

**University of  
Sheffield**

# **Developing a Novel Transgenic Zebrafish Model of Urinary Tract Cancer**

**Thesis submitted to obtain the degree of Doctor of Philosophy**

**Division of Clinical Medicine, School of Medicine and Population Health,  
University of Sheffield**

**Ibrahim Jubber**

**MRCS (Royal College of Surgeons of England, UK)**

**MBBS (University of London, UK)**

**February 2024**

## Acknowledgements

First and foremost, I'd like to express my gratitude to my supervisors Professor James Catto and Professor Stephen Renshaw for their invaluable mentorship and guidance throughout this journey.

I am indebted to Ms. Catherine Loynes for training me in several laboratory research techniques, for her advice, and help with troubleshooting throughout my PhD. I'd like to thank Renshaw lab members, past and present: Stone Elworthy, Holly Rutherford, Stuart Gaines, Clare Muir and Nils Olijhoek for their insightful suggestions and troubleshooting help during our weekly lab meetings.

A special thank you to Dr Jonathan Griffin for his assistance with histological analysis and to Dr Marcus Cumberbatch for his support during the early stages of setting up this project.

I'm grateful to technician staff Maggie Glover, Jenny Down, David Drew, Mark Kinch and Fiona Wright for their assistance. I'm also grateful to the core facilities that made this project possible: The Biological Services Aquaria for and the Light Microscope Facility.

Thank you to the Royal College of Surgeons and the National Institute for Health and Care Research (Via a Research Professorship to Professor James Catto) for allowing me to complete the research in this thesis.

Lastly, I'd like to thank my family and my wife Kristina for their unwavering support.

## Summary

Urinary tract cancers encompass cancers of the kidneys, ureters, bladder and urethra. These cancers are common and associated with substantial morbidity and mortality worldwide. The most common of these cancers overall are urothelial carcinomas which arise from the specialised epithelium (termed the urothelium) lining the urinary tract from the renal pelvis down to the urethra, but most commonly affect the bladder. The second most common of these cancers is renal cell carcinoma, an adenocarcinoma, which accounts for approximately 90% of kidney cancers and arises from renal tubular epithelial cells. Large scale sequencing projects have led to important insights on common genomic and transcriptomic alterations in these cancers. However, there is a lack of high volume *in-vivo* transgenic models of urinary tract cancers available for rigorous mechanistic testing of the roles of these genetic alterations. Zebrafish transgenic models of cancers have demonstrated advantages with respect to ease of genetic manipulation, *in-vivo* imaging and high-throughput approaches.

I performed a characterisation of the zebrafish excretory urinary tract with respect to histological characteristics and anatomical structure and demonstrate several similarities to the human system. The zebrafish kidneys converge onto two mesonephric ducts (homologous to ureters) which drain into a single saccular epithelium lined urinary bladder. The urinary bladder, in turn, drains externally via a single distinct urethra that is separate from the rectum. The zebrafish urinary epithelium expresses similar proteins to the human system. In addition, I demonstrate the development of the zebrafish urinary bladder with respect to morphological change during the larval and juvenile stages from a tubular structure that develops into a saccular expansile structure at around 6 weeks post fertilisation.

I outline my work on developing a novel transgenic zebrafish urinary tract cancer model using genomic alterations associated with bladder cancer (combination of oncogenic tissue specific *HRAS G12V* overexpression and a global *tp53* DNA binding domain mutation). This model utilises the bipartite Gal4/UAS system and generates cancers in the F0 generation. The cancers are generated by one cell stage microinjection of a plasmid containing the coding sequence for a GFP-*HRAS G12V* fusion protein (p-UAS: *GFP-HRAS\_G12V*) into a Gal4 enhancer trap zebrafish line (with and without a global *tp53* DNA binding domain mutation). We show that this pipeline results in abdominal cancers as early as 3 weeks post-fertilisation (7.1% to 14.6% abdominal tumours

between 2 weeks and 3 months for *HRASG12V* only and combination of *tp53* mutation and *HRASG12V* genomic alterations, respectively). Histological characterisation of these cancers demonstrated them to be situated in the retroperitoneal region of the urinary tract and immunohistochemistry demonstrated them to be a combination of epithelial and non-epithelial in nature. Subsequent attempts at optimisation of this urinary tract cancer model with a more tissue specific zebrafish promoter sequence (*cdh17* gene promoter) without using the Gal4/UAS system does not lead to cancers up to 3 months of age suggesting that the Gal4/UAS system is important for cancer formation in zebrafish.

# Table of Contents

<b>Acknowledgements .....</b>	<b>2</b>
<b>Summary .....</b>	<b>3</b>
<b>Table of Contents .....</b>	<b>5</b>
<b>List of Tables and Figures .....</b>	<b>11</b>
<b>Abbreviations .....</b>	<b>16</b>
<b>Gene Nomenclature.....</b>	<b>20</b>
<b>Publications Arising From Work Undertaken in This Thesis .....</b>	<b>21</b>
<b>Presentations Arising from Work Undertaken in This Thesis .....</b>	<b>21</b>
<b>Chapter 1. Introduction .....</b>	<b>22</b>
<b>1.1. The Urinary Tract in Mammals .....</b>	<b>22</b>
1.1.1. Structure.....	22
1.1.2. Function.....	22
1.1.3. Embryology.....	23
1.1.4. Histology.....	27
<b>1.2. Zebrafish .....</b>	<b>30</b>
1.2.1. Taxonomy.....	30
1.2.2. Life cycle.....	30
<b>1.3. The Zebrafish Urinary Tract .....</b>	<b>30</b>
1.3.1. Anatomy .....	30
1.3.2. Embryology.....	32
1.3.3. Homology to Mammalian Urinary Tract.....	36
1.3.3.1. Uroplakins in Zebrafish .....	36
1.3.3.2. Zebrafish Models of Lower Urinary Tract Dysfunction .....	36
<b>1.4. Cancer .....</b>	<b>37</b>
1.4.1. Overview .....	37
1.4.2. Hallmarks of Cancer .....	38
1.4.3. Aetiology and Molecular Biology.....	40
<b>1.5. Urinary Tract Cancer Overview .....</b>	<b>41</b>
<b>1.6. Bladder Cancer .....</b>	<b>42</b>
1.6.1. Epidemiology.....	42
1.6.2. Aetiology and Risk Factors .....	42

1.6.3. Pathology.....	44
1.6.4. Natural History .....	47
1.6.5. Molecular Biology.....	50
1.6.6. Molecular Subtypes of Muscle- Invasive Bladder Cancer.....	58
1.6.7. Treatment.....	62
1.6.7.1. Non-Muscle Invasive Bladder Cancer Treatment .....	62
1.6.7.2. Muscle-Invasive Bladder Cancer Treatment.....	63
1.6.7.3. Locally Advanced or Metastatic Bladder Cancer Treatment .....	64
1.6.7.4. Experimental Bladder Cancer Treatments.....	65
<b>1.7. Upper Tract Urothelial Cancer .....</b>	<b>66</b>
1.7.1. Overview, Histology, Aetiology and Diagnosis .....	66
1.7.2. Treatment.....	67
1.7.2.1. Localised Disease .....	67
1.7.2.2. Metastatic Disease .....	68
<b>1.8. Renal Cell Cancer (RCC) .....</b>	<b>68</b>
1.8.1. Overview, Histology, Aetiology and Diagnosis .....	69
1.8.2. Treatment.....	72
1.8.2.1. Localised Disease .....	72
1.8.2.2. Metastatic Disease .....	72
<b>1.9. Pre-Clinical Cancer Models Overview .....</b>	<b>73</b>
1.9.1. Cancer Models in Mice.....	73
1.9.1.1. Mouse Models of Bladder Cancer .....	74
1.9.2. Zebrafish Disease Models.....	77
1.9.2.1. Zebrafish Cancer Models.....	78
<b>1.10. Spontaneous Urinary Tract Cancers in Fish .....</b>	<b>83</b>
<b>1.11. Project Aims and Objectives .....</b>	<b>83</b>
<b>Chapter 2. Materials and Methods.....</b>	<b>85</b>
<b>2.1. Zebrafish Husbandry .....</b>	<b>85</b>
<b>2.2. Zebrafish Lines .....</b>	<b>87</b>
<b>2.3. Zebrafish One Cell Stage Microinjection .....</b>	<b>96</b>
<b>2.4. Zebrafish Dissection .....</b>	<b>98</b>
<b>2.5. Mounting Zebrafish for Fluorescent Microscopy Imaging.....</b>	<b>98</b>
<b>2.6. Zebrafish Timelapse Imaging .....</b>	<b>98</b>
<b>2.7. Fin clipping, Genomic DNA Extraction and Genotyping Zebrafish.....</b>	<b>99</b>

<b>2.8. Zebrafish <i>in situ</i> hybridisation .....</b>	<b>103</b>
<b>2.9. Whole Mount Zebrafish EdU Proliferation Assay .....</b>	<b>103</b>
<b>2.10. Whole Mount Zebrafish Immunohistochemistry.....</b>	<b>104</b>
<b>2.11. Histology .....</b>	<b>104</b>
2.11.1. Zebrafish Histology.....	104
2.11.2. Human Control Histology Samples.....	105
2.11.3. H&E staining.....	105
2.11.4. Immunohistochemistry (FFPE): ABC DAB method .....	106
2.11.5. Masson’s Trichrome .....	111
2.11.6. Histological Analysis .....	111
<b>2.12. Molecular Biology .....</b>	<b>111</b>
2.12.1. Agarose Gel Electrophoresis.....	111
2.12.2. Plasmids.....	112
2.12.3. Restriction Enzymes .....	114
2.12.4. Bacterial Transformation.....	114
2.12.5. Plasmid Purification.....	115
2.12.6. DNA/RNA Quantification.....	117
2.12.7. Plasmid DNA Confirmation.....	117
2.12.8. Plasmid Recombination (Gateway cloning).....	118
2.12.9. <i>In vitro</i> transcription (Tol2/transposase mRNA).....	118
<b>2.13. Imaging .....</b>	<b>122</b>
<b>2.14. Software .....</b>	<b>122</b>
<b>2.15. Gene and Protein Cross Species Alignment.....</b>	<b>123</b>
<b>2.16. Systematic Review .....</b>	<b>123</b>
<b>Chapter 3. Epidemiology of Bladder Cancer in 2023: A Systematic Review of Risk Factors.....</b>	<b>124</b>
<b>3.1. Introduction .....</b>	<b>125</b>
<b>3.2. Evidence Acquisition .....</b>	<b>126</b>
<b>3.3. Evidence Synthesis .....</b>	<b>126</b>
<b>3.4. Epidemiology, Incidence, Prevalence, and Mortality of Bladder Cancer .....</b>	<b>128</b>
<b>3.5. Risk Factors for Bladder Cancer .....</b>	<b>134</b>
3.5.1. Tobacco Smoking.....	135
3.5.2. e-Cigarette use .....	135
3.5.3. Cannabis use.....	136

3.5.4. Opium Consumption .....	136
3.5.5. Occupational Carcinogen Exposure.....	136
3.5.6. Dietary Factors .....	137
3.5.6.1. Regional Diets .....	137
3.5.6.2. Grain and Fibre .....	137
3.5.6.3. Alcohol.....	138
3.5.6.4. Dietary fluid consumption .....	138
3.5.6.5. Caffeine.....	138
3.5.6.6. Tea .....	139
3.5.6.7. Cow’s Milk and Dairy .....	139
3.5.6.8. Meat and Fish .....	139
3.5.6.9. Fruits and vegetables.....	139
3.5.6.10. Inflammatory Diets .....	140
3.5.6.11. Vitamins.....	140
3.5.7. Environmental Carcinogens.....	140
3.5.7.1. Arsenic .....	140
3.5.7.2. Air Pollution .....	141
3.5.7.3. Nitrates .....	141
3.5.7.4. Trihalomethanes.....	141
3.5.7.5. Routine Personal Hair Dye Use.....	142
3.5.8. Race and Comparative Genomic Landscape From Various Genomic Ancestries .....	142
3.5.9. Socioeconomic position .....	142
3.5.10. Physical Activity.....	143
3.5.11. Gene-Environment Interaction .....	143
3.5.12. Urinary Tract Inflammation .....	144
3.5.12.1. Urinary Tract Infection.....	144
3.5.12.2. Neurogenic Bladder and Long-Term Catheter.....	144
3.5.12.3. Urolithiasis.....	145
3.5.12.4. Benign Prostate Hyperplasia and Bladder Diverticulae .....	145
3.5.13. Medical Conditions (This section was written with assistance from a collaborator: Dr Sean Ong, University of Melbourne, Australia) .....	146
3.5.13.1. Pelvic Radiotherapy .....	146
3.5.13.2. Obesity.....	146
3.5.13.3. Metabolic syndrome.....	147
3.5.13.4. Diabetes.....	147
3.5.13.5. Hypertension and Hyperlipidaemia .....	147
3.5.13.6. Stroke .....	147
3.5.13.7. Asthma.....	148
3.5.13.8. Autoimmune and Rheumatological Conditions.....	148
3.5.13.9. Solid Organ Transplantation .....	148

3.5.13.10. Associations with other cancers .....	149
3.5.14. Medications (This section was written with assistance from Dr Sean Ong, University of Melbourne, Australia) .....	149
<b>3.6. Summary.....</b>	<b>149</b>
<b>Chapter 4. Analysis of the Distal Urinary Tract in Larval and Adult Zebrafish Reveals Homology to the Human System. ....</b>	<b>150</b>
<b>4.1. Introduction .....</b>	<b>151</b>
<b>4.2. Results .....</b>	<b>152</b>
4.2.1. Uroplakin Genes in the Zebrafish .....	152
4.2.2. Uroplakin-1a mRNA Expression in the Zebrafish Larval Pronephros.....	155
4.2.3. Histological Comparison Between Zebrafish and Human Excretory Urinary Tracts.....	157
4.2.4. Change in Excretory Urinary Tract Morphology Over Time .....	170
4.2.5. Characterisation of Adult Zebrafish Urinary Bladder Morphology Using <i>TgBAC(mpx:GFP)i114</i> Line .....	173
4.2.6. Isolation of Zebrafish Urinary Bladder From Dissected Adult Zebrafish .....	175
<b>4.3. Discussion .....</b>	<b>177</b>
<b>4.4. Conclusion.....</b>	<b>179</b>
<b>Chapter 5. Developing a Transgenic Model of Urinary Tract Cancer in Zebrafish Utilising An Enhancer Trap Line .....</b>	<b>180</b>
<b>5.1. Introduction .....</b>	<b>180</b>
<b>5.2. Aims and Objectives.....</b>	<b>181</b>
<b>5.3. Results .....</b>	<b>181</b>
5.3.1. Identification and Characterisation of Transgenic <i>Et(gSAIzGFFD)875b; Tg(UAS: GFP)</i> Zebrafish Line .....	181
5.3.2. Stable <i>GFP-HRAS_G12V</i> Expression in the Zebrafish Urinary Tract.....	191
5.3.3. Mosaic <i>GFP HRAS_G12V</i> Expression in the Zebrafish Urinary Tract .....	194
5.3.4. 5-Ethynyl-2-deoxyuridine Proliferation Assay .....	197
5.3.5. Design and Implementation of Zebrafish Urinary Tract Cancer Model.....	200
5.3.6. Abdominal Tumour development in Urinary Tract Cancer Model .....	204
5.3.7. Non-Abdominal Tumour Development in Urinary Tract Cancer Model.....	206
5.3.8. Histological Characteristics of H&E-Stained Tumours in the Urinary Tract Cancer Model .....	208
5.3.9. Immunohistochemical Characterisation of Zebrafish Tumours Generated During Urinary Tract Cancer Model .....	215
5.3.9.1. AE1/AE3 Epithelial Marker .....	215
5.3.9.2. Urothelial Immunohistochemistry Markers .....	221
5.3.9.3. Renal Immunohistochemistry Markers .....	224

5.4. Discussion .....	226
5.5. Conclusion.....	230
<b>Chapter 6. Developing A Transgenic Zebrafish Model of Urinary Tract Cancer Utilising the Zebrafish <i>cdh17</i> Gene Promoter .....</b>	<b>231</b>
6.1. Introduction .....	231
6.2. Aims and Objectives.....	232
6.3. Results .....	233
6.3.1. Identification of a New Urinary Tract Specific Promoter .....	233
6.3.2. Generation of Tg( <i>cdh17</i> Gal4); Tg(UAS: Kaede) Stable Line.....	238
6.3.3. Characterisation of Kaede Expression Pattern in Tg( <i>cdh17: Gal4</i> ) <i>sh681</i> ; Tg(UAS: Kaede) <i>s1999t</i> From Larval To Adult Stages.....	241
6.3.4. Generation of Plasmids to Drive GFP-HRAS-G12V Expression Under Control of the <i>cdh17</i> promoter. ....	244
6.3.5. Generation of plasmids to drive oncogenic <i>erbb2</i> and <i>pik3ca</i> expression under control of the zebrafish <i>cdh17</i> promoter. ....	246
6.3.6. Testing Newly Generated Plasmids Designed to Drive Oncogenic <i>HRAS</i> , <i>erbb2</i> and <i>pik3ca</i> Under the Control of the Zebrafish <i>cdh17</i> Promoter .....	249
6.3.7. Design of urinary tract cancer model utilising <i>cdh17</i> promoter/driver.....	252
6.3.8. Mosaic expression of GFP-HRAS_G12V and GFP-CAAX in the Distal Mesonephros Under the Control of the Zebrafish <i>cdh17</i> Promoter at 3 Weeks Post Fertilisation .....	254
6.3.9. Identification of Zebrafish Abnormalities in New Urinary Tract Cancer Model .....	255
6.3.10. Histological Analysis of Zebrafish With Macroscopic Abnormalities in Cancer Model Utilising <i>cdh17</i> Promoter .....	256
6.4. Discussion .....	261
6.5. Conclusions .....	262
<b>Chapter 7. Overall Discussion and Future Work .....</b>	<b>263</b>
7.1. Overall Discussion .....	263
7.2. Future Work.....	266
7.3. Conclusions .....	271
<b>References.....</b>	<b>272</b>

## List of Tables and Figures

Table 1. TNM classification for Bladder Cancer. ....	46
Table 2. EORTC Scoring System to Determine Risk of Recurrence and Progression of Bladder Cancer. ....	49
Table 3. Probabilities of Bladder cancer Recurrence and Progression After 1 and 5 years Respectively Based on EORTC Scores .....	50
Table 4. TNM Classification for Kidney Cancer. ....	71
Table 5. Zebrafish Lines Maintained During This Project. ....	95
Table 6. Reagents Used for Immunohistochemistry Experiments. ....	110
Table 7. Plasmids Used During This Project. ....	114
Table 8. Bladder Cancer Risk Factor Summary According to International Agency for Research on Cancer Monographs. ....	134
Table 9. Spatial Reporter Gene Expression Pattern in <i>Et(gSAIzGFFD)875b; Tg(UAS: GFP)</i> Zebrafish Line. ....	191
Figure 1. Embryology of the Human Urinary Tract. ....	24
Figure 2. Embryological Development of the Urinary Bladder and Trigone. ....	26
Figure 3. H&E-Stained Histology Section of Bladder Urothelium. ....	28
Figure 4. H&E-Stained Histology Section of Bladder Wall. ....	29
Figure 5. Adult Zebrafish Kidney Exposed Along Dorsal Abdominal Wall. ....	32
Figure 6. Zebrafish Embryo Pronephros Segmentation. ....	34
Figure 7. Schematic of Zebrafish Mesonephrogenesis. ....	36
Figure 8. The Hallmarks of Cancer. ....	40
Figure 9. Simplified Two Pathway Model for Molecular Basis of Bladder Cancer Initiation and Progression. ....	52
Figure 10. Common FGFR3 Genomic Alterations in Bladder Cancer. ....	53
Figure 11. Key Signalling Pathways Implicated in Bladder Cancer Tumourigenesis: MAPK and PI3K signalling. ....	55
Figure 12. Mutation Frequency Identified From Whole Exome Sequencing Data for Non-Muscle Invasive Bladder Cancer and Muscle Invasive Bladder Cancer. ....	57
Figure 13. Proposed Molecular Subtypes of Muscle Invasive Bladder Cancer and Potential Treatment Options. ....	61
Figure 14. Schematic of The Gal4/UAS System. ....	81

Figure 15. One Cell Stage Microinjection Technique.....	97
Figure 16. Genotyping for <i>GFF</i> transgene and <i>tp53 zdf1</i> mutation.....	102
Figure 17. Generating <i>tol2</i> mRNA from pCS2 transposase plasmid (tol2 kit 396).....	121
Figure 18. CONSORT Diagram for Systematic Review. ....	127
Figure 19. Global Map of Incidence (Age-Standardized) Rates for Males and Females in 2020. ...	130
Figure 20. Global Map of Prevalence for Males and Females in 2020. ....	131
Figure 21. Global Map of Mortality (Age-Standardized) Rates for Males and Females in 2020.....	132
Figure 22. Estimated Number of New Bladder Cancer Cases Between 2020 and 2040 (Both Sexes). .....	133
Figure 23. Alignment of Human, Mouse and Zebrafish Uroplakin Protein Amino Acid Sequences. .....	154
Figure 24. Expression of <i>uroplakin 1a</i> in Zebrafish Larvae Using <i>in situ</i> Hybridisation.....	156
Figure 25. Anatomy of Adult Zebrafish Mesonephric Ducts and Urinary Bladder. ....	158
Figure 26. Anatomy of Adult Zebrafish Urethra. ....	159
Figure 27. Alignment of Human and Zebrafish GATA3 amino acid sequences.....	160
Figure 28. Expression of GATA3 in Zebrafish and Human Urinary Bladder Tissue Sections Using Immunohistochemistry. ....	161
Figure 29. Alignment of Human and Zebrafish Uroplakin-1a and Uroplakin-2 Amino Acid Sequences.....	162
Figure 30. Expression of Uroplakins in Zebrafish and Human Urinary Bladder Tissue Sections Using Immunohistochemistry. ....	163
Figure 31. Amino acid Alignment of Zebrafish and Human CD44 and Cytokeratin 5 Sequences...	165
Figure 32. Expression of Urothelial Basal Cell Layer Markers in Zebrafish and Human Urinary Bladder Tissue Sections Using Immunohistochemistry. ....	166
Figure 33. Negative (No Primary Antibody) Controls for Immunohistochemistry. ....	167
Figure 34. Structure of Zebrafish Mesonephric Duct and Urinary Bladder Wall. ....	169
Figure 35. Analysis of Morphological Development of the Zebrafish Urinary Bladder Using GFP expression in the <i>TgBac(mpx: GFP) i114</i> Zebrafish Line Between 2- and 3- Weeks Post Fertilisation. .....	171
Figure 36. Analysis of Morphological Development of the Zebrafish Urinary Bladder Using GFP Expression in the <i>TgBAC(mpx: GFP)i114</i> Zebrafish Line Between 4-Weeks Post Fertilisation and Adult Stages.....	172

Figure 37. Analysis of Morphology of Adult Zebrafish Urinary Bladder Using GFP Expression in <i>TgBAC(mpx:GFP)i114</i> Zebrafish Line. ....	174
Figure 38. Dissection of Zebrafish Distal Urinary Tract.....	176
Figure 39. Early GFP Expression in the Zebrafish Pronephros of the <i>Et(gSAIzGFFD)875b; Tg(UAS:GFP)</i> Enhancer Trap Zebrafish Line.....	184
Figure 40. GFP Expression in Zebrafish <i>Et(gSAIzGFFD)875b; Tg(UAS:GFP)</i> Line Between 2- and 4 Days Post Fertilisation. ....	186
Figure 41. GFP Expression in Zebrafish <i>Et(gSAIzGFFD)875b; Tg(UAS:GFP)</i> Line Between 2- and 3 Weeks Post Fertilisation. ....	187
Figure 42. GFP Expression in Urinary Tract of Dissected Zebrafish <i>Et(gSAIzGFFD)875b; Tg(UAS:GFP)</i> Line At 4 Weeks Post Fertilisation. ....	189
Figure 43. GFP Expression in Urinary Tract of Dissected Zebrafish <i>Et(gSAIzGFFD)875b; Tg(UAS:GFP)</i> Line At 6 Weeks Post Fertilisation. ....	190
Figure 44. Attempt at Generating Stable Transgenic Zebrafish <i>Et(gSAIzGFFD)875b; Tg(UAS:GFP-HRAS_G12V)</i> Line for Use in a Urinary Tract Cancer Model. ....	193
Figure 45. Mosaic <i>GFP-HRAS_G12V</i> Expression in Zebrafish Distal Pronephros at 4 Days Post Fertilisation.....	196
Figure 46. Optimisation of EdU Proliferation Assay to Visualize Proliferation in Zebrafish Pronephros Using Fluorescence Microscopy.....	199
Figure 47. Schematic of the Zebrafish Urinary Tract Cancer Model Pipeline. ....	203
Figure 48. Zebrafish Tumours Generated in Urinary Tract Cancer Model.....	205
Figure 49. Non-Abdominal Tumours in the Zebrafish Urinary Tract Cancer Model. ....	207
Figure 50. Histological Characteristics of Zebrafish Distal Abdominal/Pelvic Cancers in Urinary Tract Cancer Model. ....	210
Figure 51. Histological Characteristics of Zebrafish Proximal Abdominal Cancers in Urinary Tract Cancer Model. ....	211
Figure 52. Histological Characteristics of Zebrafish Proximal Abdominal Cancers in Urinary Tract Cancer Model. ....	212
Figure 53. Histological Features of Cancer in Urinary Tract Cancer Model: Nuclear Pleomorphism and Prominent Mitosis. ....	213
Figure 54. No Evidence of Macroscopic Tumours in <i>tp53</i> Mutant & <i>HRAS_G12V</i> and <i>tp53</i> Wild Type & <i>HRAS_G12V</i> Endpoint 3-Month-Old Zebrafish.....	214

Figure 55. Immunohistochemistry Validation of AE1/AE3 (Pan-Cytokeratin) Antibody in Zebrafish Epithelia.....	216
Figure 56. Immunohistochemistry Using AE1/AE3 (Pan-Cytokeratin) Antibody in Distal Abdominal/Pelvic Tumours in Zebrafish Urinary Tract Cancer Model. ....	218
Figure 57. Immunohistochemistry using AE1/AE3 (Pan-Cytokeratin) Antibody in Proximal Abdominal Tumours in Zebrafish Urinary Tract Cancer Model. ....	219
Figure 58. Immunohistochemistry Using AE1/AE3 (Pan-Cytokeratin) Antibody in Proximal Abdominal Tumours in Zebrafish Urinary Tract Cancer Model. ....	220
Figure 59. Immunohistochemistry Using GATA 3 Antibody in IHC Determined Epithelial Tumours Generated in Zebrafish Urinary Tract Cancer Model.....	222
Figure 60. Immunohistochemistry Using Uroplakin-1a Antibody in IHC Determined Epithelial Tumours Generated in Zebrafish Urinary Tract Tumours in Urinary Tract Cancer Model. ....	223
Figure 61. Optimization of Pax8 Immunohistochemistry in Zebrafish Kidney.....	225
Figure 62. Zebrafish <i>In Vivo</i> Mosaic Expression Patterns of Zebrafish <i>enpep</i> Promoter .....	235
Figure 63. Zebrafish <i>In Vivo</i> Mosaic Expression Pattern of Zebrafish <i>cdh17</i> Promoter.....	236
Figure 64. Alignment of Zebrafish and Human CDH17 Amino Acid Sequences. ....	237
Figure 65. Generation of <i>Tg(cdh17: Gal4)sh681</i> ; <i>Tg(UAS: Kaede)s1999t</i> and <i>Tg(cdh17: Gal4)shs681</i> Stable Transgenic Zebrafish Lines.....	239
Figure 66. Identification of Founder with Single Transgene Insertion in Newly Generated <i>Tg(cdh17: Gal4)sh681</i> ; <i>Tg(UAS: Kaede)s1999t</i> and <i>Tg(cdh17: Gal4)shs681</i> Stable Transgenic Zebrafish Lines. ....	240
Figure 67. Fluorescence Microscopy of Stable <i>Tg(cdh17: Gal4)sh681</i> ; <i>UAS: Kaede)s1999t</i> Transgenic Zebrafish Larvae at 4 days, 2 Weeks and 3 Weeks Post Fertilisation.....	242
Figure 68. Fluorescence Microscopy of Stable <i>Tg(cdh17: Gal4)sh681</i> ; <i>UAS: Kaede)s1999t</i> Transgenic Zebrafish Line at 6-Weeks Post Fertilisation. ....	243
Figure 69. Generating pDestTol2CG2- <i>cdh17: GFP-HRAS_G12V</i> and pDestTol2CG2- <i>cdh17: GFP-CAAX</i> expression vectors.....	245
Figure 70. Designing Zebrafish Middle Entry Plasmids Containing <i>erbB2</i> and <i>pik3ca</i> Coding Sequences With Mutations Associated With Urothelial Bladder Cancer. ....	247
Figure 71. Generating pDestTol2CG2- <i>cdh17: erbB2_A301F-GFP</i> and pDestTol2CG2- <i>cdh17: pik3ca_E545K-GFP</i> Plasmids.....	248
Figure 72. One Cell Stage Zebrafish Microinjection of Newly Constructed <i>cdh17: GFP-HRAS_G12V</i> and <i>cdh17: GFP-CAAX</i> Expression Vectors and Subsequent Fluorescence Microscopy. ....	250

Figure 73. One Cell Stage Zebrafish Microinjection of Newly Constructed <i>cdh17: erbb2_A301F-GFP</i> and <i>cdh17: pik3ca_E545K-GFP</i> Expression Vectors and Subsequent Fluorescence Microscopy ...	251
Figure 74. Schematic of New Zebrafish Urinary Tract Cancer Model Utilising Zebrafish <i>cdh17</i> Gene Promoter. ....	253
Figure 75. Mosaic Expression of GFP-HRAS_G12V and GFP-CAAX in Distal Mesonephros Under the Control of the <i>cdh17</i> Gene Promoter. ....	254
Figure 76. Macroscopic Phenotypes in <i>tp53<sup>zdf1/zdf1</sup></i> , <i>Tg(cdh17: GFP-HRAS_G12V)</i> and <i>tp53<sup>zdf1/zdf1</sup></i> , <i>Tg(cdh17: GFP-CAAX)</i> Zebrafish Between 2 Weeks and 3 Months.....	255
Figure 77. H&E-Stained Sections of Approximately 4-Week Post Fertilisation <i>tp53<sup>zdf1/zdf1</sup></i> , <i>Tg(cdh17: GFP- HRAS_G12V)</i> Zebrafish Culled Due To Heart Swelling. ....	257
Figure 78. H&E-Stained Sections of Approximately 6-Week Post Fertilisation <i>tp53<sup>zdf1/zdf1</sup></i> , <i>Tg(cdh17: GFP- HRAS_G12V)</i> Zebrafish Culled Due To Heart Swelling. ....	258
Figure 79. H&E-Stained Sections of Approximately 6-Week Post Fertilisation <i>tp53<sup>zdf1/zdf1</sup></i> , <i>Tg(cdh17: GFP- HRAS_G12V)</i> Zebrafish Culled Due To Abdominal Swelling. ....	259
Figure 80. H&E-Stained Sections of Approximately 2-month-old <i>tp53<sup>zdf1/zdf1</sup></i> , <i>Tg(cdh17: GFP- HRAS_G12V)</i> Zebrafish Culled Due To Abdominal Swelling. ....	260

## Abbreviations

ABC: Avidin-Biotin Complex

ADC: Antibody Drug Conjugates

APOBEC: Apolipoprotein B mRNA Editing Enzyme, Catalytic Polypeptide)

ASR: Age-standardised rate

ATG: Adenine-Thymine-Guanine (Start codon which signals the start of protein translation)

BAC: Bacterial Artificial Chromosome

BBN: N-butyl-N-(4-hydroxybutyl) nitrosamine

BC: Bladder Cancer

BCG: Bacillus Calmette-Guerin

BF: Brightfield

BLAST: Basic Local Alignment Search Tool

BMP: Bone Morphogenetic Protein

BRCA: Breast Cancer Gene

BrdU: 5'-bromo-2'- deoxyuridine

BSA: Bovine Serum Albumin

CI: Confidence Interval

CIS: Carcinoma in situ

Cl: Chloride

CRISPR: Clustered Regularly Interspaced Short Palindromic Repeats

CS: Corpuscle of Stannius

CT: Computerised Tomography

DAB: 3,3'-Diaminobenzidine

DAPI: 4',6-diamidino-2-phenylindole

DE segment: Distal early (renal) segment

DF: Dark Field

dH<sub>2</sub>O: Distilled Water

DL segment: Distal late (renal) segment

DPF: Days Post Fertilisation

DPX: Dibutylphthalate Polystyrene Xylene

DNA: Deoxyribonucleic Acid

*E. Coli: Escherichia Coli*

EDTA: Ethylenediaminetetraacetic acid  
EDU: 5-ethynyl-2'-deoxyuridine  
ENU: N-ethyl-N-nitrosourea  
EGFR: Epidermal Growth Factor Receptor  
EMT: Epithelial- Mesenchymal Transition  
EORTC: European Organisation for Research and Treatment of Cancer  
ERK: Extracellular signal-regulated kinase  
Et: Enhancer trap  
ETOH: Ethanol  
FFPE: Formalin-Fixed Paraffin Embedded  
FGFR: Fibroblast Growth Factor Receptor  
F0 or F1 or F2: F stands for filial generation and describes a generation in a line breeding experiment.  
G: Gravitational Force  
GFF: Transcriptional activator Gal4-VP16 (Modified version of Gal4)  
GFP: Green Fluorescent Protein  
GST: Glutathione S-transferase  
GWAS: Genome Wide Association Study  
HRAS: Harvey rat sarcoma virus  
HRNMIBC: High risk non-muscle invasive bladder cancer  
HRP: Horse Radish Peroxidase  
H2O2: Hydrogen Peroxide  
IARC: International Agency for Research on Cancer  
IHC: Immunohistochemistry  
KRAS: Kirsten rat sarcoma virus  
LB: Luria-Bertani  
MA: Meta-Analysis  
MAPK: Mitogen-activated protein kinase  
Mg: Magnesium  
MET: Mesenchymal-Epithelial Transition  
MIBC: Muscle-invasive bladder cancer  
MMC: Mitomycin C  
mM: Millimolar

MMR: Mismatch Repair  
mRNA: Messenger Ribonucleic Acid  
MS222: Tricaine Methanesulfonate  
mTOR: Mammalian target of rapamycin  
NAC: Neoadjuvant chemotherapy  
NAT2: N-acetyl transferase 2  
NMIBC: Non-muscle invasive bladder cancer  
NRAS: Neuroblastoma Ras Viral Oncogene Homolog  
OR: Odds ratio  
ORF: Open reading frame  
PCR: Polymerase Chain Reaction  
PCT: Proximal Convoluted Tubule  
PD segment: Pronephric Duct (Renal segment)  
PD-1: Programmed Cell Death Protein 1  
PD-L1: Programmed Cell Death Ligand 1  
PFA: Paraformaldehyde  
PI3K: Phosphoinositide 3-kinase  
POD: Podocytes  
PST: Proximal Straight Tubule  
PTEN: Phosphatase and tension homolog gene  
RAS: Rat sarcoma (Family of genes)  
RB: Retinoblastoma  
RCC: Renal Cell Carcinoma  
RNA: Ribonucleic Acid  
RPM: Revolutions per minute  
RR: Risk Ratio  
RT: Radiotherapy  
RTK: Receptor Tyrosine Kinase  
SCC: Squamous Cell Carcinoma  
SOC: Super Optimal Broth  
SNP: Single Nucleotide Polymorphism  
SR: Systematic Review  
SV40: Polyomavirus Simian Virus 40

TAE: Buffer solution containing a mixture of Tris base, acetic acid and EDTA

TALENS: Transcription Activator-Like Effector Nucleases

TAM: Tumour Associated Macrophage

Tg: Transgenic

TKI: Tyrosine Kinase Inhibitor

TNM: Tumour, node, metastasis (Cancer staging classification system)

UAS: Upstream Activating Sequence

UBC: Urothelial Bladder Carcinoma

UCC: Urothelial Cell Carcinoma

UPK: Uroplakin

UTUC: Upper tract urothelial carcinoma

VHL: Von-Hippel Lindau

WNT: Wingless-related integration site

WPF: Weeks Post Fertilisation

WT: Wild type

ZFIN: Zebrafish Information Network

µg: Microgram

µl: Microliter

µM: Micromolar

## Gene Nomenclature

Standard gene nomenclature has been used to describe and differentiate zebrafish, human and mouse genes (1-3). The following table describes the nomenclature differences between the species for genes and proteins. These are differentiated by letter case and italicisation and an example is shown in the table below using the *TP53* tumour suppressor gene as an example:

<b>Species</b>	<b>Gene</b>	<b>Protein</b>
Zebrafish	Lower case & italicised e.g. <i>tp53</i>	First letter upper case, the rest lower case and no italics e.g. Tp53
Mouse	First letter upper case, the rest lower case and all italicised e.g. <i>Tp53</i>	All letters upper case and no italics e.g. TP53
Human	All letters upper case and italicised e.g. <i>TP53</i>	All letters upper case and no italics e.g. TP53

## **Publications Arising From Work Undertaken in This Thesis**

**Jubber I**, Ong S, Bukavina L, Black PC, Comperat E, Kamat AM, Kiemeney L, Lawrentschuk N, Lerner SP, Meeks JJ, Moch H, Necchi A, Panebianco V, Sridhar SS, Znaor A, Catto JWF, Cumberbatch MG. Epidemiology of Bladder Cancer in 2023: A Systematic Review of Risk Factors. *Eur Urol.* 2023;84(2):176-90.

**Jubber I**, Morhardt DR, Griffin J, Cumberbatch MG, Glover M, Zheng Y, Rehman I, Loynes CA, Hussain SA, Renshaw SA, Leach SD, Cunliffe VT, Catto JWF. Analysis of the distal urinary tract in larval and adult zebrafish reveals homology to the human system. *Disease models & mechanisms.* 2023;16(7).

## **Presentations Arising from Work Undertaken in This Thesis**

**Jubber I**, Griffin J, Cumberbatch M, Loynes CA, Glover M, Morhardt D, Zheng Y, Leach S, Cunliffe V, Renshaw SA, Catto J. Developing a Novel Transgenic Zebrafish Model of Bladder Cancer. *Zebrafish Disease Models 15; 2022; Sheffield, United Kingdom (Oral Presentation).*

**Jubber I**, Cumberbatch M, Glover M, Griffin J, Morhardt D, Zheng Y, Rehman I, Kawakami K, Loynes C, Hussain S, Leach S, Renshaw S, Cunliffe V, Catto J. Analysis of the urinary tract in *Danio rerio* (Zebrafish) reveals homology to the mammalian system. *Zebrafish Disease Models 15; 2022; Sheffield, United Kingdom (Poster Presentation).*

# Chapter 1. Introduction

## 1.1. The Urinary Tract in Mammals

### 1.1.1. Structure

The urinary tract in mammals is composed of paired retroperitoneal kidneys which have filtration and excretion function. The functional unit of a kidney is a nephron which consist of a glomerulus, proximal convoluted tubule, loop of Henle, distal convoluted tubule and collecting ducts. The glomerulus has filtration function and the region from the proximal convoluted tubule to collecting ducts has reabsorption function (approximately 90% of the initial filtrate) (4).

Following reabsorption, the remaining fluid constitutes urine and this travels from the collecting ducts into the collecting system of the kidney which includes the calyces leading to the renal pelvis, ureter and urinary bladder. Therefore, the urinary tract can be categorised into three main regions: the filtration region (i.e. the glomerulus), the reabsorption region (i.e. the proximal convoluted tubule to collecting ducts) and the urinary excretory or transport region (i.e. the renal calyces, renal pelvis, ureter, urinary bladder) (4).

Histologically, the proximal tubule, loop of Henle and distal convoluted tubule are lined by one layer of cuboidal epithelial cells and the collecting ducts are lined by cuboidal and columnar epithelial cells. The renal calyces, renal pelvis, ureters, urinary bladder and urethra are lined by transitional epithelium or urothelium (4).

### 1.1.2. Function

The function of the urinary collecting system (renal calyces and renal pelvis) and the ureters are to transport urine to the urinary bladder with minimal reabsorption of urinary contents. The function of the urinary bladder is low pressure urine storage and voluntary urine release at socially appropriate times when the bladder has filled to a significant volume. In humans, control of urinary bladder function is a complex process involving multiple neural pathways including the cerebral cortex and the pontine micturition centre (5).

### **1.1.3. Embryology**

Mammals develop three kidney structures of increasing complexity during embryogenesis. In chronological order, the kidney structures that develop are the pronephros, the mesonephros, and metanephros. The latter of these structures forms the permanent kidney (Figure 1). All three kidney structures derive from the intermediate mesoderm (6).

The pronephros in mammals is vestigial and is composed of paired pronephric tubules and ducts. The pronephric ducts develop into the paired mesonephric ducts as they grow caudally and induce the mesonephric nephrons in the adjacent mesenchyme to develop and join the mesonephric ducts. The mesonephric ducts (Wolffian ducts) extend caudally and terminate by joining the cloaca.

The ureteric bud develops as an outgrowth from the mesonephric duct and ascends cranially. The metanephros forms as a result of reciprocal induction events between the metanephric mesenchyme and the ascending ureteric bud. The metanephric mesenchyme induces branching of the ureteric bud, which gives rise to collecting ducts, renal pelvis and ureter. The mesenchyme, in turn, is induced to develop vesicles in a mesenchymal-to-epithelial transition (MET) to give rise to metanephric tubules and nephrons (7).

The kidneys start developing caudally close the tail of the mammalian embryo. Vascular buds originating from the early kidney structures develop towards and join the common iliac arteries. As the embryo elongates, the kidneys ascend from the sacral vertebrae, reaching their final anatomical position at the lumbar level. This is believed to be driven, in part, by longitudinal growth of the lumbosacral vertebrae and a reduced flexion at the lumbar level. As the kidneys ascend, they utilise blood vessels at increasingly more proximal levels until the renal arteries are reached in the lumbar region (8). Following development of the metanephros, the mesonephros

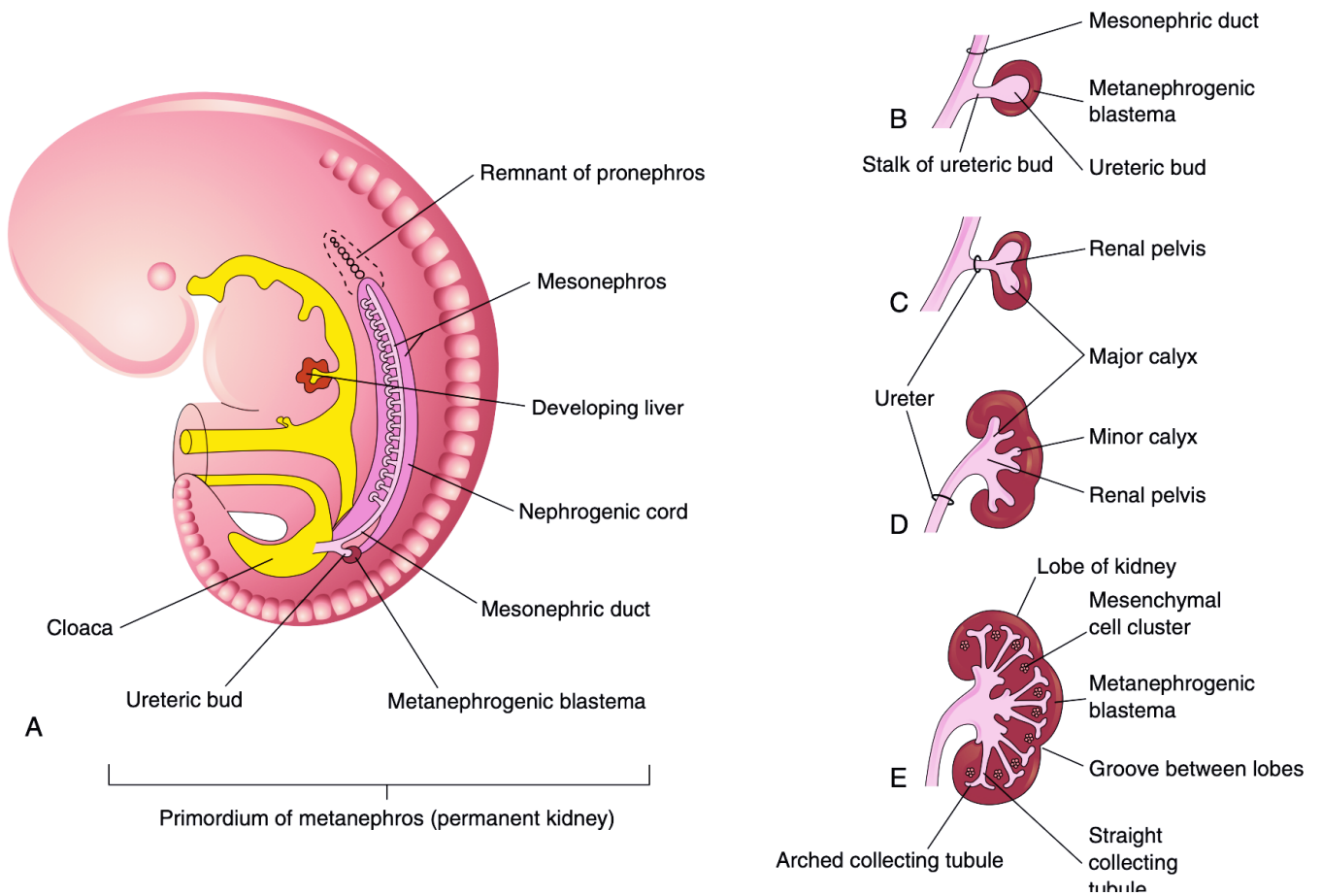


**Figure 1. Embryology of the Human Urinary Tract.**

(A) Lateral orientation 5-week-old embryo. (B-E) Stages of development of the ureteric bud and intermediate mesoderm into the ureter, renal pelvis and kidney that occurs from week 5-8 gestation. Adapted From Moore KL, Presaud TVN, Torchia MG. *The Developing Human: Clinically Oriented Embryology*. 11th ed. Philadelphia, PA, USA: Elsevier; 2019 (9). Re-used with permission.

The urinary bladder and urethra are predominantly derived from the anterior/ventral urogenital sinus, which develops as a result of the cloaca portioning into a dorsal anorectal canal and a ventral urogenital sinus separated by the uro-rectal septum at around 4-6 weeks gestation (Figure 2). The allantois is the canal that drains urine from the foetus and runs with the umbilical cord. This canal closes to form the urachus and subsequently the anatomical median umbilical ligament (6).

The trigone forms as a result of a poorly understood remodelling process whereby the common nephric duct, which is the portion of the mesonephric (Wolffian) ducts distal to the ureteric bud, fuses to the anterior urogenital sinus and migrates distally to open into the pelvic part of the urogenital sinus (precursor to urethra). The distal ureters migrate to open directly into the urogenital sinus (bladder precursor). The region of urinary bladder between the two ureters and the urethra is known as the bladder trigone (10) (Figure 2). Common nephric duct apoptosis is believed to play an important role in this process (11). Based on these embryological descriptions and its unique appearance, the bladder trigone was traditionally believed to be derived from the mesonephric duct (mesodermal in origin) in contrast to the rest of the urinary bladder urothelium which is derived from the urogenital sinus (endodermal in origin). However, cell lineage analysis utilising a mouse reporter line labelling mesonephric duct origin cells has suggested that the common nephric duct does not give rise to the trigone but is removed by apoptosis leading to migration of the ureters to the bladder (11). Tissue recombination experiments investigating mesenchymal-epithelial interactions in urinary bladder tissues have also suggested that the bladder trigone epithelium is endodermal in origin. Following recombination of trigone epithelium with foetal urogenital sinus mesenchymal tissue, prostatic epithelial tissue was induced suggesting bladder trigone tissue is endodermal in origin (12).

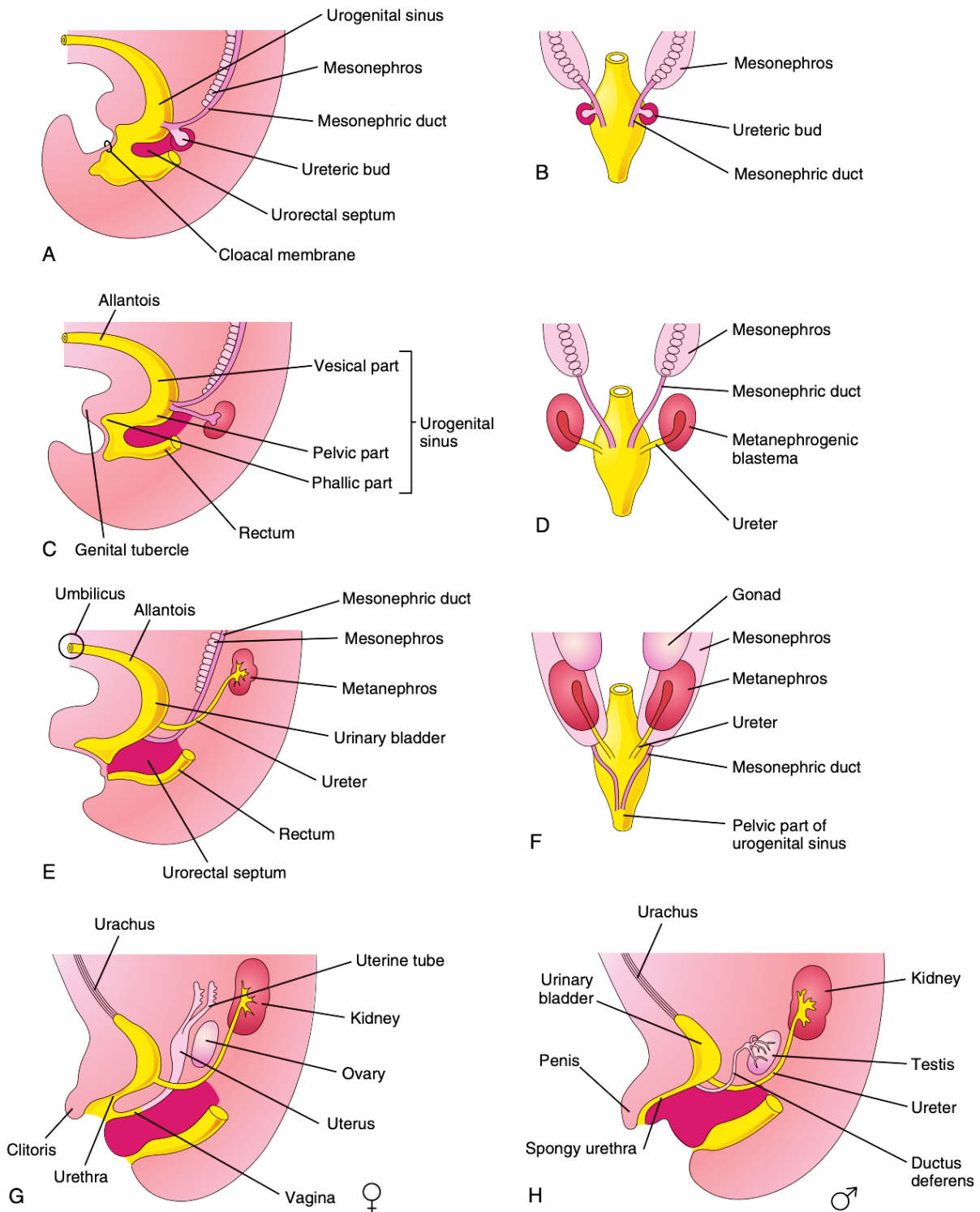


**Figure 2. Embryological Development of the Urinary Bladder and Trigone.**

(A, C, E, G and H) Lateral and (B, D and F) dorsal views of embryo demonstrating urinary bladder and trigone development from 5-weeks to 12-weeks gestation. The trigone is a triangular region within the urinary bladder between the two ureters and the urethra and is best appreciated in figures 2G and 2H. Adapted From Moore KL, Presaud TVN, Torchia MG. *The Developing Human: Clinically Oriented Embryology*. 11th ed. Philadelphia, PA, USA: Elsevier; 2019 (9). Re-used with permission.

Numerous congenital urological conditions develop as a result of abnormal embryological development of the kidneys and ureters (renal agenesis, malrotated kidney, ectopic kidney, horseshoe kidney, ectopic ureter) and bladder (urachal abnormalities [urachal cysts, urachal sinus and urachal fistula] and bladder exstrophy) (13).

#### **1.1.4. Histology**

The mammalian urothelium or transitional epithelium is a multi-layered epithelium lining renal the pelvis, ureter, and urinary bladder. The urothelium is composed of three main cell types: basal, intermediate and superficial. The superficial apical layer of cells are also termed 'umbrella cells.' The umbrella cells have tight junctions and are covered on their apical surface by proteins called uroplakins which form plaques (Figure 3). The urothelium is believed to possess barrier function that is reliant on the tight junctions of the umbrella cells and the uroplakin proteins, which reduce the permeability of the cells to small molecules (14).

The urothelium has one of the slowest growth rates amongst epithelial layers in mammals under normal conditions (15). However, urothelial proliferation increases significantly following injury leading to the development of differentiated superficial cells within two weeks (16). It is believed to be the basal cells that are the progenitor cells that proliferate and differentiate into intermediate and superficial cells following response to injury (17). The urothelium is surrounded by a lamina propria layer which consists of loosely collagenised stroma. The lamina propria, in turn, is surrounded by a muscle layer (Figure 4) (18).

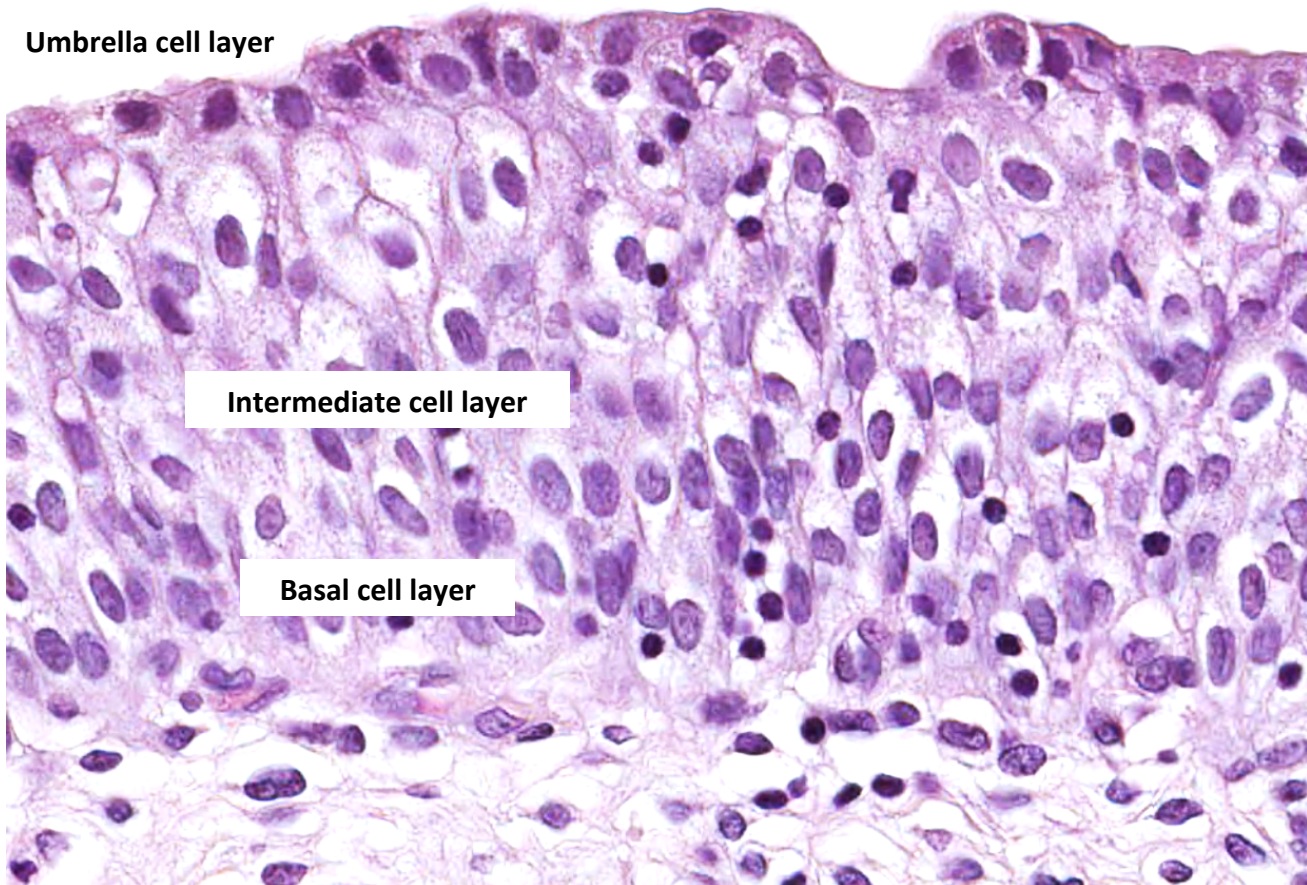


**Figure 3. H&E-Stained Histology Section of Bladder Urothelium.**

Adapted from The Human Protein Atlas Webpage (19). Re-used with permission.

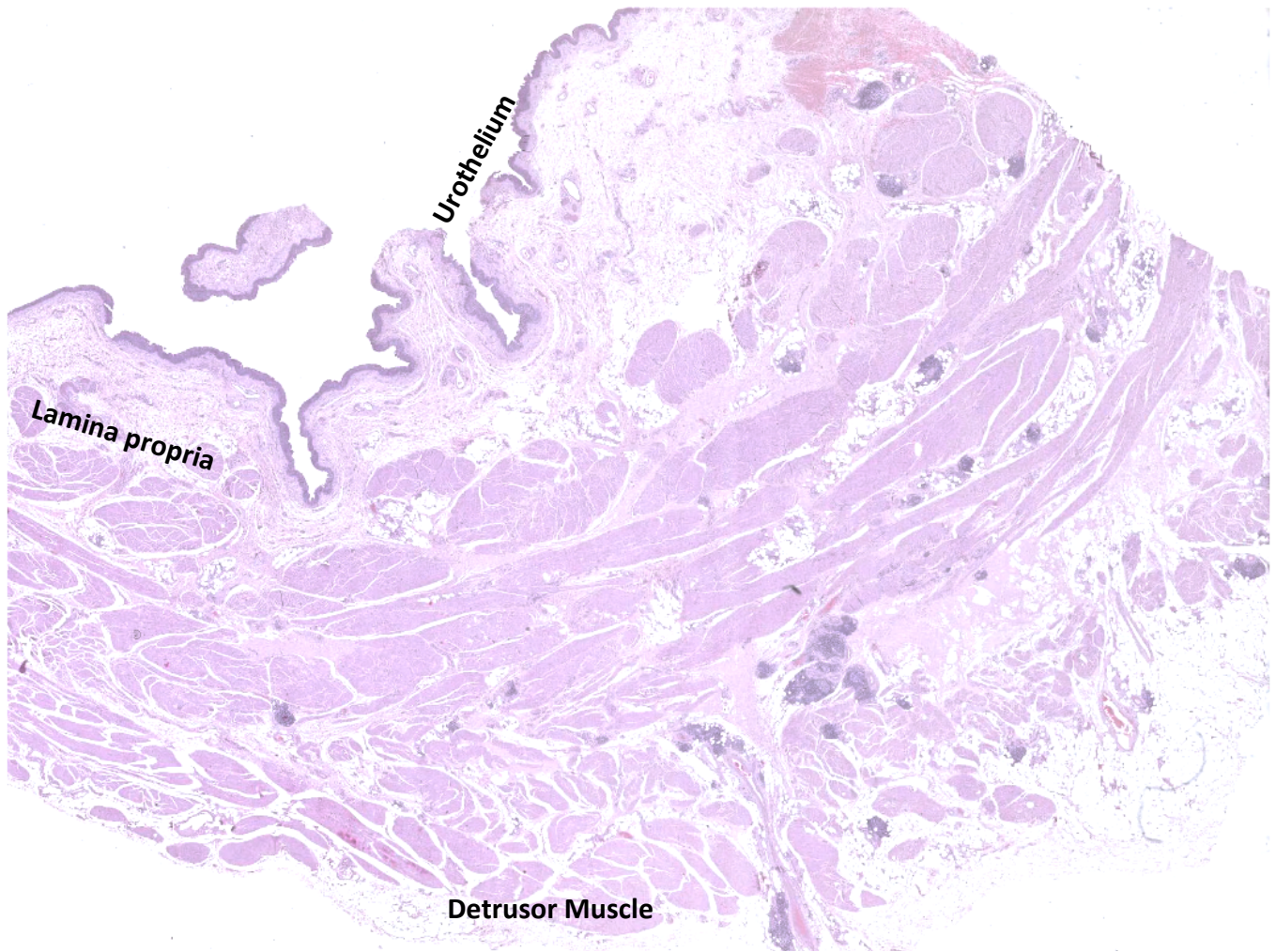


**Figure 4. H&E-Stained Histology Section of Bladder Wall.**

Adapted from The Human Protein Atlas Webpage (19). Re-used with permission.

## **1.2. Zebrafish**

### **1.2.1. Taxonomy**

Zebrafish (*Danio rerio*) are a freshwater fish native to India and South Asia. They derive from the genus, *Danio*, and the family, *Cyprinidae*. They belong to a group called teleosts which account for approximately 96% of all fish species. Teleosts are ray finned fish and are characterised by a mobile maxilla and premaxilla, which enables them to protrude their jaw, and symmetrical tails (20).

### **1.2.2. Life cycle**

The zebrafish life cycle comprises four broad developmental stages: embryonic, larval, juvenile and adult. The life cycle begins with fertilisation. A mating pair of zebrafish (male and female) release sperm and eggs, respectively. The embryonic stage lasts from fertilisation to around 3 days post fertilisation when the embryos hatch from their chorion and become larvae (21). Zebrafish begin to feed independently on day 5 post fertilisation and stop relying on their yolk for nourishment. This is also the point at which they become protected animals under UK Home Office legislation. The larval stage lasts until around 4 weeks post fertilisation when the zebrafish transitions into the juvenile stage. The juvenile stage continues until around 3 months post fertilisation which is the approximate point of sexual maturity (22). The zebrafish lifespan within the laboratory environment is around 30 to 36 months.

## **1.3. The Zebrafish Urinary Tract**

### **1.3.1. Anatomy**

The adult zebrafish urinary tract comprises a retroperitoneal mesonephric kidney which is situated along the dorsal abdominal wall. This kidney can be categorised anatomically into different regions from cranial to caudal: head, trunk and tail and has a characteristic shape and pigmented colouration (Figure 5). Whole mount *in-situ* hybridisation studies in zebrafish support the presence of a functional segmentation pattern in the adult mesonephros with the presence of a glomerulus, proximal convoluted tubule, proximal straight tubule, distal early segment (or tubules) and distal late segment (or tubules) (23, 24). It is difficult to differentiate between proximal and distal tubules with H&E staining. Unlike in mammals, the interstitium of the zebrafish kidney also

contains haematopoietic cells. Haematopoietic tissue is also contained in the stroma of the spleen as zebrafish bones do not have a medullary cavity. Endocrine cells (interrenal and chromaffin cells) are situated in the anterior kidney adjacent to major blood vessels. The interrenal cells are homologous to the adrenal cortex and the chromaffin cells are homologous to the adrenal medulla. Another endocrine tissue located in the zebrafish kidney is the Corpuscle of Stannius which is situated in the caudal aspect of the zebrafish kidney and is involved in calcium homeostasis as well as blood pressure regulation and osmoregulation (24).

Very little is known about the excretory component of the zebrafish urinary tract i.e. distal to the distal late segment of the mesonephros. For example, a comprehensive histological characterisation of the anatomy of zebrafish does not describe the excretory urinary system distal to nephrons responsible for urine transport to the external environment (24). Previous literature has reported that all zebrafish nephrons drain via a common segment, and this has been described as “possibly a collecting duct or ureter to the cloaca.” The majority of literature on zebrafish anatomy reports the absence of a urinary bladder structure in adult zebrafish (25). There is one report of a urinary bladder in adult zebrafish in a textbook but this report is not referenced (26). In this, the structure of the adult zebrafish urinary bladder was described as consistent with that of teleosts in that it is continuous with the collecting ducts. The origin of the urinary bladder is reported to be from the mesonephric ducts and, therefore, mesodermal origin in contrast to the urinary bladder in higher vertebrates which is predominantly endodermal in origin except for the trigone, which has traditionally been believed to be mesodermal in origin. The zebrafish urinary bladder has been described as composed of a mucosa of cuboidal epithelium surrounded by a thin coat of smooth muscle (26). Within this one previous description of a urinary bladder in zebrafish, its function is not elucidated (26). It is important to note that the zebrafish swim bladder structure is not linked in any way the urinary bladder. The swim bladder is a two chambered organ filled with air that maintains balance and controls buoyancy (27).

In freshwater rainbow trout, another teleost, the urinary bladder has been reported to hold urine for approximately 30 minutes prior to releasing urine in bursts and likely always retains a small residual volume. This is thought to be advantageous in avoiding olfactory signals to potential predators. During the urine storage period, the bladder actively reabsorbs sodium and chloride aiding the function of the kidney in salt conservation (28). The teleost urinary bladder has therefore been described as a ‘morphological extension of the kidney’ (29). Furthermore, the

urinary bladder has been utilised as a model for kidney tubular function in fish (29). The urinary bladder in teleosts, therefore, is likely to have a hybrid function as having both storage and emptying function in addition to tubular function.

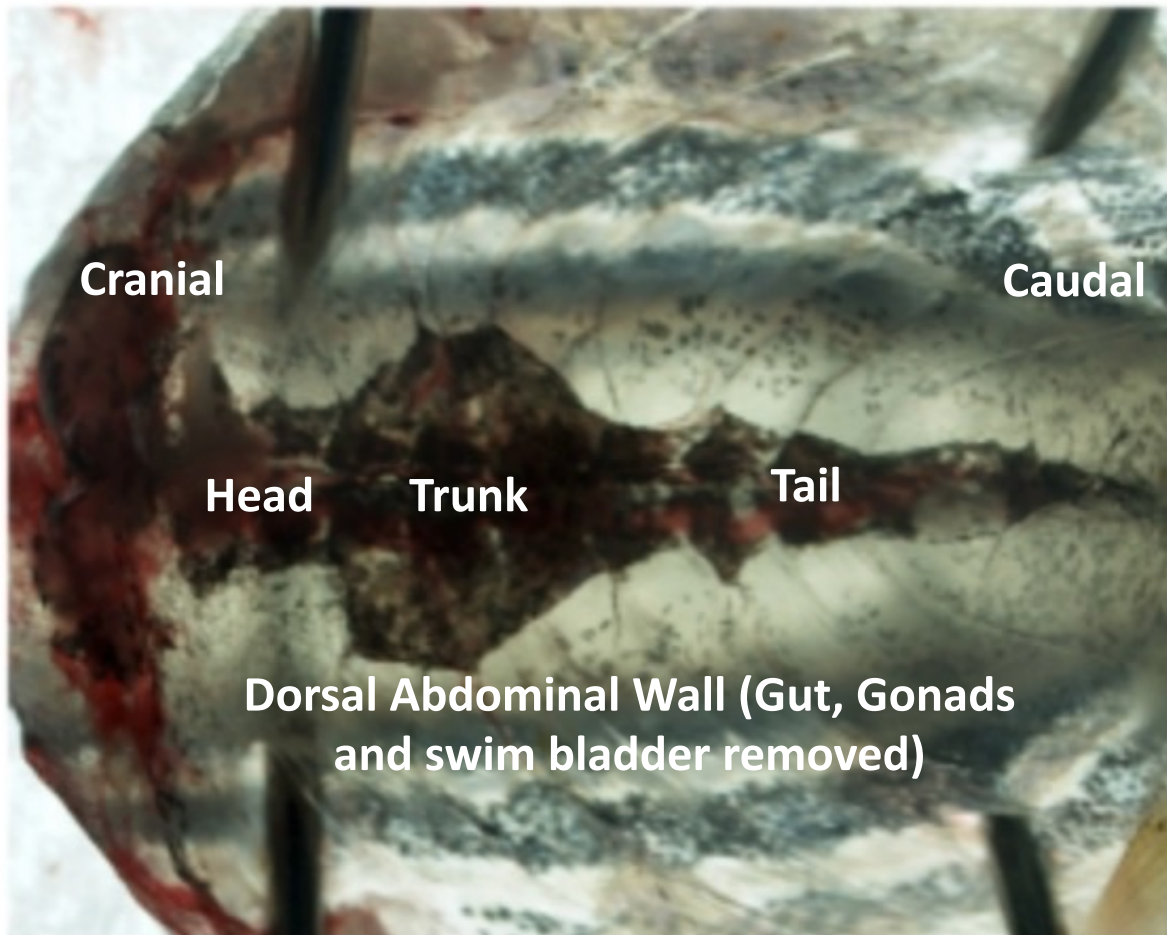


**Figure 5. Adult Zebrafish Kidney Exposed Along Dorsal Abdominal Wall.**

Internal surface of dorsal abdominal wall shown. Anterior abdominal wall has been opened and internal organs (gut, gonads and swim bladders have been removed to expose the urinary tract). Figure adapted from Gerlach et al 2011 (30). Image re-used with permission.

### 1.3.2. Embryology

In contrast to the mammalian kidney, which develops the pronephros, mesonephros, and metanephros, only the pronephric and mesonephric kidneys develop in the zebrafish. The zebrafish pronephros, in contrast to its mammalian counterpart, is fully functional and has a key role in osmoregulation (31).

Structurally the pronephros is comprised of two nephrons with glomeruli that are fused in the midline anteriorly. Two pronephric tubules join the glomerulus to the pronephric ducts, which course posteriorly and in the midline prior to their contact with the cloaca (31). Like in mammalian kidneys, the glomeruli are involved in blood filtration, and the pronephric tubules have roles in osmoregulatory function and solute secretion and reabsorption (32).

The pronephros originates from the intermediate mesoderm on either side of the midline. The most anterior cells develop podocytes that migrate to the centre and recruit endothelial cells to form the glomerulus. The remaining intermediate mesoderm undergoes a mesenchymal-to-epithelial transition (MET) to form a tubular epithelium that fuses with the cloaca, a common exit passage for waste substances from the intestines and pronephros (33).

Cells contributing to the cloaca and distal pronephros arise from the ventral mesoderm. At around 24 hours post-fertilisation, the pronephros tubular cells migrate ventrally towards the ectodermal cells of the cloaca. Between 24 hours and 30 hours post-fertilisation, the pronephros joins the cloaca which, in turn, opens to the environment. This process is dependent on Bone Morphogenetic Protein (BMP) signalling (34) and the nephrocystin 4 (*nphp4*) gene (35).

Gene expression analysis has demonstrated the zebrafish pronephros has multiple discrete domains: two proximal tube segments (proximal convoluted and proximal straight [PCT and PST]), two distal tube segments (Distal early and Distal late [DE and DL]), and a pronephric duct (Figure 6) (36). The gene expression patterns are analogous to those in the mammalian kidneys (36). In particular, the expression of solute transporters and renal transcription factors is highly conserved. The zebrafish PCT and PST express solute transporter genes found in the proximal tubules of mammals such as *slc9a3* and *slc4a4*. The zebrafish DE segment expresses *slc12a1*, which is a marker of the ascending limb of the loop of Henle in the mammalian kidney and the DL segment expresses *slc12a3*, which is a marker of the distal convoluted tubule in the mammalian kidney (36).

The zebrafish DL segment has been described as a distal tubule/nephric duct hybrid segment. It has been shown to express genes that are expressed in kidney tubules such as *slc12a3* and *clcnk*. The segment also expresses genes that are expressed in the mammalian nephric duct: *ret1*, *gata3*, and *emx1* (36-38). The posterior tip of the DL segment also migrates distally and fuses to the

cloaca, which is typical mammalian nephric duct behaviour. It is, therefore, likely that the pronephric DL segment is a distal tubule and nephric duct hybrid (32).

The pronephric duct expresses *gata3*, which is not present in the proximal pronephric segments, nor is it present in the mesonephric nephrons. The *gata3* expression has been demonstrated using whole mount *in situ* hybridisation (ISH) of larvae in the terminal segment of the pronephros but not seen in the mesonephric nephrons (23, 36).

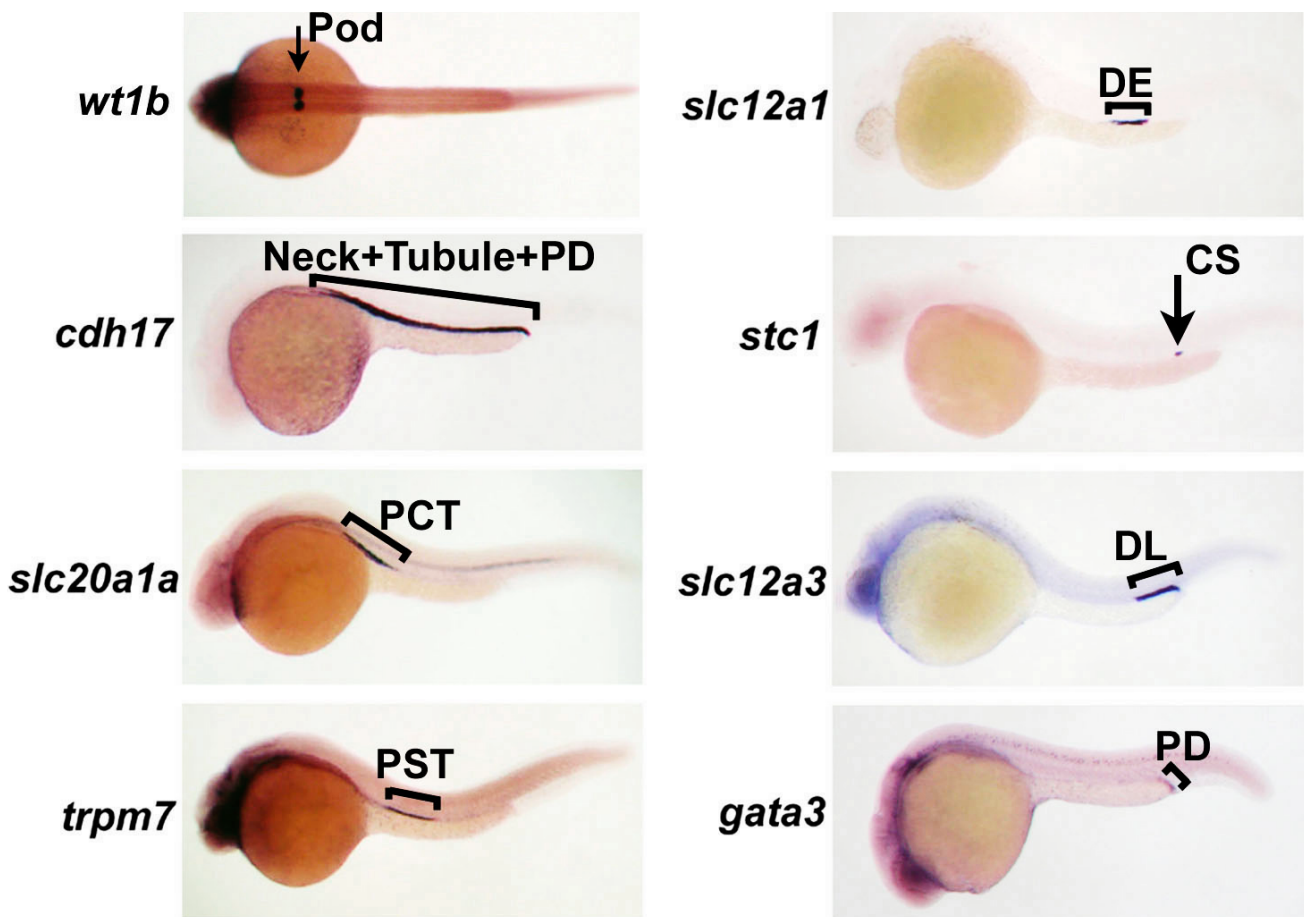


**Figure 6. Zebrafish Embryo Pronephros Segmentation.**

Whole mount *in situ* hybridisation of zebrafish embryos demonstrating pronephros segmentation. Pod: Podocytes, PCT: proximal convoluted tubule, PST: proximal straight tubule, DE: distal early, CS: corpuscle of Stannius, DL: distal late, PD: pronephric duct. Adapted from Wingert et al 2007 (36). Re-used with permission.

Pronephros development and the segmentation pattern during pronephros development is believed to be driven by retinoic acid signalling by inducing proximal pronephros segments and restricting the development of distal segment fates. Caudal transcription factors, which include *cdx1a* and *cdx4*, are believed to play a role in the anteroposterior position of the pronephros progenitors by regulating the site of retinoic acid production (36).

The mesonephros develops at around ten days post-fertilisation during the transition from larva to juvenile. This development is thought to occur due to higher osmoregulatory demands secondary to increased size (23). The first mesonephric nephrons form on top of the pronephric DE segment and become functional by the 6mm stage based on a study utilising filtration of a fluorescent tracer (23). Further mesonephric nephrons develop in this region during the juvenile period from caudal to cranial. These nephrons are believed to arise from *wt1b* expressing basophilic progenitor cells using an MET process (23, 39). This is believed to be dependent on the *wnt9a* gene, which is expressed in the distal pronephros segments though the existence of a functioning Wingless-related integration site (WNT) signal is not yet known (40). This theory is based on the reciprocal induction occurring in mammals that involves a similar MET process that relies on *WNT9b* expression from the ureter (41).

The pronephros becomes a scaffold for mesonephros formation. The mesonephric nephrons that develop on the DE segment of the pronephros initially only develop PCT, PST, and DE segments and use the mesonephric DE segment to fuse to the pronephric DE segment (Figure 7) (23). The pronephric DE and DL segments, which drain caudally to the pronephric duct, are all believed to be precursors to the collecting duct/ureter segments in the adult urinary tract (23, 39).

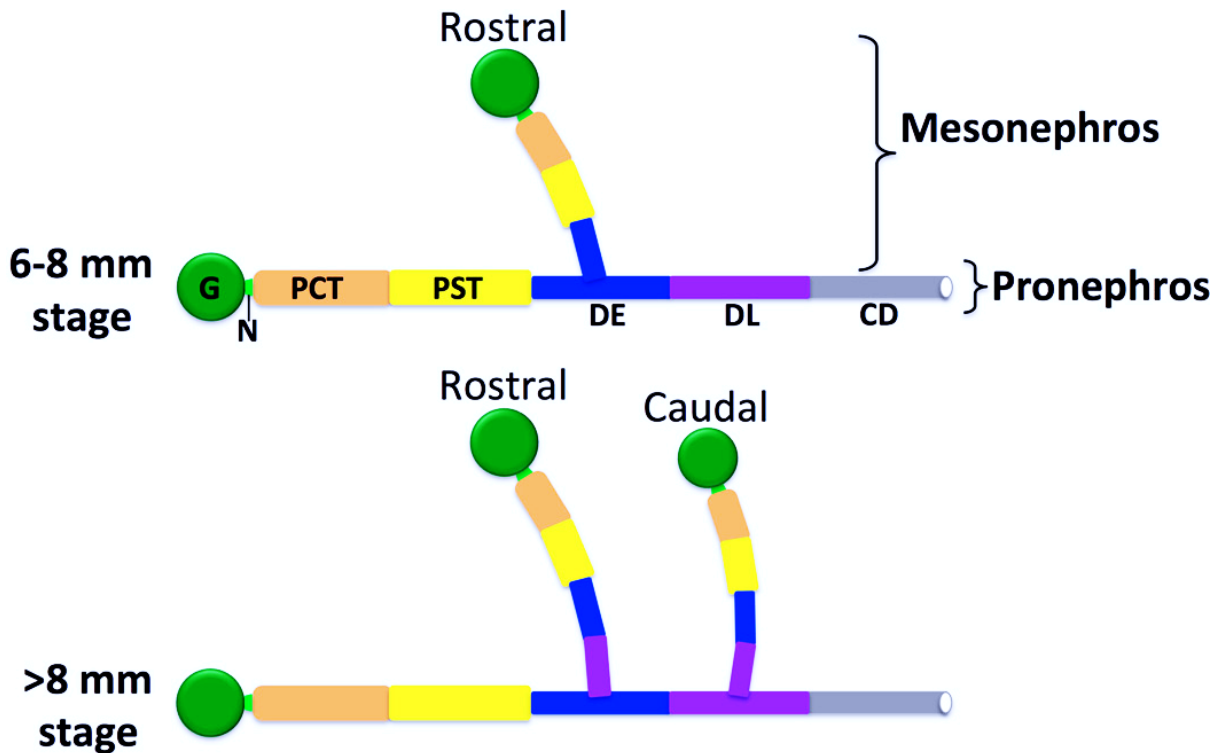


**Figure 7. Schematic of Zebrafish Mesonephrogenesis.**

Mesonephric nephrons develop and fuse to the existing pronephric distal early (DE) and distal late (DL) tubule segments which drain via the collecting duct (CD) or ureter segment. Adapted from Diep et al 2015 (23). Re-used with permission.

### 1.3.3. Homology to Mammalian Urinary Tract

#### 1.3.3.1. Uroplakins in Zebrafish

The zebrafish pronephric tubules and ducts have been shown to express uroplakin proteins, which are characteristic of mammalian urothelium and are believed to have a key role in barrier function (42, 43). Uroplakin-3a like protein called Upk31 is expressed on the luminal surface of the pronephric tubules and ducts, and *upk31* morpholinos lead to embryos with reduced pronephros function believed to be due to their effects on pronephric tubule epithelial cell development and polarisation (42).

#### 1.3.3.2. Zebrafish Models of Lower Urinary Tract Dysfunction

Congenital lower urinary tract obstruction has been modelled in the zebrafish pronephric duct. Causes of congenital anatomical lower urinary tract obstruction in humans include posterior urethral valves in males (at the level of the prostatic urethra) and anterior urethral valves, also known as urethral atresia, in both sexes. Exome sequencing of human patients with congenital lower urinary tract obstruction identified a nonsense variant in the *BNC2* gene which is expressed

in human urothelial cells. The *bcn2* gene is also expressed in the pronephric duct of zebrafish. Knockdown of *bcn2* in zebrafish causes a lower urinary tract obstruction phenotype manifesting as pronephric duct obstruction and dilatation of the cloaca (44).

Human bladder exstrophy, which is a rare congenital malformation of the anterior abdominal wall and urinary bladder, has been modelled in zebrafish. Bladder exstrophy has been linked to the *WNT* gene family. Knockdown of *wnt3* in zebrafish leads to cloacal abnormalities that include expansion of the cloacal lumen as well as possible rupture of the cloaca (25). This is supportive of homology between the zebrafish and human urinary lower urinary tract.

## **1.4. Cancer**

### **1.4.1. Overview**

The definition of cancer has evolved over time. The defining feature of cancer, according to the World Health Organisation (WHO) is “the rapid creation of abnormal cells that grow beyond their usual boundaries and which then invade adjoining parts of the body and spread to other organs” (45).

Cancer incidence and mortality is increasing globally reflecting ageing populations, population growth, evolving exposures to risk factors which, in many cases, is linked to industrialisation and socioeconomic development (46). In both sexes combined, the highest cancer incidences worldwide occur in female breast, lung, prostate, nonmelanoma skin cancer, and colon (46).

The traditional model of cancer development was based on accumulation of mutations secondary to environmental carcinogens which activate various signalling pathways and, in turn, drive cancer progression. However, this traditional model has increasingly been replaced by the notion that environmental carcinogens can promote cancer formation in cells that have pre-existing oncogenic mutations through inflammation and tissue damage. These oncogenic mutations can arise from normal endogenous processes in tissues. This notion was driven in part by recent data from mouse cancers suggests that some carcinogens do not induce mutations, with mutations arising from endogenous processes in tissues (47). Furthermore, cancer associated mutations can accumulate in normal human tissues during ageing without causing cancer until a separate process drives

cancer formation (48). It is important to note, however, that this is contrary to the established model of cancer development.

A recent study using both mouse models of lung cancer and 3D cell culture tested the hypothesis that air pollution can initiate cancer in healthy lung cells with pre-existing mutations. Mice with oncogenic *Egfr* or *Kras* mutations develop faster growing lung cancers within weeks of exposure to air pollution compared to mice without these mutations. Furthermore, DNA sequencing data from normal healthy lung tissue in individuals with cancer demonstrated mutations in *Egfr* or *Kras* genes suggesting that a further tumour promoting process is required. This study also demonstrated increased expression of interleukin 1-beta in air pollution induced lung cancer in mice suggesting that air pollution can result in macrophage infiltration into the lungs which, in turn, can release interleukin 1-beta and drive inflammation which can promote cancer formation (49).

#### **1.4.2. Hallmarks of Cancer**

Hanahan and Weinberg in 2000 (50) and 2011 (51) proposed six hallmarks of cancer to explain the processes involved in cancer development and progression i.e. important capabilities acquired by normal human cells transforming into cancers that are necessary for the development of cancer (Figure 8). These are: proliferation, evasion of growth suppression, activation of invasion and metastasis, enablement of replicative immortality, induction of angiogenesis and resisting cell death which are all linked to genome instability.

A key development described in subsequent reviews (51, 52) is the addition of two more hallmarks: altering energy metabolism (or reprogramming cellular metabolism) and evasion of immune destruction. In addition, cancer enabling characteristics were described: genomic instability and tumour promoting inflammation. These hallmarks are relevant in all cancers, but differences exist in how and to what degree different cancers demonstrate these features. The most recent review by Hanahan et al (52) also described four emerging hallmarks and enabling characteristics: unlocking phenotypic plasticity, non-mutational epigenetic reprogramming, polymorphic microbiomes and cellular senescence.

Unlocking phenotypic plasticity is a capability that allows disruption of cellular differentiation through either cellular dedifferentiation, blocked cellular differentiation or trans-differentiation (change from one differentiated cell type to another) to drive uncontrolled proliferation and cancer. Non-mutation epigenetic reprogramming is the notion that change in gene expression can result from epigenetic factors/changes such as chromatin modification in the absence of mutations and can contribute to cancer development. Polymorphic microbiomes are a concept that variability in the microbiome in different tissues can modulate cancer hallmark capabilities through mutagenesis, DNA damage, disruption of DNA repair and many other mechanisms. Cellular senescence, although traditionally believed to be only a protective mechanism against cancer, can also drive carcinogenesis through activation of a senescence-associated secretory phenotype (SASP) which can, through signalling molecules signal to other cells to utilise cancer hallmark capabilities (52).

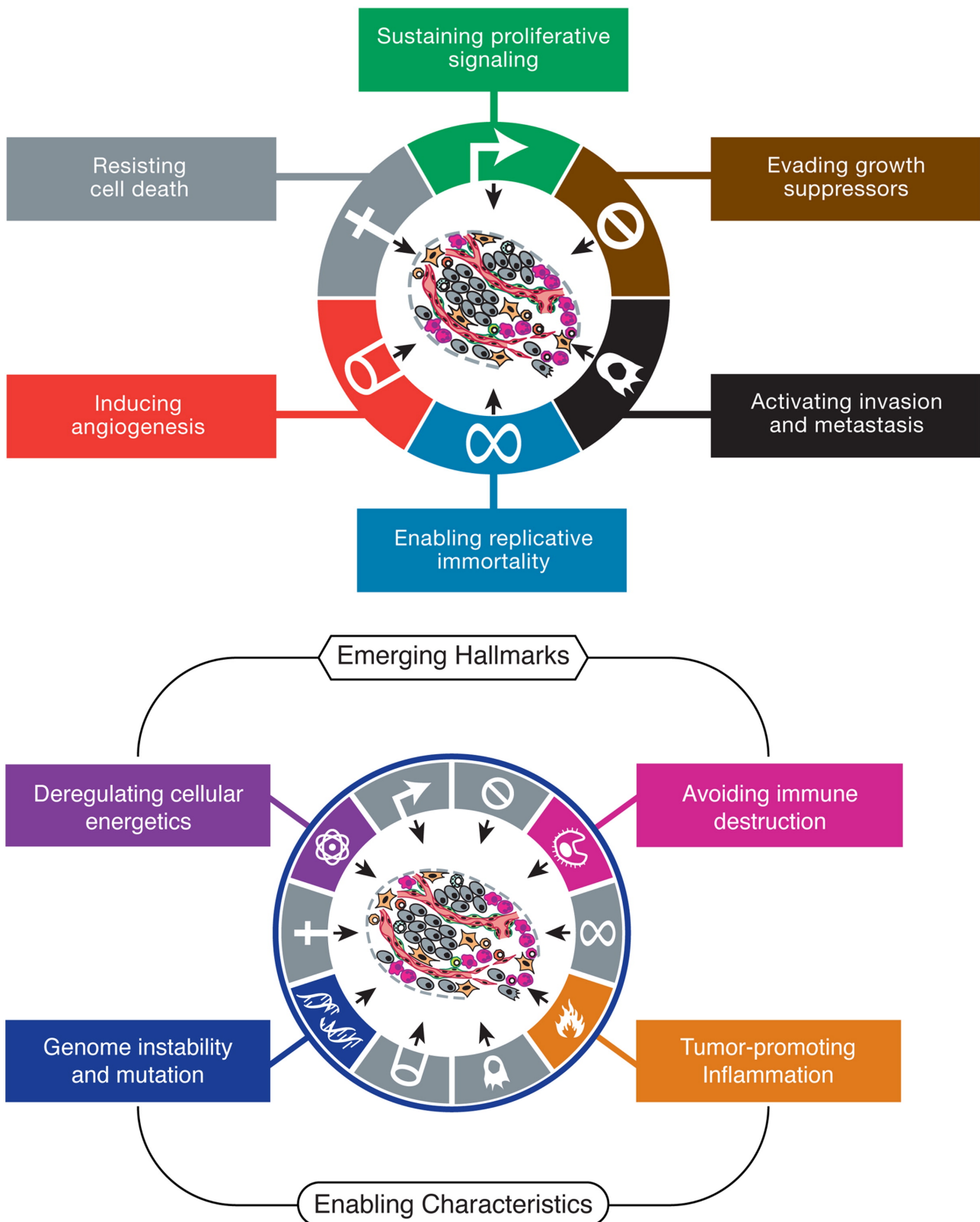


**Figure 8. The Hallmarks of Cancer.**  
Adapted from Hanahan et al 2011(51). Re-used with permission.

### 1.4.3. Aetiology and Molecular Biology

Cancer is caused by both intrinsic risk factors and non-intrinsic risk factors. Intrinsic risk factors are inevitable spontaneous genetic mutations due to random error in DNA replication and these are

non-modifiable. Non-intrinsic risk factors include external factors such as carcinogens, viruses and lifestyle factors (e.g. smoking, diet, physical activity) which are modifiable. Non-intrinsic risk factors also include endogenous risk factors which are related to individual characteristics e.g. biological ageing, inflammation, hormones and genetic susceptibility. For some cancers, there have been clear associations made with specific environmental factors and as a result, successful cancer prevention. Examples of these clear associations include tobacco smoking and lung cancer, sun/ultraviolet light exposure and skin cancer, human papilloma Virus (HPV) and cervical cancer, *Helicobacter pylori* (*H. pylori*) and gastric cancer and viral hepatitis infection and hepatocellular cancer (53). Intrinsic and non-intrinsic risk factors can interact and the degree to which one or the other will contribute to a specific cancer is likely to vary in different cancer types and different individuals (53). Therefore, it is likely that cancer risk is still modifiable in the presence of an intrinsic mechanism (53).

Hereditary cancer can occur via intrinsic and non-intrinsic mechanisms (53). It is estimated that intrinsic mechanisms account for approximately 10-30% of overall cancer incidence (53). Significant heritability has been reported in prostate cancer (42%), colorectal cancer (35%) and breast cancer (27%) (54). Similarly, a study of over 80,000 monozygotic twins and over 120,000 same-sex dizygotic twins reported 33% excess familial risk for all cancer and that almost 60% of prostate cancer was believed to be linked to genetic factors (55). Many heritable cancer mutations and germline cancer syndromes involve genes involved in DNA repair which can increase mutation rates. Alternatively, heritable cancer mutations and germline cancer syndromes may be linked to genetic alterations that lead to greater susceptibility to non-intrinsic risk factors (53).

### **1.5. Urinary Tract Cancer Overview**

Urinary tract cancers (excluding prostate cancer) include cancers of the kidneys, ureters, bladder and urethra. These cancers are common and associated with substantial morbidity and mortality worldwide (56-58). The most common of these cancers overall are urothelial carcinomas which arise from the specialised epithelium (termed the urothelium) lining the urinary tract from the renal pelvis down to the urethra but most commonly affect the bladder (approx. 90-95% of all urothelial carcinomas) (59). Renal cell carcinoma, an adenocarcinoma, accounts for approximately 90% of kidney cancers and arises from renal tubular epithelial cells (60) and will be discussed later in the introduction.

## **1.6. Bladder Cancer**

### **1.6.1. Epidemiology**

Bladder cancer (BC) is the 7<sup>th</sup> commonest cancer worldwide in men and 9<sup>th</sup> when all genders are considered. There were an estimated 430 000 new BC cases and 165 000 deaths from BC worldwide in 2012, and three-quarters of new cases were in men. Male: female ratios range from 6:1 to 2:1 in different regions across the world (56). In contrast, female patients have a worse prognosis than male patients (61). The incidence of BC increases in older age groups, with incidences rising sharply above the age of 50. There is a high overall prevalence with over 1.3 million cases over a five-year period worldwide (56). Incidence and mortality rates (adjusted for age) differ widely across different geographical regions. The highest rates are observed in North America and Europe whilst the lowest are seen in Central America, West Africa, and Asia (56, 62). The geographic differences may reflect variations in smoking prevalence and occupational exposures (56).

### **1.6.2. Aetiology and Risk Factors**

The strongest modifiable risk factor for BC is smoking. Smoking carries an attributable risk of 50% (56, 63). Tobacco smoke contains known carcinogens, including, polyaromatic hydrocarbons, aromatic amines and N-nitroso compounds which cause DNA damage (64, 65). The pooled relative risk (RR) for current smokers versus never smokers in BC was 3.47 (95 CI 3.07 -3.91) in a meta-analysis comprising 83 studies (63). With regards to tobacco type, there was no statistically significant difference in BC risk between black and blond tobacco use in a French case control study (66), nor was there a difference in BC risk between plain and filter cigarette use in a Canadian case control study (67).

Occupational exposures are the second commonest risk factor for BC. Around 10% of BCs occur following occupational exposures (68). Potential occupational carcinogens include 2-naphthylamine, 4-aminobiphenyl, toluene, 4,4'-methylenebis (2-chloroaniline), diesel exhausts, polyaromatic hydrocarbons (PAH), and metalworking fluids (69). Other modifiable risk factors include arsenic in drinking water, chlorination of drinking water, use of pioglitazone, cyclophosphamide, and pelvic radiotherapy (56).

Genetic risk factors include inherited polymorphisms in genes encoding carcinogen detoxification enzymes N-acetyltransferase 2 (NAT-2) and Glutathione S-transferase (GSTM1). NAT-2 regulates the detoxification of aromatic amines (established carcinogens) through acetylation. Genetic carriers of the slow variant polymorphism have an increased risk of BC. Glutathione S-transferase detoxifies polyaromatic hydrocarbons. Homozygous deletion of the *GSTM1* gene carries an increased risk of BC (70). Gene polymorphisms in these genes, therefore, play a key role in individuals with occupational or environmental carcinogen exposures.

Genome-wide association studies (GWAS) demonstrate multiple genetic loci that harbour variants associated with BC including: 1p13.3 (*GSTM1*), 2q37.1 (*UGT1A*), 3q26.2 (*TERC*), 3q28 (*TP63*), 4p16.3 (*TACC3-FGFR3*), 5p15.33 (*TERT-CLPTM1L*), 8p22 (*NAT2*), 8q24.21 (*MYC*), 8q24.3 (*PSCA*), 11p15.5 (*LSP1*), 13q34, (*MCF2L*), 15q24 (*CYP1A2*), 18q12.3 (*SLC14A1*), 19q12 (*CCNE1*), 20p12.2 (*JAG1*) and 22q13.1 (*CBX6*, *APOBEC3A*) (71). These genes have a range of functions including carcinogen detoxification genes (*GSTM1* and *NAT2*) which encode carcinogen detoxification enzymes Glutathione S-transferase M1 and N-acetyl transferase 2, telomerase components (*TERC* and *TERT*), transcription factors (*TP63*, *MYC*), receptor tyrosine kinase (*FGFR3*), Cell cycle control (*CCNE1*) (72), cytidine deaminase (*APOBEC*) (73), solute transport (*SLC14A1*) (74), metabolic processes (*UGT1A* (75), *CYP1A2* (76)) and Notch signalling (*JAG1*) (77). These susceptibility loci were estimated to contribute 12% of the familial risk of BC (71).

A recent up-to-date meta-analysis of 32 BC GWASs including over 13,700 BC cases and over 343,000 controls of European ancestry revealed several novel BC susceptibility loci: 6p.22.3 (*CDKAL1*), 6p.22.3 (*CASC15*), 7q36.3 (*LOC389602*), 8q21.13 (*PAG1*), 9p21.3 (*MTAP/CDKN2A*), 9q31.1 (*SMC2*) 10q22.1 (*COL13A1*), 19q13.33 (*SULT2B1-FAM83E*). These are involved in tumour suppression and cell cycle regulation (*CDKN2A*) (78), polyamine metabolism (*MTAP*) (79), intermediary in EGFR/RAS signalling (*FAM83E*) (80). The function of some of these genes (*CDKAL1*, *CASC15*, *PAG1*, *COL13A1*, *SULT2B1*, *SMC2*) and their potential mechanistic link to BC is poorly understood.

Chronic inflammation is also linked to BC, particularly the squamous cell subtype (81). Causes of chronic bladder inflammation include urinary tract infection and chronic bladder mucosa irritation such as long term catheterisation. It is also believed that the early cancer changes can lead to a chronic inflammatory microenvironment which can, in turn, drive many hallmarks of cancer which

include proliferation, angiogenesis and invasion. The chronic inflammatory microenvironment includes cells that promote inflammation such as macrophages and myeloid derived suppressors cells, amongst others (81). Tumour associated macrophages (TAMs) are grouped according to their polarisation states into M1 and M2, with M2 receptors believed to promote carcinogenesis. A high TAM density in BC samples is associated with a poor prognosis (82). Furthermore, high counts of CD163 positive (M2-polarized specific cell surface receptor) macrophages in the stroma of BC samples is linked with failure of an established bladder cancer treatment, intravesical bacille Calmette-Guerin (BCG) (83). Both of these studies however had small patient numbers.

An in-depth up to date systematic review of the epidemiology and risk factors for BC is presented in Chapter 3.

### **1.6.3. Pathology**

Urothelial Cell Carcinomas (UCC), previously referred to as Transitional Cell Carcinoma (TCC), represent the majority of BCs (>90%). Less common BC histological subtypes include squamous cell carcinoma (SCC) and adenocarcinoma (84).

Grading of urothelial carcinoma is based on the extent of preservation of architecture of the urothelial cell layer and nuclear atypia (abnormal appearance of nuclei). High grade carcinoma is characterised by several nuclear abnormalities: nuclear enlargement, nuclear pleomorphism, prominent nucleoli. High grade features also include prominent mitotic activity in the upper urothelial layers, absent umbrella cell layer, disordered cell layering and variability in polarity (85).

Urothelial neoplasms can have papillary or non-papillary morphology. Papillary carcinomas are exophytic with papillae that contain central fibrovascular cores and covered by neoplastic epithelium. In low grade papillary carcinoma of the urothelium, there is minimal fusing of the papillae and a small degree of abnormalities of the urothelial cells/nuclei. There may be occasional mitosis, but this is limited to the basal urothelial layer and there is often minimal variation in nuclear size. High grade papillary carcinoma is characterised by a greater degree of abnormalities of the urothelial cells/nuclei including fusing of papillae, nuclear atypia, frequent mitosis and nuclear pleomorphism. Non-papillary urothelial carcinomas can be flat non-invasive lesions (e.g. carcinoma in situ) or invasive lesions. Urothelial carcinoma in situ is a flat lesion whereby the urothelial cell layer is replaced by cells that demonstrate cytological atypia. There is often nuclear

pleomorphism, enlarged and irregular hyperchromatic nuclei, high nuclear-to-cytoplasmic ratio and mitotic figures (86).

There are various histological classifications reported for BC, but the clinical outcome and treatment is primarily determined by invasiveness. The invasiveness of BC is determined by the presence or absence of underlying detrusor muscle invasion. Non-muscle invasive bladder cancer (NMIBC) represents approximately 80% of cases, and muscle-invasive bladder cancer (MIBC), represents approximately 20% of cases. The cancer stage correlates with prognosis and informs treatment options (87). The TNM (tumour, node, metastasis) classification system is used to formally stage BC according to the local tumour stage, the presence and extent of lymph node metastases, and the presence and extent of distant metastases (Table 1) (88).

<b>T - Primary Tumour</b>		
Tx	Primary tumour cannot be assessed	
T0	No evidence of primary tumour	
Ta	Non-invasive papillary carcinoma	
Tis	Carcinoma in situ: "flat tumour"	
T1	Tumour invades subepithelial connective tissue	
T2	Tumour invades muscle	
	T2a	Tumour invades superficial muscle (inner half)
	T2b	Tumour invades deep muscle (outer half)
T3	Tumour invades perivesical tissue:	
	T3a	Microscopically
	T3b	Macroscopically (extravesical mass)
T4	Tumour invades any of the following: prostate stroma, seminal vesicles, uterus, vagina, pelvic wall, abdominal wall	
	T4a	Tumour invades prostate stroma, seminal vesicles, uterus, or vagina
	T4b	Tumour invades pelvic wall or abdominal wall
<b>N - Regional Lymph Nodes</b>		
Nx	Regional lymph nodes cannot be assessed	
N0	No regional lymph node metastasis	
N1	Metastasis in a single lymph node in the true pelvis (hypogastric, obturator, external iliac, or presacral)	
N2	Metastasis in multiple regional lymph nodes in the true pelvis (hypogastric, obturator, external iliac, or presacral)	
N3	Metastasis in a common iliac lymph node(s)	
<b>M - Distant Metastasis</b>		
M0	No distant metastasis	
	M1a	Non-regional lymph nodes
	M1b	Other distant metastasis

**Table 1. TNM classification for Bladder Cancer.**

Another histological feature which has important implications for prognosis is the presence of histological variants of urothelial carcinoma. These are cancers which are predominantly urothelial in nature with components of the cancer that are not urothelial. These may be associated with a worse prognosis, although data conflict. The most common variants are squamous, sarcomatoid and micropapillary. In the squamous variant, there is evidence of squamous production such as intracellular keratin. The sarcomatoid variant has histological features resembling a sarcoma. The micropapillary variant often has small papillary clusters of neoplastic cells within lacunae and there is an absence of fibrovascular cores.

Immunohistochemistry plays a key role in the diagnosis of these histological variants (86).

Immunohistochemical markers can be used to aid the diagnosis of urothelial carcinoma in more complex clinical scenarios where there is diagnostic uncertainty e.g. differentiating between urothelial carcinoma and secondary malignancies in the urinary tract and in identifying the origin of a metastatic lesion of unknown primary. Immunohistochemical markers used in clinical practice to this end include GATA3 and Uroplakin-2 (89, 90).

#### **1.6.4. Natural History**

For consistency, there is a standard terminology used to describe the natural history of urothelial cell carcinoma: 'recurrence' and 'progression'. In NMIBC, 'recurrence' is the subsequent diagnosis of a NMI urothelial cell carcinoma of the bladder the same stage (or less) as a previous NMI urothelial cell carcinoma of the bladder. Progression in NMIBC is the subsequent diagnosis of a BC of a more advanced stage (91).

NMIBCs have a high recurrence rate (31-78% at 5 years) but have a lower likelihood of progression to muscle invasion (0.8-45% at 5 years). The European Organisation for Research and Treatment of Cancer (EORTC) put together a scoring system from seven trials performed in NMIBC. The calculated score then corresponds to risks of recurrence and progression at one and five years. Recurrence and progression to muscle invasion are dependent on number of tumours, tumour size, previous recurrences, whether the tumour has invaded the lamina propria layer, presence of carcinoma in situ, and the histological grade of the tumour. Previous disease recurrence and number of tumours are the most heavily weighted risk factors with respect to determining risk of

future recurrence. In contrast, disease stage and grade are the most heavily weighted risk factors with respect to determining risk of future disease progression (Tables 2 and 3) (92).

Risk Factor	Recurrence	Progression
<b>Number of tumours</b>		
Single	0	0
2 to 7	3	3
≥8	6	3
<b>Tumour size</b>		
<3 cm	0	0
≥3 cm	3	3
<b>Prior recurrence rate</b>		
Primary	0	0
≤1 rec/yr	2	2
>1 rec/yr	4	2
<b>T category</b>		
Ta	0	0
T1	1	4
<b>CIS</b>		
No	0	0
Yes	1	6
<b>Grade</b>		
G1	0	0
G2	1	0
G3	2	5
<b>Total score</b>	0–17	0–23

**Table 2. EORTC Scoring System to Determine Risk of Recurrence and Progression of Bladder Cancer.**

Recurrence score	% Probability of Recurrence at 1 year (95% CI)	% Probability of Recurrence at 5 years (95% CI)
0	15% (10%, 19%)	31% (24%, 37%)
1–4	24% (21%, 26%)	46% (42%, 49%)
5–9	38% (35%, 41%)	62% (58%, 65%)
10–17	61% (55%, 67%)	78% (73%, 84%)

Progression score	% Probability of progression at 1 year (95% CI)	% Probability of progression at 5 years (95% CI)
0	0.2% (0%, 0.7%)	0.8% (0%, 1.7%)
2–6	1.0% (.4%, 1.6%)	6% (5%, 8%)
7–13	5% (4%, 7%)	17% (14%, 20%)
14–23	17% (10%, 24%)	45% (35%, 55%)

**Table 3. Probabilities of Bladder cancer Recurrence and Progression After 1 and 5 years Respectively Based on EORTC Scores**

MIBCs have a poor prognosis with a 5-year survival of 55% for primary MIBC (no history of previous superficial BC) and 28% for progressive MIBC (history of superficial BC) (93). Survival largely depends on pathological stage, lymph node metastases and lymphovascular invasion. The 5- year survival following first line platinum based chemotherapy treatment (gemcitabine and cisplatin [GC] or methotrexate, vinblastine, doxorubicin and cisplatin [MVAC]) for metastatic disease is 13.0-15.3% and 5-year progression free survival is 9.8%-11.3% (94).

### 1.6.5. Molecular Biology

A two-pathway model has traditionally been used to describe BC pathogenesis based on early histological and cytogenetic analysis (95, 96). According to this model, low grade and high-grade tumours have a distinct natural history. Low grade tumours frequently arise from hyperplasia and are molecularly characterised by loss of heterozygosity of chromosome 9 (95). In contrast, high grade tumours, which include carcinoma in situ (CIS), are genetically unstable tumours believed to develop from flat dysplasia and associated with progression to MIBC. These tumours are believed to be induced by *TP53* mutations (95) and *RB1* mutations (97) (Figure 9). Early studies of genomic alterations in BC evaluated somatic mutations in specific candidate genes including *FGFR3* (98, 99) and *PIK3CA* (100, 101) which are more frequent in low grade tumours and *HRAS* (102) which are

uniformly distributed across all grades (103). Mutations in *FGFR3* and *TP53* have been almost found to be mutually exclusive in studies of patient urothelial cancer samples (104, 105). This suggests that they represent separate pathways of tumourigenesis.

Activation of the RAS genes and upstream *FGFR3* can activate both MAPK and PI3K cascades, the two most implicated signalling pathways in urothelial cancer. Both of these signalling pathways may converge downstream on the mammalian target of rapamycin (mTOR) (103).

Mutations in *FGFR3* and *RAS* have also been found to be mutually exclusive. However, these two genetic mutations have not been reported to be associated with differing stage or grade of tumours. This suggests that these two genetic mutations represent different pathways that lead to a similar phenotype (106).

It is not entirely clear why different genomic alterations lead to different bladder cancer phenotypes or subtypes. What is known is that the *FGFR3* and *RAS* mutations, which are more common in lower grade bladder cancers, affect the MAPK and PI3K intracellular signalling cascades resulting in proliferation (103). In contrast, the *TP53* and *RB1* mutations, which are more common in higher grade and muscle invasive bladder cancers, are often loss of function mutations in key tumour suppressors and are therefore likely to have wide ranging effects on cell cycle arrest, apoptosis, senescence and DNA repair in response to DNA damage (95, 97). It is possible that these differences in downstream cellular pathways that occur with these two mutation categories are responsible for the different bladder subtypes that occur.

## Low grade pathway

## High-grade pathway

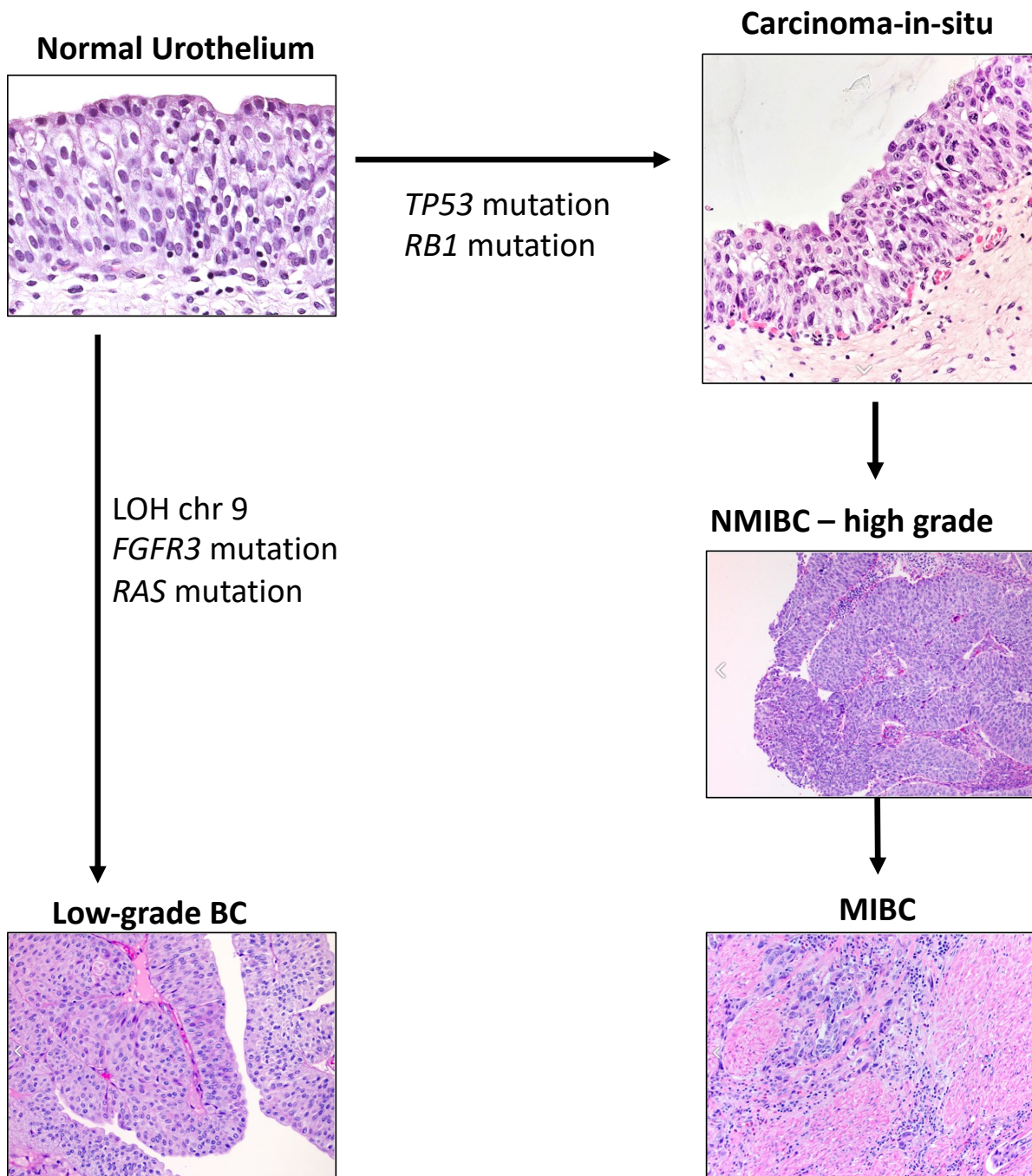


**Figure 9. Simplified Two Pathway Model for Molecular Basis of Bladder Cancer Initiation and Progression.**

Histology images in figure re-used with permission from Human Protein Atlas (Normal Urothelium Image) (19) and Pathology Outlines (Rest of Images in Figure) (107). Pathology outlines images contributed by Dr Nicole K. Andeen (low-grade BC and NMIBC-high grade images), Maria Tretiakova (low-grade BC, NMIBC-high grade and MIBC images) and Ana-Maria Catana (Carcinoma-in situ image).

Fibroblast growth factor receptors (FGFRs) are transmembrane receptor tyrosine kinases (RTKs) (108). Binding of a FGFR by its corresponding growth factor triggers dimerization of the receptor, phosphorylation of tyrosine residues and activation of multiple signalling cascades including the RAS-MAPK (Mitogen activated protein kinase) pathway (108). Abnormal activation of FGFR3 can occur in multiple ways including: *FGFR3* point mutation, FGFR3 fusion proteins, upregulated expression of wild type *FGFR3* and isoform switching. The most common mutation is S249C followed by Y375C (109). These FGFR3 point mutations are activating mutations. FGFR3 S249C, for instance, can self-dimerise through a disulfide bond leading to constitutive activation of FGFR signalling in a ligand independent way (110).

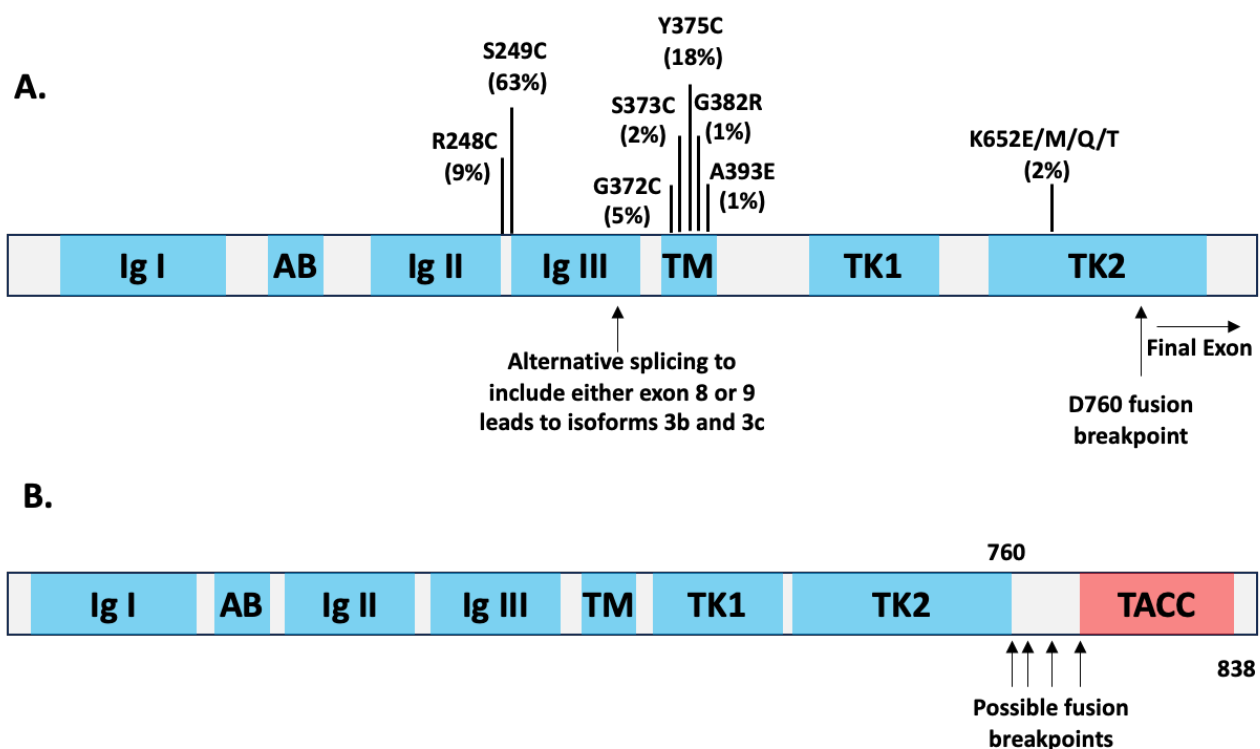


**Figure 10. Common FGFR3 Genomic Alterations in Bladder Cancer.**

(A) Structure of FGFR3 isoform 3b/c with mutation hot spots and position of translocations in relation to structure. (B) Structure of FGFR3 fusion protein: FGFR3-TACC3 (associated with BC) (111). Abbreviations: AB: Acid box, Ig: Immunoglobulin domain, TM: Transmembrane domain, TK: Split tyrosine kinase domain.

PI3K/AKT is an important signal transduction pathway that regulates apoptosis, survival and proliferation. Activating mutations in *PIK3CA* are believed to activate the PI3K/AKT pathway and are more common in low grade cancers but are found in all BC grades. The most common mutations identified in BC and other cancers are E542K, E545K and H1047R. The mutations in BC mainly consists of helical domain mutations (112). RAS proteins can activate the PI3K pathway through direct contact with the p110 $\alpha$  protein (catalytic subunit protein encoded by *PIK3CA* gene) (113).

Oncogenic activation of *RAS* genes activates the MAPK pathway. Mutations in the *RAS* genes (*HRAS*, *NRAS*, *KRAS*) have been identified in all stages and grades of BC. RAS is a GTPase protein which is involved in signal transduction in multiple intracellular pathways including RAF, MEK and ERK which are involved in cell division. Mutations in RAS in hotspots such as codon 12 (G12V) leads to loss of GTPase function and constitutive activation of the protein in its GTP-bound form (114). FGFR3 activation can also activate the MAPK pathway (115).

Most MIBCs have alterations in genes that have roles in cell cycle checkpoint. *TP53* is a tumour suppressor gene that has been implicated in high grade cancers. The *TP53* gene encodes the TP53 protein which is a DNA-binding transcription factor that regulates cell cycle function (116). Mutations are commonly missense mutations affecting the DNA binding domain. This affects the activation of genes involved in cell cycle regulation. Inactivation of tumour suppressor genes *RB1* and *CDKN2A* are also seen in MIBC (116).

Receptor tyrosine kinases (RTKs [e.g. FGFR3, EGFR]) may be activated in BC by ligand binding, mutation, or overexpression. RTKs activate RAS leading to activation of the RAS-RAF-MEK-ERK cascade which in turn, contribute to phosphorylation of substrates. This can lead to cell cycle progression and proliferation. Activated RTKs also bind to p85 (which is the regulatory subunit of PI3K [P110]) recruiting the PI3Kinase enzyme. The PI3Kinase enzyme phosphorylates phosphatidylinositol-4,5-bisphosphate (PIP2) to form PIP3. PI3kinase can also be activated directly by RAS. PIP3 recruits 3-phosphoinositide-dependent protein kinase 1 (PDK1) and activates AKT through phosphorylation leading to regulation of other proteins and intracellular signalling effects. Activation of MDM2 represses tumour suppressor p53 transcriptional activity thereby driving tumourigenesis (117) (Figure 11).

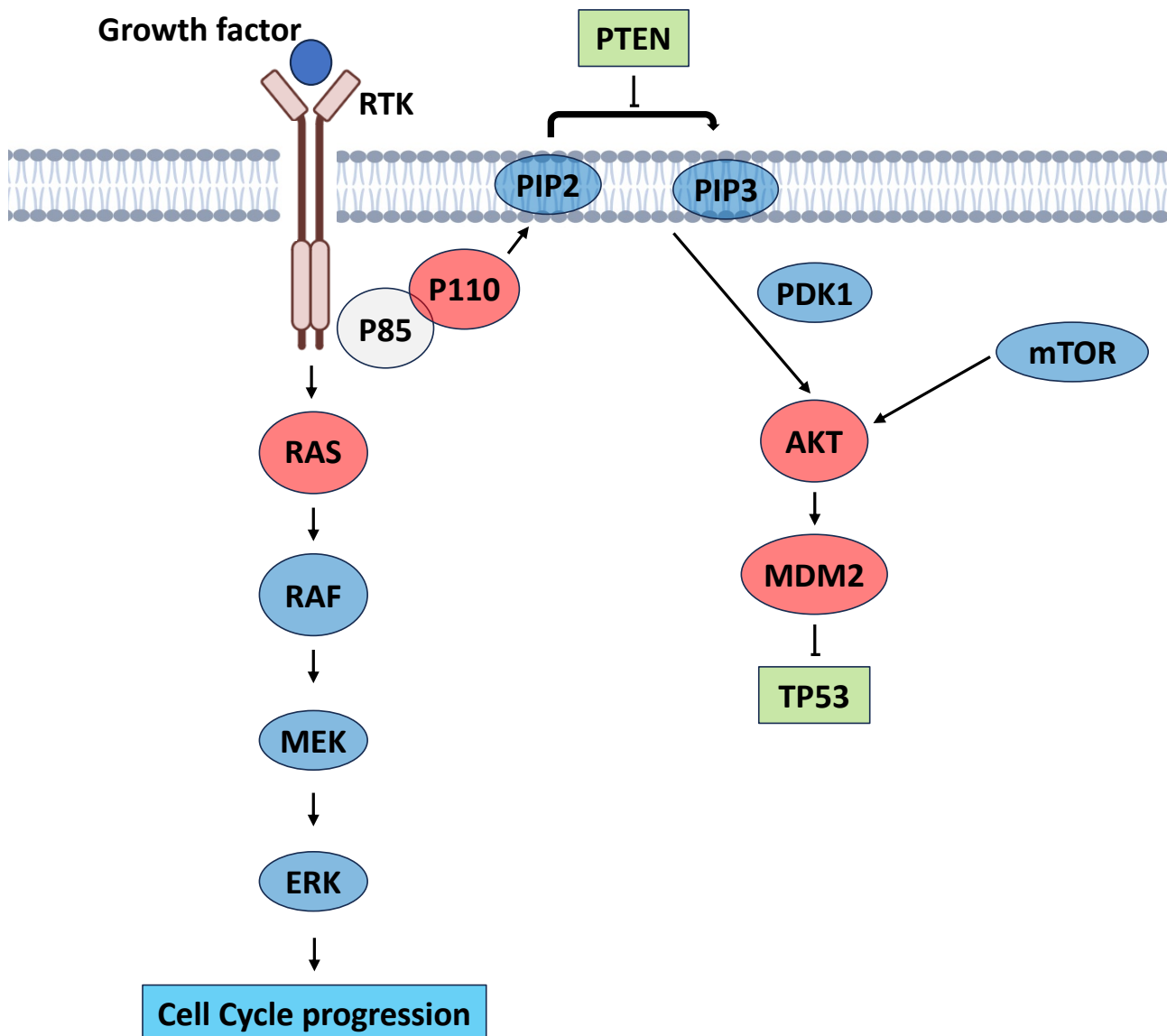


**Figure 11. Key Signalling Pathways Implicated in Bladder Cancer Tumourigenesis: MAPK and PI3K signalling.**

Proteins that are activated in BC are red (RAS, PI3K [p110], AKT, MDM2) and proteins that are inactivated in BC are green (PTEN and p53) (117).

Whole exome sequencing analysis of NMIBC and MIBC samples has revealed further insights into genomic alterations in BC. The Cancer Genome Atlas (TCGA) reported somatic DNA alterations and copy number alterations in 412 MIBC patients. The most common somatic mutations ( $\geq 12\%$  frequency) were in *TP53* (48%), *KMT2D* (28%), *KDM6A* (26%), *ARID1A* (25%), *PIK3CA* (22%), *KMT2C* (18%), *RB1* (17%), *EP300* (15%), *FGFR3* (14%), *STAG2* (14%), *ATM* (14%), *FAT1* (12%), *ELF 3* (12%), *CREBBP* (12%) and *ERBB2* and *SPTAN1* (12%) (118). Somatic copy number alterations were seen in *CDKN2A* and *RB1* (Deletion) and *E2F3* and *EGFR* (Amplification) (118, 119) (Figure 12). These genes fall into multiple different categories: chromatin modifying genes (*KMT2D*, *KDM6A*, *ARID1A*,

*KMT2C*, *STAG2*, *CREBBP* and *EP300*), a lipid kinase (*PIK3CA*), tumour suppressor genes (*TP53*, *RB1*, *ELF3*, *ATM*, *CDKN2A*), receptor tyrosine kinases (*ERBB2*, *EGFR*, *FGFR3*) and a transcription factor (*E2F3*).

Whole exome sequencing of 24 NMIBC samples followed by next generation sequencing of 58 additional samples showed the most common somatic mutations ( $\geq 12\%$  frequency) were in: *FGFR3* (79%), *PIK3CA* (54%), *KDM6A* (52%), *STAG2* (37%), *KMT2D* (30%), *ARID1A* (18%), *EP300* (18%), *KMT2C* (15%), *CREBBP* (15%), *RHOB* 13%) and *HRAS* 12%)(120) (Figure 12). The function of these genes includes an RTK (*FGFR3*), lipid Kinase (*PIK3CA*), chromatin modifying genes (*KDM6A*, *STAG2*, *KMT2D*, *ARID1A*, *EP300*, *KMT2C*, *CREBBP*) and GTPases (*HRAS*, *RHOB*).

These datasets confirm previously reported differences in the mutational landscape between NMIBC and MIBC. There is an absence of *TP53* mutations in lower grade BCs and a higher frequency of *FGFR3* and *PIK3CA* mutations in lower grade BCs. Other notable findings in the data from these sequencing studies are the high incidence of mutations in the *STAG2* gene and a significantly higher number of mutations in *KDM6A*, *RAS* and *RHOB* genes in NMIBC compared to MIBC. In addition, there is an absence of alterations in *CDKN2A* and *RB1* genes in NMIBC which are altered in  $>10\%$  MIBCs (120).

A particularly novel finding from the TCGA MIBC sequencing data was the significant number of somatic mutations in chromatin remodelling genes *KMT2D*, *KDM6A*, *ARID1A*, *KMT2C* and *EP300* (118). Epigenetic alterations such as DNA methylation, histone modification and chromatin remodelling are involved in regulating gene expression. Chromatin-modifying gene mutations were also common in next-generation sequencing of NMIBC samples where they were found common across grade and stage (120).

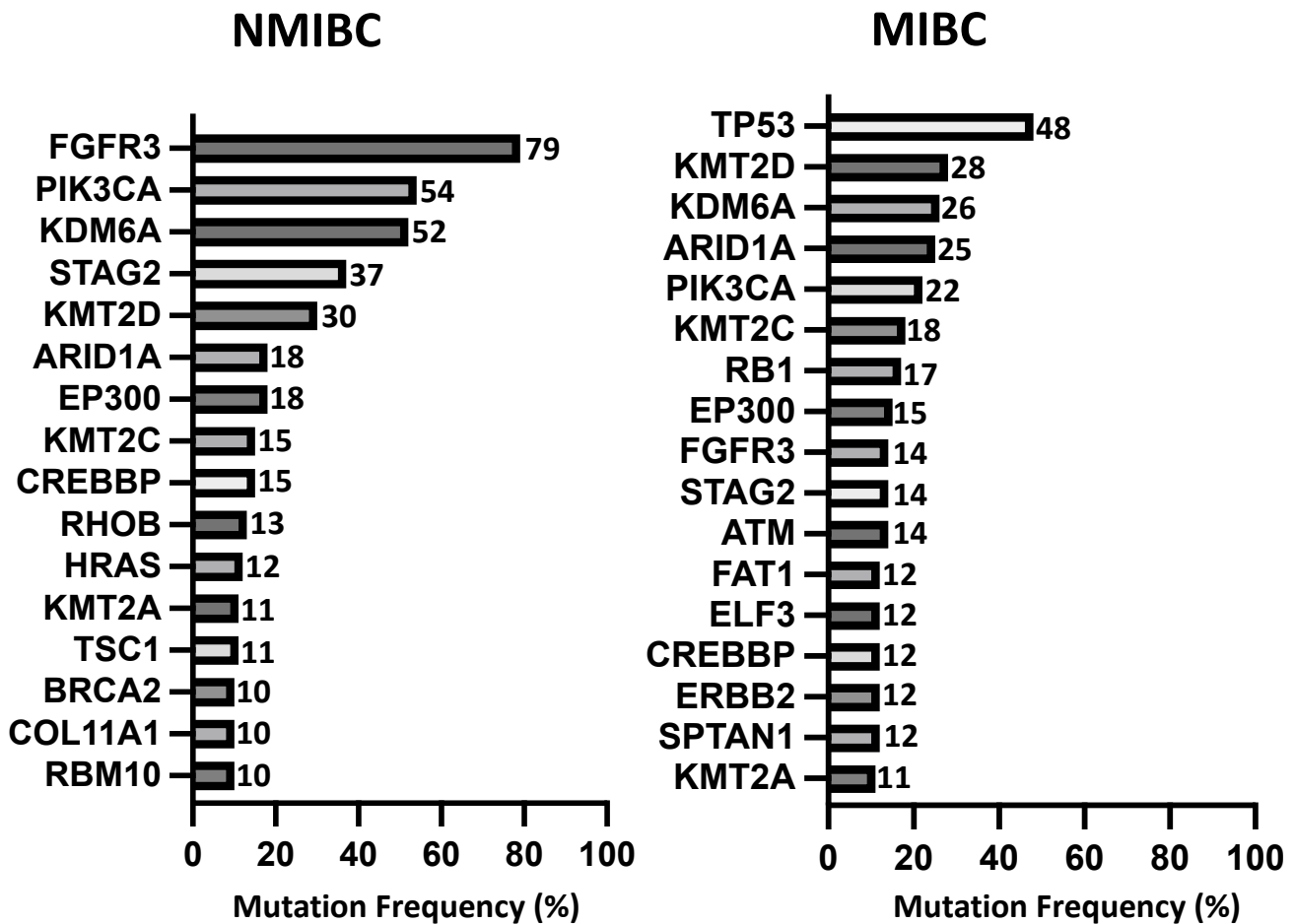


Figure 12. Mutation Frequency Identified From Whole Exome Sequencing Data for Non-Muscle Invasive Bladder Cancer and Muscle Invasive Bladder Cancer.

Graph produced using data from Hurst et al 2017 (120) and Robertson et al 2017 (118).

MIBC has one of the highest mutational loads (somatic mutation frequency) of any cancer that was studied in the TCGA with a mean of 8 mutations per Mb, behind only lung carcinoma and melanoma (118). The mutational load is lower in NMIBC in comparison to MIBC with a mean of 2 mutations per Mb in NMIBC (120). This is an important finding as mutational burden is associated with neoantigen load which may have implications for immunotherapy sensitivity (118).

Anti-viral apolipoprotein B mRNA editing enzyme catalytic polypeptide (APOBEC) are a family of enzymes that function as cytosine deaminases and likely have a physiological function in the restriction of retroviruses by inducing mutations in the virus genome. High mutational load in BC is predominantly believed to be driven by APOBEC mediated mutagenesis (Up to 67% of single nucleotide variants) (73, 118, 121). Mutations have been identified in BC that are consistent with the APOBEC mutational signature. This signature is characterised by the deamination, in exposed single stranded DNA, of cytosine bases to uracil in 5' TCA and TCT contexts which gives rise to cytosine to thymine (C->T) and cytosine to guanine (C->G) mutations (121). In a transgenic mouse model, human *APOBEC3* expression has been demonstrated to play an important role in inducing specific somatic mutational signature at cytosine bases in BC (122). In MIBC, patients with a mutational profile characterised by a high APOBEC signature, high mutation burden, and a high predicted neoantigen load have the best 5-year survival probability (75%) (118). This has been hypothesised to be due to a host immune response to the high mutation load limiting cancer growth and progression (118).

Findings from *in vitro* data has suggested that BK polyomavirus reactivation could potentially be a BC carcinogen in immunocompromised patients by driving APOBEC mediated mutations (123). Polyomaviruses are often childhood infections with 70-80% of the healthy population testing positive by adulthood. In healthy individuals without immunocompromise, these viruses are often asymptomatic and can remain latent in the proximal tubule cells of the kidneys. Reactivation of the viruses can occur during periods of immune compromise causing sloughing of infected cells in the urine into the bladder. In urothelial cell lines, BK virus was demonstrated to infect differentiated urothelial cells and increase APOBEC3A and B protein levels and deaminase enzyme activity. BK virus induced cells to re-enter the cell cycle from the G0 phase and arrest in the G2 phase via blocking retinoblastoma protein tumour suppressor function. However, further evidence is required to demonstrate that mutations in BC are due to BK virus infection and not the result of other initiators of APOBEC- mediated mutagenesis (123).

#### **1.6.6. Molecular Subtypes of Muscle- Invasive Bladder Cancer**

RNA sequencing data from The Cancer Genome Atlas (TCGA) identified and described five mRNA expression subtypes: luminal-papillary (35%), luminal-infiltrated (19%), luminal (6%), basal-squamous (35%), and neuronal (5%) associated with overall survival and potential sensitivity to

treatment (118). The broad categories of basal and luminal subtypes are similar to intrinsic breast cancer subtypes where gene expression profiling was used to show molecular subtypes of breast cancer that have different clinical behaviours (luminal and basal) (124).

Luminal subtypes of MIBC exhibit high expression of urothelial differentiation markers (*FOXA1*, *GATA3*, *Cytokeratin 20*) and uroplakins (*UPK2* and *UPK1A*). The luminal subtypes were further subdivided based on epithelial-to-mesenchymal transition (EMT) signature genes, myofibroblast makers and wild type p53 signature genes. The luminal subtype is characterised by expression of genes that are highly expressed in differentiated urothelial cells (*KRT20* and *SNX31*). This is suggestive that this subtype derives from intermediate cells that express markers of superficial umbrella cells. Potential targeted therapies for this subtype were not proposed when formulating this molecular classification.

The luminal papillary subtype encompasses tumours with papillary morphology, and these were enriched with somatic alterations in *FGFR3*, *CDKN2A* and *STAG2*. This subtype also had low CIS signature scores as well as high expression of sonic hedgehog signalling markers. This group has a low likelihood of response to cisplatin-based chemotherapy based on preliminary data (125). Tyrosine kinase inhibitors of *FGFR3* have been proposed as treatment options due to the high incidence of *FGFR3* alterations.

The luminal infiltrated subtype had lower purity likely to be due to the lymphocytic infiltrates. There was also high expression of smooth muscle signature genes as well as epithelial to mesenchymal transition (EMT) signature genes. This subtype has high expression of immune markers programmed death ligand 1 (*PD-L1*), programmed cell death protein 1 (*PD-1*) and *CTLA4* and was associated with a wild type *TP53* signature. With regards to treatment, the luminal infiltrated subtype is characterised by resistance to cisplatin-based chemotherapy and sensitivity to immune checkpoint inhibition therapy with atezolizumab in locally advanced or metastatic disease following platinum-based chemotherapy failure (126).

The basal squamous subtype, more common in females, had high expression of basal and stem cell markers (*CD44*, *KRT5*, *KRT6A*, *KRT14*) and squamous differentiation markers (*TGM1*, *DSC3*, *PI3*). The basal squamous subtype also demonstrated high expression of *PD-L1* and *CTLA4* immune markers as well as other features of immune infiltration. The subtype has high expression of CIS

signature genes and loss of sonic hedgehog and BMP signalling which suggests this subtype develops from basal cells and CIS lesions. Both cisplatin based neoadjuvant chemotherapy (NAC) and immune checkpoint therapy (PD-L1 inhibitors, PD-1 inhibitors and anti-CTLA4 treatment) have been proposed as treatment options.

The neuronal subtype had high expression of neuronal differentiation markers and neuroendocrine markers and had mutations in cell cycle regulators *TP53* and *RB1* as well as amplification of transcription factor *E2F3*. This subtype had the poorest survival. Etoposide-cisplatin NAC has been proposed as a treatment regime based on the treatment regime for neuroendocrine tumours at other sites.

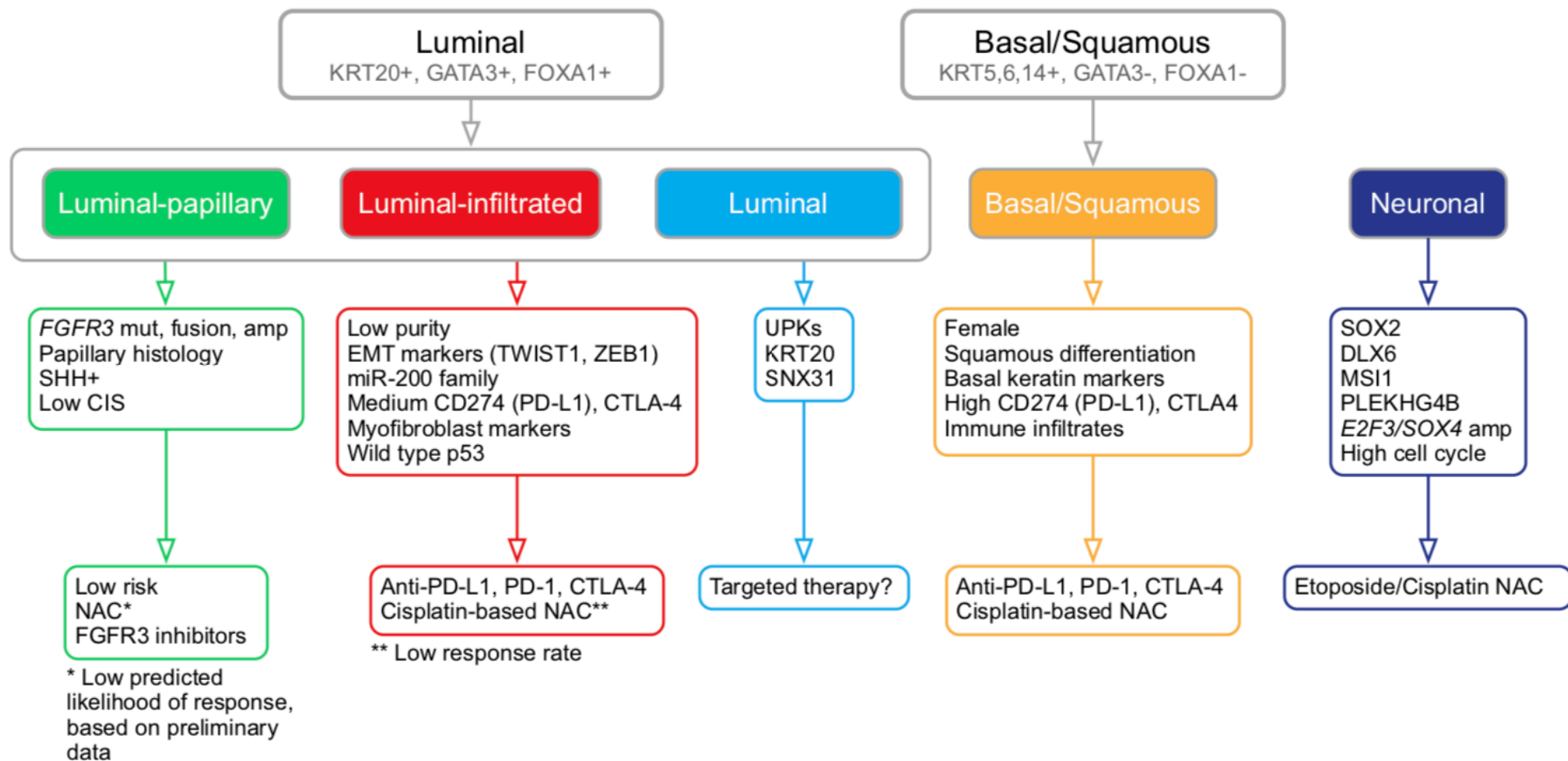


**Figure 13. Proposed Molecular Subtypes of Muscle Invasive Bladder Cancer and Potential Treatment Options.**

Adapted from Robertson et al 2017 (118) and re-used with permission.

### **1.6.7. Treatment**

Treatment for BC starts with transurethral resection of bladder tumour (TURBT). This enables resection of the tumour which can provide symptomatic relief and allows histopathological examination and diagnosis. Subsequent treatment is dependent on grade and stage of the disease as well as the overall general health and co-morbidities of patients. Treatment options for NMIBC include surveillance cystoscopy alone (to detect recurrences), adjuvant intravesical treatments (chemotherapy [mitomycin] and immunotherapy [BCG]) and surgery (radical cystectomy and urinary diversion). The choice of treatment depends on disease grade, previous bladder cancer, size of tumour and number of tumours.

#### **1.6.7.1. Non-Muscle Invasive Bladder Cancer Treatment**

The most administered intravesical agent for BC is mitomycin (MMC). MMC is an antibiotic with anti-tumour activity and works by inducing DNA cross linking in BC cells. It is often administered as a single instillation into the bladder immediately following a TURBT to act on potential residual tumour cells. This approach has been demonstrated to result in a 39% reduction in the odds of BC recurrence (OR=0.61,  $p<0.0001$ ) (127) but not on progression. Mitomycin instillations can also be given as a longer weekly treatment over the course of several weeks for BC (128).

Intravesical Bacillus Calmette-Guerin (BCG) instillations are used to reduce the rate of both recurrence and progression of high-risk non muscle invasive bladder cancer including Carcinoma In Situ (CIS). A maintenance BCG regimen (i.e. 27 instillations over 3 years) is associated with a 27% reduction in odds of progression to muscle-invasive disease (OR=0.73,  $p=0.001$ ) at a median follow up of 2.5 years. The mechanism of action is not fully understood but is believed to stimulate the immune system and upregulate several cytokines including interleukins 6 and 8. The cellular immune response is believed to lead to destruction of the tumour cells (129).

There are emerging novel treatments for patients who do not respond to BCG. Intravesical Nadofaragine Firadenovec is a treatment that contains a recombinant adenovirus that carries the human interferon alfa-2b cDNA into the bladder urothelial cells. It leads to complete response in 45.5% of patients with BCG unresponsive non-muscle invasive BC at 12 months (130). Preliminary work has suggested that Atezolizumab (an anti-programme cell death ligand 1 [PD-L1] treatment), with and without BCG treatment may be a promising treatment for BCG-unresponsive CIS (131).

Radical cystectomy and urinary diversion is also a possible treatment in patients with high-risk non-muscle invasive bladder cancer. Indications for this treatment are high grade disease (G3), lamina propria invasion (T1 disease) or recurrent, large lower grade disease (G1 or G2 pTa).

#### **1.6.7.2. Muscle-Invasive Bladder Cancer Treatment**

Treatment options for MIBC include surgery (radical cystectomy, bilateral pelvic lymph node dissection and urinary diversion) with or without neoadjuvant chemotherapy (132) or bladder preserving treatments which include radiotherapy and chemoradiation (133). Treatment decisions are based on patient fitness and choice.

Radical surgery takes the form of radical cystectomy, bilateral pelvic lymph node dissection and urinary diversion. This treatment carries significant risks with a reported early complication rate of 28% and a reported peri-operative death risk of 2.5%. Potential short-term peri-operative complications include bleeding/haematoma, chest/urine infections, wound infections or wound dehiscence, bowel ileus, urine leak secondary to uretero-ileal anastomotic leak, bowel leak secondary to small bowel anastomotic leak and pelvic collection/abscess (134).

Long term oncological outcomes for surgery are largely dependent on the pathological stage and presence of lymph node metastases. Overall recurrence free survival at 5 years for patients undergoing radical cystectomy is 68%. Recurrence free survival (5-year) ranges from as high as 92% for patients with no evidence of cancer in their cystectomy pathological

specimen to as low as 50% for pT4 disease (see Table 1 for TNM staging of Bladder Cancer) and 35% in the presence of lymph node metastases (134).

Radical radiotherapy is an alternative treatment for MIBC and involves a dose of 66Gy over 6 weeks targeted to the urinary bladder. It is not an effective treatment for carcinoma in situ, squamous cell carcinoma or adenocarcinoma. Radical radiotherapy has been shown to be similar to surgery with respect to oncological outcomes in a single institution series (135). However, there were concerns regarding the patient selection in this series with more aggressive disease in the radical surgery group and higher than usual peri-operative mortality in the radical surgery group (136).

Neoadjuvant chemotherapy prior to radical surgery with a platinum based regimen has been reported to be associated with a 5% absolute survival benefit at 5 years (137). The recommended treatment is a cisplatin combination regime and is only recommended for patients with MIBC (138).

Adjuvant chemotherapy following radical surgery with a platinum-based chemotherapy agent is a recommended option for patients in whom the surgical pathology demonstrates MIBC or the presence of lymph node metastases (i.e. higher chance of recurrence), providing they did not receive neoadjuvant chemotherapy prior to radical surgery (139). Programme cell death protein 1 (PD-1) inhibitor nivolumab as an adjuvant treatment following radical surgery has demonstrated prolonged disease-free survival in patients who are at a higher risk of recurrence (e.g. presence positive of lymph nodes) (140).

### **1.6.7.3. Locally Advanced or Metastatic Bladder Cancer Treatment**

In patients with locally advanced (invading the pelvic side wall or rectum [pT4b based on TNM classification of bladder cancer]) or metastatic disease, the mainstay of treatment is platinum-based chemotherapy regimens (94). However, there is recent increasing evidence for benefits of immunotherapies. Programme cell death protein 1 (PD-1) is a molecule that is expressed on activated T cells and binds to programme cell death ligand 1 (PD-L1) to curtail the immune response. Tumours can express PD-L1 to stop T cell activation. Anti PD-1

and PD-L1 agents are immune checkpoint inhibitor treatments have been developed to increase T cell activation resulting in an anti-tumour response. Current indications for immune checkpoint inhibitors (e.g. PD-1 inhibitor pembrolizumab or PD-L1 inhibitor atezolizumab) are situations where patients with locally advanced or metastatic urothelial cancer either are not suitable for traditional chemotherapy regimens (141, 142) or have progressed on traditional chemotherapy regimens (143, 144). These drugs have also been approved as maintenance therapy (e.g. PD-L1 inhibitor avelumab) in patients who have responded to and completed a platinum-based chemotherapy regime but still need further maintenance treatment (145).

Antibody drug conjugates (ADC) have been shown to be effective treatments in metastatic urothelial cancer that has progressed on chemotherapy and PD-1/PD-L1 inhibitors. Enfortumab vedotin is an ADC targeting nectin-4 and has been reported to significantly prolong survival compared to standard chemotherapy (median overall survival benefit of approximately 4 months and median progression free survival benefit of approximately 2 months) in patients who had disease progression following PD-1 or PD-L1 inhibitor treatment (146).

There is evidence for targeted treatment based on the presence of *FGFR3* mutations. *FGFR3* inhibitors (e.g. erdafitinib) which target the FGFR3 receptor tyrosine kinase have shown survival benefits in patients with locally advanced or metastatic urothelial cancer who have progressed after platinum-based chemotherapy and have *FGFR3* alterations (147).

#### **1.6.7.4. Experimental Bladder Cancer Treatments**

Sacituzumab Govitecan is an ADC targeting trophoblast cell surface antigen 2 (TROP-2) and has been evaluated in a phase II study in patients with metastatic urothelial cancer progressing on platinum-based chemotherapy and checkpoint inhibitors. It was shown to have an acceptable safety profile and its efficacy was good (median progression-free survival and overall survival of 5.4 months [95% CI: 3.5 -7.2 months] and 10.9 months [95% CI: 9.0 to 13.8 months]) (148). It is currently only recommended in the context of clinical trials (149).

## **1.7. Upper Tract Urothelial Cancer**

### **1.7.1. Overview, Histology, Aetiology and Diagnosis**

Upper urinary tract cancers include urothelial cancers of the upper tracts (kidneys and ureters) and renal cell carcinoma. Renal cell carcinoma will be discussed later in the introduction chapter. Upper tract urothelial cancer (UTUC) constitutes a small proportion of urothelial cancers (approximately 5-10%). Histologically these cancers are urothelial carcinomas arising from the urothelium lining the renal calyces, renal pelvis and ureters. They have an estimated incidence (age standardised) of 4.7 cases per 100,000 in Western countries (150). Due to similarities at the histological level, diagnosis and treatment approaches have traditionally been extrapolated from data on urothelial BC (151).

UTUCs can occur in association with BC at the same time (synchronous) or at different times (metachronous). Concurrent BC is present in 17% of UTUC (152). Furthermore, 41% of American males with UTUC have a previous history of BC (153), BC recurrence occurs in 40% of UTUC cases within a median follow up of 45 months (154) and contralateral upper urinary tract recurrence occurs in 2-5% at a median follow up of 33 months (155). It remains unclear whether these phenomena are due to intraluminal seeding or intraepithelial spread of tumours (monoclonal theory) or if individual tumours develop in different parts of urothelium independently from each other due to carcinogenic exposures that effect the entire urothelium (multiclonal theory) (156).

Over half of UTUCs are invasive at diagnosis compared to 15-25% of BC patients with MIBC (157). However, UTUC and urothelial BC have similar behaviours when stage and grade are considered (158). Like BCs, UTUC are more common in men. Some risk factors are similar between urothelial BC and UTUC such as tobacco smoking and occupational exposures. However, there are also risk factors with greater risk for UTUC than urothelial BC such as phenacetin, aristocholic acid (159) and Lynch syndrome (160).

Somatic gene mutations are mostly similar to those identified in BC but with differing frequencies. Whole exome sequencing data of UTUCs identified mutations in *FGFR3* (74%), *KMT2* (59%), *PIK3CA* (26%), *TP53* (22%) and *KDM6A* (22%), *CDKN2* (19%). Mutation rates overall are comparable between UTUC and BC (mean 5.8/mb and median 3.4/mb for UTUC vs mean 7.7/mb and 5.5/mb for BC) (161). Germline mutations in DNA mismatch repair (MMR) genes leading to microsatellite instability associated with Lynch syndrome are also associated with UTUC. Examples of mismatch repair genes that are implicated in Lynch syndrome include: *MLH1*, *MSH2*, *MSH6* and *PMS2*. Loss of mismatch repair protein expression has been reported in 18.8% of UTUC cases (162).

UTUC is diagnosed mainly with computer tomography (CT) scanning but ureteroscopy with or without biopsies can be used as an adjunct in cases where there is diagnostic uncertainty (59).

## **1.7.2. Treatment**

### **1.7.2.1. Localised Disease**

Choice of treatment depends on stage of disease, patient fitness and patient choice. The gold standard treatment for UTUC is radical nephroureterectomy with excision of bladder cuff. Excision of the bladder cuff is important because there is a high risk of recurrence in unexcised ureteric stump. A single intravesical dose of mitomycin C post operatively has been demonstrated to reduce subsequent BC recurrence risk (absolute risk reduction 11% and relative risk reduction of 40%) (163). There is also evidence for four cycles adjuvant cisplatin-based chemotherapy for radical nephroureterectomy with a disease-free survival of 71% (95% CI: 61-79) for chemotherapy vs 46% (36-56) for surveillance alone at 3 years (164).

Alternatively, less invasive treatment with nephron sparing surgery is an option in a specific subset of patients with low grade, low stage and small volume (<1cm) disease. This treatment has the advantage of reducing the morbidity associated with the more invasive

treatment of nephroureterectomy. In the aforementioned specific subset of cases with low risk and low volume disease, nephron sparing surgery is reported to be oncologically equivalent (165). Nephron sparing surgery can also be used in cases where nephroureterectomy would be detrimental to their health i.e. patients with a single kidney or significant chronic renal impairment (165). Endoscopic management with ureteroscopy or percutaneous access and laser fulguration is a treatment option in well selected patients with low stage disease. Oncological outcomes are reported to be adequate in well selected patients. However, approximately 20% of these patients will progress to radical nephroureterectomy (166).

#### **1.7.2.2. Metastatic Disease**

Metastatic UTUC, like metastatic BC, is associated with a poor prognosis. Data informing treatment of metastatic UTUC is sometimes extrapolated from studies performed on patients with both upper and lower tract urothelial carcinomas. Platinum-based chemotherapy regimens are the standard treatments used. Patients with upper and lower urothelial carcinoma treated with platinum-based chemotherapy have similar overall and progression free survival at a median follow up of 4.8 years (167). Maintenance avelumab (PD-L1 inhibitor) can be used in patients who have responded to initial platinum-based chemotherapy (median overall survival 21.4 months for treatment vs 14.3 months for best supportive care)(145). In patients who progress on platinum-based chemotherapy, immune checkpoint inhibitor pembrolizumab (PD-1 inhibitor) can be used to prolong survival by approximately 3 months compared to standard chemotherapy (median overall survival 10.3 months vs 7.4 months) (168). In patients who progress on pembrolizumab, antibody drug conjugate enfortumab vedotin has been reported to prolong survival by approximately 4 months (median overall survival 12.9 vs 9.0 months) compared to standard chemotherapy (146).

### **1.8. Renal Cell Cancer (RCC)**

### 1.8.1. Overview, Histology, Aetiology and Diagnosis

Renal cell cancers (RCC) are adenocarcinomas that arise from the renal tubular epithelial cells. It is the 14<sup>th</sup> commonest malignancy globally overall (9<sup>th</sup> commonest in men and 14<sup>th</sup> commonest in women). It is estimated there were 431, 288 new cases in 2020 (57). In total, approximately 75% of RCCs are clear cell RCCs (ccRCC) which arise from the proximal tubule. Less common subtypes of RCC include papillary RCC (10% and arise from distal tubular epithelium), chromophobe RCC (5% and arise from distal tubular epithelium), collecting duct carcinoma (1% and arise from collecting ducts) and renal medullary carcinoma (1% and arise from distal tubular epithelium)(169). The majority of RCCs are detected incidentally on imaging (57). Symptoms are often a late sign associated with local growth of the tumour, metastatic disease, or paraneoplastic syndromes.

Histologically, the most common subtype of RCC (clear cell RCC [ccRCC]) is characterised by malignant cells arising from the proximal tubular epithelium and which have a distinct cell membrane, clear cytoplasm and arranged in 'nests' surrounded by thin-walled blood vessels. The clear cytoplasm is a result of cytoplasmic glycogen, lipids and cholesterol. The glycogen can be stained for using periodic-acid Schiff (PAS). The cytoplasm can also be granular and eosinophilic (18). Nuclear abnormalities are graded using the Furhman grading system which groups nuclear abnormalities (E.g. nuclear size, pleomorphism, presence of nucleoli) according to their severity (170).

Risk factors for RCC include obesity, hypertension, smoking, and chronic kidney disease. Inherited cancer syndromes caused by germline mutations also predispose to renal cell cancer. The following inherited cancer syndromes predispose to RCC:

- von Hippel Lindau syndrome (mutation in *VHL* gene [tumour suppressor])
- Hereditary leiomyomatosis and RCC (mutation in *FH* gene [encodes fumarate hydratase enzyme])
- Hereditary papillary RCC (mutation in *MET* gene [receptor tyrosine kinase and proto-oncogene])
- Birt-Hogg-Dubé (mutation in *FLCN* gene [encodes folliculin protein] (57).

Other common germline mutations have been identified in the following genes: *BAP1* (encodes BRCA1 associated protein 1), *SDHB/SDHC/SDHD* (tumour suppressors and encode subunits of succinate dehydrogenase enzyme complex), *TSC1/TSC2* (tumour suppressors that encode hamartin and tuberin proteins), and *MITF* (encodes melanocyte inducing transcription factor) (57). Somatic gene mutations have also been reported in RCC include *VHL*, *PBRM1* (tumour suppressor gene and encodes Protein polybromo-1 which is involved in chromatin remodelling), *BAP1* and *SETD2* (encodes a histone methyltransferase) (171).

Renal cell carcinoma is diagnosed with computer tomography (CT) scanning and the disease is staged according to the TNM classification (Table 4) (172).

<b>T - Primary Tumour</b>		
Tx	Primary tumour cannot be assessed	
T0	No evidence of primary tumour	
T1	Tumour $\leq$ 7 cm or less in greatest dimension, limited to the kidney	
	T1a	Tumour $\leq$ 4 cm or less
	T1b	Tumour $>$ 4cm but $\leq$ 7cm
T2	Tumour $>$ 7 cm in greatest dimension, limited to the kidney	
	T2a	Tumour $>$ 7cmbut $\leq$ 10cm
	T2b	Tumours $>$ 10 cm, limited to the kidney
T3	Tumour extends into major veins or perinephric tissues but not into the ipsilateral adrenal gland and not beyond Gerota's fascia	
	T3a	Tumour extends into the renal vein or its segmental branches, or invades the pelvicalyceal system or invades peri-renal and/or renal sinus fat, but not beyond Gerota fascia
	T3b	Tumour grossly extends into the vena cava below diaphragm
	T3c	Tumour grossly extends into vena cava above the diaphragm or invades the wall of the vena cava
T4	Tumour invades beyond Gerota fascia (including contiguous extension into the ipsilateral adrenal gland)	
<b>N - Regional Lymph Nodes</b>		
Nx	Regional lymph nodes cannot be assessed	
N0	No regional lymph node metastasis	
N1	Metastasis in regional lymph node(s)	
<b>M - Distant Metastasis</b>		
M0	No distal metastasis	
M1	Distant metastasis	

**Table 4. TNM Classification for Kidney Cancer.**

## **1.8.2. Treatment**

Treatments for renal cell cancer include surgery (Radical or partial nephrectomy) and immunotherapy. Choice of treatment will depend on stage of disease as well as patient factors.

### **1.8.2.1. Localised Disease**

Nephron sparing surgery or partial nephrectomy has advantages over full nephrectomy with respect to preserving renal function which may be associated with cardiovascular benefits. Partial nephrectomy can be offered to all suitable patients with T1 cancer (localised cancer <7cm) and to patients with T2 tumours associated with a solitary kidney or chronic kidney disease if it is feasible (173). Radical nephrectomy is the treatment of choice for RCCs staged T2 as well as T1 RCC unsuitable for partial nephrectomy e.g. close to the renal hilum (173). In patients with RCC associated with renal vein or inferior vena caval involvement, then there is evidence for radical nephrectomy and removal of tumour thrombus (173).

### **1.8.2.2. Metastatic Disease**

In total, one quarter of newly diagnosed RCC patients will have metastatic disease and 30% of patients will progress to metastatic disease following nephrectomy. Cytoreductive nephrectomy is surgery to remove the kidney in the setting of metastatic RCC. This is a palliative treatment in most patients with metastatic disease and further systemic treatment is necessary to improve survival. However, cytoreductive nephrectomy may be curative in a subset of patients with a single metastatic deposit if the kidney and the metastatic deposit is removed (173).

There is evidence for the use of tyrosine kinase inhibitors (e.g. Sunitinib or pazopanib) in metastatic RCC, with particularly good evidence for benefit in the clear cell subtype of RCC. Furthermore, there is emerging evidence for checkpoint inhibition (e.g. Nivolumab or Pembrolizumab) in addition to TKIs in metastatic RCC. The first line standard of care now is combination TKI and checkpoint inhibitor treatment e.g. nivolumab combined with cabozantinib or pembrolizumab combined with axitinib or pembrolizumab combined with

Lenvatinib (173). These combinations have demonstrated a survival benefit with respect to progression free survival and overall survival (174).

### **1.9. Pre-Clinical Cancer Models Overview**

Cancer models are an important component of cancer research as they can help with elucidating biological mechanisms, establishing causal relationships, identification of novel treatments and understanding tumour microenvironment interactions (175). Several pre-clinical models exist with different strengths and weaknesses and the choice of model largely depends on the research question. For example, studying the interaction between cancer and immunity necessitates a model system with intact immunity e.g. immunocompetent animal models (175).

Broadly speaking, pre-clinical models can be categorised into animal and non-animal models. Animals used in animal models include mice, zebrafish, and drosophila. Animal models can be autochthonous (i.e. tumour initiation from the native organisms' normal cells), allografts (i.e. tumour cell implantation from other animal tumours from the same species) or xenograft (i.e. tumour cell implantation from human tumours). Non-animal models include *in vitro* cell culture and 3D culture or organoids (175).

#### **1.9.1. Cancer Models in Mice**

The main advantages of modelling cancer in mice are the presence of close homology of different organs and tissues to the human systems, the ability to recreate the complex tumour microenvironment interactions present in human cancer and the ability to study the immune responses and interactions (175).

Carcinogen induced or genetically engineered (GEM) mouse models of cancer offer the advantage of cancer developing in its native cells and tissues. However, carcinogen induced mouse models of cancer often have long timelines, have a low propensity to metastasise and have variable penetrance. For GEM models of cancer, modelling the complex genetic profile of human cancer is often limited by the use of a discrete number of oncogenic

genomic alterations. Allograft and xenograft mouse models of cancer have the advantage of the potential to generate large numbers of synchronous tumours that can be used in intervention studies. However, human xenografts require the mice to be immunodeficient resulting in the absence of adaptive immunity (175).

#### **1.9.1.1. Mouse Models of Bladder Cancer**

Transgenic mouse models of BC have led to numerous insights into the genetic alterations and signalling pathways driving BC. Mouse models to date have tested the roles of activating mutations in *FGFR3*, *RAS* (*HRAS* and *KRAS*), Beta-Catenin ( $\beta$ -catenin) and loss of function genetic alterations in *RB1*, *TP53* and *PTEN* tumour suppressor genes as well as different combinations of genetic alterations (176). This has enabled study into the role of the MAPK, WNT, PI3 kinase and mTOR signalling pathways in BC. The majority of the transgenic bladder cancer models in mice have utilised the mouse uroplakin-2 (*Upk2*) promoter, which is the 3.6kb 5' upstream sequence of the mouse *Upk2* gene(176). The Cre Lox system has often be used to conditionally express (or overexpress) or inactivate a gene of interest to the urothelium (176).

In mice, urothelial specific expression of the SV40T, which is an oncoprotein that inactivates TP53 and retinoblastoma proteins, leads to urothelial carcinoma. The severity depends on the number of copies of the *SV40T* transgene. A low number of copies of the *SV40T* transgene led to a carcinoma in situ (CIS) phenotype, and a high number of copies develop CIS, MIBC and as metastatic disease (177).

Constitutively active *Hras* alone can drive low grade non-invasive papillary BC in mice. A transgenic mouse model whereby constitutively active rabbit *Hras* gene (Q61L) is expressed in the urothelium gives rise to urothelial hyperplasia at an early onset and low grade non-invasive papillary tumours. In this model, tumour latency was dependant on number of copies of the *Hras* transgene (178). However, this finding was not replicated in another more recent study utilising a mouse model where *Hras* Q61L was expressed under the control of the *Upk2* promoter (utilising the Cre Lox system) by 12 months. In this model, there was evidence of urothelial hyperplasia but not a cancer phenotype suggesting there

was a tumour suppressor mechanism stopping progression to cancer. There was no observable phenotype (no hyperplasia or cancer) when the *Ras* oncogene *Kras* G12D was used in the same study (179). The different findings of these two studies with respect to the development of cancer could be explained by different transgenic methods used to generate the cancers. Zhang et al used a rabbit 3kb *Hras* genomic fragment, harbouring the Q61L mutation, under the direct control of a 3.6kb fragment of the murine *Upk2* gene promoter. Furthermore, Zhang et al evaluated mouse founders with different numbers of transgene copies (one founder had 2 transgene copies, one founder had 30 transgene copies and one founder had 48 transgene copies (178). Ahmed et al, in contrast, utilised the murine *Upk2* gene promoter and the rabbit *Hras* Q61L oncogene (2 transgene copies in the mouse genome) in conjunction with the Cre Lox system (179).

Mice expressing a constitutively active *Hras* transgene and have had knockout of *Tp53* (using the Cre Lox system) in the urothelium develop CIS and MIBC suggesting that activation of RAS signalling in combination with *Tp53* loss leads to urothelial cancer progression (180). This is supported by another mouse model in which homozygous *Tp53* mutation and constitutively active *Hras* leads to urothelial proliferation that is greater and earlier onset than activated *Hras* only mice with a proportion of the mice with both genetic alterations developing high-grade cancer. It is important to note that in this model, transgenic mice heterozygous for the *Tp53* mutation and have constitutively active *Hras* do not develop tumours more frequently or have higher tumour pathological grades than the constitutively active *Hras* only mice suggesting that *Tp53* mutations must be homozygous to interact with oncogenes to induce BC (181).

Loss of p53 tumour suppressor function alone does not lead to BC. Mice homozygous for *Tp53* mutation resulting in knockout do not show evidence of urothelial cancer until they reach seven months of age when the mortality rate is high due to other cancers (thymic lymphomas and soft tissue sarcoma) (181). These findings are mirrored with loss of function of the retinoblastoma tumour suppressor function. Tissue-specific homozygous knockout of *Rb1* in the mouse urothelium does not increase the rate of urothelial proliferation but does activate the p53 pathway leading to apoptosis. Additional urothelial-specific knockout of *Tp53* results in hyperplasia, nuclear abnormalities, and low-grade papillary bladder tumours

but not invasive tumours. Mice deficient in functioning TP53 and RB1 are, however, more sensitive to carcinogen-induced invasive cancer with 50% of BBN exposed mice deficient in both TP53 and RB1 (knockouts) developing invasive urothelial cancer. This suggests that the combination of loss of TP53 and RB1 can be cooperative in driving invasive urothelial cancer in conjunction with other carcinogens (182).

In a mouse model utilising the Cre Lox system, urothelium specific inactivation of both *Tp53* and *Pten* tumour suppressor genes led to CIS, high grade invasive carcinoma with areas of transitional cell, squamous and sarcomatoid carcinoma and stained positive for cytokeratin suggesting that they were epithelial in origin. There was evidence of metastatic spread to regional lymph nodes as well as distant sites such as the spleen, liver and diaphragm. There was no evidence of BC in mice with loss of function of *Tp53* alone or *Pten* alone. Key markers of the mTOR signalling pathway (AKT and mTOR) were upregulated in mouse BCs and an mTOR inhibitor (rapamycin) prevented tumours from developing suggesting that the mTOR signalling pathway played an important role in driving these BCs (183).

Previous studies reported expression of a mutated *Fgfr3* transgene alone or in combination with other genetic events in the urothelium does not lead to cancer. A transgenic mouse model in which a mutant *Fgfr3* transgene (K644E and K644M which are murine equivalents of human K652E and K652M) is expressed under the control of the *Upk2* promoter utilising the Cre Lox system does not lead to urothelial hyperplasia, dysplasia or carcinoma. However, when *Fgfr3* mutations were introduced alongside overexpression of *Kras*, tumours develop suggesting that *FGFR3* acts with other genetic alterations to drive tumourigenesis (184).

Although *Fgfr3* K644E or K644M mutations alone in mice have previously not driven BC, a recent study has demonstrated that a different *FGFR3* mutation (S249C [constitutively active form]) alone can drive BC. A genetically engineered mouse model of BC expressing human *FGFR3* 249C under the control of the *urop1akin-2* promoter developed focal papillary non-invasive urothelial cancer resembling the luminal papillary subtype. Higher levels of *FGFR3* expression levels were associated with higher tumour frequency and more multifocal tumours (185).

WNT signalling and PI3 kinase pathways can cooperate to drive BC. A transgenic mouse model with urothelial specific expression of activated  $\beta$ -catenin (causing accumulation of  $\beta$ -catenin and activation of WNT signalling) under the control of the *Upk2* promoter led to urothelial hyperplasia but not cancer. High level of the PTEN tumour suppressor protein were observed suggesting this was stopping tumour development in this model (186). Combination of PTEN deficiency and  $\beta$ -catenin accumulation (and resulting WNT signalling activation) led to papillary BC that was dependant on PI3 kinase signalling (associated high levels of pAKT signalling and downstream mTOR activation) (186).

The WNT signalling pathway can also cooperate with the RAS pathway to drive BC. Although one study previously reported that constitutively active *Hras* Q61L or *Kras* G12D oncogene (activation of RAS pathway) did not lead to BC in mice. Mice with a combination of increased beta-catenin expression (and activation of WNT signalling) and RAS activation developed papillary BC with associated upregulation of MAPK signalling markers (pERK1/2 and pMEK1/2) and WNT signalling markers (SOX9). These tumours were sensitive to MEK inhibition (179).

### **1.9.2. Zebrafish Disease Models**

The zebrafish (*Danio rerio*) is an important vertebrae model of human disease. It has numerous advantages for genetic studies including high fecundity, ex vivo fertilisation and embryogenesis, optically transparent embryos and larvae, rapid embryological development, and low housing costs (187). A key advantage of using zebrafish to model disease is the ability to perform live in *vivo* imaging at the cellular level (188, 189). Around 70% of human genes have a homolog in zebrafish (190). They are also highly amenable to efficient transgenic approaches (191). Mosaic (F0) transgenic zebrafish can be generated at a rate of up to 1000 animals per day. Furthermore, stable transgenic founders can arise from up to 50% of injected mosaic F0 animals using modern Tol2 transposon-based transgenesis techniques. The completely transparent adult mutant 'Casper' line, which is the result homozygous mutation in both *nacre* and *roy* genes enable *in-vivo* imaging of tumour development and metastases (192).

### 1.9.2.1. Zebrafish Cancer Models

Tumour suppressor genes in zebrafish have been demonstrated to have conserved function. Zebrafish with a homozygous mutation in the *tp53* binding domain (M214K which is orthologous to human methionine-246 also in the DNA binding domain) have been demonstrated to develop peripheral nerve sheath tumours, angiosarcomas, germ cell tumours, and leukaemia (193, 194). Zebrafish with a homozygous mutation in the *brca* gene are prone to testicular neoplasias in adulthood, and tumours in multiple tissues develop in combination with homozygous *tp53* mutation (195). Somatic inactivation of the *rb1* tumour suppressor in mosaic adult zebrafish (F0 generation) utilising TALEN genome editing leads to tumorigenesis in 11-33% of embryos developing tumours as early as 3.5 months of age. They predominantly develop brain lesions that exhibit features of neuroectodermal-like and glial-like tumours. Adult zebrafish with heterozygous germline *rb1* mutations do not develop cancers and adult zebrafish with homozygous *rb1* mutation have high mortality rates during the larval stages (196).

It has been demonstrated in a zebrafish model that germline homozygous inactivation of the *vhl* gene leads to abnormalities in the pronephros epithelium (Predominantly proximal pronephros) that mirror clear cell renal cell cancer features. The phenotype in the zebrafish pronephros was evaluated during the larval stages (up to 8.5 days post fertilisation) and characterised by an increased tubule diameter, prominent eosinophilic cytoplasm, numerous cytoplasmic vesicles, disorganised cilia, greater lipid vesicles (confirmed with BOPIDY staining) and higher glycogen content in the epithelium (confirmed with periodic acid Schiff staining), increased cellular proliferation (confirmed with BrdU staining) and apoptosis (investigated using immunofluorescence for activated caspase 3) (197). HIF2a inhibitor treatment led to more organised nuclei, reduced number of lipid vesicles and increased pronephros luminal diameter. However, a gross cancer phenotype was not seen in this model and the homozygous mutant *vhl* zebrafish embryos are not viable beyond 13 days post fertilisation possible due to cardiac abnormalities (197). The absence of a gross cancer phenotype was mirrored in a mouse model of *Vhl* mutation where there was also

cellular proliferation, accumulation of cellular lipids and renal cysts and but not cancer (198).

Oncogenes also have conserved function in zebrafish. This was first demonstrated when the mouse *c-Myc* oncogene was overexpressed in the lymphoid tissue utilising the *rag2* promoter led to lymphoma that shared similarities to human acute T cell lymphoblastic leukaemia (T-ALL). More severe cancer occurred in a homozygous *tp53* mutant background (188). Furthermore, RAS signalling, involved in regulating cell division, has been shown to be conserved in zebrafish. Human oncogenic constitutively active *HRAS\_G12V* occurs when a GGC codon is substituted with a GTC codon (G12V). When the sequence is fused to the *GFP* sequence and microinjected into fertilised eggs, approximately 20% developed neoplasias (nevi, melanomas, and lymphomas) (199).

Zebrafish have successfully been used to interrogate oncogenic pathways in haematological cancers (188), melanoma (200), thyroid cancer (201), pancreatic cancer (202), hepatocellular carcinoma (203), intestinal cancers (204), brain cancer (205) and rhabdomyosarcoma (206) which very often resemble human tumours. These models often drive mammalian oncogenes under the control of a tissue-specific promoter or they knockdown zebrafish orthologues of human tumour suppressor genes. Melanoma models are the most widely used zebrafish cancer models due to the superficial and easily visualised nature of the cancer. In these models, human activated *BRAF V600E* (the most common oncogene associated with human nevi and melanoma) driven under the control of the *mitfa* promoter leads to nevi, but in *tp53* deficient fish, human activated *BRAF V600E* leads to invasive melanomas, which share similarities with human melanomas. This suggests that *BRAF* activation leads to the development of nevi and that p53 and *BRAF* pathways cooperate to give rise to melanoma (200).

RAS signalling can drive proliferation, an early hallmark of cancer, in the zebrafish larval intestine. A zebrafish model of intestinal cancer expressing *kras G12D* (tagged to GFP) in a posterior intestine enhancer trap line led to an epithelial tumour phenotype evident at five days post fertilisation (204). This model utilised the Gal4/UAS system which can help avoid the potential toxic effect of oncogene overexpression that potentially hinders the

development of stable transgenic lines. In this system, tissue specific expression of genes of interest relies on the expression of two transgenes together. Gal4, a transcriptional activator, can be expressed under the control of a tissue specific promoter or enhancer and a gene of interest is placed downstream of an upstream activating sequence (UAS). When the Gal4 driver gene is not present, transgenes positioned downstream of UAS (upstream activating sequence) are not expressed (204, 207). A schematic of the Gal4/UAS system utilising the zebrafish *cm1c* gene promoter and GFP is shown in Figure 14. This intestinal tumour model demonstrated the tumour phenotype by measurement of fluorescent area with fluorescence microscopy, measurement of the intestinal cell counts by DAPI staining and measurement of the number of mitotic cells using pH3 (phosphorylated histone H3) and BrdU staining. In addition, the study used quantitative real time PCR (qPCR) to confirm oncogene expression. Although this study demonstrates that *kras* G12D can drive proliferation in the zebrafish intestinal cells, there was no evidence of tumour invasion during the study period. Therefore, the lesions cannot yet be confirmed to be cancers (204).

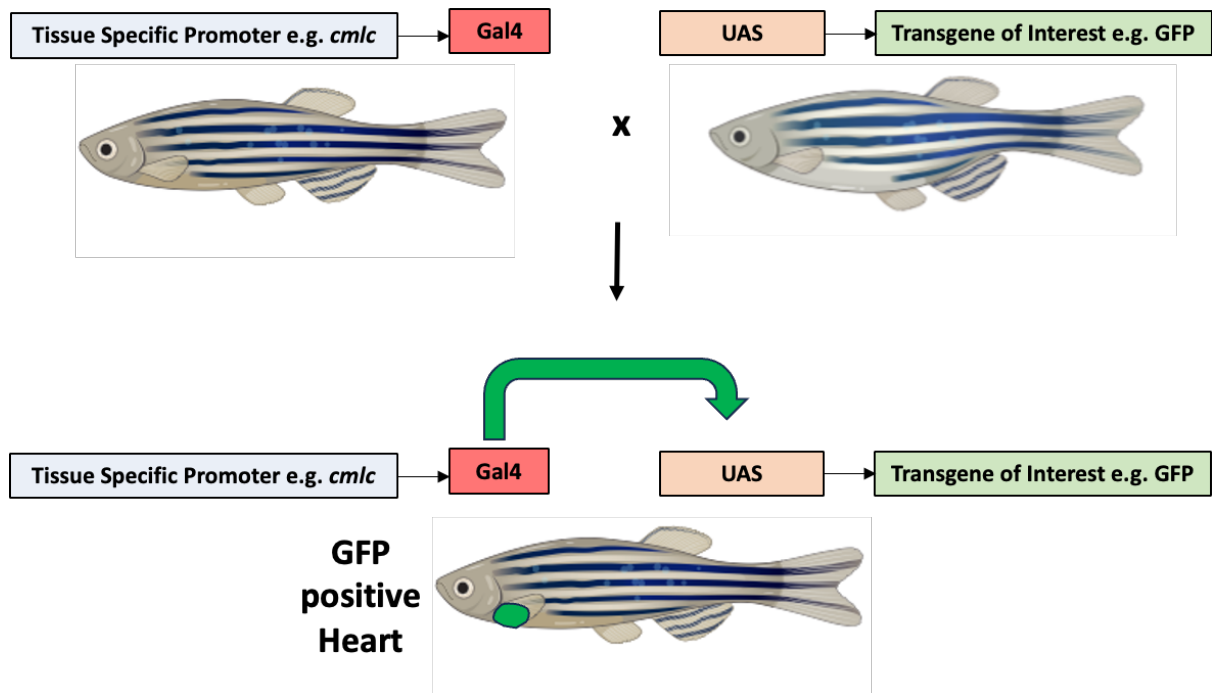


**Figure 14. Schematic of The Gal4/UAS System.**

In this schematic, the zebrafish *cmc* (cardiac myosin light chain) gene promoter, which drives gene expression in the zebrafish heart, and the reporter gene *GFP* (green fluorescent protein) are used to illustrate how the system works. *Gal4*, a transcriptional activator, is placed downstream of the heart specific *cmc* promoter in one zebrafish line and *GFP* is placed downstream of the upstream activating sequence (UAS) in another zebrafish line. *GFP* is expressed only in tissues where the upstream activating sequence is expressed. In offspring that possess both components, the Gal4 transcriptional activator binds to the upstream activating sequence (UAS) initiating expression of *GFP* under the control of the heart specific *cmc* gene promoter resulting in zebrafish with GFP positive hearts.

Most transgenic zebrafish models of cancer generated stable transgenic lines whereby the transgenes are integrated into the genome of every cell in the organism and are heritable from generation to generation. However, transient expression of oncogenes in a mosaic pattern in F0 zebrafish have also been investigated (205, 206, 208). This approach utilises one cell stage microinjection of exogenous DNA, which randomly integrates into the zebrafish genome. The result of the mosaic approach is transgene integration and expression in some of the somatic cells in a tissue but not necessarily all of the cells. Furthermore, there is variation in the proportion of somatic cells that express the transgene across different individual F0 zebrafish (208). This method was utilised in a zebrafish model of brain cancer whereby human oncogenic *KRAS* G12V was transiently expressed under the control of the cytokeratin 5 (*krt5*) and glial fibrillary acidic protein (*gfap*) promoters and led to brain tumourigenesis (205). This method has been hypothesised to more closely recapitulate human tumourigenesis, which more commonly arises due to genetic alterations in somatic cells (208).

Allograft zebrafish cancer models exist for several cancer types. The main advantage over mouse transplantation cancer models is the ability to graft more animals in less time and lower cost as well as better imaging resolution of the engrafted cancer cells (209).

Transplanted zebrafish T cell lymphoma cells (driven by *MYC*) transplanted into irradiated adult zebrafish migrate to the thymus suggesting the zebrafish thymus gland is a supportive microenvironment for T cell lymphoma cells (188). Other zebrafish cancers that have been successfully transplanted include B cell acute lymphoblastic leukaemia, melanoma, pancreatic cancer, hepatocellular carcinoma, and Ewing's sarcoma (209). Transplantation of fluorescently labelled cancer cells enables the study of the tumour initiation and metastatic progression (210).

Xenotransplantation of human cancer cells into zebrafish embryos that have not yet developed a fully functional immune system has been reported (211). Fluorescent labelled human pancreatic cancer cells (derived from human patients) transplanted into the yolk sac of 2-day old zebrafish embryos disseminated and spread to the liver, gut and intestines. Transplantation of human non-malignant pancreatic cells using the same technique failed to

metastasise suggesting that this model could demonstrate the progression behaviour of human cancer (211).

### **1.10. Spontaneous Urinary Tract Cancers in Fish**

There is no literature on spontaneous urinary tract cancer development in zebrafish. Other fish species have been demonstrated to develop urinary tract cancers(212). There are 10 cases described of the *Astronotus ocellatus* species of fish (Also known as the Oscar species [from cichlid family](213)) developing epithelial tumours of the urinary tract. Four neoplasms in the National Cancer Institute's Registry of Tumours in Lower Animals archive have been reported as likely originating from the 'transitional epithelium of the renal collecting ducts and urinary bladder' in the Oscar species. These tumours were interpreted as being 'urothelial adenopapillomas of the urinary bladder'. There are two lesions of the mesonephric duct that have been described in another teleost species, the rainbow trout, that were exposed to Methylnitronitrosoguanidine (MNNG) (212).

### **1.11. Project Aims and Objectives**

The aims and objectives of my project are as follows:

1. To perform an up-to-date systematic review of the epidemiology and risk factors for bladder cancer.
2. To perform a characterisation of the zebrafish urinary tract and determine the homology of the zebrafish system to the human system with respect to structure and histological characteristics.
3. To develop a dissection technique to isolate the urinary bladder from culled adult zebrafish that can be used for future downstream applications.
4. To study the development of the zebrafish urinary bladder with respect to morphological change during the larval and juvenile stages.
5. To identify and characterise spatial and temporal reporter gene expression pattern of transgenic zebrafish urinary tract reporter lines in order to determine their feasibility for use in a cancer model.

6. To develop a transgenic zebrafish urinary tract cancer model using genomic alterations associated with bladder cancer (combination of *HRAS* overexpression and *tp53* mutation).
7. To histologically analyse potential zebrafish urinary tract tumours arising from my newly developed model.

## Chapter 2. Materials and Methods

### 2.1. Zebrafish Husbandry

Zebrafish were housed and raised in accordance with UK Home Office legislature (Animals (Scientific Procedures) Act 1986) at the approved biological services aquaria, Bateson centre, University of Sheffield under PPL5320710 and PILI82542068. Zebrafish were maintained using standard conditions. These include maintenance at a temperature of 28 degrees in a closed aquarium system with a continuous recirculating water supply. The aquaria facility maintained a daily light cycle of 14 hours of light and 10 hours of dark (214).

Zebrafish embryos were acquired either through pair mating or marbling. Pair mating involved placing a male and female zebrafish in a specific zebrafish pair mating tank with a divider in between the day before. The following morning the divider was released at the onset of lights turning on (at 8am) to allow mating to occur. Alternatively, marbling involved placing a marbling tank into a tank of zebrafish (containing males and females) the night before and collecting zebrafish embryos the following day. Zebrafish embryos were collected using a strainer. Zebrafish embryos were placed into a petri dish of E3 media. 10xE3 media is made up as follows: 2.867 g sodium chloride (5.00 mM), 0.127 g potassium chloride (0.17 mM), 0.483 g calcium chloride dihydrate (0.33 mM), 0.817 g magnesium sulphate heptahydrate (0.33 mM) and deionised water up to 1 litre, followed by autoclave. The 10x stock is subsequently diluted to 1x working solution as follows in deionised water and 1 drop of methylene blue (Sigma 50484) is added per litre of 1x working solution. Unfertilised embryos were removed later that day to avoid contamination.

Pre 5.2pf zebrafish embryos were raised in a petri dish of E3 media with no more than 60 animals per plate in an incubator. Dead embryos were removed from the plate to avoid contamination of the E3 media.

Zebrafish were placed on the aquarium system from day 5.2 post fertilisation (pf) at the point of independent feeding. After day 5.2pf, zebrafish were fed twice daily at which point

their health condition was also observed. Procedures performed on zebrafish prior to day 5.2pf were not subject to home office legislation.

Zebrafish were sacrificed with a schedule 1 technique which usually involved an overdose of tricaine anaesthesia (primary method) and a secondary method which included: confirmation of cessation of circulation under a microscope, destruction of the brain with a pin, or confirmation of rigor mortis.

The only regulated procedures performed on zebrafish post 5.2pf were a) immersion fixation culling and b) imaging under anaesthetic followed by recovery. Immersion fixation is a technique whereby zebrafish were anaesthetised in tricaine followed by immersion in fixative to maximally preserve tissues for downstream histological applications. Imaging under anaesthetic followed by recovery involves anaesthetising zebrafish to perform imaging followed by recovery from the anaesthetic under close observation and return to its tank.

## 2.2. Zebrafish Lines

The zebrafish lines (Mutant/transgenic or wild type) used and maintained during this project are below in Table 5.

Zebrafish Line Name	Transgenic/Mutant/Enhancer Trap/Wild Type	Stable vs F0 generation	Presence of Transgene Selection Marker in Line (Yes/No)	Origin	Reference (If present)
<i>Et(gSAIzGFFD)875b; Tg(UAS: GFP)</i>	Transgenic and Enhancer trap	Stable	No	Kawakami Lab, National Institute of Genetics, Mishima, Japan	(215)
<i>tp53<sup>+/zdf1</sup></i>	Mutant	Stable	N/A	Originally from Zebrafish International Resource Centre (ZIRC). Kind gift from Dr Catarina Enriques	(194)

<p><i>tp53<sup>+/zdf1</sup>,</i>  <i>Et(gSAIzGFFD)875b;</i>  <i>Tg(UAS: GFP)</i></p>	<p>Mutant and Enhancer trap</p>	<p>Stable</p>	<p>No</p>	<p>Generated from crosses, screening for GFP and genotyping offspring in Biological Services Aquaria, Bateson Centre, University of Sheffield</p>	<p>N/A</p>
<p><i>tp53<sup>+/zdf1</sup>,</i>  <i>Et(gSAIzGFFD)875b</i></p>	<p>Mutant and Enhancer trap</p>	<p>Stable</p>	<p>No</p>	<p>Generated from crosses, screening for GFP and genotyping offspring in Biological Services Aquaria, Bateson Centre, University of Sheffield</p>	<p>N/A</p>

<i>Et(gSAIzGFFD)875b</i>	Enhancer trap	Stable	No	Generated from crosses, screening for GFP and genotyping offspring in Biological Services Aquaria, Bateson Centre, University of Sheffield	(215)
<i>tp53<sup>zdf1/zdf1</sup>, Et(gSAIzGFFD)875b</i>	Mutant and Enhancer trap	Stable	No	Generated from crosses, screening for GFP and genotyping offspring in Biological Services Aquaria, Bateson Centre, University of Sheffield	N/A
<i>Tg(UAS: Kaede)s1999t</i>	Transgenic	Stable	No	Renshaw Lab, Biological Services Aquaria, Bateson Centre, University of Sheffield	(216)

<i>Tg(cdh17: Gal4)</i> <i>sh681; Tg(UAS:</i> <i>Kaede) s1999t</i>	Transgenic	Stable	Yes ( <i>cdh17: Gal4</i> cassette contains <i>cmc:GFP</i> sequence leading to a GFP heart marker)	Made by Ibrahim Jubber	N/A
<i>Tg(cdh17: Gal4)</i> <i>sh681</i>	Transgenic	Stable	Yes ( <i>cdh17: Gal4</i> cassette contains <i>cmc:GFP</i> sequence leading to a GFP + as a selection marker)	Made by Ibrahim Jubber	N/A
<i>TgBAC(mpx: eGFP)</i> <i>i114</i>	Transgenic	Stable	No	Renshaw Lab , Biological Services Aquaria, Bateson Centre, University of Sheffield	(217)

<p><i>Tg(UAS: eGFP HRAS_G12V)io006</i></p>	<p>Transgenic</p>	<p>Stable</p>	<p>Yes (<i>UAS: GFP HRAS_G12V</i> cassette contains <i>cmc</i>:GFP sequence leading to a GFP + heart as a selection marker)</p>	<p>Dr Yi Feng, University, of Edinburgh</p>	<p>(218, 219)</p>
<p><i>Tg(UAS: GFP- CAAX)ed204</i></p>	<p>Transgenic</p>	<p>Stable</p>	<p>Yes (<i>UAS: eGFP- CAAX</i> cassette contains <i>cmc</i>:GFP sequence leading to a GFP + heart as a selection marker)</p>	<p>Dr Yi Feng, University of Edinburgh</p>	<p>(220)</p>

Wild type (Nacre)	Wild Type	Stable	N/A	Biological Services Aquaria, Bateson Centre, University of Sheffield	(221)
Wild type (AB)	Wild Type	Stable	N/A	Biological Services Aquaria, Bateson Centre, University of Sheffield	N/A
<i>tp53<sup>zdf1/zdf1</sup>,</i> <i>Et(gSAIzGFFD)875b;</i> <i>Tg(UAS: GFP-</i> <i>HRAS_G12V)</i>	Mutant, Transgenic and Enhancer trap	F0 generation (for UAS GFP HRAS_G12V component) and stable for GFF transgene and p53 mutation	Yes ( <i>UAS: GFP</i> <i>HRAS_G12V</i> cassette contains <i>cmIc:GFP</i> sequence leading to a GFP + heart as a selection marker)	Made by Ibrahim Jubber	N/A

<p><i>tp53<sup>zdf1/zdf1</sup>,</i>  <i>Et(gSAIzGFFD)875b;</i>  <i>Tg(UAS: GFP- CAAX)</i></p>	<p>Mutant, Transgenic and  Enhancer trap</p>	<p>F0 generation (for UAS  GFP CAAX component)  and stable for GFF  transgene and p53  mutation</p>	<p>Yes (<i>UAS: GFP-</i>  <i>CAAX</i> cassette  contains  <i>cmc:GFP</i>  sequence  leading to a GFP  + heart as a  selection  marker)</p>	<p>Made by Ibrahim Jubber</p>	<p>N/A</p>
<p><i>Et(gSAIzGFFD)875b;</i>  <i>Tg(UAS: GFP-</i>  <i>HRAS_G12V)</i></p>	<p>Transgenic and Enhancer trap</p>	<p>F0 generation (for UAS  GFP HRAS_G12V  component) and stable  for GFF transgene</p>	<p>Yes (<i>UAS: GFP-</i>  <i>HRAS_G12V</i>  cassette  contains  <i>cmc:GFP</i>  sequence  leading to a GFP  + heart as a  selection  marker)</p>	<p>Made by Ibrahim Jubber</p>	<p>N/A</p>

<p><i>Et(gSAIzGFFD)875b;</i> <i>Tg(UAS: GFP- CAAX)</i></p>	<p>Transgenic and Enhancer trap</p>	<p>F0 generation (for UAS GFP CAAX component) and stable GFF transgene</p>	<p>Yes (<i>UAS: GFP- CAAX</i> cassette contains <i>cmIc:GFP</i> sequence leading to a GFP + heart as a selection marker)</p>	<p>Made by Ibrahim Jubber</p>	<p>N/A</p>
<p><i>tp53<sup>zdf1/zdf1</sup>,</i> <i>Et(gSAIzGFFD)875b;</i> <i>Tg(cdh17: GFP- HRAS_G12V)</i></p>	<p>Mutant, Transgenic and Enhancer trap</p>	<p>F0 generation (for Cdh17 GFP HRAS_G12V component) and stable for GFF transgene and p53 mutation</p>	<p>Yes (<i>cdh17: GFP- HRAS_G12V</i> cassette contains <i>cmIc:GFP</i> sequence leading to a GFP + heart as a selection marker)</p>	<p>Made by Ibrahim Jubber</p>	<p>N/A</p>

<p><i>tp53</i><sup>zdf1/zdf1</sup>,  <i>Et(gSAIzGFFD)875b</i>;  <i>Tg(cdh17: GFP-CAAX)</i></p>	<p>Mutant, Transgenic and  Enhancer trap</p>	<p>F0 generation (for  Cdh17 GFP CAAX  component) and stable  for GFF transgene and  p53 mutation</p>	<p>Yes (<i>cdh17: GFP-CAAX</i> cassette  contains  <i>cmIc:GFP</i>  sequence  leading to a GFP  + heart as a  selection  marker)</p>	<p>Made by Ibrahim Jubber</p>	<p>N/A</p>
--	--	---	--	-------------------------------	------------

**Table 5. Zebrafish Lines Maintained During This Project.**

New zebrafish lines sent from other facilities only came from zebrafish facilities that were approved by the biological services aquaria at the Bateson Centre, University of Sheffield. New zebrafish lines sent from other labs outside of the biological services aquaria were held in a quarantine facility to prevent spread of disease. Offspring embryos were then bleached before being taken out of quarantine and put on the main biological services aquarium system.

The *Et(gSAIzGFFD)875b; Tg(UAS: GFP)* enhancer trap and transgenic zebrafish were outcrossed to *tp53<sup>+/zdf1</sup>* zebrafish (originally from ZIRC and kindly donated by Dr Caterina Enriques) and the offspring were screened for GFP negative to identify those without the *UAS: GFP* transgene. These offspring were genotyped once they reached adulthood (Minimum 3 months of age) for the *GFF* transgene (see methods for *GFF* primers) and the *tp53 zdf1* mutation (see methods for *tp53* primers and restriction digest). The *tp53<sup>+/zdf1</sup>* zebrafish (Heterozygous for mutation) that were positive for the *GFF* transgene were raised to adulthood and incrossed. The offspring were subsequently genotyped once they reached adulthood for the presence of the *GFF* transgene (see methods for *GFF* primers) and for homozygous and wild type for the *tp53 zdf1* mutation (see methods for *p53* primers and restriction digest).

### **2.3. Zebrafish One Cell Stage Microinjection**

Zebrafish one cell stage microinjection was performed following a training programme approved by the biological services aquaria (It is a regulated procedure to raise zebrafish embryos that were injected at the one cell stage). The day before injection, zebrafish were paired using pair mating tanks with a divider in between males and females. The following morning, at the onset of the lights coming on (8am), eggs were collected and injected within 15 minutes. Injections were performed using glass capillary needles prepared in advance using a micropipette puller (Sutter Instrument Model P-1000 Flaming). The Injection mixture was composed of *tol2* mRNA (50ng/ul), plasmid (10-50ng/ul), RNase free water (Qiagen 169041483) and phenol red. A WPI Pneumatic PicoPump PV820 injection rig was used for microinjection. A graticule was used to measure the injection volume to be delivered. A

total of 0.5-1nl was used for injection. The eggs were pipetted on a petri dish and aligned against a histology slide under a microscope. The injection was performed through the chorion and either into the cell or the yolk (Figure 15). The injected eggs were subsequently added to a petri dish of E3 and placed in an incubator with no more than 50-60 embryos per petri dish. Dead or unfertilised eggs were removed later in the day to prevent contamination of the E3 media.

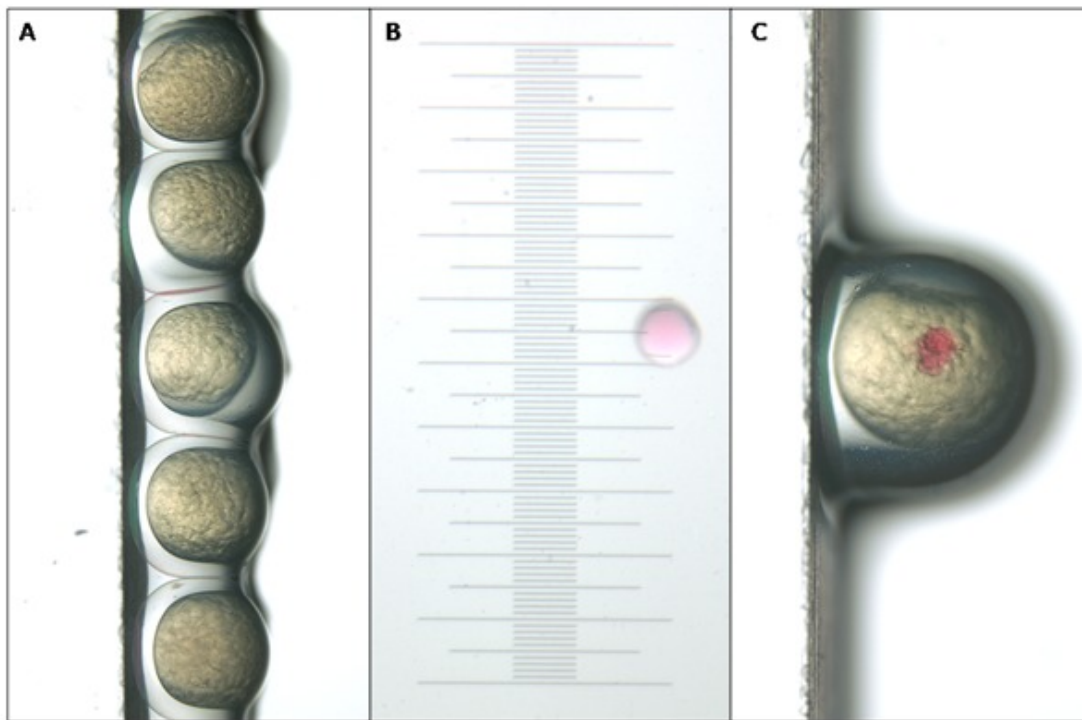


**Figure 15. One Cell Stage Microinjection Technique.**

(A) One cell stage embryos are lined up in a petri dish against a microscope slide. (B) The injection volume is calibrated using a graticule. (C) Microinjection is performed into the yolk of the one cell stage embryos and successful injection is confirmed by the presence of a distinct red dot in the yolk (due to the presence of phenol red in the injection mixture). Adapted from Rosen et al 2009 (222). Image re-used with permission.

## **2.4. Zebrafish Dissection**

Zebrafish dissection was performed on zebrafish between the ages of 4 weeks old to adults. They were sacrificed using a schedule 1 technique (Immersion in tricaine followed by destruction of the brain). The technique to dissect open the zebrafish in order to expose the kidney/urinary tract was modified from Gerlach et al 2011 (30). Equipment required included 4% agarose dissection plate (Molecular grade agarose, Meridian biosciences BIO-41025), tricaine MS222 bath, Leica light microscope, dissection pins, spring scissors and fine forceps. The 4% dissection plate was made using the same technique as an agarose gel (16g molecular grade agarose per 100mls distilled water) and poured into a petri dish and left to set. Following schedule 1 cull, the head was removed followed by incision of the ventral abdominal wall from the cut end of the head to the anal fin. The lateral abdominal walls were pinned to the dissection plate so that the ventral surface of the zebrafish was facing up. The gut, swim bladders, gonads and loose areolar tissue was removed to expose the urinary tract along the dorsal abdominal wall.

## **2.5. Mounting Zebrafish for Fluorescent Microscopy Imaging**

In order to image zebrafish live, they were first anaesthetised. The ages of the zebrafish that were imaged ranged from embryos at around 20 hours post fertilisation up to a maximum of 4 weeks post fertilisation at the juvenile stage. This involved adding tricaine anaesthetic to zebrafish either in E3 media or aquarium water. The zebrafish were then mounted in 1% low gelling temperature agarose (Sigma A9414) with tricaine anaesthesia in a 4 well mounting dish (Ibidi). In order to make the 1% low gelling temperature agarose, 0.1g of low gelling temperature agarose powder was added to 9.5mls E2 and 420 ul of tricaine was added to this. It was microwaved until the powder was dissolved and the temperature was maintained at 42 degrees in a heat block until it was needed. Anaesthetised zebrafish were oriented laterally with the head on the left and the tail on the right under a microscope and the warm low gelling temperature agarose was added and allowed to set.

## **2.6. Zebrafish Timelapse Imaging**

Live timelapse imaging performed on the Zeiss Z1 Lightsheet microscope. Zebrafish embryos were first dechorionated. The Lightsheet microscope chamber was filled with E3 with tricaine (1ml per 25mls). 1% low gelling temperature agarose was placed on the zebrafish and they were then drawn up into a capillary. The capillary was loaded into the Lightsheet system for imaging. Fluorescent microscope (GFP channel) and brightfield channel images were taken every 15 minutes.

## **2.7. Fin clipping, Genomic DNA Extraction and Genotyping Zebrafish**

Zebrafish genotyping via fin clipping was performed by the Bateson Centre Aquaria Genotyping service (By Lisa Van Hateren). Zebrafish were first anaesthetised in tricaine (4.2ml per 100mls aquarium water). No greater than 1/3 of the caudal fin was clipped and placed into a PCR tube containing 100 $\mu$ l 50mM sodium hydroxide. Fin clipped zebrafish were then placed into a single tank with an assigned number that corresponded to a number on the PCR tube.

To extract DNA from the fin clip samples, the sample was boiled at 98°C for 5 mins followed by cooling the tube at 4°C for 10 mins. A total of 10 $\mu$ l (1/10 volume of sodium hydroxide) 1M Tris pH 8 was then added and the sample was vortexed. Finally, the sample was spun down for 10 minutes at full speed (4,200 RPM).

The PCR reactions for genotyping zebrafish were assembled as follows (Total volume of reaction was 10 $\mu$ l): 1 $\mu$ l Genomic DNA, 2 $\mu$ l 5x FirePol PCR Master mix (Thistle Scientific) 0.2 $\mu$ l forward primer (10 $\mu$ M) , 0.2 $\mu$ l reverse primer (10 $\mu$ M) and 6.6 $\mu$ l Water.

The primers used for genotyping are below:

Primer name	Primer sequence	Source of Primer Sequences
<i>tp53</i> Forward Primer	ACATGAAATTGCCAGAGTATGTGTC	Zebrafish International Resource Centre
<i>tp53</i> Reverse Primer	TCGGATAGCCTAGTGCGAGC	
<i>GFF</i> Forward Primer	TATCGAGCAGGCTTGTGACA	Designed (Primer 3) and optimised by Ibrahim Jubber
<i>GFF</i> Reverse Primer	ATCAGTCTCCACACTTGCCA	

The PCR settings used for genotyping are below:

#### ***GAL4FF* (Also referred to as *GFF*) Transgene**

Step 1: Initial Denaturation	95°C for 2 mins
Step 2: Denaturation	95°C for 30 sec
Step 3: Annealing	62°C for 30 sec
Step 4: Elongation	72°C for 30 sec
Step 5: Repeat steps 2-4	Go to step 2, Cycle x29
Step 6: Final Elongation	72°C for 10 min
Step 7: End Stage	Hold at 12 °C

#### **Zebrafish *tp53* gene**

Step 1: Initial Denaturation	95°C for 3 mins
Step 2: Denaturation	95°C for 30 sec
Step 3: Annealing	53°C for 30 sec
Step 4: Elongation	72°C for 30 sec
Step 5: Repeat steps 2-4	Go to step 2, Cycle x39
Step 6: Final Elongation	72°C for 5 min
Step 7: End Stage	Hold at 12 °C

Genotyping for the zebrafish *tp53* mutation (*M214K*, *zdf1*) utilises the Restriction Fragment Length Polymorphism (RFLP) assay. This system is used to detect a mutation that either creates or removes a site that is recognised by a specific restriction enzyme. The *tp53 zdf1* mutation creates a mutation site recognised by the MbolI restriction enzyme. An MbolI restriction enzyme digest was used to genotype for the presence of the *tp53* mutation using the following quantities: MbolI enzyme (NEB) (0.5µl), water (0.5ul), PCR reaction mixture containing amplified DNA fragment (4ul). The incubation temperature used was 37 degrees for a total of 2 hours.

PCR reaction for the *GFF* transgene produces a band size of 334bp on gel electrophoresis. PCR reaction for the wild type *tp53* gene produces a band size of 336bp on gel electrophoresis. MbolI diagnostic digest of the *tp53* gene fragment in the presence of homozygous *M214K* mutation (from the PCR reaction) results in digestion into two fragments – 196bp and 140bp on gel electrophoresis. Heterozygous *tp53 M214K* mutation results in 3 bands- the wild type 336bp band and the two digest bands – 196bp and 140bp on gel electrophoresis. Agarose gel electrophoresis of the genotyping process for *GFF* transgene (PCR only) and *tp53 zdf1* mutation (PCR and diagnostic digest) is shown below (Figure 16).

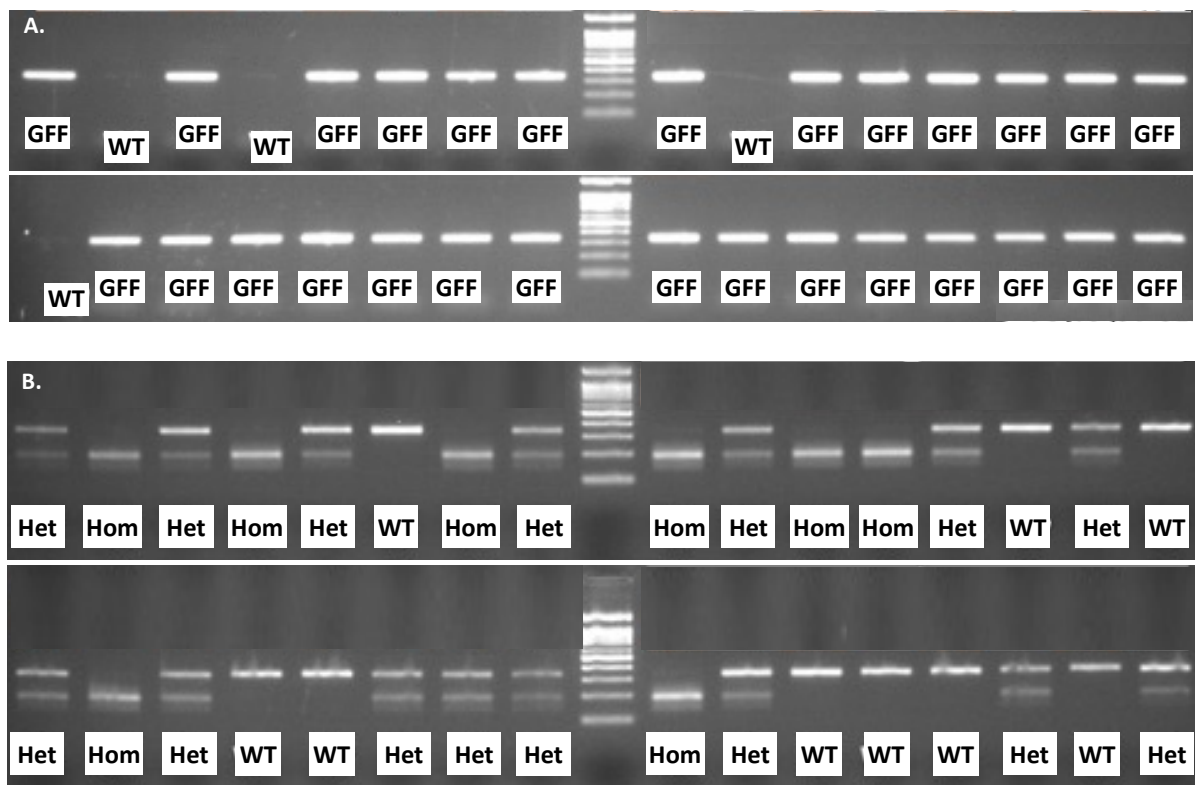


**Figure 16. Genotyping for *GFF* transgene and *tp53 zdf1* mutation.**

Agarose gel electrophoresis of PCR amplified DNA fragments from genomic DNA. (A) Representative example of genotyping on 32 zebrafish PCR amplified DNA samples from genomic DNA using PCR primers for *GFF* transgene. *GFF* DNA fragment length: 334bp. (B) Representative example of genotyping of 32 zebrafish PCR amplified DNA samples from genomic DNA using primers for zebrafish *tp53* gene followed MbolI diagnostic digest to identify zebrafish with *tp53 zdf1* mutation. Wild type (WT) band is 336bp. Homozygous *tp53<sup>zdf1/zdf1</sup>* mutant (Hom) is two bands: 196 and 140bp. Heterozygous *tp53<sup>+/zdf1</sup>* mutant (Het) has all 3 bands.

## 2.8. Zebrafish *in situ* hybridisation

This work was performed by laboratory technician Maggie Glover. For digoxigenin-labelled RNA probe production, the probe for *uroplakin 1a* was synthesized from linearized plasmid DNA obtained from a plasmid vector containing the coding sequence. The coding sequence was contained in the p-express 1 plasmid. The Zebrafish Information Network (ZFIN) was searched for details regarding zebrafish *upk1a* cDNA (MGC: 136832, Accession number: GenBank: BC115285). A cDNA clone for *upk1a* was obtained from Source BioScience, Nottingham, UK. This *upk1a* cDNA clone was then inserted in the p-Express 1 vector between EcoRV (744) and NOT1 (735) restriction sites. For the antisense *uroplakin 1a* probe, the p-express 1 plasmid was linearized using the EcoRI restriction enzyme and the T7 RNA polymerase enzyme was used for transcription. For the sense *uroplakin 1a* probe, the p-express 1 plasmid was linearized using the NotI restriction enzyme and the SP6 RNA polymerase enzyme was used for transcription. Whole-mount *in situ* hybridization was performed using standard procedures (223).

## 2.9. Whole Mount Zebrafish EdU Proliferation Assay

The 5-ethynyl-2'-deoxyuridine (EdU) proliferation assay was performed in whole mount zebrafish larvae using the Click-it EdU Cell Proliferation Kit (Thermofisher C10340) with Alexa Fluor 647 dye (Thermofisher C10340). Unless otherwise stated all washes and incubation steps were performed at room temperature with light shaking (4 RPM). 10mM EdU (diluted in DMSO) or DMSO as a control (1 in 20 dilution in RNase free water) was injected into the yolk (2nl volume) at 3 dpf and the larvae were incubated in E3 for 20 hours in the dark at 28 degrees before fixation in 4% PFA for 30 minutes. The larvae were washed in PBST (0.5% Triton X in PBS [OXOID, BR0014G]) and subsequently incubated in 3% Bovine Serum Albumin (BSA) diluted in PBST for 1 hour. The larvae were incubated in reaction mix (1x Clickit reaction buffer [440µl], copper protectant [10µl], Alexa Fluor picolyl azide [1.2µl] and 1x Clickit EdU buffer additive [50µl]) for 30minutes. The reaction mix was scaled up as necessary using the same ratios.

At this stage, whole mount immunohistochemistry staining for GFP was performed (See section 2.10. ). Following a PBST wash, the larvae were subsequently stained with Hoechst 33342 (1:1000 dilution in PBST) for 30 minutes. The protocol was completed with a PBST wash. The whole mount zebrafish were kept in the dark until imaging.

## **2.10. Whole Mount Zebrafish Immunohistochemistry**

Zebrafish larvae underwent whole mount immunohistochemistry staining with an anti-GFP antibody (abcam6556, rabbit polyclonal). This protocol involved fixation with 4% PFA for 30 minutes at room temperature. Fixation was followed by permeabilization (performed by washing in 0.5% triton X in PBS (PBST) for 5 minutes at room temperature on a rocker three times). Zebrafish larvae were incubated in 5% sheep serum block (diluted in PBST) for 2 hours followed by incubation in the anti-GFP antibody (1:200 dilution in, diluted in 5% sheep serum in PBST) overnight at 4 degrees on a shaker. This was followed with a PBST wash followed by incubation with a secondary antibody (Goat Anti-Rabbit IgG H&L Alexa Fluor 488 [abcam ab150077], 1:250 dilution, diluted in 3% sheep serum in PBST) for 2 hours at room temperature. This step is followed by a PBST wash.

## **2.11. Histology**

### **2.11.1. Zebrafish Histology**

Zebrafish were fixed by immersion fixation in 4% PFA for 2-4 days at 4 degrees. Immersion fixation is a regulated procedure that involves immersion in tricaine anaesthetic until the zebrafish is non-responsive, followed by immersion in 4% PFA. The 4% PFA was either purchased in solution (Sigma Aldrich 1004965000) or made up from powder (Fisher Scientific P/0840/53) in PBS and heated overnight on a heated stirrer at 70 degrees until dissolved.

Zebrafish aged older than 3 weeks were decalcified in 0.25-0.5M EDTA for 2-4 days (either purchased [Invitrogen AM9262] or made up from powder [Fisher Scientific D/0700/53] in distilled water) and then placed in 70% ETOH. Zebrafish were then placed on the tissue processor by the histology technician team. Tissue processor settings were as below:

<b>Tissue processing reagent</b>	<b>Duration</b>
70% alcohol	2 hours
70% alcohol	2 hours
70% alcohol	2 hours
95% alcohol	2 hours
95% alcohol	2 hours
100% ETOH	2 hours
100% ETOH	2 hours
Xylene 1	2-3 hours
Xylene 2	2-3 hours
Wax 1	2-3 hours
Wax 2 (Under vacuum)	2-3 hours

Processed zebrafish were then wax embedded in cassettes. They were oriented in 3 possible orientations: (1) sagittal [enables lateral surface to lateral surface sectioning], (2) coronal [enables ventral to dorsal sectioning] or (3) transverse [enables caudal to rostral sectioning]. Zebrafish wax specimens were sectioned on a microtome at 3.5 – 5 micron thickness on charged slides.

### **2.11.2. Human Control Histology Samples**

Human urinary bladder and ureter specimens were obtained with the ethical approval of the South Yorkshire Research Ethics Committee (REC reference number: 10/H1310/73).

### **2.11.3. H&E staining**

Wax sections were first dewaxed in two xylene pots for 5 minutes each. Sections were then transferred to two absolute alcohol pots for 3 minutes each. Sections were then rehydrated by transferring them to 95% or 90% alcohol followed by 70% alcohol pots for 3 minutes each. A 1-minute rinse in tap water is then performed followed by immersion in Gill's haematoxylin to stain the nuclei for approximately 1 minute. The Gill's haematoxylin is then

washed under tap water until the water runs clear. The sections are then immersed in pots of increasing alcohol concentrations for 3 minutes each (70% and 90% or 95%). The sections are then immersed in 1% eosin in 95% alcohol for approximately 1 minute to stain the extracellular matrix and cytoplasm. The sections are then immersed in two consecutive pots of absolute alcohol for 3 minutes each and then two consecutive pots of xylene for 5 minutes. Finally, cover slips are mounted to the slides using Dibutylphthalate Polystyrene Xylene (DPX) mountant.

#### **2.11.4. Immunohistochemistry (FFPE): ABC DAB method**

The ABC DAB method was used for immunohistochemistry. All reagents used for FFPE immunohistochemistry are listed in Table 6. Wax sections were first dewaxed in two xylene pots for 5 minutes each. Sections were then transferred to an absolute alcohol pot for 5 minutes followed by a second absolute alcohol pot for 3 minutes. Sections were then rehydrated by transferring them to a 95% alcohol pot for 3 minutes. To block endogenous peroxidases, sections were immersed in 3% hydrogen peroxide. Heat induced antigen retrieval was performed either with an antigen retrieval pressure cooker or a microwave and antigen retrieval solution. For some of the experiments (details below), avidin/biotin block (Vector laboratories/2B Scientific SP-2001) was applied to the slides. Non-specific binding sites were blocked either with animal sera (10% goat or rabbit sera) or 10% casein (Sigma B6429-500ml, diluted in PBS). The primary antibody was applied for either 1 hour at room temperature or overnight in the fridge (diluted in 2% animal sera or 1% casein). A biotinylated secondary antibody was diluted in 2% sera or 1% casein and applied for 1 hour. The avidin-biotin complex (ABC) solution (Vector laboratories/2B Scientific Vectastain Elite ABC-HRP Kit, Peroxidase, Standard PK-6100) was applied for a total of 30 minutes. The DAB substrate (Vector laboratories/2B Scientific DAB substrate kit, peroxidase [HRP] SK-4100) was applied for 2-9 minutes. Slides were subsequently stained with Gill's haematoxylin for approximately 1 minute and rinsed with tap water for 2 minutes. Finally, slides were dehydrated by immersing in pots with increasing concentrations of alcohol (3 minutes each) followed by immersing in a pot of xylene. Cover slips were mounted to the slides with DPX mountant.

<b>Primary Antibody name</b>	<b>Reference (if available)</b>	<b>Origin and code</b>	<b>Host species and clonality</b>	<b>Antigen retrieval</b>	<b>Dilution</b>	<b>Non-specific block</b>	<b>Primary antibody Incubation details</b>	<b>Secondary antibody</b>
Uroplakin 1a (N-16)	Not available	Santa cruz sc-15170	Goat polyclonal	0.01M citrate boiled in microwave	1:400 dilution for zebrafish and 1:200 human	Rabbit sera	Overnight at 4 degrees	Biotinylated Rabbit anti-goat 1:200 dilution (Vector Laboratories now 2b Scientific)
Uroplakin 2 (k-18)	Not available	Santa cruz sc-15179	Goat polyclonal	0.01M citrate boiled in microwave	1:400 dilution for zebrafish tissue and 1:100 to 1:400 dilution for human tissue	Rabbit sera	Overnight at 4 degrees	Biotinylated Rabbit anti-goat 1:200 dilution (Vector Laboratories now 2b Scientific)

Cytokeratin 5/6	(224)	Dako M7237	Mouse monoclonal	Dako pH 9 in pressure cooker	1:100 to 1:200 dilution for zebrafish tissue and 1:100 dilution for human tissue	Goat sera	Overnight at 4 degrees	Biotinylated Goat anti- mouse 1:200 dilution (Vector Laboratories now 2b Scientific).
Gata3	(225)	Sigma Aldrich SAB2100898	Rabbit poly- clonal	Dako pH 6 in pressure cooker	1:400 dilution for zebrafish tissue and 1:100 dilution for human tissue	Goat sera	Overnight at 4 degrees	Biotinylated Goat anti- rabbit 1:200 dilution (Vector Laboratories now 2b Scientific),

CD44	(226)	Sigma Aldrich SAB1405590	Mouse mono- clonal	Dako pH 6 in pressure cooker	1:400 dilution for zebrafish tissue and 1:50 dilution for human tissue	Goat sera	Overnight at 4 degrees	Biotinylated Goat anti- mouse 1:200 dilution (Vector Laboratories now 2b Scientific).
AE1/AE3	(227)	Abcam 961	Mouse mono- clonal	Dako pH 6 in pressure cooker	Pre-diluted	Casein	1 hour at room temp	Biotinylated Goat anti- mouse 1:200 dilution (Vector Laboratories now 2b Scientific).

Pax8	(228)	Abcam 227707	Rabbit mono- clonal	EDTA pH8 100x (Abcam, ab93680 ) in pressure cooker	1:100 and 1:200	Casein	1 hour at room temperature	Biotinylated Goat anti- rabbit 1:200 dilution (Vector Laboratories now 2b Scientific)
------	-------	-----------------	---------------------------	---	--------------------	--------	-------------------------------	--

**Table 6. Reagents Used for Immunohistochemistry Experiments.**

### **2.11.5. Masson's Trichrome**

Bouin's fixative was heated to 56 degrees for 1 hour. Sections were deparaffinised in decreasing concentrations of ethanol followed by hydration in distilled water. Tissue sections were mordanted in Bouin's solution for 1 hour at 56 degrees to improve staining quality and then subsequently rinsed in tap water until the yellow colour disappeared. Weigert's haematoxylin was applied onto the slides for 15 minutes. Slides were then washed in tap water and immersed in 1% acid alcohol (5mls HCL made up to 100mls in 70% ETOH) five times. Ponceau fuchsin (0.5% Ponceau 2R in 1% acetic acid and 0.5% acid fuchsin in 1% acetic acid [Mix 2 parts ponceau and 1 part acid fuchsin]) was then applied to the slides for 8 minutes followed by a wash in distilled water. Slides were dipped in phosphomolybdic acid (5% phosphomolybdic acid in distilled H<sub>2</sub>O) solution until the red colouration in the connective tissue lightened to colourless and this was followed by a wash in tap water. Slides were then dipped in light green stain (2% light green in 2% acetic acid) until the connective tissue stained. Slides were subsequently washed in tap water, and this was followed by dehydration through a series of increasing concentrations of alcohol. Finally, slides were immersed in xylene and then mounted with DPX mountant.

### **2.11.6. Histological Analysis**

All histology images were reviewed with a pathologist.

## **2.12. Molecular Biology**

### **2.12.1. Agarose Gel Electrophoresis**

Agarose gel electrophoresis was performed to either quantify DNA or RNA or determine nucleotide sequence size. Molecular grade agarose was added to 1xTAE (diluted from a 50x stock) and heated in the microwave until dissolved. A 50xTAE solution is made up of 242 g Tris base, 57.1ml Glacial Acetic Acid, 100mls 500mM EDTA pH 8 and then made up to 1 litre in distilled water. Sybre Safe DNA gel stain (Invitrogen S33102) was subsequently added (3ul per 50mls of liquid agarose). The agarose liquid was then added to a mould with a comb and allowed to set. The gel tank was filled to the fill line with TAE and the set gel was added. DNA ladder was pipetted into the well (NEB or Bioline). The loading buffer was added to

each sample (x6 concentration, NEB B7024S) and samples were loaded. Voltage and time depended on the nature of the nucleotide fragments that needed separating. Samples were interpreted on a UV gel reader in a dark room.

### 2.12.2. Plasmids

The following plasmids used during this project are listed below in Table 7:

Plasmid Name	Type of plasmid	Selective Antibiotic Resistance	Origin	Reference if available
pDestTol2CG2- <i>UAS:GFP- HRAS_G12V</i>	Expression vector	Carbenicillin	Dr Yi Feng	Not available
pDestTol2CG2- <i>UAS:GFP-CAAX</i>	Expression vector	Carbenicillin	Dr Yi Feng	Not available
pDestTol2CG2, <i>crya:Venus-UAS: fgfr3-2A-eGFP</i>	Expression vector	Carbenicillin	Dr Alexa Burger	(229)
pDestTol2CG2, <i>crya:Venus- UAS:eGFP</i>	Expression vector	Carbenicillin	Dr Alexa Burger	(229)
pDestTol2CG2- <i>cdh17:GFP- HRAS (G12V)</i>	Expression vector	Carbenicillin	Made by Ibrahim Jubber	Not available
pDestTol2CG2- <i>cdh17: GFP- CAAX</i>	Expression vector	Carbenicillin	Made by Ibrahim Jubber	Not available
pDestTol2CG2- <i>cdh17:erbb2(A301F)- GFP</i>	Expression vector	Carbenicillin	Made by Ibrahim Jubber	Not available

pDestTol2CG2- <i>cdh17: pik3ca</i> (E545K)- GFP	Expression vector	Carbenicillin	Made by Ibrahim Jubber	Not available
pDestTol2CG2- <i>cdh17: Gal4</i>	Expression vector	Carbenicillin	Dr Iain Drummond	Not available
pT2KXIGdeltaIN- <i>enpep: GFP</i>	Expression vector	Carbenicillin	Dr Martin Lowe	Not available
pDestTol2CG2- <i>enpep: Gal4</i>	Expression vector	Carbenicillin	Dr Freek Van Eeden	Not available
pME- GFP- <i>HRAS(G12V)</i>	Gateway entry clone	Kanamycin	Dr Yi Feng	Not available
pME- GFP -CAAX	Gateway entry clone	Kanamycin	Tol2 kit	(230)
pME- <i>erb2 (A301F)</i> - GFP	Gateway entry clone	Kanamycin	Designed by Ibrahim Jubber and synthesised by Thermofisher	Not available
pME- <i>pik3ca</i> (E545K)- GFP	Gateway entry clone	Kanamycin	Designed by Ibrahim Jubber and synthesised by Thermofisher	Not available
p5E- <i>cdh17</i>	Gateway entry clone	Kanamycin	Dr Iain Drummond	Not available
p3E- <i>polyA</i>	Gateway entry clone	Kanamycin	Tol2 kit	(230)
p3E-GFP- <i>poly A</i>	Gateway entry clone	Kanamycin	Tol2 kit	(230)

p5E-4x UAS	Gateway entry clone	Kanamycin	Tol2 kit	(230)
pDestTol2CG2 (Contains <i>cmlc: GFP</i> nucleotide sequence for GFP+ heart selection marker)	Destination vector	Carbenicillin and Chloramphenicol	Tol2 kit	(230)
pCS2FA-transposase	Vector used as template for <i>in vitro</i> transcription of tol2/transposase mRNA	Carbenicillin	Tol2 kit	(230)

**Table 7. Plasmids Used During This Project.**

### 2.12.3. Restriction Enzymes

The following restriction enzymes were used during this project and were purchased from NEB: MbolI, NcoI, NotI, Bamh1, KpnI and Sall. Restriction enzyme digest reactions were performed according to the enzyme manufacturer's instructions. Briefly, restriction enzyme reactions consisted of the DNA sample, enzyme, enzyme buffer and nuclease free water (Qiagen 169041483). The total volume of the reactions was either 50ul or 30ul. The restriction enzyme reaction was subsequently run out on a gel to confirm successful digestion and the gel appearance was compared against a simulated successful diagnostic digest using SnapGene® software (from Dotmatics; available at [www.snapgene.com](http://www.snapgene.com)).

### 2.12.4. Bacterial Transformation

Plasmids were transformed using top ten chemically competent E coli (Thermofisher C404010). A total of 1-3 ul of plasmid was added to competent cells (1 vial of 50 ul used for up to 3 transformation reactions) and incubated on ice for 30 minutes. The bacteria were subsequently heat shocked for 30 seconds at 42 degrees using a pre-heated water bath. A total of 250ul of SOC media was added to the reaction. The reaction was then placed in a

shaking incubator at 37 degrees for 1 hour. The reaction was then spread on a prewarmed selective agar plate (Containing appropriate antibiotic at 50 µg/ml for kanamycin and carbenicillin or 30 µg/ml for chloramphenicol) and incubated overnight at 37 degrees in a regular incubator.

The following morning, single bacterial colonies were isolated with clean pipette tips and placed into 50mls of LB broth with appropriate antibiotic (at 50 µg/ml for kanamycin and carbenicillin or 30 µg/ml for chloramphenicol) in a conical flask with a soft bung. The bacteria were grown overnight in a shaking incubator at 37 degrees (12-16 hours).

#### **2.12.5. Plasmid Purification**

Following 12-16 hours of incubation of bacterial culture originating from a single bacterial colony (bacteria containing the plasmid), a glycerol stock was always made. To make a glycerol stock, 500ul of bacterial culture was added to 500ul of glycerol (Sigma G5516) in labelled cryovial and placed in the -80 degrees freezer.

The Nucleobond Midi DNA purification kit (Macherey Negel 740410.50) was used to isolate and purify plasmid from the bacterial culture. This is a column-based purification method. There are 3 types of prep in this kit depending on the amount of plasmid DNA required. The most common purification performed was midi prep (High copy plasmid purification). Manufacturer's instructions were followed. Briefly, this had the following steps (Summarised):

1. Cultivation and harvesting of bacterial cells: Centrifugation (4500-6000xg for 30 minutes followed by removal of supernatant.
2. Cell lysis: Addition of buffers S1, S2 and S3.
3. Equilibration of the column: Adding buffer N2 to Midi AX100 column and discarding the flow through.
4. Clarification of lysate and binding of plasmid to column: Pouring the lysate into folded filter paper positioned over the equilibrated Nucleobond column and discarding the flow through.

5. Washing the DNA in the column: Adding buffer N3 to the column and discarding the flow through.
6. Elution: Adding buffer N5 to the column and collecting the flow-through containing plasmid DNA.
7. Precipitation of a DNA pellet: Adding room temperature isopropanol to the eluted plasmid DNA, centrifugation at maximum speed for 30 minutes and removing the supernatant.
8. Washing DNA pellet: Adding room temperature 70% ethanol to the DNA pellet and centrifugation, centrifugation at maximum speed for 10 minutes followed by removal of the ethanol.
9. Drying of DNA pellet: Allowing the DNA pellet to dry at room temperature for 5 to 10 minutes.
10. Reconstitution of DNA: Dissolving the pellet in an appropriate volume of RNase free water (Depending on the desired concentration).

In situations needing a quick and efficient method to extract plasmid DNA from culture for to confirm plasmid identify but not for downstream plasmid use, a modified 'dirty' mini prep protocol was performed using the nucleobond plasmid purification kit (Macherey Negel). This method involves growing 5-6mls of bacterial culture containing the plasmid (single colony in LB broth incubated for 12-16 hours). A total of 2mls of grown culture (from the total 5-6mls bacterial culture) was used for this protocol. An initial centrifugation step was performed to pellet the bacterial cells for 1 minute at full speed. Once the supernatant was removed, the cell lysis step involved resuspending the bacterial cells in 250ul of solution S1. A total of 250ul of solution S2 was added and the mixture was inverted six times and incubated for 2 minutes at room temperature. A total of 250ul of S3 solution was added to this mixture followed by centrifugation at maximum speed for 10 minutes to precipitate impurities (white flocculate). The supernatant was transferred to a new 1.5ml Eppendorf. The precipitation step involved adding 750ul isopropanol, mixing vigorously and centrifugation for 10 minutes at maximum speed. The supernatant containing impurities was discarded. The precipitated DNA pellet was washed by adding 1ml 70% ethanol, mixing and centrifuging at room temperature at maximum speed for 10 minutes. The supernatant containing impurities and alcohol was discarded. The pellet containing pure plasmid DNA

was left to air dry at room temperature for 10 minutes. Finally, the pure DNA pellet was resuspended in an appropriate volume of RNase free water.

#### **2.12.6. DNA/RNA Quantification**

Several methods were used to estimate DNA/RNA concentration including: Nanodrop spectrophotometer, Beckman spectrophotometer, Qubit fluorometer 3.0 (Invitrogen) and Gel electrophoresis. Manufacturer's instructions were followed for the devices used.

The Qubit fluorometer enables more accurate nucleic acid quantification but requires the use of reagents and does not provide estimates of purity such as the 260/280 and 260/230 ratios that spectrophotometric methods provide. In order to quantify DNA with a Qubit fluorometer, the Qubit dsDNA quantitation broad range kit was used (Invitrogen Q32850). The kit contains a fluorogenic dye (Qubit dsDNA broad range reagent), buffer (Qubit dsDNA broad range buffer) and two standard solutions (used to calibrate the Qubit device). The dsDNA quantification involves first preparing a working solution from the fluorogenic dye and the buffer (by diluting the Qubit dsDNA broad range reagent in the Qubit dsDNA broad range buffer at a ratio of 1:200). The working solution amount can be scaled up as necessary as 200ul of working solution is needed for each sample including standards. The standards are prepared by adding 190ul of working solution to 10ul of standard solution. DNA samples are prepared for quantification by adding a total of 1-20ul of sample topped up with working solution to a total volume of 200ul. The samples are vortexed and incubated at room temperature for 2 minutes. The standards and samples are then analysed on the Qubit fluorometer following on screen instructions.

#### **2.12.7. Plasmid DNA Confirmation**

Methods used to confirm plasmid identify included:

1. Restriction enzyme digest

And/Or

2. Sanger sequencing using generic primers e.g. M13F or with specifically designed primers (Genewiz). This method is able to sequence a maximum of approximately 1200bp in one read.

And/Or

3. Whole plasmid next generation sequencing (Plasmidsaurus, USA).

#### **2.12.8. Plasmid Recombination (Gateway cloning)**

Gateway cloning technology was used to assemble expression vectors from 4 components: p5' entry vector, Middle entry vector, p3' Entry vector and a destination vector (pDestTol2CG2). LR reactions were used to make expression vectors from entry clones and destination vectors. A total of 20 femtomoles of each component plasmid were assembled topped up to 8ul in nuclease free water. The starting concentration of each component plasmid had to be low enough to facilitate accurate pipetting of 20 femtomoles. This reaction was assembled in a 1.5 ml Eppendorf at room temperature. LR clonase II PLUS enzyme (Invitrogen by ThermoFisher Scientific 12538120, stored in -80 degree freezer) was thawed on a cold block for approximately 2 minutes. The enzyme mix was briefly vortexed twice. 2ul of this enzyme mix was added to the plasmid components assembled in a 1.5ml Eppendorf and briefly vortexed twice. The reaction was then incubated at 25 degrees C overnight. The following morning, 1ul of Proteinase K solution was added to terminate the reaction. The reaction was then briefly vortexed and centrifuged and incubated at 37 degrees C on a hot block for 10 minutes then put in fridge. A total of 3ul of the reaction mix was then transformed in 50ul of top 10 E coli competent cells (See section on bacterial transformation for further details) for plasmid replication.

#### **2.12.9. *In vitro* transcription (Tol2/transposase mRNA)**

Tol2 (transposase) mRNA was synthesised to facilitate transposition of plasmid DNA into the zebrafish genome following one cell stage microinjection. The tol2 (transposase) mRNA was synthesised using an *in vitro* transcription reaction from template DNA (p-CS2 transposase plasmid, tol2 kit 396).

The p-CS2 transposase plasmid was first linearised with the NOT1 restriction enzyme (Buffer r3.1) in a digest reaction at 37 degrees overnight. Successful linearisation was confirmed using gel electrophoresis. The linearised plasmid DNA was purified using QIAquick PCR purification kit (Qiagen 28104). This kit purifies DNA fragments from enzymes and buffers. Manufacturer's instructions were followed. This involved adding 5 volumes of buffer PB to 1 volume of the linearised plasmid DNA from the digest reaction and then mixed. The sample was added to a QIAquick spin column placed in a 2ml Eppendorf and the column was centrifuged for 1 minute to bind the pure linearised DNA. The flow through was discarded. The DNA in the column was washed by adding 0.75ml Buffer PE to the column and centrifugation was performed for 1 minute. The flow through was discarded. The column was subsequently placed in a clean Eppendorf and the DNA was eluted by adding 30- 50ul buffer EB to the column and centrifugation was performed for 1 minute.

An *in vitro* transcription reaction was performed using the mMMESSAGE SP6 polymerase kit (Invitrogen AM1340) using manufacturer's instructions. The *in vitro* transcription reaction (total volume 20ul) requires the following components: linear template DNA (pCS2 transposase plasmid, SP6 RNA polymerase enzyme mix (2ul), 10x reaction buffer (2ul) and ribonucleotides (10ul) and RNase free water. The reaction was scaled by as necessary with the same proportions. The reaction was incubated in a PCR tube in a PCR machine for 2 hours at 37 degrees. The reaction is then terminated using TURBO DNase enzyme and incubating at 37 degrees for 15 minutes.

The RNA was subsequently purified using phenol chloroform method or RNeasy MinElute clean up protocol using the RNeasy MinElute cleanup kit (Qiagen 74204). Both techniques were used during the course of this project. The phenol chloroform method was performed according to the mMessage mmachine kit manual. This method precipitates RNA and removes all enzyme and most of the free nucleotides. The phenol chloroform method involved adding 115ul nuclease free water and 15ul ammonium acetate stop solution followed by mixing thoroughly. Phenol/chloroform extraction was then performed. An equal volume phenol was then added followed by centrifugation at 4 degrees for 15 minutes. The top layer was carefully transferred to a new tube. An equal volume of chloroform was

added, and this was then followed with centrifugation at 4 degrees for 15 minutes. The top aqueous phase was transferred to a new tube. The RNA was precipitated by 1 volume of isopropanol and mixing thoroughly. The mixture containing the precipitated RNA was chilled at -20 degrees for at least 2 hours. Centrifugation of the mixture was performed at maximum speed at 4 degrees for 20 minutes to pellet the RNA followed by removal of the supernatant containing any impurities. The RNA pellet was washed with 1ml of 70% ethanol (RNase-free), and this was centrifuged at 4 degrees at maximum speed for 20 minutes. The pellet was dried at room temperature for 10 minutes and resuspended in an appropriate volume of RNase free water depending on the desired concentration.

The RNeasy MinElute clean protocol (Qiagen) is a column-based extraction method and was performed according to the manufacturer's instructions. The sample was adjusted to a volume of 100ul with RNase free water. A total of 350ul of buffer RLT was added and mixed thoroughly. A total of 250ul of 100% ethanol (Fisher E/0665DF/17) was added to the diluted mixture. In order to isolate the RNA, the sample was added to an RNeasy MinElute spin column and centrifuged for 15 seconds at maximum speed. The flow through containing impurities was discarded. The RNA in the column was washed by adding 500ul of buffer RPE and centrifugation performed at maximum speed for 15 seconds. A further washing step was performed by adding 500ul 70% ethanol to the spin column and centrifugation performed at maximum speed for 2 minutes. Elution of the RNA was performed by adding a minimum of 10ul of RNase free water (Depending on the desired concentration) to the column (placed in a new Eppendorf) and centrifuging the column for 1 minute at maximum speed. The RNA was transferred to ice and stored at -80 degrees until needed.

The purified RNA was quantified using both nanodrop spectrophotometry and gel electrophoresis. For gel electrophoresis, 0.5ul of RNA is mixed with 2ul H<sub>2</sub>O and 2ul loading dye and run on a gel at 120 volts for 15 minutes to confirm the presence of two distinct bands (Figure 17).

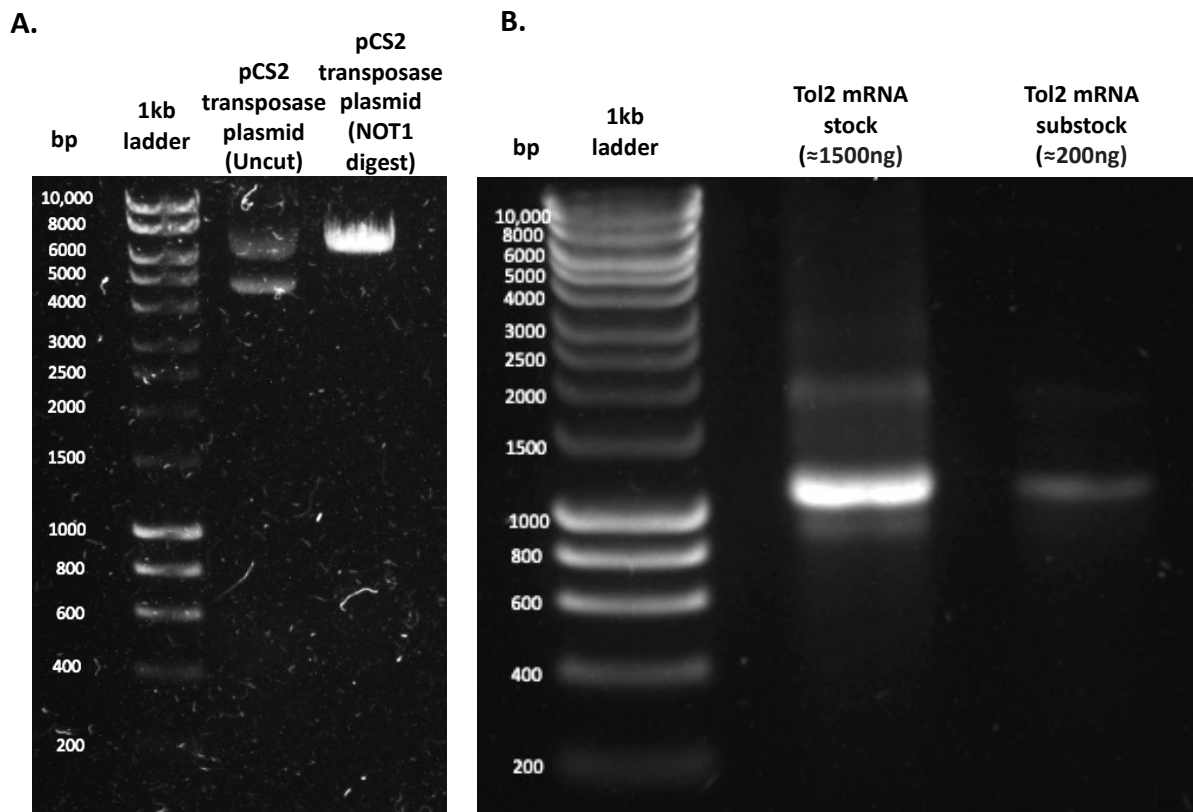


**Figure 17. Generating *tol2* mRNA from pCS2 transposase plasmid (tol2 kit 396).**

(A) Agarose gel electrophoresis of linearized pCS2 transposase plasmid (tol2 kit 396) using NotI restriction enzyme digest (with undigested plasmid for comparison) (B) *tol2* transposase mRNA fragment generated using in vitro transcription from linearized pCS2 *tol2* transposase plasmid.

### 2.13. Imaging

The following microscopes were used to take fluorescent microscope pictures:

Microscope Name	Type of Microscope
Leica M205 FA and DFC365 FX	Fluorescent Stereo
Zeiss Z1	Lightsheet
Perkin Elmer Spinning Disc	Confocal
Nikon Eclipse TE2000-U	Fluorescent inverted
Nikon SMZ Extended Focus	Brightfield Stereo
3DHISTECH Panoramic Slide Scanner	N/A (Slide Scanner)

For fluorescent microscopy, a BF or DF channel was taken in addition to a fluorescent channel. Images were formatted in FIJI to add scale bars and create merged brightfield and GFP channel images. Microscope settings (Exposure time, gain etc) were stored in the meta data of the imaging files.

### 2.14. Software

The following software were used during this project:

Software	Manufacturer
FIJI version 2.14.0/1.54f	Open-Source Software
Qupath v0.5.0	Open-Source Software
Zen Lite (Zeiss) Blue edition	Zeiss
NIS elements (Nikon)	Nikon
Volocity	Quorum Technologies
Leica Application Suite X	Leica
SnapGene® v4.3.11	Dotmatics (available at <a href="http://snapgene.com">snapgene.com</a> )

### **2.15. Gene and Protein Cross Species Alignment**

Gene and protein sequences were downloaded from Ensembl (Release 111) (231) or UniProt (232). For alignment of sequences, either the online Basic Local Alignment Search (BLAST) tool (233) or the CLUSTAL OMEGA feature in SnapGene® software (from Dotmatics; available at [www.snapgene.com](http://www.snapgene.com)) were used.

### **2.16. Systematic Review**

Systematic review was performed according to the accepted Preferred Reporting Items for Systematic Reviews and Meta-Analyses (PRISMA) method (234). These are evidence-based guidelines on how to conduct and present a rigorous systematic review and/or meta-analysis.

## **Chapter 3. Epidemiology of Bladder Cancer in 2023: A Systematic Review of Risk Factors**

Work in this chapter contributed to the following publication:

**Jubber I**, Ong S, Bukavina L, Black PC, Comperat E, Kamat AM, Kiemeny L, Lawrentschuk N, Lerner SP, Meeks JJ, Moch H, Necchi A, Panebianco V, Sridhar SS, Znaor A, Catto JWF, Cumberbatch MG. Epidemiology of Bladder Cancer in 2023: A Systematic Review of Risk Factors. *Eur Urol.* 2023;84(2):176-90.

### 3.1. Introduction

In 2018, Bladder cancer (BC) was the 10<sup>th</sup> commonest cancer worldwide (235). Incidence rates were higher in men for whom it was the sixth commonest cancer. Highest incidence rates were seen in the developed world (235). Most BCs are urothelial carcinoma (UC) in subtype (remainder include squamous cell, sarcoma, lymphoma and adenocarcinoma) and approximately 75% of these are non–muscle-invasive BC (NMIBC) (236). NMIBC has a high prevalence due to its indolent natural history and high recurrence rate. Around one-quarter of BCs, and most non-UC subtypes, are muscle invasive (MIBC) which require systemic chemotherapy and/or immunotherapy, and radical treatment (cystectomy or radiotherapy), or palliation (237). Most BCs present with either haematuria or storage lower urinary tract symptoms while the remainder are asymptomatic or incidental findings (238).

The demographics of BC are evolving reflecting an improved understanding of the human exposome and the changing nature of industrialization (239). For example, around half of BCs are attributed to cigarette smoking although the rate of smoking has declined in many countries (240-242). Similarly, workplace regulations have reduced exposure to high-risk carcinogens (243). Here, we update previous reports (56, 244), by searching the literature to compile a contemporary picture of BC demographics and epidemiology.

### **3.2. Evidence Acquisition**

A systematic literature search was performed using PubMed and Embase on 21.1.22 and 6.9.22 utilising a combination of subject headings and free text words. Further details of the search strategy are in supplementary files. The search was restricted to manuscripts published since 2018. Manuscripts were excluded if they were not in English, had <50 subjects (for epidemiological studies), or were not human studies. Conference abstracts were also excluded. Two authors (I.J and S.O) reviewed the abstracts using a priori inclusion and exclusion criteria and Covidence software (Cochrane library). Conflicts were resolved between the authors or with the involvement of a third author (M.G.C). Reference lists of included manuscripts were also searched. Systematic reviews (SR) and meta-analyses (MA) were included. We report our findings in accordance with the Preferred Reporting Items for Systematic Reviews and Meta-analyses (PRISMA) guidelines(245). The review was registered with the PROSPERO database (CRD42022341359) on 20.7.22.

### **3.3. Evidence Synthesis**

The literature search, after removal of duplicates, identified 5,177 studies, of which 334 full-text articles were included. A total of 15 articles were identified by searching references, including 349 full-text articles (Figure 18). Information on study type, number of study subjects or number of studies and confounding factors adjusted for were extracted for quality assessment. For MAs, specific information on included studies and heterogeneity were extracted.

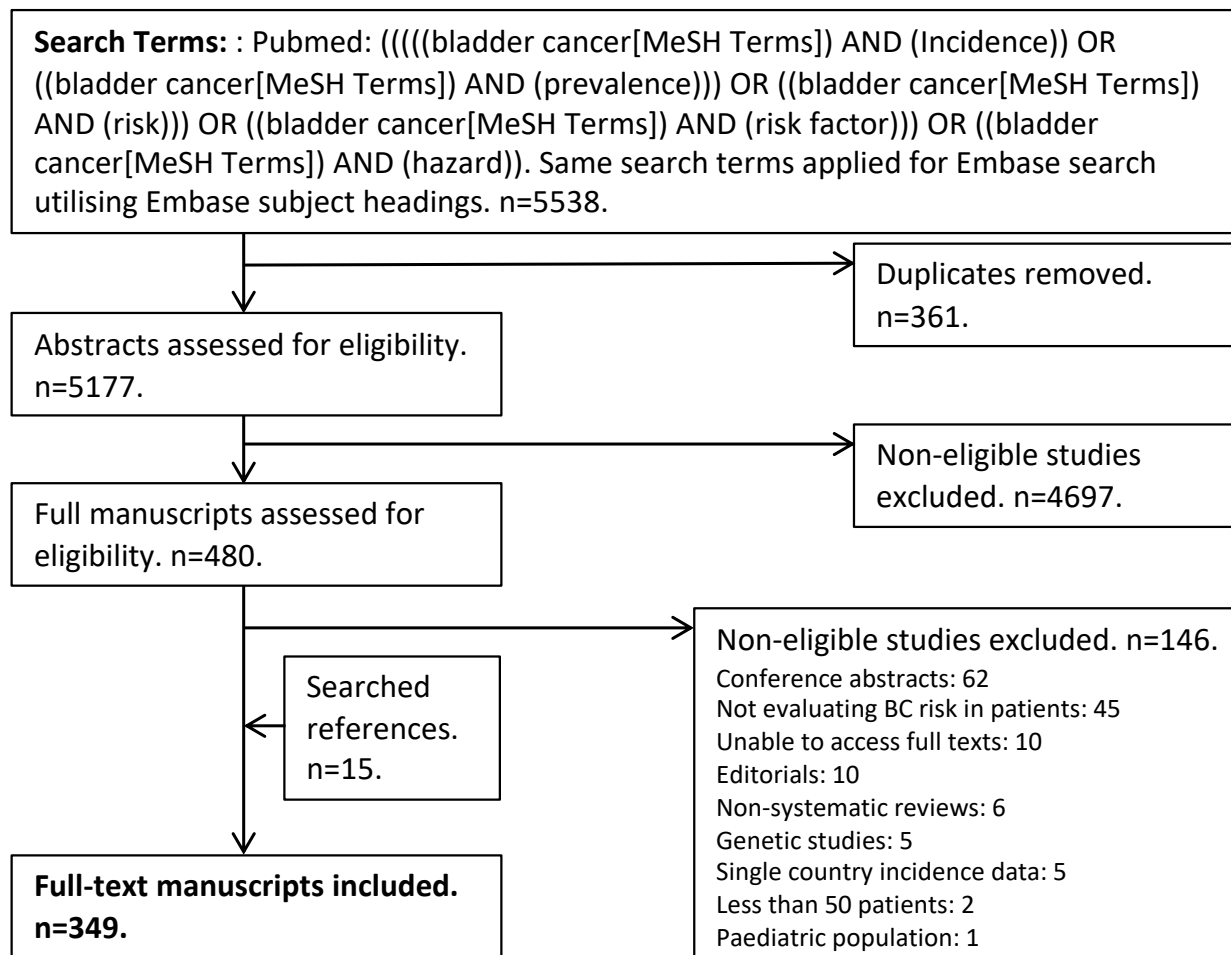


**Figure 18. CONSORT Diagram for Systematic Review.**

Search captured all articles from 1 April 2018 until 6 September 2022. BC = bladder cancer.

### **3.4. Epidemiology, Incidence, Prevalence, and Mortality of Bladder Cancer**

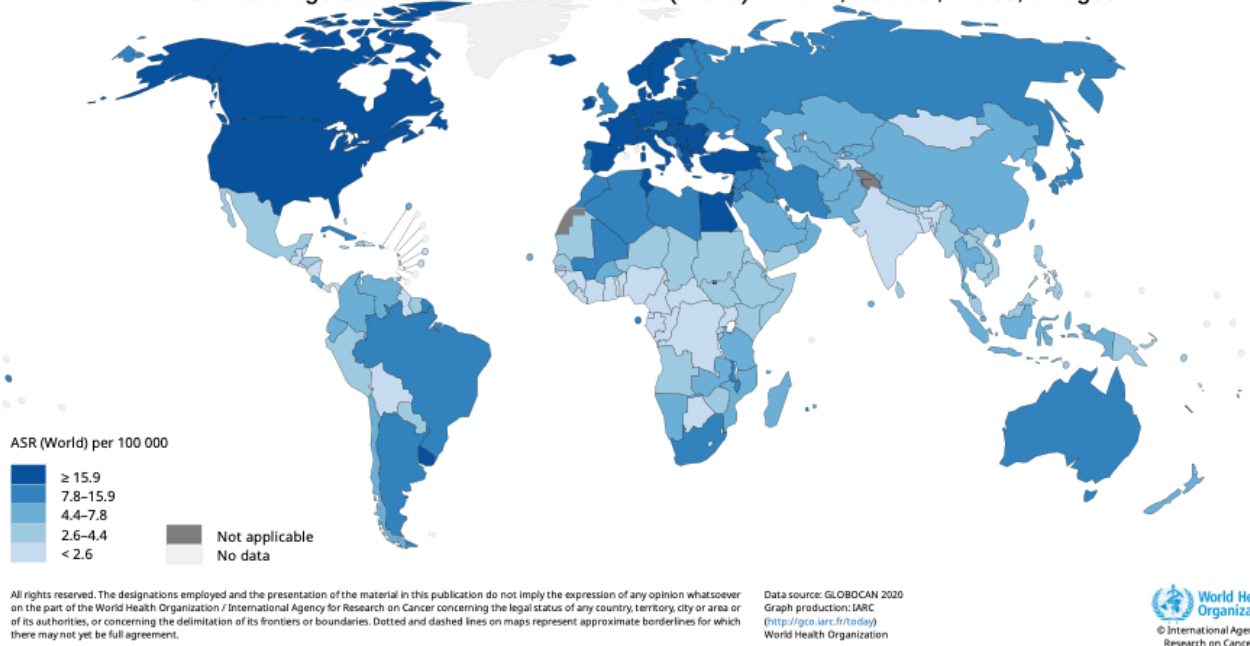
According to GLOBOCAN, there were 573, 000 new BC cases and 213, 000 deaths worldwide in 2020 (46, 246, 247). Over three-quarters of new BC cases occurred in men. BC incidence is strongly correlated with increasing age. In males and females, age specific incidence rates start to rise from ages 50-54. A significantly sharper rise occurs in males between ages 55-59. The highest incidence rates for BC occur in the over 85 years age category in males and females (248).

Commonly used epidemiological measures for incidence and mortality are age-standardised incidence rates and age-standardised mortality rates. These measures take into account the effects of age which is important for making regional comparisons where the age distributions may differ significantly. Age standardised incidence rates (ASR, per 100, 000 persons per year) for both sexes combined were highest in Europe (11), North America (11), North Africa (8.9), and West Asia (8.6) and lowest in West (2.0) and Middle Africa (1.6), Central America (2.2), and South-Central Asia (1.9). Male: female ratios of age-standardised incidence rates (ASR, per 100,000 persons) vary by region from 6:1 to 2:1. In West Asia the ASR is 15 vs 2.6 for men and women respectively (ratio of 6:1) and in East Africa the ASR is 4.2 vs 2.4 for men and women respectively (ratio of 2:1). The 5-year prevalence worldwide in 2020 was 1,721,000 cases. The combined age standardised mortality rates (ASR, per 100, 000 persons per year) for both sexes were highest in North Africa (5.2), South Europe (3.3), and West Asia (3.2). GLOBOCAN world maps of BC incidence and mortality rates are shown in (Figures 19, 20, 21).

In men, BC is the sixth most common cancer worldwide (5% of all cancers excluding non-melanoma skin cancer) and in women it is the 17<sup>th</sup> most common cancer site (1.5% of female cancer incidence). BC has the 9<sup>th</sup> highest five-year prevalence (22 per 100,000 persons) overall. With regards to disability-adjusted life years (DALYs), BC ranks as the 15<sup>th</sup> highest (54 years of total health lost per 100,000 individuals)(249).

Globally, estimated ASRs for incidence have not significantly changed from 1990 to 2019, reflecting diverging incidence trends in different world areas. According to estimates, there have been significant increases in East Asia (percentage change: 56%), North Africa and Middle East (53%) and Central Europe (50%). With regards to estimated age standardised mortality rates, there were overall decreases worldwide, but a significant increase was noted in central Asia (18%)(250). GLOBOCAN predictions of future BC disease burden (based on demographic changes only) by continent estimate the greatest percentage increases in incident BC cases from 2020 to 2040 will be in Africa (100.6%), Latin America and the Caribbean (85%), Asia (79%) and Oceania (70%) (Figure 22) (251). This is likely to reflect the forecasted industrialisation and ageing population in these areas.

Estimated age-standardized incidence rates (World) in 2020, bladder, males, all ages



Estimated age-standardized incidence rates (World) in 2020, bladder, females, all ages

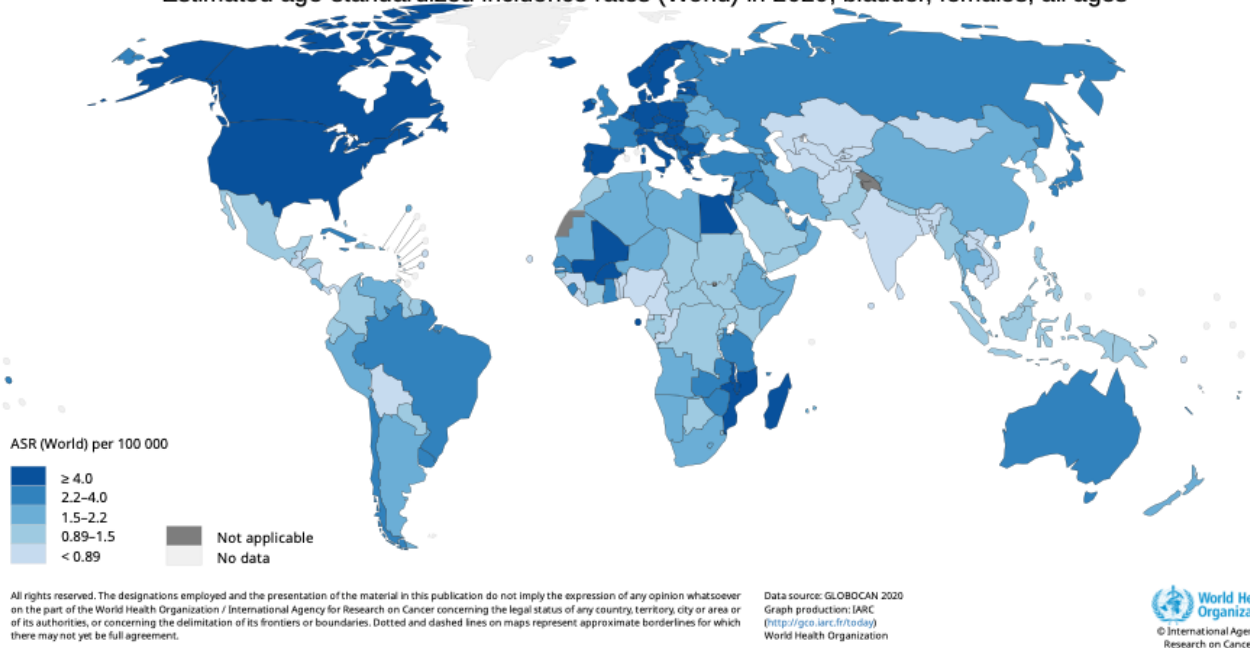
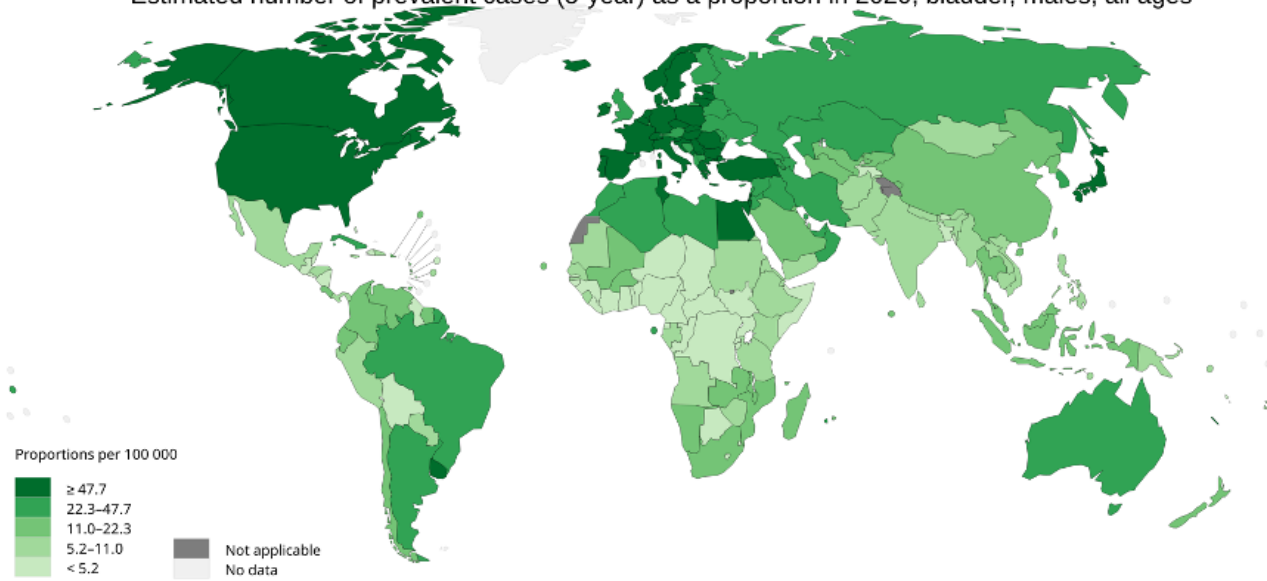


**Figure 19. Global Map of Incidence (Age-Standardized) Rates for Males and Females in 2020.**

From Global Cancer Observatory: Cancer Today tool by the International Agency for Research on Cancer (246).

Estimated number of prevalent cases (5-year) as a proportion in 2020, bladder, males, all ages

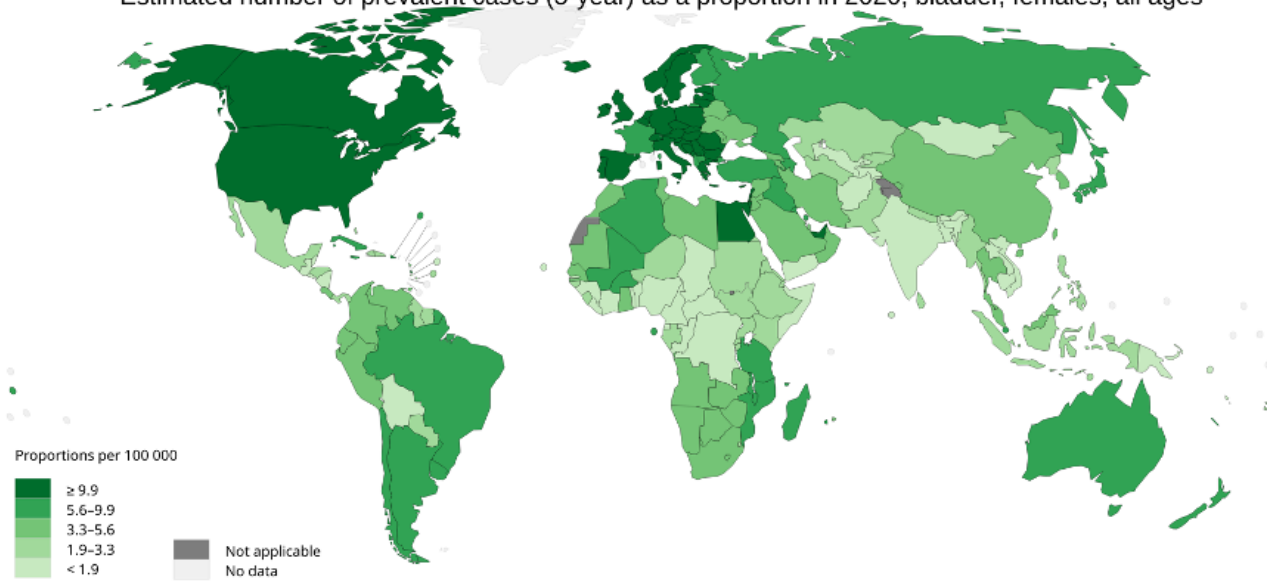


All rights reserved. The designations employed and the presentation of the material in this publication do not imply the expression of any opinion whatsoever on the part of the World Health Organization / International Agency for Research on Cancer concerning the legal status of any country, territory, city or area or of its authorities, or concerning the delimitation of its frontiers or boundaries. Dotted and dashed lines on maps represent approximate borderlines for which there may not yet be full agreement.

Data source: GLOBOCAN 2020  
Map production: IARC  
(<http://gis.crc.iarc.fr/>)  
World Health Organization

 World Health Organization  
© International Agency for Research on Cancer 2020  
All rights reserved

Estimated number of prevalent cases (5-year) as a proportion in 2020, bladder, females, all ages



All rights reserved. The designations employed and the presentation of the material in this publication do not imply the expression of any opinion whatsoever on the part of the World Health Organization / International Agency for Research on Cancer concerning the legal status of any country, territory, city or area or of its authorities, or concerning the delimitation of its frontiers or boundaries. Dotted and dashed lines on maps represent approximate borderlines for which there may not yet be full agreement.

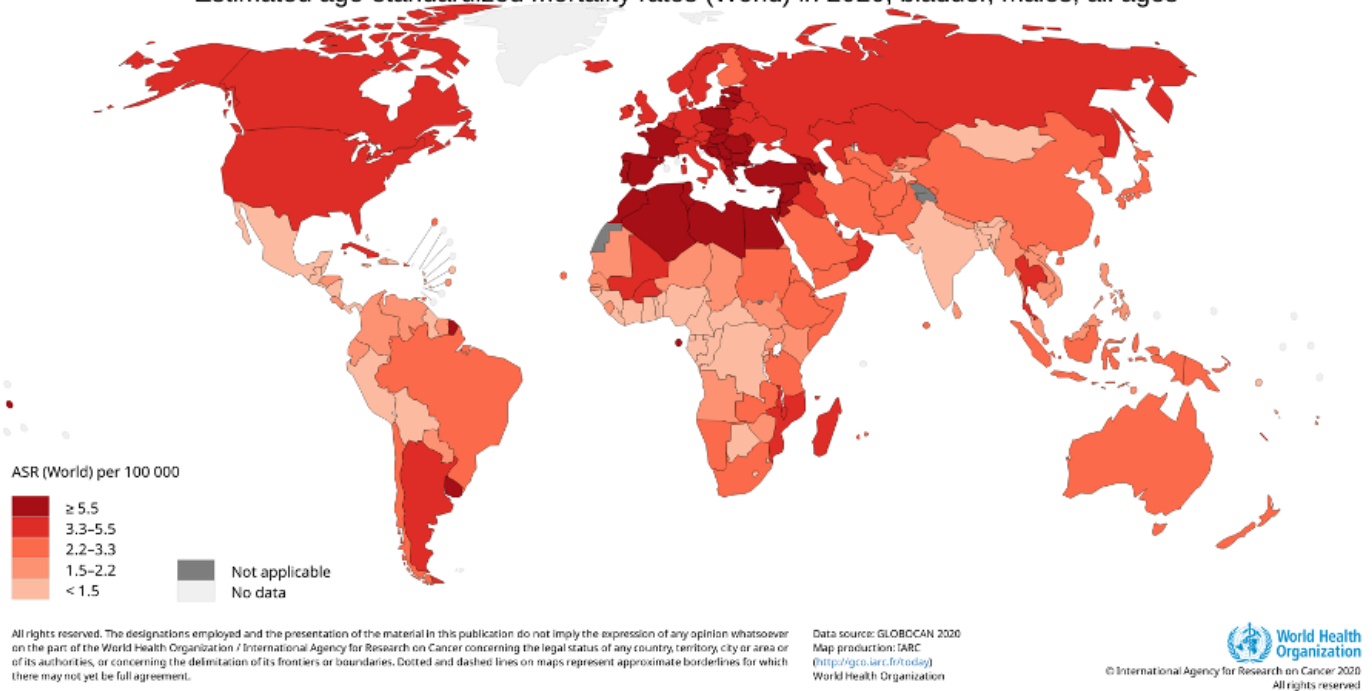
Data source: GLOBOCAN 2020  
Map production: IARC  
(<http://gis.crc.iarc.fr/>)  
World Health Organization

 World Health Organization  
© International Agency for Research on Cancer 2020  
All rights reserved

**Figure 20. Global Map of Prevalence for Males and Females in 2020.**

From Global Cancer Observatory: Cancer Today tool by the International Agency for Research on Cancer (246).

Estimated age-standardized mortality rates (World) in 2020, bladder, males, all ages



Estimated age-standardized mortality rates (World) in 2020, bladder, females, all ages

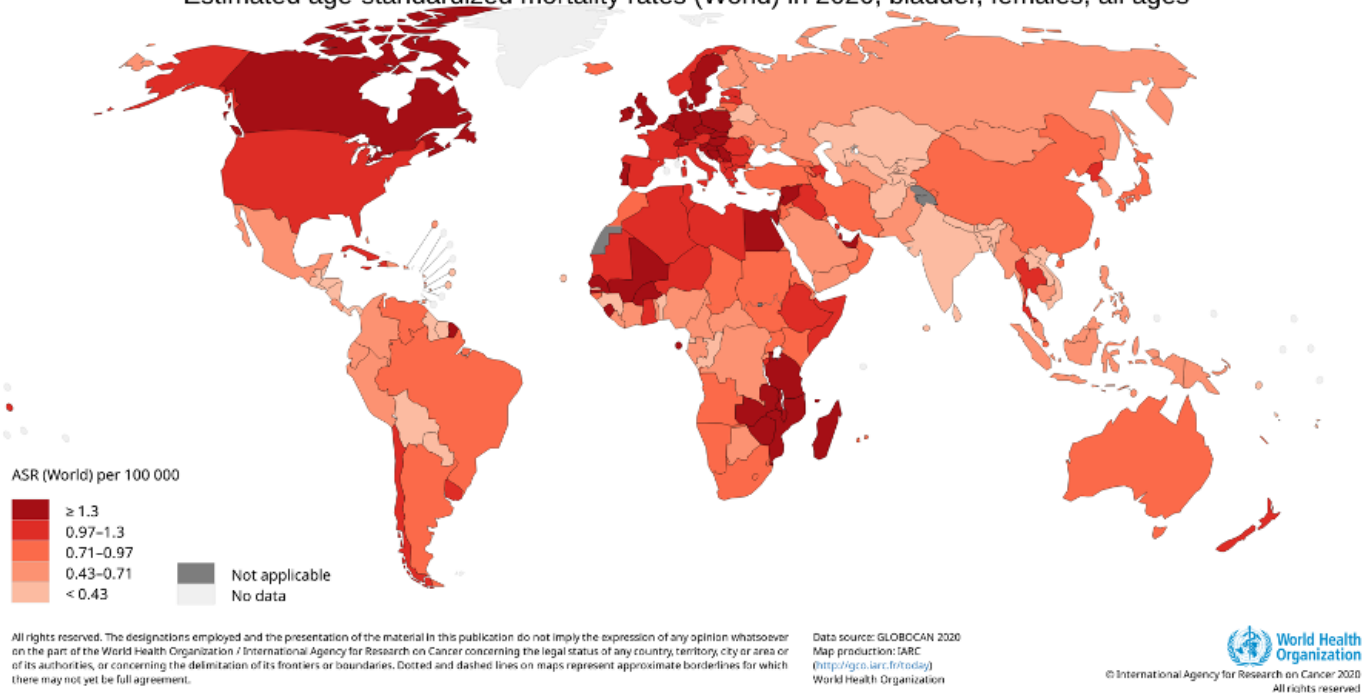
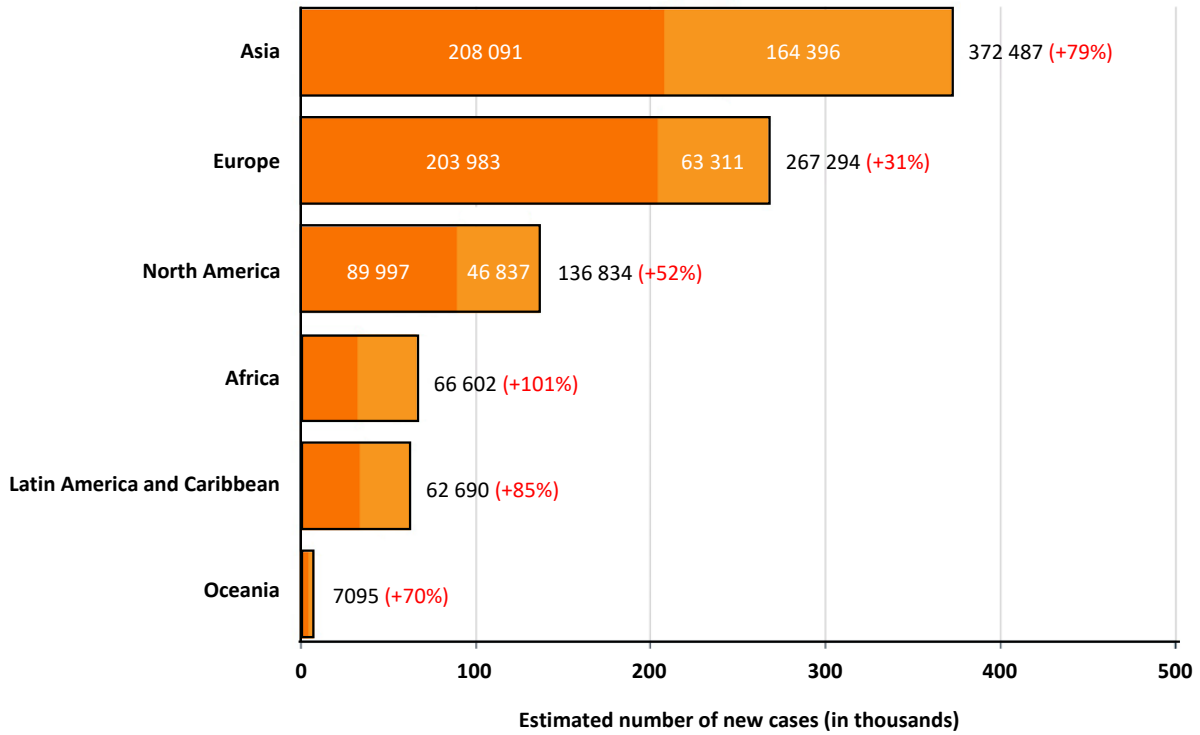


**Figure 21. Global Map of Mortality (Age-Standardized) Rates for Males and Females in 2020.**

From Global Cancer Observatory: Cancer Today tool by the International Agency for Research on Cancer (246).



Totals	
2020	573,278
2040	913,002

**Figure 22. Estimated Number of New Bladder Cancer Cases Between 2020 and 2040 (Both Sexes).**  
Adapted from Global Cancer Observatory: Cancer Tomorrow tool by the International Agency for Research on Cancer (251)

### 3.5. Risk Factors for Bladder Cancer

Most BCs are associated with external risk factors. In total, 4.3% of BC patients have a first-degree relative with BC (252) and up to 50% of urothelial cancer patients have a family history of cancer (253). The International Agency for Research on Cancer (IARC) has reported sufficient evidence for the following risk factors in BC: tobacco smoking, various occupational exposures (aluminum, rubber production, painters, firefighters, occupational exposure to various dyes [e.g. magenta, auramine] or dye intermediates [ e.g. 4-aminobiphenyl] and paint), environmental exposures (X radiation or gamma radiation, arsenic), medications (cyclophosphamide and chlornaphazine), opium consumption and Schistosoma infection (Table 8) (254).

#### Smoking

- Tobacco Smoking

#### Occupations

- Aluminum production
- Rubber manufacturing industry
- Dye Industry (Magenta, Auramine)
- Painter
- Firefighter
- Dry cleaning\*
- Hairdressers or barbers\*
- Printing processes\*
- Textile manufacturing \*

#### Environmental Factors

- Arsenic and inorganic arsenic compounds
- X and Gamma Radiation
- Outdoor air pollution\*
- Diesel Exhaust\*

#### Occupational Agents

- Benzidine (Dye manufacturing)
- 4-aminobiphenyl (Dye and rubber manufacturing)
- *ortho*-Toluidine (Dye and rubber manufacturing)
- 2-Naphthylamine (Dye and rubber manufacturing)
- 4-Chloro-*ortho*-toluidine\* (Dye manufacturing)
- 2- Mercaptobenzothiazole\* (Rubber manufacturing)
- Tetrachloroethylene\* (Dry cleaning, automotive and metalwork industries)
- Soot\*
- Coal Tar Pitch\*

#### Diseases and Medications or Drugs

- Chlornaphazine
- Schistosomiasis
- Cyclophosphamide
- Opium Consumption
- Pioglitazone\*

Adapted IARC list of classifications for bladder cancer with sufficient or limited evidence for humans<sup>21</sup>. \*Agents with limited evidence for bladder cancer in humans. Note that all risk factors without an asterisk correspond to a group 1 IARC classification (carcinogenic to humans).

**Table 8. Bladder Cancer Risk Factor Summary According to International Agency for Research on Cancer Monographs.**

### **3.5.1. Tobacco Smoking**

Approximately 50% of BC cases are caused by tobacco smoking (255). A cohort study of 422,010 subjects with 30 years follow-up demonstrated between two- and three-times increased risks of BC with smoking (HR: 2.32, 95% CI 1.98-2.73 in males and HR: 2.75, 95% CI 2.07-3.64 in females)(256).

In a pooled analysis of seven Australian cohorts (including 364, 426 subjects), the percentage BC risk attributed to ever smoking was estimated to be 44% (95% CI: 35-52%) overall, 53% (95% CI: 43-62%) in men and 19% (1.1-33%) in women (257). However, significantly higher values have been reported previously (255).

In a meta-analysis (MA) of 52 studies, BC risk is directly proportional to smoking intensity up to 20 cigarettes/day (RR: 2.52, 95% CI: 2.41-2.64 for 10 cigarettes/day and RR 3.27, 95% CI: 3.16-3.38 for 20 cigarettes/day) but plateaus thereafter. In contrast, BC risk increases without plateau with smoking duration (258).

BC risk decreases with time since smoking cessation. In a prospective cohort of 143,279 post-menopausal women, BC risk in ex-smokers was 25% lower within the first ten years following smoking cessation (HR: 0.75, 95% CI: 0.56-0.99) and continued to decrease with time. However, risks of BC remained higher in ex-smokers compared to never-smokers 30 years after quitting smoking (HR: 1.92; 95% CI, 1.43–2.58)(259).

A MA of 14 studies (646, 526 subjects) demonstrated increased BC risk with lifetime second hand smoking exposure in non-smokers (RR: 1.22, 95% CI: 1.06-1.40) compared to unexposed non-smokers (260).

### **3.5.2. e-Cigarette use**

E-cigarette vapour may contain a number of carcinogenic compounds (e.g. formaldehyde and acrolein). A study of 23 subjects found two carcinogenic compounds (o-toluidine and 2-naphthylamine) at higher concentration in the urine of e-cigarette users (261). Similarly, a systematic review (SR) of 22 studies found numerous carcinogenic compounds linked to BC

in the urine of e-cigarette users (262). However, there is no published epidemiological bladder cancer data for e-cigarette use as yet.

### **3.5.3. Cannabis use**

Previous data on cannabis and BC risk has been inconsistent, with two previous studies reporting both increased and decreased BC risk respectively. A cohort study of over 150,000 subjects reported no association between previous cannabis use and BC risk overall but reduced BC risk in female subjects on subgroup analysis (HR: 0.42, 95% CI: 0.19-0.94)(263). This study is limited by potential recall bias and lack of adjustment for key confounding factors such as occupation.

### **3.5.4. Opium Consumption**

Opium consumption has previously been linked to increased BC risk in several case control studies. A prospective cohort study of over 50, 000 subjects with a median 10 years follow up showed increased BC risk for ever users of opium (smoking and ingestion) compared to never users (HR: 2.86, 95% CI: 1.47-5.55) (264).

### **3.5.5. Occupational Carcinogen Exposure**

Occupational carcinogen exposure is the second most frequent BC risk factor for industrialised countries. An estimated 5.7% of new BCs are due to occupational carcinogen exposure (265).

A Nordic cohort study of 14.9 million subjects (including 111,458 BC cases) reported the highest smoking adjusted standardised incidence ratios (SIRs) in chimney sweeps (SIR: 1.29, 95% CI: 1.05–1.56), waiters (SIR: 1.22, 95% CI: 1.07–1.38), hairdressers (SIR: 1.14, 95% CI: 1.02–1.26), cooks and stewards (SIR: 1.12, 95% CI: 1.01–1.25), printers (SIR: 1.11, 95% CI: 1.04–1.18), seamen (SIR: 1.09, 95% CI: 1.03–1.14) and drivers (SIR: 1.08, 95% CI: 1.05-1.10) (266).

Firefighters are exposed to numerous combustion products from fires such as polyaromatic hydrocarbons, volatile organic compounds, diesel exhaust, asbestos, metals (cadmium and arsenic) and particulate matter. Some of these agents are either known bladder cancer carcinogens (such as polyaromatic hydrocarbons) or suspected bladder cancer carcinogens (such as diesel exhaust) (267). A MA of 14 studies demonstrated increased BC risk in firefighters (summary risk estimate: 1.12, 95% CI: 1.04-1.21) (268). Although, this increased risk is most likely related to the combustion product exposure, firefighters are exposed to other factors which are not necessarily related to combustion products such as heat stress, radiation and shift work. These factors may also contribute to the increased bladder cancer risk (267). It is important to note the individual studies had varying levels of adjustment for potential confounders and there was poorly defined exposure information (268).

### **3.5.6. Dietary Factors**

Previous studies investigating diet/fluid consumption and BC risk have yielded inconsistent results. The World Cancer Research Fund Continuous Update Project reported that there was limited suggestive evidence of reduced BC risk with fruit and vegetables and tea intake(269).

#### **3.5.6.1. Regional Diets**

A MA of 13 studies (including 646,222 subjects) demonstrated reduced BC risk with high adherence to a Mediterranean diet overall (HR: 0.85, 95% CI: 0.77-0.93)]. Subgroup analysis showed reduced BC risks in males and not in females (270). In contrast, Western diet was associated with an exaggerated BC risk overall (HR for highest vs lowest tertile: 1.54, 95% CI: 1.37-1.72). Subgroup analysis revealed increased risks in males with no observed differences noted in females (271).

#### **3.5.6.2. Grain and Fibre**

A MA of 13 cohort studies (including 574,726 subjects) reported reduced BC risk with higher intake of total whole grain (HR for highest vs lowest tertile: 0.87, 95% CI: 0.77-0.98). Similar

findings were reported for total dietary fibre (HR for highest vs lowest tertile: 0.86, 95% CI: 0.76-0.98)(272).

### **3.5.6.3. Alcohol**

The association between BC and alcohol is controversial. While there was no association between increased alcohol intake and BC risk overall in an Australian cohort 226,162 of subjects (273), a MA subgroup analysis of a Japanese population demonstrated increased BC risk with heavy alcohol consumption (moderate alcohol intake defined as  $\leq 30$ g of ethanol/day, heavy intake defined as the most heavy volume of alcohol consumed) (RR: 1.31, 95% CI: 1.08–1.58) (274). Furthermore, heavy consumption of spirit drinks was associated with increased BC risk in males (RR: 1.42, 95% CI: 1.15–1.75) (274).

### **3.5.6.4. Dietary fluid consumption**

Previous data on dietary fluid consumption and BC risk have been conflicting. Increased fluid may reduce carcinogen exposure by diluting urine. However, increased fluid may increase exposure to potential carcinogens such as arsenic. In a MA of 20 studies, while total fluid intake did not correlate to BC risk overall, subgroup analysis by sex demonstrated male predisposition to BC development with increased fluid intake (RR: 1.37, 95% CI: 1.04-1.81 for highest vs lowest intakes). Increased BC risks were also observed with total fluid intake > 3000ml/day and with tap water consumption (RR: 1.33, 95% CI: 1.02-1.73 for highest vs lowest categories) (275) but not non-tap water. However, most studies evaluated were retrospective, and categories of fluid intake were often poorly defined.

### **3.5.6.5. Caffeine**

A pooled analysis of 12 cohorts (including 501, 604 subjects) reported increased BC risk with coffee consumption > 500mls per day (HR: 1.56, 95% CI: 1.38-1.77) and 180-500mls per day (HR: 1.39, 95% CI: 1.23-1.58) compared to no coffee. However, analysis stratified by sex and smoking demonstrated the link was restricted to male smokers suggesting the findings may have been influenced by residual confounding of smoking (276).

#### **3.5.6.6. Tea**

Greater tea consumption was associated with reduced BC risk overall in a pooled analysis of 12 cohort studies (HR: 0.84, 95% CI: 0.75–0.95 for high consumption). However, no evidence of association was seen for females and never smokers in subgroup analysis(277) suggesting a possible modulation of the effect by tobacco carcinogens. This study is limited by the lack of granularity in tea consumption data and the lack of data on other potential confounding factors e.g. occupation.

#### **3.5.6.7. Cow's Milk and Dairy**

A Swedish cohort study previously reported a 38% reduced BC risk with high culture milk intake (278). However, overall, the literature on dairy products has previously been inconsistent. Dairy products were not associated with BC risk overall in a pooled analysis of 13 studies, but reduced BC risks were seen for yoghurt (HR: 0.85, 95% CI: 0.75-0.96 for moderate consumption) (279). This analysis did not adjust for occupation.

#### **3.5.6.8. Meat and Fish**

There has previously been inconsistent data on the relationship between meat and BC risk. A MA of 11 studies (including 518, 545 subjects) demonstrated increased BC risk with a high intake of organ meat (HR for highest vs lowest tertile: 1.21, 95% CI: 1.05- 1.38). On subgroup analysis, fish consumption was linked to lower BC risk in men (HR: 0.79, 95% CI: 0.65- 0.97) but not in women (280). This work is limited by a lack of data on food preparation methods and other potential BC risk factors such as occupation.

#### **3.5.6.9. Fruits and vegetables**

A pooled analysis of 13 cohort studies (including 535, 713 subjects) demonstrated a small decrease in BC risk only in women (HR: 0.92; 95% CI 0.85-0.99) with increasing fruit consumption by 100g per day but not in men (281). Potential explanations for the sex difference include hormonal factors and micturition habits. A pooled analysis of 13 cohort studies showed higher intake of total vegetables was associated with reduced BC risk in

women but not men (highest vs lowest tertile HR: 0.79, 95% CI: 0.64-0.98)(282). An important limitation of these studies is the limited data on confounding factors.

#### **3.5.6.10. Inflammatory Diets**

Chronic inflammation has previously been implicated in BC and diet is reported to modulate inflammation. Results from three North American prospective cohort studies (Including 218, 074 subjects) did not demonstrate an association between diets with greater inflammatory potential and BC risk (283).

#### **3.5.6.11. Vitamins**

A SR of 6 studies evaluated the association between Vitamin D levels and BC. In total, 5 out of the 6 studies demonstrated an association between low serum vitamin D levels and BC risk (OR ranging from 1.28 to 3.71) (284). The potential mechanism involved with this association is poorly understood. However, it has been postulated that bladder cancer development may be linked to Toll-like receptor signalling and immune responses controlled by vitamin D receptor signalling. Further work is needed to confirm this postulated mechanism (284).

Increased BC risk was reported with high vitamin B1 consumption (HR: 1.14, 95% CI: 1.01-1.29) compared to low consumption. Subgroup analysis showed this association only in men. (285). This study is limited by the absence of data on numerous potential confounding factors.

### **3.5.7. Environmental Carcinogens**

Arsenic in the drinking water, which the IARC has classified as a group 1 carcinogen (286), has established links to BC risk. Air pollution is classified by the IARC as a group 1 carcinogen based on associations with lung cancer.

#### **3.5.7.1. Arsenic**

Although there is significant evidence that high levels of arsenic in drinking water is a risk factor for BC, there has previously been uncertainty about the exposure levels required for carcinogenicity. A MA of 8 studies specifically evaluating low levels of exposure (exposure greater than 150 µg/L was excluded) and did not show a statistically significant increased risk of BC with an increase in arsenic levels of 10 µg/L (RR: 1.02, 95% CI: 0.97-1.07) (287). This suggests that arsenic is carcinogenic only at higher levels.

#### **3.5.7.2. Air Pollution**

Diesel exhaust emissions and outdoor air pollution exposure have been established as carcinogens by the IARC based on evidence for lung cancer (group 1)(254, 288) and are both reported to have limited evidence for BC. A pooled analysis of 2 case-control studies (5121 subjects) reported increased BC risk (OR: 1.61, 95% CI: 1.08–2.40) with high level of cumulative diesel exhaust exposure (289).

There were no statistically significant associations with BC for air pollution in a pooled analysis from a European cohort (290) or a Spanish case control (291).

#### **3.5.7.3. Nitrates**

Previous studies on nitrates and BC risk have not been conclusive. A MA of 5 studies showed no significant association between nitrates in drinking water and BC risk (292). Most study populations were in developed countries with relatively low nitrate concentrations.

#### **3.5.7.4. Trihalomethanes**

Drinking water disinfection is a widespread public health measure to protect against waterborne infections and the most common disinfectant used globally is chlorine. However, disinfection byproducts form as a result of drinking water disinfection and trihalomethanes (and haloacetic acids) are the predominant disinfection byproduct classes that form following chlorination. Long term exposure to trihalomethanes has previously been linked to increased BC risk in case control studies. In a cohort study of 58,672 individuals with 16 years of follow-up, there was no association between high drinking

water trihalomethane (THM) exposure and BC risk. This study evaluated THM concentrations up to around 20 µg/L, reflecting European chlorinated drinking water. However, individual drinking water consumption data was lacking (293).

#### **3.5.7.5. Routine Personal Hair Dye Use**

Although there is some evidence of increased cancer risk with occupational exposure to hair dyes, previous data on personal hair dye use and BC risk have been conflicting. A prospective cohort study (including 117, 200 women) reported no significant association between ever users of permanent hair dyes and BC (294).

#### **3.5.8. Race and Comparative Genomic Landscape From Various Genomic Ancestries**

A UK cohort study of 52, 779, 123 subjects reported lower age standardised rates for BC in Asian and black ethnic categories compared to white (295). These data should be interpreted with caution as the differences in BC incidence rates between races can reflect different smoking patterns and environmental exposures. An analysis of the molecular effects of ancestry in cancer demonstrated enrichment in HRAS mutations in BCs from patients with East Asian ancestry compared to European ancestry (296).

#### **3.5.9. Socioeconomic position**

An analysis of GLOBOCAN data demonstrated positive correlations between gross domestic product (GDP) per capita and BC incidence in men ( $r=0.48$ ) and women ( $r=0.44$ ). However, this association was not significant in multivariable linear regression adjusting for tobacco smoking(297).

A cohort study reported higher BC incidence in more deprived socio-economic groups in Canada (based on income and education levels) over an 18-year period (298). An important drawback of these is the absence of data on smoking.

### 3.5.10. Physical Activity

A North American prospective cohort study of 141 288 post-menopausal women demonstrated reduced BC risk with more physically activity ( $\geq 15$  MET [metabolic equivalent of task] hours/week of total physical activity HR: 0.74, 95% CI: 0.59-0.94,  $\geq 8.75$  MET hours/week of walking HR: 0.79, 95% CI: 0.63-0.98, and  $\geq 11.25$  MET hours/week of moderate to vigorous activity HR: 0.76, 95% CI: 0.61-0.94 (299). In contrast, data from a Japanese cohort of 76, 795 subjects (300) and Korean cohort of 162, 220 subjects(301) reported no association with BC risk.

### 3.5.11. Gene-Environment Interaction

N-Acetyltransferase 2 and Glutathione S transferases are enzymes involved in the detoxification of carcinogens linked to BC such as arylamines and polyaromatic hydrocarbons. Previous reports on the role of N-Acetyltransferase 2 (*NAT-2*) and Glutathione S transferase (*GSTM1*, *GSTT1*) gene polymorphisms and BC risk have been inconsistent.

In a MA of 54 case-control studies (including 31, 929 subjects), the slow acetylator genotype of *NAT-2*, an enzyme important for catalysing N-acetylation of arylamines, was associated with increased BC risk compared to the rapid and intermediate genotype (OR: 1.46, 95%: 1.30-1.63) (302).

An analysis of genetic associations of plasma metabolites revealed an association between caffeine metabolite 5-acetylamino-6-formylamino-3-methyluracil (AFMU), a potential BC carcinogen which is a product of NAT2 activity, and single nucleotide polymorphism (SNP) rs1495741 near the N-acetyltransferase 2 (*NAT2*) gene which showed linkage disequilibrium with a SNP, rs35246381, that has previously been reported to be associated with urinary AFMU (303).

A MA of 84 studies demonstrated that both the *GSTM1* and *GSTT1* null genotypes, were associated with increased BC risk in the overall population (OR: 1.40, 95% CI: 1.31–1.48 for *GSTM1* and OR:1.11, 95% CI: 1.01-1.22 for *GSTT1*)(304). A MA of 34 case control studies

showed the GSTP1 gene polymorphism (313 A/G rs1695) was also associated with increased BC risk (GG vs AA; OR: 1.33, 95% CI 1.04–1.69) (305).

A SR of 5 studies demonstrated arsenic (+3 oxidation state) methyltransferase (AS3MT) gene polymorphisms (rs3740393 and rs11191438 polymorphisms) were associated with increased BC risk potentially because of regulating inorganic arsenic metabolism (306).

### **3.5.12. Urinary Tract Inflammation**

#### **3.5.12.1. Urinary Tract Infection**

Whilst the association between schistosomiasis, an infectious disease caused by parasitic flatworms called schistosomes, and BC risk (squamous cell carcinoma of the bladder) is well established (254), the association with non-schistosomiasis urinary tract infection is less well defined. A MA of 8 studies demonstrated increased BC risk with urinary tract infections (RR 1.33, 95% CI: 1.14–1.55) (307)

#### **3.5.12.2. Neurogenic Bladder and Long-Term Catheter**

Neurogenic bladder is a broad term used to refer to bladder dysfunction caused by diseases of the central and peripheral nervous system such as stroke, Parkinson's Disease, spinal cord injury and spina bifida. Patients with neurogenic bladders can have bothersome urinary tract symptoms such as hesitancy, poor stream, urgency and frequency. They may also have urinary retention or urinary incontinence and may require catheterisation to manage this (308).

There have been previous reports of increased BC risk in neurogenic bladder patients with a higher incidence of squamous cell histology, but the causes are unclear. The proposed pathophysiology is secondary to chronic irritation due to long term catheters and recurrent urinary tract infections. A cohort study with 7004 subjects reported that BC was diagnosed in 0.5% of spinal cord injury (SCI) patients. 95% of BCs had a >10 years latency between the onset of SCI and BC diagnosis. Long-term catheters (LTC) were the bladder emptying method in 22% of BC cases suggesting a BC risk independent of LTCs. An important

limitation is the absence of data on key BC risk factors i.e. smoking (309). A SR of 15 studies reported a comparable overall incidence of BC of 0.33% (Range: 0.11%-7.4%) in the neurogenic bladder population (310) (vs 0.5% in spinal cord injury patients in Bothig et al 2020 described above) (309).

A Canadian cohort study of 147, 612 subjects demonstrated increased BC risk with LTCs (HR: 4.80, 95% CI: 4.26-5.42). BC risk was highest among patients in the two longest catheter duration quintiles (2.9–5.9 and 5.9–15.5 years) (311). It is important to note that there could be a detection bias as patients with neurogenic bladder and long-term catheters are more likely to be under regular hospital follow up.

### **3.5.12.3. Urolithiasis**

Previous work on urolithiasis and BC has been inconsistent. A MA of 13 studies demonstrated an increased risk of BC in patients with urolithiasis (OR: 1.87, 95% CI, 1.45–2.41) (312). This may be due to the associated chronic irritation and inflammation. The BC risk was increased with bladder stones (OR: 2.17, 95% CI: 1.52-3.08) and kidney stones (OR: 1.39, 95% CI: 1.06-1.82). Important potential confounders such as smoking occupation were not adjusted for the majority of included studies. There is also a potential surveillance bias as patients with urolithiasis are likely to have had more follow up imaging than the general population.

### **3.5.12.4. Benign Prostate Hyperplasia and Bladder Diverticulae**

BPH has previously been proposed as a risk factor possibly due to prolonged contact time of urothelium with urine carcinogens, but the data has been inconsistent. A retrospective cohort of 35,092 subjects demonstrated increased BC risk with BPH (HR: 4.11, 95% CI: 2.70–6.26) (313).

A cohort study of 10, 662 subjects demonstrated increased BC risk with bladder diverticulae (HR: 2.63, 95% CI: 1.74–3.97) (314). This may be due to prolonged urothelial contact with

urinary carcinogens due to urinary stasis. This study did not evaluate the association between bladder diverticulae and intra diverticulae BCs specifically.

### **3.5.13. Medical Conditions (This section was written with assistance from a collaborator: Dr Sean Ong, University of Melbourne, Australia)**

Previous studies have evaluated medical conditions, but the evidence for certain conditions has been inconsistent. As numerous medical conditions and treatments are intrinsically linked, it is difficult to ascertain the effect of specific conditions and treatments on BC risk.

#### **3.5.13.1. Pelvic Radiotherapy**

Previous studies investigating secondary BC following pelvic radiotherapy (RT) have had inconsistent results. A cohort study of 440,792 subjects with six years follow-up reported increased BC risk with external beam radiotherapy (EBRT) for prostate cancer compared to radical prostatectomy (HR: 1.41, 95% CI: 1.33-1.51) (315). There were similar findings in a cohort of 84,397 subjects (316) and a MA of 15 studies (including 619,479 subjects) (317). A cohort study (including 318,058 subjects) with a median follow up of approximately 10 years demonstrated increased BC risk with brachytherapy (HR 1.58; 95% CI 1.46-1.72) (318). Whole exome sequencing of muscle invasive BCs demonstrated distinct genomic profiles in BCs with previous RT (increased frequency of short insertions and deletions [indels])(319).

Increased secondary BC risks were also reported following RT for gynaecological cancer (HR: 2.69, 95% CI: 2.29-3.16)(320).

#### **3.5.13.2. Obesity**

Previous data on obesity and BC risk is inconsistent. A cohort study of 11,823,876 men demonstrated increased BC risks with higher BMI categories but only in participants with waist circumference >90cm suggesting abdominal obesity to play a key role (321).

A pooled analysis of 6 cohort studies (including 811,633 subjects) showed no significant association between raised BMI and BC risk overall in men but and an inverse association

between raised BMI and BC risk overall in women (HR: 0.90, 95% CI: 0.82-0.99). Analysis of BC subtypes showed an association between raised BMI and NMIBC in men (HR: 1.09, 95% CI: 1.01-1.18) (322). This study is limited by lack of data on potential confounders such as co-morbidities and physical activity.

### **3.5.13.3. Metabolic syndrome**

Previous research on metabolic syndrome (which comprises central obesity, insulin resistance, hypertriglyceridemia, hypercholesterolaemia, hypertension and reduced high density lipoprotein [HDL]) and BC risk has been inconclusive. A SR and MA of 4 studies demonstrated increased BC risk with metabolic syndrome (RR 1.09, 95% CI, 1.02 to 1.17) (323). This study did not specify the confounding factors that were adjusted for in individual studies and there may be a confounding effect from medications.

### **3.5.13.4. Diabetes**

In a cohort of 95, 796 subjects, there was no significantly increased risk of BC in the T2DM group after 16 years follow up (324). Similar findings were reported in a cohort of 148, 208 women (325). However, increased BC risk were reported in a Korean cohort of over 25 million subjects with a mean follow up period of 8.6 years (HR: 1.28, 95% CI: 1.23-1.33). This study is limited by potential misclassification of diabetic subjects and did not adjust for smoking and diabetic medications (326).

### **3.5.13.5. Hypertension and Hyperlipidaemia**

A pooled prospective cohort study of 811, 633 men and women reported no association between raised cholesterol and BC risk. However, there was increased BC risk with increasing blood pressure in men (HR: 1.09, 95% CI: 1.02-1.17) but not women. An important limitation is the potential confounding effect of drug treatments, occupational and environmental exposures on the results (322).

### **3.5.13.6. Stroke**

A cohort study of 944, 633 subjects reported increased BC risk in the stroke population (HR 1.43; 95% CI: 1.17-1.76) (327). However, smoking status and other specific medical comorbidities were not adjusted for.

### **3.5.13.7. Asthma**

Previous reports on asthma or atopic disease and BC risk have had inconsistent results. A MA of 7 studies (2, 171, 549 subjects) found an increased BC risk in patients with current or previous asthma (HR 1.46; 95% CI: 1.18–1.80)(328). A proposed mechanism is associated oxidative stress, reactive oxygen species and resulting DNA damage.

### **3.5.13.8. Autoimmune and Rheumatological Conditions**

A MA of 10 cohort studies reported increased BC risk (HR 1.92; 95% CI 1.15–3.21) with systemic lupus erythematosus (SLE) (329). Similar findings have been reported for vasculitis. A cohort study of 9910 subjects reported increased BC risk with antibody-associated vasculitis (AAV) (HR: 2.70 95% CI: 1.20-6.10) (330). Similarly, a cohort study of 359, 860 subjects reported increased BC risk with gout (HR 1.15 95% CI: 1.01-1.30)(331). These studies did not adjust for treatments in their analyses. There was no significant association between Inflammatory Bowel Disease (IBD) and BC risk in two MAs (332, 333).

### **3.5.13.9. Solid Organ Transplantation**

Several studies have previously reported increased BC risk following kidney transplant believed to be due to immunosuppressive therapy. However, there have also previously been conflicting reports. A cohort study (including 3069 subjects) reported an incidence of solid organ malignancy of 3.6% in kidney transplant recipients. Of the solid organ malignancies reported, 5.3% were BCs (0.20% BC overall in kidney transplant patients)(334).

A study of 11,004 liver transplant patients reported a risk of de novo malignancy of 2.1% at 1 year, 13% at 5 years and 28% at 10 years. Of the reported malignancies, 1.1% were BCs (335). It is important to note that the potential effect of key BC risk factors such as smoking were not considered.

### **3.5.13.10. Associations with other cancers**

A cohort study of 10,734 men with non-seminoma testicular cancer demonstrated increased BC risk compared to the general population (SIR: 1.47, 95% CI: 1.07- 1.59) potentially related to effects of cisplatin-based chemotherapy, radiation from surveillance imaging and radiotherapy (336).

### **3.5.14. Medications (This section was written with assistance from Dr Sean Ong, University of Melbourne, Australia)**

The IARC has classified cyclophosphamide and chlornaphazine as having sufficient evidence for BC (254). Exploratory evidence showed increased BC risks for pioglitazone(337, 338), ranitidine (339), levothyroxine(340) and angiotensin 2 receptor blockers (341). No significant association was seen for SGLT2 inhibitors (342), Metformin (343), Aspirin (344, 345), Statins (346), ACE inhibitors, calcium channel blockers or diuretics(341). There were mixed results for reports on androgen deprivation therapy (347) and 5- alpha reductase inhibitors (348-350).

## **3.6. Summary**

BC is a significant global health problem. Whilst the incidence of BC has not significantly changed globally, increased incidence and mortality have been noted in specific regions of the world likely to represent evolving carcinogen exposures. Smoking and specific occupational exposures are the most established risk factors. There is emerging evidence for a number of risk factors including specific dietary factors, gene-external risk factor interactions, and pelvic radiotherapy.

## **Chapter 4. Analysis of the Distal Urinary Tract in Larval and Adult Zebrafish Reveals Homology to the Human System.**

Work in this chapter contributed to the following publication:

**Jubber I**, Morhardt DR, Griffin J, Cumberbatch MG, Glover M, Zheng Y, Rehman I, Loynes CA, Hussain SA, Renshaw SA, Leach SD, Cunliffe VT, Catto JWF. Analysis of the distal urinary tract in larval and adult zebrafish reveals homology to the human system. *Disease models & mechanisms*. 2023;16(7).

#### 4.1. Introduction

The urinary tract is essential for the regulation of extracellular fluid and the excretion of metabolites. In humans, the urinary tract is composed of a multifunctional kidney, with excretory, metabolic, and endocrine roles, and an excretory component. The excretory component comprises two propulsive drainage tubes (ureters) leading to a contractile expansive storage vesicle (urinary bladder) with intermittent outflow via the urethra. Micturition (passing urine) occurs under voluntary and involuntary neurological control. The embryological development of the urinary tract is characterised by complex interactions between various tissues.

In humans, the distal excretory component of the urinary tract begins development at approximately 4 weeks gestation. The cloaca is partitioned by the uro-rectal septum to form the ventral urogenital sinus and the dorsal anorectal canal. The urogenital sinus develops into the urinary bladder and urethra. The mesonephric ducts fuse with the urogenital sinus and the ureteric bud develops as an outgrowth from the distal mesonephric duct. The ureteric bud is involved in reciprocal induction events with the metanephric mesenchyme giving rise to the collecting ducts, renal pelvis, and ureters. The distal mesonephric duct and ureteric bud undergo a remodelling process whereby the ureters fuse with the urogenital sinus and subsequently migrate superiorly and laterally to form the vesicoureteric junctions and the trigone. The distal mesonephric ducts migrate inferiorly to empty into prostatic urethra and form the ejaculatory duct (Figures 1 and 2) (351).

The resultant excretory system is lined by urothelium; a multi-layered epithelium with a terminally differentiated superficial layer as well as intermediate and basal cell compartments (352). The superficial layer is composed of 'umbrella cells' which are characterised by the expression of uroplakin proteins. Uroplakin proteins are from a superfamily of tetraspanins and highly evolutionarily conserved across species (353). They form an asymmetric unit membrane on the apical surface of the superficial urothelial layer and are expressed on the cell membrane and within the cytoplasm. Uroplakin proteins have been reported to have barrier function with respect to water permeability (354, 355). There are 4 important members in humans: Uroplakin-1a, 1b, 2, and 3. Basal cell layers express

transcription factor tumour protein 63 (TP63 or p63) (356) and high molecular weight cytokeratins such as cytokeratin 5 (KRT5) (357).

*Danio rerio* (zebrafish) models have been used to study the biology of the kidney. The zebrafish embryonic and larval kidney (pronephros) is comprised of two crescent shaped nephrons fused in the midline that course from the glomerulus to the pronephric ducts and cloaca (32). The mesonephros (the permanent adult kidney structure in zebrafish) develops at around 10 days post fertilisation (dpf) during the transition from larva to juvenile as the osmoregulatory demands of the fish increase (23). Whilst the zebrafish kidneys have been well characterised, the distal excretory component of the urinary tract is not well studied and it is unclear whether a bladder and urethra exist or if urine exits the body separately from the intestinal tract (26, 358).

Here we describe the zebrafish distal excretory urinary tract. We identify features similar to those observed in larger teleosts and mammals, including a urinary bladder that leads to a distinct urethra transporting urine externally.

## **4.2. Results**

### **4.2.1. Uroplakin Genes in the Zebrafish**

As uroplakin expression is characteristic of human urothelium, we searched for conserved orthologues within the zebrafish genome. We identified three candidate genes: *uroplakin-1a* (ENSDARG00000021866.9), *uroplakin-2-like* (ENSDARG00000103164.2) and *uroplakin-3-like* (ENSDARG00000092872.2). *Uroplakin-1b* is a uroplakin gene which exists in mammals but not in zebrafish. Protein alignment of the zebrafish and human uroplakin genes revealed structural homology and inter-species conservation (Figure 23). Uroplakin-1a is a member of the tetraspanin superfamily of transmembrane proteins, which have 4 transmembrane helices (3 clustered towards the N terminus and 1 at the C terminus). Uroplakin-2 and 3 have a single transmembrane domain towards the C terminus.

Mammalian Uroplakin-1a and 1b interact with Uroplakin-2 or 3a to form two heterodimers that can subsequently exit the endoplasmic reticulum. The two components of this dimer (1a/1b and 2/3a) function together as a unit (353).

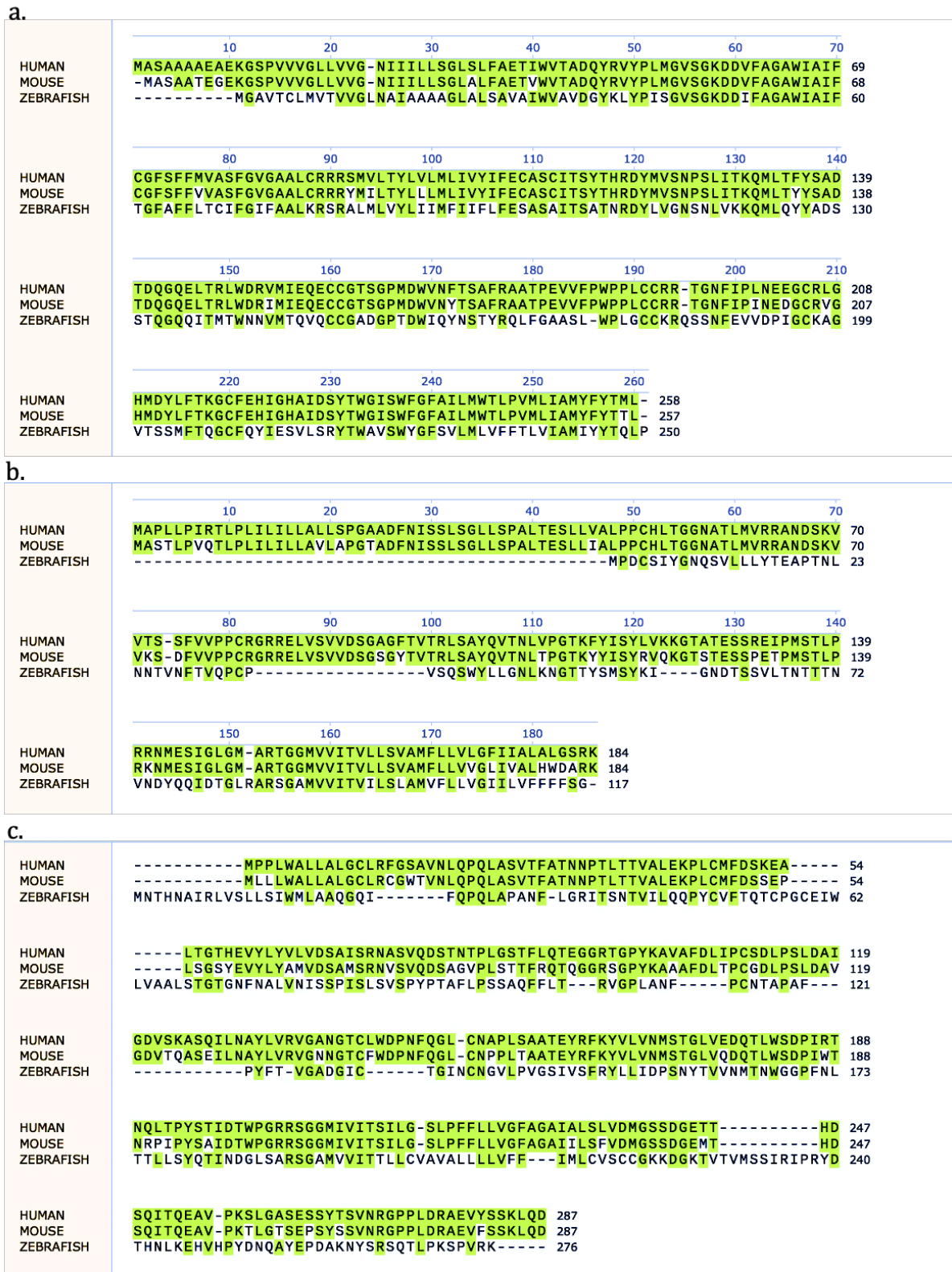


**Figure 23. Alignment of Human, Mouse and Zebrafish Uroplakin Protein Amino Acid Sequences.** (a) Uroplakin 1a, (b) Uroplakin 2, (c) Uroplakin 3a. SnapGene® software (from Dotmatics; available at [snappgene.com](http://snappgene.com)) used for alignment. Human sequence used as reference. Alignment highlighted in green.

#### 4.2.2. Uroplakin-1a mRNA Expression in the Zebrafish Larval Pronephros

Uroplakin-1a is the most highly conserved uroplakin and the only member present in zebrafish from the Uroplakin-1a/1b component of the dimer. Uroplakin-1a is known to line the urothelium in the human urinary tract (urethra, urinary bladder, ureters and renal collecting system) and is highly specific.

The zebrafish pronephros is a functioning urinary tract system which starts to function at around 48 hours post fertilisation. The zebrafish pronephros continues to function during the larval stages and represents the precursor to the final zebrafish urinary tract, the mesonephros.

In order to determine homology between the human urinary tract and the zebrafish pronephros (early urinary tract), *in situ* hybridisation for *uroplakin-1a* was performed. We observed *uroplakin 1a* expression from around 96 hpf (hours post fertilization) in the zebrafish larval pronephros (Figure 24).

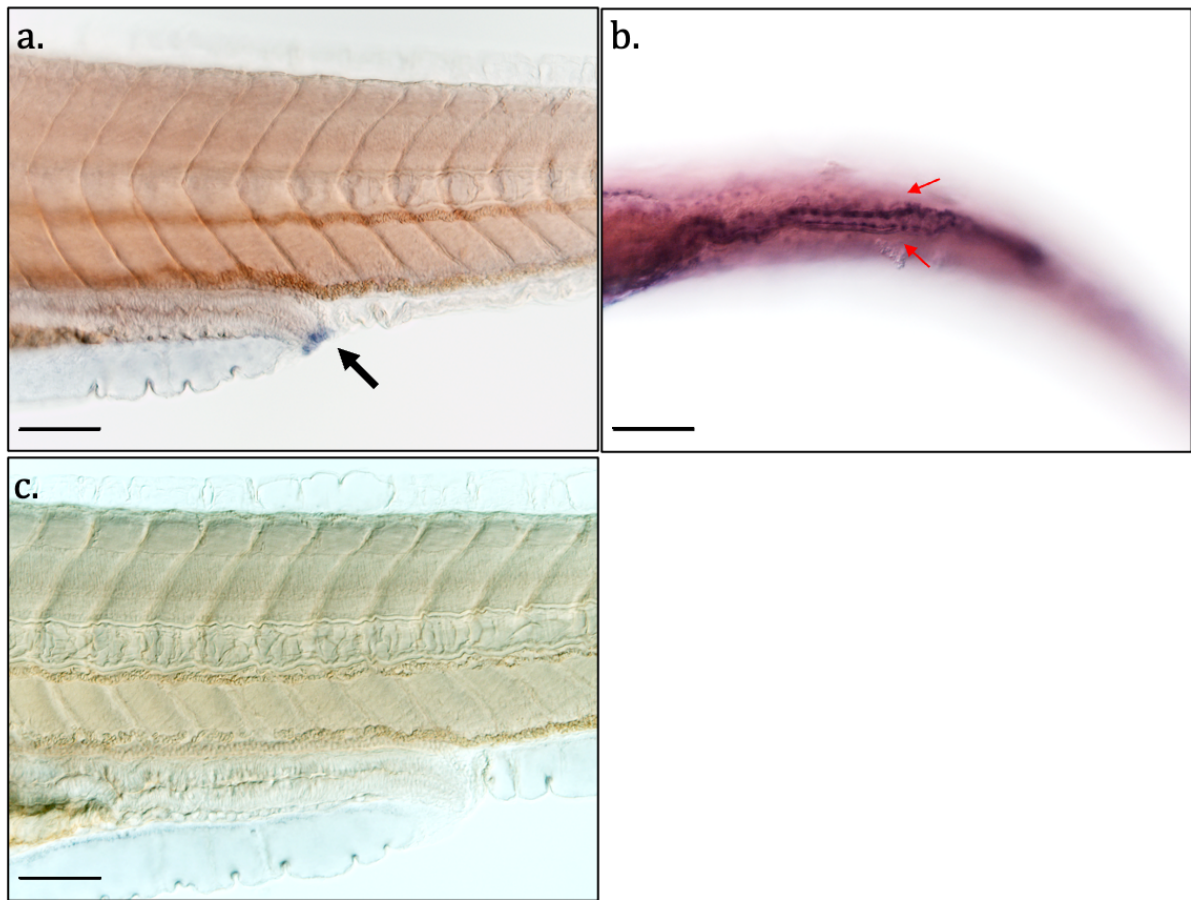


**Figure 24. Expression of *uroplakin 1a* in Zebrafish Larvae Using *in situ* Hybridisation.**

(a) *uroplakin-1a* expression in the cloaca (Black arrow) at 96 hours post fertilisation (hpf) in the lateral view. (b) *uroplakin-1a* expression in the two pronephric ducts (red arrows) as they drain from the kidney towards the cloaca at 120 hpf in the ventral view. (c) Sense Control for *Uroplakin 1a In Situ* Hybridisation in Zebrafish larvae at 96 hpf. Scale bar= 50µm. Scale bars=50µm. Images shown are from 1 experiment. Performed by technician Maggie Glover.

### 4.2.3. Histological Comparison Between Zebrafish and Human Excretory Urinary Tracts

To explore any similarity between the anatomical structures of zebrafish and human excretory urinary tracts, we sectioned and stained adult zebrafish from the kidney to the cloacal region in transverse, coronal and sagittal orientations. Microscopy revealed two mesonephric ducts leaving the distal kidney, traveling inferiorly and caudally before fusing into a single collecting vesicle, with features of a urinary bladder (Figure 25). This structure closely resembles the ureters and urinary bladder in humans. In contrast to human urothelium (which has multiple layers and different cell types), the zebrafish urinary bladder epithelium appeared one to two cells thick and all cells had a similar appearance (regardless of luminal proximity).

Similarities between adult zebrafish and humans were also observed in the anatomy and morphology of the urinary tract structures distal/inferior to the urinary bladder. The urinary bladder in adult zebrafish, as for humans, leads to a urethra and urethral orifice which excretes urine (Figure 26). Furthermore, H&E and Masson's trichrome staining demonstrated that the urethra in both males and female adult zebrafish is lined by an epithelial layer surrounded connective tissue rich in collagen (Figure 26). This histological characteristic is also present in the human urethra. In female adult zebrafish, the urethra and oviduct are separate tubes throughout their lengths (Figure 26). However, in male adult zebrafish the ejaculatory duct joins into the urethra, enabling ejaculation to occur via the urethra, which closely resembles ejaculation in male humans (Figure 26).

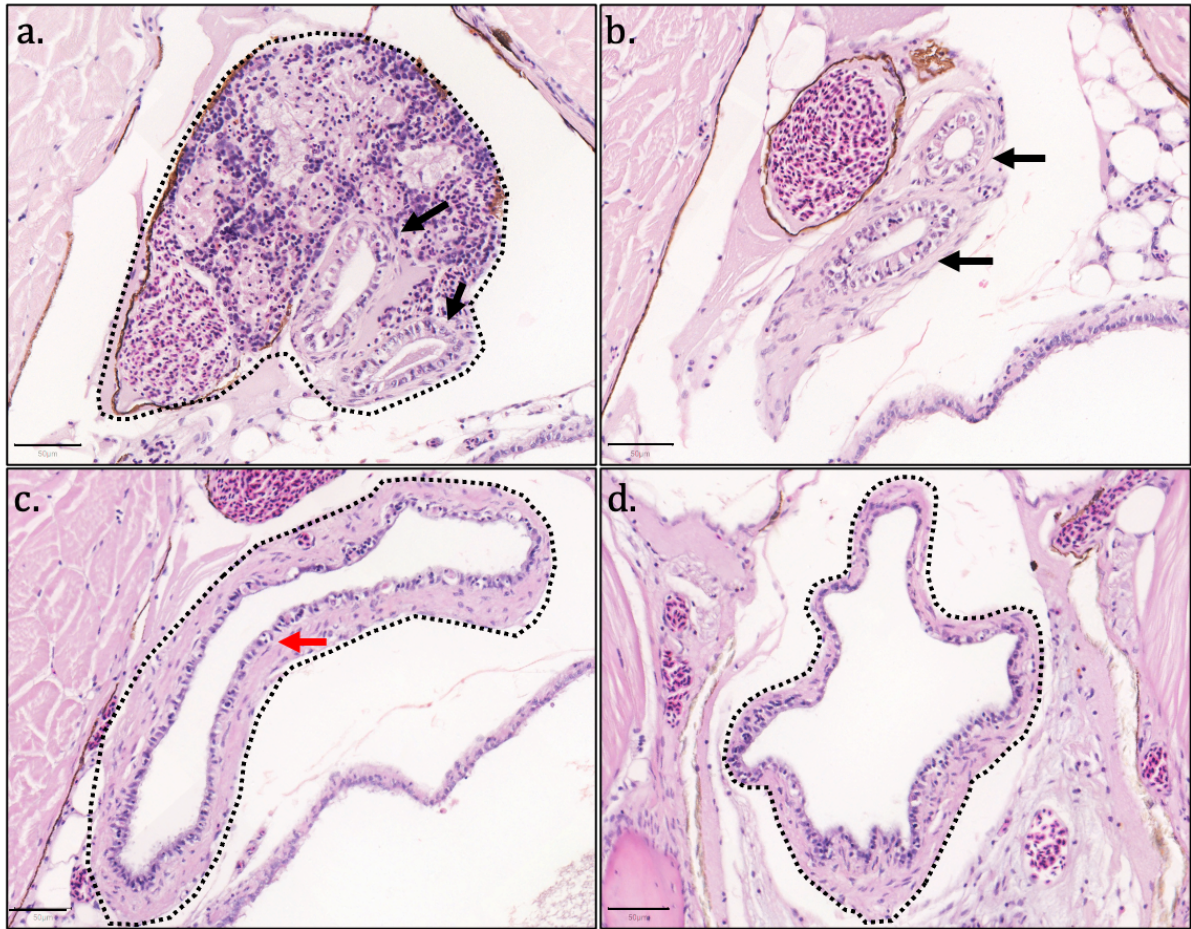


**Figure 25. Anatomy of Adult Zebrafish Mesonephric Ducts and Urinary Bladder.**

H&E-stained adult zebrafish (female) sections in transverse orientation from cranial to caudal. (a) Kidney (black dotted outline) converges onto two mesonephric ducts (Black arrows). (b) Two mesonephric ducts (black arrows) inferior to kidney in retroperitoneum. (c) The two mesonephric ducts unite into a single urinary bladder (black dotted outline) lined by epithelial cells (red arrow). (d) Inferior aspect of urinary bladder (black dotted outline). Images shown are of sections from 1 adult zebrafish. Scale bars=50 $\mu$ m. Histological staining performed by histology technician Maggie Glover.

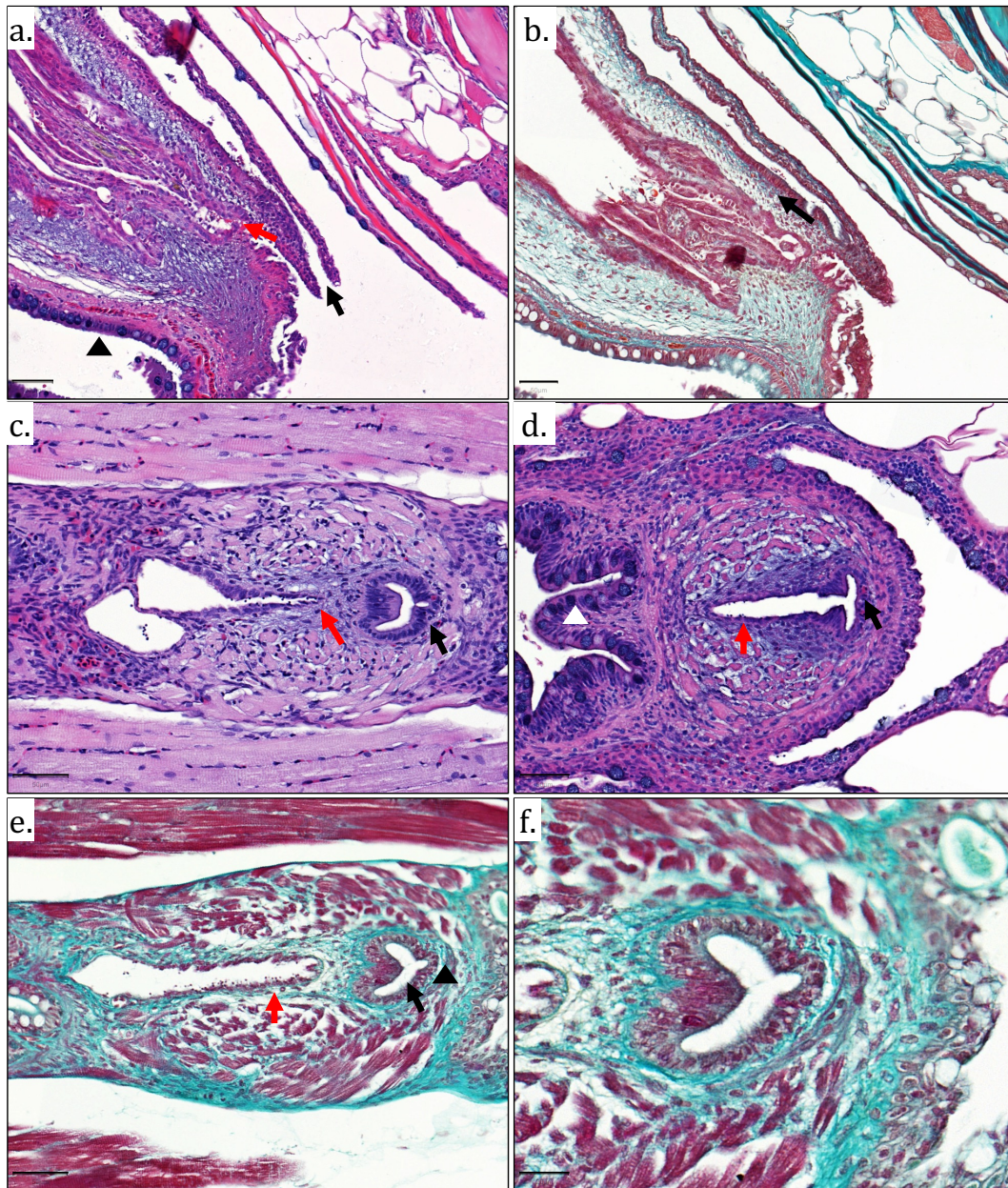


**Figure 26. Anatomy of Adult Zebrafish Urethra.**

(a) H&E stain (sagittal orientation) of adult female zebrafish cloacal region demonstrating distinct and separate urethral orifice (black arrow), oviduct (red arrow) and rectum (black triangle). (b) Masson's trichrome demonstrating connective tissue (light green colouration, black arrow) surrounding female urethra. (c) H&E stain (coronal orientation) of adult male zebrafish cloacal region demonstrating urethra (black arrow), ejaculatory duct (red arrow). (d) H&E stain (coronal orientation) of adult male zebrafish cloacal region demonstrating ejaculatory duct (red arrow) opening into urethra (black arrow) and distinct separate rectum (white arrow). (e) Masson's trichrome stain of male adult cloacal region (coronal orientation) demonstrating muscle fibres surrounding ejaculatory duct (red arrow) and connective tissue (light green colouration, black triangle) surrounding urethra (black arrow). (f) Masson's trichrome stain of male zebrafish urethra at higher magnification. Scale bars =50 $\mu$ m for (a-e) and 20 $\mu$ m for (f). Images shown are of sections from 2 adult zebrafish (Male and female) for Masson's trichrome staining. Histological staining performed with assistance from histology technician Fiona Wright.

To understand protein conservation between the zebrafish and human excretory urinary tracts, we determined the expression of various proteins that are characteristic of human urothelium.

GATA3 is a pioneer transcription factor and urothelial differentiation marker that is highly expressed in normal human urothelium (359). Amino acid alignment of zebrafish and human GATA3 proteins revealed significant homology (Figure 27). Immunohistochemistry revealed strong nuclear GATA3 expression in the zebrafish urothelium that matches human urothelial expression (Figure 28).

<b>Zebrafish</b>	1	MEVSPEQHRWVTHH-----TVGQHPETHHPGLGHSYMDPSQYQLAEDVDVLFNIDGQSNH-	55
<b>Human</b>	1	MEV+ +Q RWV+HH GQHP+THHPGL HSYMD +QY L E+VDVLFNIDGQ NH	60
<b>Zebrafish</b>	56	-PYYGNPVRA-VQRYPPPHSSQMCRPSSLHGSLPWL DGGKSIGPHHSTSPWNLGPFPKT	113
<b>Human</b>	61	PYYGN VRA VQRYPP H SQ+CRP LLHGSLPWL DGGK++G HH+ SPWNL PF KT	120
<b>Zebrafish</b>	114	SLHHSSPGPLSVYPPASSSSLSAGHSSPHLFTFPPTPKDVSPDPAISTSGSGSSVRQED	173
<b>Human</b>	121	S+HH SPGPLSVYPPASSSSLS GH+SPHLFTFPPTPKDVSPDP++ST GS S RQ++	180
<b>Zebrafish</b>	174	KECIKYQVSLAESMKLDSAHSR-SMASIGAGASSAHHPIATYPSYVPDYGPGLFPPSSLI	232
<b>Human</b>	181	KEC+KYQV L +SMKL+S+HSR SM ++G +SS HHPI TYP YVP+Y GLFPPSSL+	240
<b>Zebrafish</b>	233	GGSSSSYGSKTRPKTRSSSEGRECVNCGATSTPLWRRDGTGHYLCNACGLYHKMNGQNRP	292
<b>Human</b>	241	GGSPTGFGCKSRPKARSST-GRECVNCGATSTPLWRRDGTGHYLCNACGLYHKMNGQNRP	299
<b>Zebrafish</b>	293	LIKPKRRLSAARRAGTSCANCQTTTTTLWRRNANGDPVCNACGLYYKLHNINRPLTMKKE	352
<b>Human</b>	300	LIKPKRRLSAARRAGTSCANCQTTTTTLWRRNANGDPVCNACGLYYKLHNINRPLTMKKE	359
<b>Zebrafish</b>	353	GIQTRNRKMSSKSKKSHDSMEDFSKSLMEKNSSFPAALSRHMTSF---PPFSHSGH	409
<b>Human</b>	360	GIQTRNRKMSSKSKK HDS+EDF KNSSF+PAALSRHM+S PFSHS H	414
<b>Zebrafish</b>	410	MLTTPTPMHPSSSLPFASHHPSSMVTAMG	438
<b>Human</b>	415	MLTTPTPMHP SSL F HHPSSMVTAMG	443

**Figure 27. Alignment of Human and Zebrafish GATA3 amino acid sequences.**

GATA3 primary Ab directed towards N terminus region of human GATA3 protein (Dotted red). Amino acid alignment performed using the online National Center for Biotechnology Information (NCBI) BLAST tool (233).

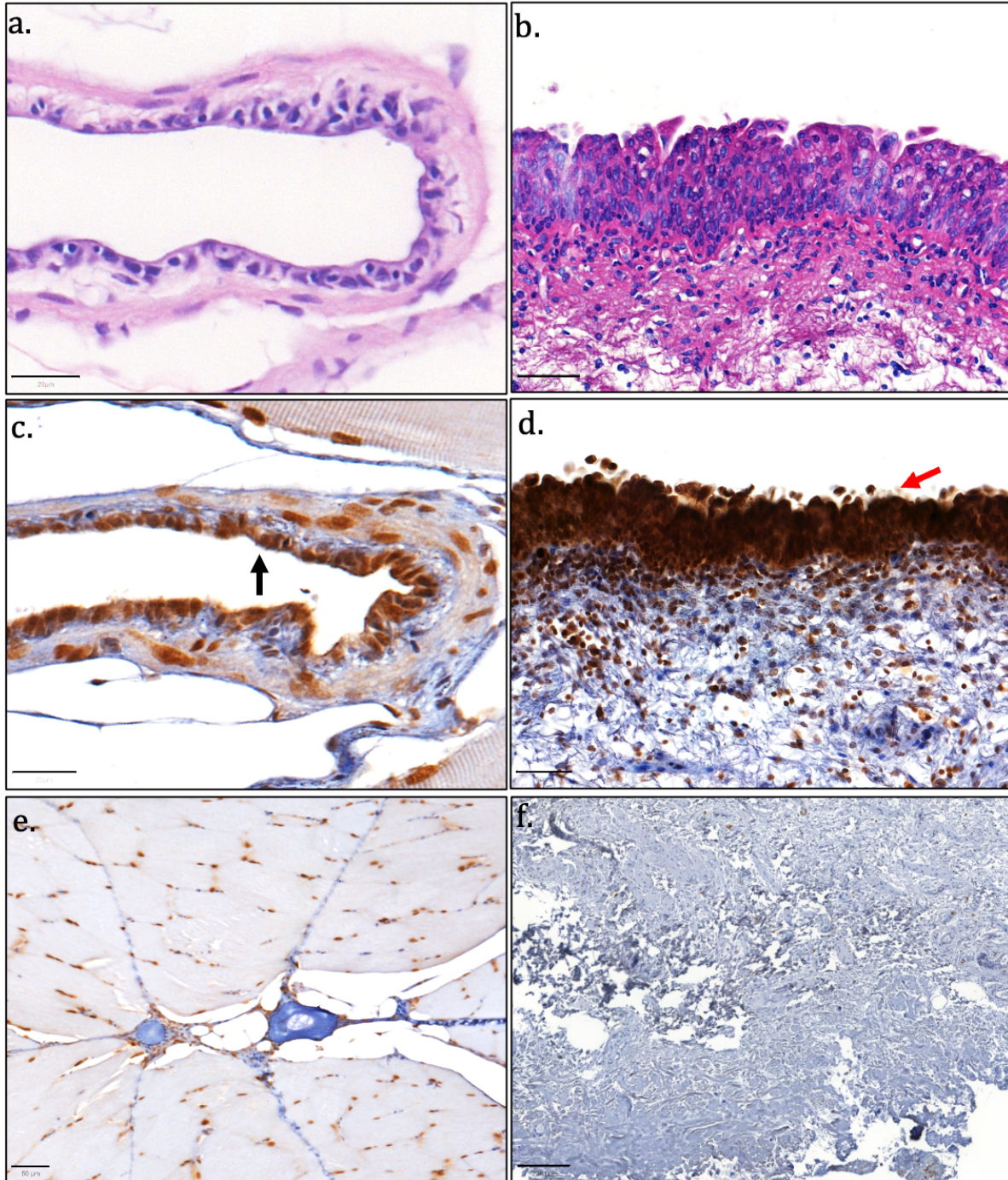


**Figure 28. Expression of GATA3 in Zebrafish and Human Urinary Bladder Tissue Sections Using Immunohistochemistry.**

(a) Hematoxylin and eosin stain of coronal zebrafish urinary bladder section and (b) Human urinary bladder sections for reference. (c) Nuclear expression of Gata3 in zebrafish urinary bladder urothelium (black arrow). (d) Nuclear expression of GATA3 in human urinary bladder urothelium (red arrow). (e) GATA3 antibody stain on zebrafish tail shown for negative control. (f) GATA3 antibody stain on human bladder lamina propria and detrusor muscle shown for negative control. Zebrafish images shown are of sections from 1 adult zebrafish. Scale bar=20 $\mu$ m for (a) and (c). Scale bar=50 $\mu$ m for (b), (d) and (e). Scale bar = 200 $\mu$ m for (f).

Uroplakins are tetraspanin dimers that are characteristic of mammalian urothelium (352). Amino acid sequence alignment demonstrated similarities between human and zebrafish sequences (Figure 29). Immunohistochemistry revealed cytoplasmic and membranous expression of Uroplakin-1a and Uroplakin-2l within the epithelium of the zebrafish urinary bladder and mesonephric duct, in a pattern similar to that seen in human urothelium (Figure 30).

**a.**

Zebrafish	15	NAIAAAAGLALSAVAIWVAVDGYKLYPISGVSGKDDIFAGAWIAIFTGFAFFLTCIFGIF	74
Human	24	N I +GL+L A IWV D Y++YP+ GVSGKDD+FAGAWIAIF GF+FF+ FG+	83
Zebrafish	75	AALKRSRALMLVYLIIMFIIIFLFESASAITSATNRDYLVGNSNLVKKQMLQYYADSSTQG	134
Human	84	AAL R R+++L YL++M I+++FE AS ITS T+RDY+V N +L+ KQML +Y+ + QG	143
Zebrafish	135	QQITMTWNNVMTQVQCCGADGPTDWIQYNSTYRQLFGAASL-WPLGCCKRQSSNFVVDP	193
Human	144	Q++T W+ VM + +CCG GP DW+ + S +R WP CC+R + NF ++	202
Zebrafish	194	IGCKAGVTSSMFTQGCFQYIESVLSRYTWAWSWYGFSVLMLVFFTLVIAMIYYTQL	249
Human	203	GC+ G +FT+GCF++I + YTW +SW+GF++LM ++IAM +YT L	258

**b.**

Zebrafish	1	MPDCSIYGNQSVLLLYTEAPTNLNNTVNFTVQPCVPSQ-----SWYLL	43
Human	48	+P C + G + L++ + + T +F V PC + S Y +	106
Zebrafish	44	GNLKNGTTYSMSYKI----GNDTSSVLTNTTNNVNDYQQIDTGLRARGAMVVITVILSL	99
Human	107	NL GT + +SY + ++S + +T + + I G+ AR+G MVVITV+LS+	165
Zebrafish	100	AMVFLLVGIILVFFFSS	116
Human	166	AM L++G I+ S	182
Human	166	AMFLLVLGFIIALALGS	182

**Figure 29. Alignment of Human and Zebrafish Uroplakin-1a and Uroplakin-2 Amino Acid Sequences.**

(a) Alignment of Human and Zebrafish Uroplakin-1a amino acid sequences (Uroplakin 1a primary Ab directed towards amino acids 100-150 of human Uroplakin1a protein (Dotted red). (b) Alignment of Human and Zebrafish Uroplakin 2 amino acid sequences (Uroplakin 2 primary Ab directed towards last 50 amino acids (C terminus) of human Uroplakin-2 protein (Dotted red). Note human Uroplakin 2 protein is 184 amino acids in length. Amino acid alignment performed using the online National Center for Biotechnology Information (NCBI) BLAST tool (233).

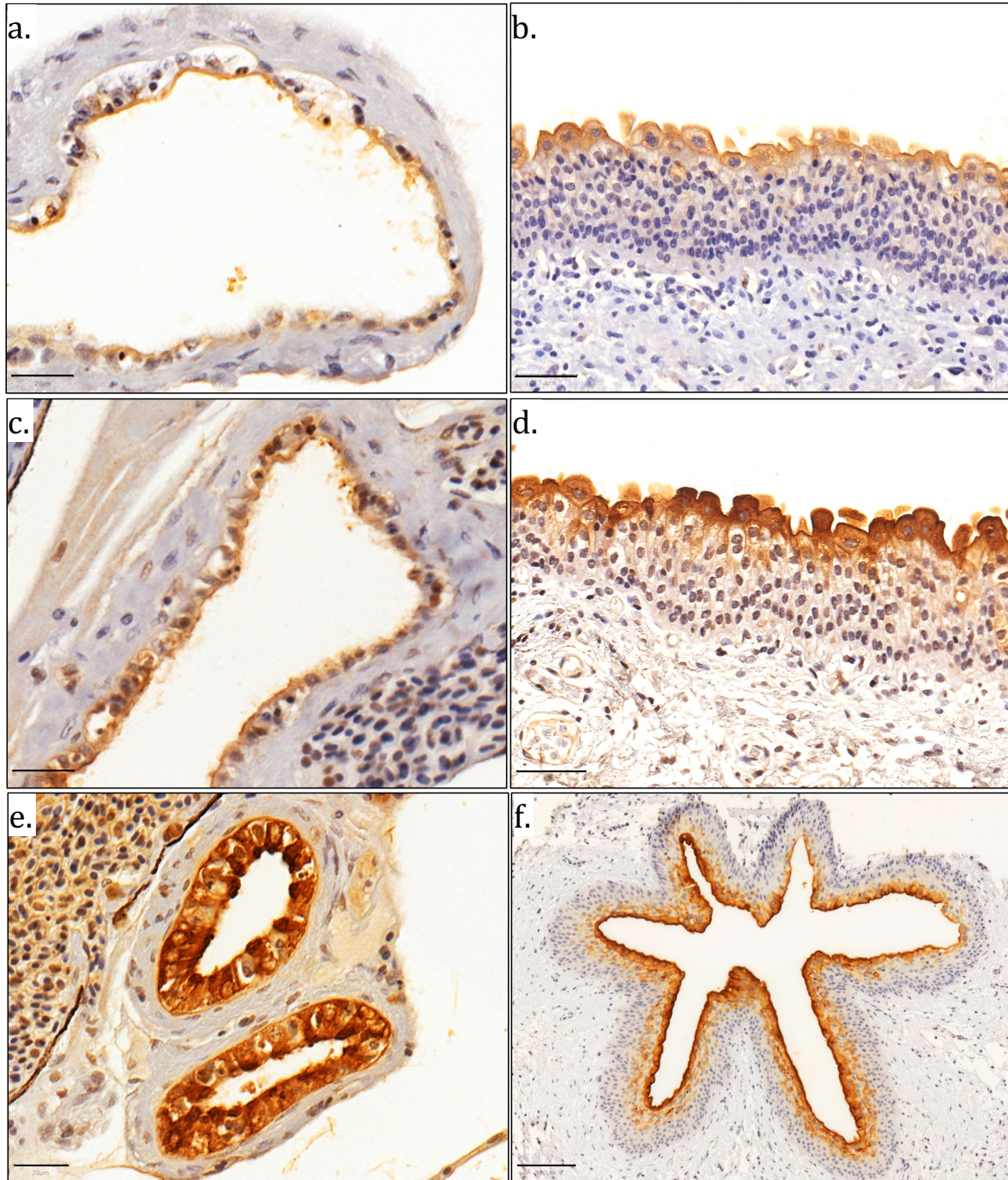


**Figure 30. Expression of Uroplakins in Zebrafish and Human Urinary Bladder Tissue Sections Using Immunohistochemistry.**

(a) Cytoplasmic and membranous expression of urothelium-specific protein Uroplakin 1a (Upk1a) in zebrafish urinary bladder urothelium. (b) Cytoplasmic UPK1A expression in human urinary bladder urothelium. (c) Uroplakin-2l (Upk2l) expression in zebrafish urinary bladder. (d) UPK2 expression in human urinary bladder. (e) Upk2l expression in zebrafish mesonephric duct epithelium. (f) UPK2 expression in human ureter urothelium. Scale bar= 20 $\mu$ m for (a), (c) & (e). Scale bar=50 $\mu$ m for (b) & (d). Scale bar= 100 $\mu$ m for (f). Representative images shown are of sections from 1 adult zebrafish. IHC Performed by technician Maggie Glover, University of Sheffield.

Having demonstrated expression of proteins found in the superficial urothelial layer, we next sought to perform immunohistochemistry for known markers of human basal urothelial layers KRT5 (357) and basal and stem cell marker CD44 (360). The immunogen for the CD44 antibody was the full length 361 amino acid human protein and the immunogen for the KRT5 antibody is the full length 590 amino acid human KRT5 protein. Amino acid alignments for zebrafish and human KRT5 and CD44 revealed significant homology for KRT5 and a small amount of homology for CD44 (Figure 31).

Cytoplasmic KRT5 expression was confirmed in both the zebrafish urinary bladder and mesonephric duct epithelium. However, there was a difference between the expression of KRT5 between zebrafish and human urothelium: KRT5 was expressed throughout the zebrafish urinary epithelium but only in the basal cell layer of the human urothelium (Figure 32). The basal and stem-like marker CD44 showed cytoplasmic expression in the zebrafish urinary bladder urothelium in a similar manner to the human urinary bladder urothelium (Figure 32).

No primary antibody controls for immunohistochemistry are shown in Figure 33.

a.				
Zebrafish	70	SCSYSGVFHVQGKERYSLTFDDAQRCLCERLSTTLANLTQVKTAFNSGMETCRYGWINSSQ	129	
Human	27	+C ++GVFHV+ RYS++ +A LC+ ++TL + Q++ A + G ETCRYG+I TCRFAGVFHVEKNGRYSISRTEAADLCKAFNSTLPTMAQMEKALSIGFETCRYGFI-EGH	85	
Zebrafish	130	LVILRKTPNLNCARNQTDVIIKTS DGKKYDALCYNDKDKSKKNCTEAID	178	
Human	86	+VI R PN CA N T V I TS+ +YD C+N +++CT D VVIPRIHPNSICAANNTGVYILTSNTSQYDTCFNASAPPEEDCTSVTD	134	
Zebrafish	359	CCIVVYRKRLFQKQTLVINSTVAAAE-----NGSAATHQEMVTLNNTDT	404	
Human	666	CI V +R GQK+ LVINS A E NG A+ +QEMV L+N ++ VCIAVNSRRRCGQKKLVLVINSNGGAVEDRKPSGLNGEASK-SQEMVHLVNKES	717	
b.				
Zebrafish	123	PGGVVPIAVTVNQNLAPLNLEIDPNIQVVRTQEKEQIKTLNNRFASFIDKVRFLQQN	182	
Human	137	PGG I VTNQ+LL PLNL+IDP+IQ VRT+E+EQIKTLNN+FASFIDKVRFLQQN PGG---IQEVTVNQSLLTPLNLQIDPSIQVRTEEREQIKTLNNKFASFIDKVRFLQQN	193	
Zebrafish	183	KVLETKWLLQEQ--TTTRSNDAMFEAYIANLRRQLDGLGNEKMKLEGELKNMQNLVED	240	
Human	194	KVL+TKW+LLQEQ T R N++ +FE YI NLRRQLD + E+ +L+ EL+NMQ+LVED KVLDTKWTLLEQGTQTVRQNLPLFEQYINLRRQLDSIVGERGRLDSELNMQDLVED	253	
Zebrafish	241	FKNKYEDEINKRAAVENEFVLLKKDVDAAAYMNKVELEAKVDSLQDEINFLRAIFEEELRE	300	
Human	254	FKNKYEDEINKR ENEFV+LKKDVDAAAYMNKVELEAKVD+L DEINF++ F+ EL + FKNKYEDEINKRTTAENEFVMLKKDVDAAAYMNKVELEAKVDALMDEINFMKMFFDAELSQ	313	
Zebrafish	301	LQSIKIDTSVVVEMDNSRNLMDAIVA EVAQYEDIANRSRAEAEESWYKQKFEEMQSSAG	360	
Human	314	+Q+ + DTSVV+ MDN+RNL D+D+I+AEV+AQYE+IANRSR EAESWY+ K+EE+Q +AG MQTHVSDTSVVLSDNRRNLDLDSIIAEVKAQYEEIANRSRTEAESWYQTKYEELQQTAG	373	
Zebrafish	361	KYDDLRLNTKAEIADLNRMI SRLQNEIEAVKQORANLEAQIAEAEERGELAVKDAKLRIK	420	
Human	374	++GDDLRLNTK EI+++NRMI RL+ EI+ VK Q ANL+ IA+AE+RGELA+KDA+ ++ RHGDDLRLNTKHEISEMNRMIQRLRAEIDNVKKQCANLQNAIADAEQRGELALKDARNKLA	433	
Zebrafish	421	DLEDALQRAKQDMARQVREYQELMNVKLALDIEIATYRKLLEGEESRIA	469	
Human	434	+LE+ALQ+AKQDMAR +REYQELMN KLALD+EIATYRKLLEGEE R++ ELEELQKAKQDMARLLREYQELMNTKLALDVEIATYRKLLEGEECRLS	482	

**Figure 31. Amino acid Alignment of Zebrafish and Human CD44 and Cytokeratin 5 Sequences.**

(a) Zebrafish Cd44b and human Cd44 sequences aligned using online BLAST tool. Homology is seen to human Cd44. Sequence homology is seen between at human amino acid sequences 27-134 (N terminus region) and human amino acid sequence 666-717 (C-terminus region). Note that human CD44 amino acid sequence is 742 amino acids long and zebrafish CD44b amino acid sequence is 405 amino acids long. (b) Zebrafish and human CK5 sequences aligned using online BLAST tool. Homology is seen to human CK5 amino acids 137-482. Note that human cytokeratin 5 is 590 amino acids long. Amino acid alignment performed using online National Center for Biotechnology Information (NCBI) BLAST tool (233).

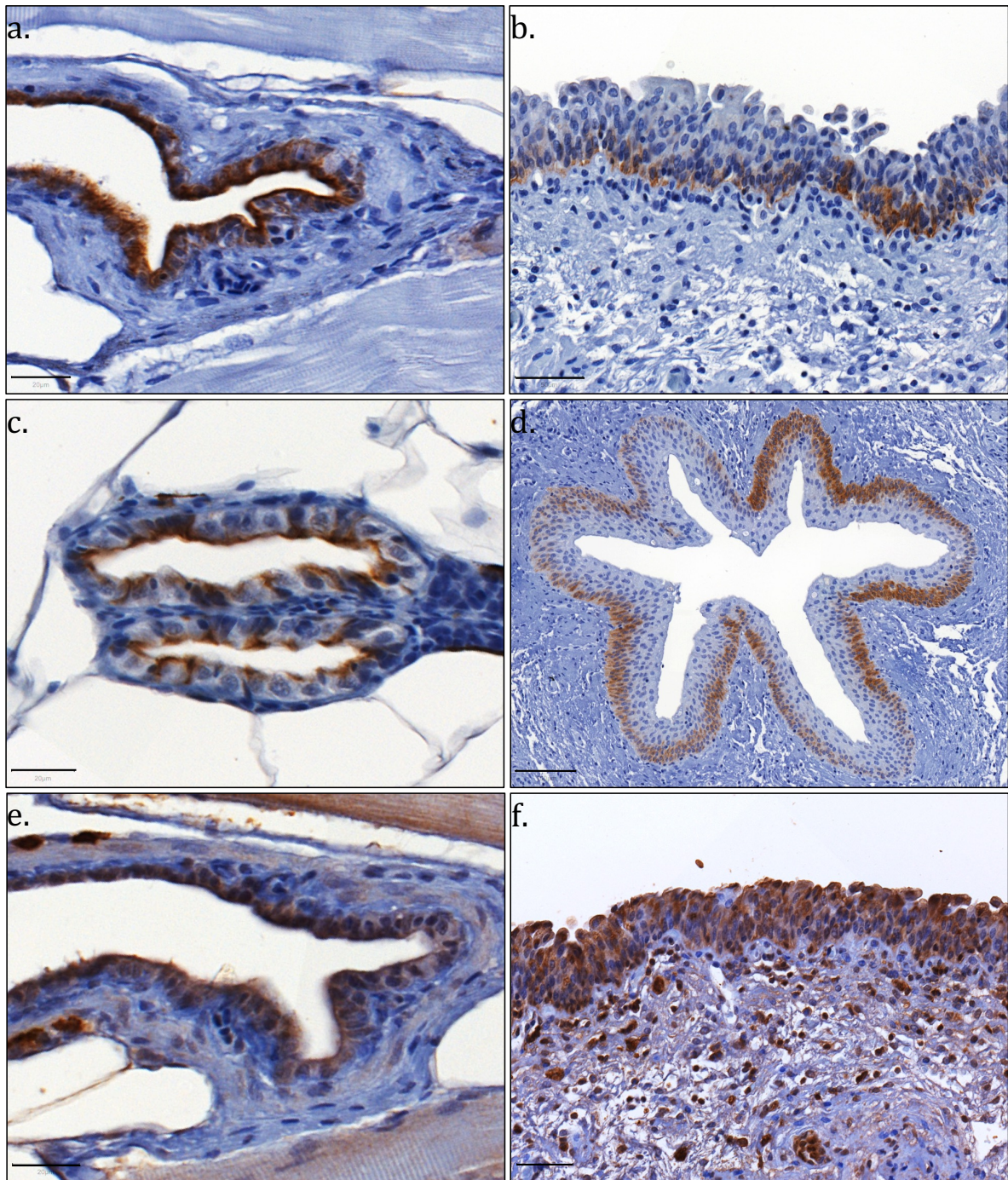


**Figure 32. Expression of Urothelial Basal Cell Layer Markers in Zebrafish and Human Urinary Bladder Tissue Sections Using Immunohistochemistry.**

(a) Cytoplasmic expression of Krt5 in zebrafish urinary bladder urothelium. (b) Cytoplasmic KRT5 in human urinary bladder urothelium. (c) Cytoplasmic Krt5 expression in zebrafish mesonephric duct epithelium. (d) Cytoplasmic KRT5 expression in human ureter urothelium. (e) Cytoplasmic CD44 expression in zebrafish urinary bladder urothelium. (f) Cytoplasmic CD44 expression in human urinary bladder urothelium. Scale bar = 20 $\mu$ m for (a), (c), (e). Scale bars=50 $\mu$ m for (b) and (f). Scale bar=100 $\mu$ m for (d). Images shown are of sections from 1 adult zebrafish.

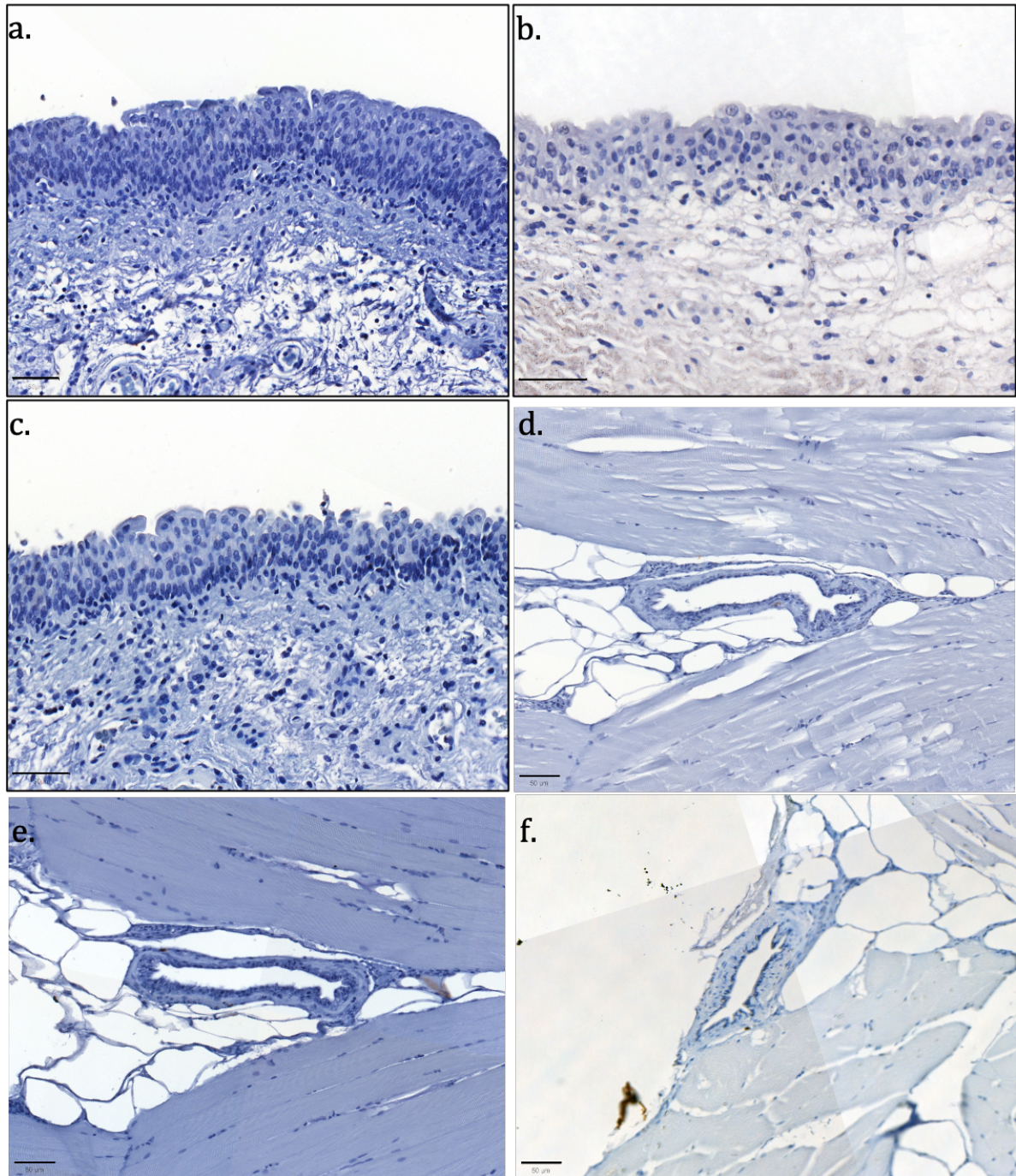


**Figure 33. Negative (No Primary Antibody) Controls for Immunohistochemistry.**

(a) No primary antibody control for biotinylated goat anti-rabbit secondary antibody, (b) No primary antibody control for biotinylated rabbit anti-goat secondary antibody. (c) No primary antibody control for biotinylated goat anti-mouse secondary antibody. (d) No primary antibody control for biotinylated goat anti-rabbit secondary antibody. (e) No primary antibody control for biotinylated goat anti-mouse secondary antibody. (f) No primary antibody control for biotinylated rabbit anti-goat secondary antibody. Scale bars= 50µm.

Masson's trichrome staining demonstrated that the wall of the zebrafish mesonephric ducts and urinary bladder have a connective tissue layer rich in collagen deep to the epithelial layer. Similar to the zebrafish mesonephric duct, the human ureter also has a connective tissue layer deep to the epithelial layer (Figure 34). However, the human ureter has a muscle layer deep to the connective tissue (lamina propria) layer which is not present in the zebrafish mesonephric duct. Masson's trichrome staining demonstrated the zebrafish urinary bladder wall has, deep to the epithelial layer, a connective tissue layer and a deeper thin layer of muscle fibres. The structure of the human urinary bladder wall follows a similar pattern (Figure 34).

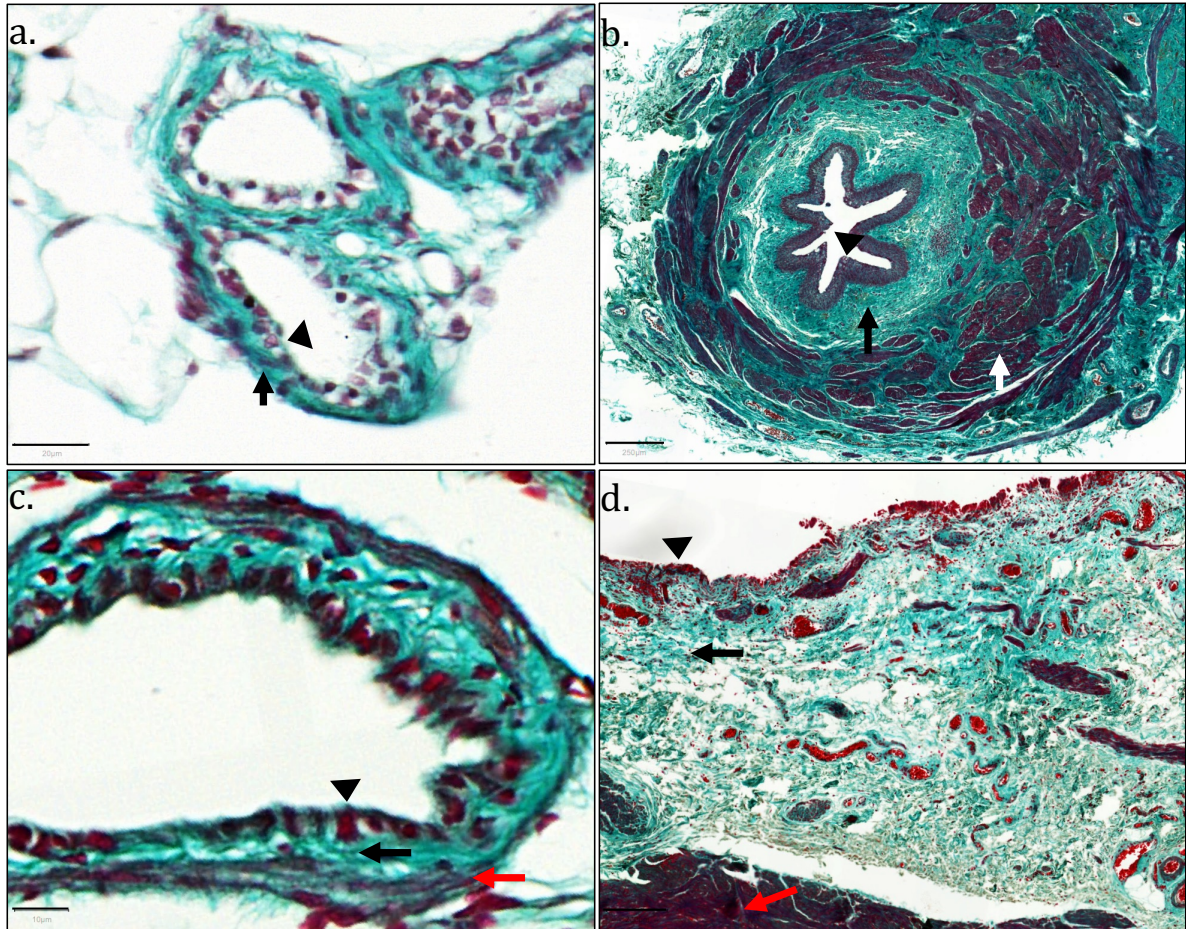


**Figure 34. Structure of Zebrafish Mesonephric Duct and Urinary Bladder Wall.**

(a) Masson's trichrome stain of zebrafish mesonephric duct sections (coronal orientation) demonstrating connective tissue layer (light green colouration, black arrow) deep to epithelial layer (black triangle). (b) Masson's trichrome of human ureter section, for comparison, demonstrating connective tissue layer (light green colouration, black arrow) deep to epithelial layer (black triangle) and muscle layer (white arrow). (c) Masson's trichrome stain of zebrafish urinary bladder section (Coronal orientation) demonstrating, deep to epithelial layer (black triangle), a connective tissue layer (light green colouration, black arrow) and thin muscle fibres (red fibres, red arrow). (d) Masson's trichrome stain of human urinary bladder section demonstrating, deep to epithelial layer (black triangle), a connective tissue layer (light green colouration, black arrow) and a muscle layer (red fibres, red arrow). Scale bar=20  $\mu\text{m}$  for (a), 250  $\mu\text{m}$  for (b), 10  $\mu\text{m}$  for (c) and 200  $\mu\text{m}$  for (d). Images shown are of sections from 1 adult zebrafish. Performed with assistance from Fiona Wright, histology technician, University of Sheffield.

#### 4.2.4. Change in Excretory Urinary Tract Morphology Over Time

I performed optimisation of a technique to dissect open zebrafish and perform fluorescence microscopy of their urinary tract in order to characterise the reporter gene expression in specific regions of the urinary tract in another adult zebrafish line (Data shown in Chapters 5 and 6). This optimisation was carried out on the *Tg(mpx:GFP)i114* zebrafish line (217), which is a transgenic reporter line with green fluorescent protein (GFP) expression in neutrophils. As the zebrafish kidney is also the site of haematopoiesis, the *Tg(mpx:GFP)i114* zebrafish line would be likely to have GFP expression in the adult zebrafish kidney and thus would serve as a good positive control to show, as a proof of concept, that the technique of dissecting open zebrafish and performing fluorescence microscopy of their urinary tract was working.

During the process of imaging the *Tg(mpx:GFP)i114* zebrafish line, it was noticed, for the first time, that this line labelled the zebrafish urinary tract (tubules, mesonephric ducts and urinary bladder) and gut in addition to neutrophils. As there are, to date, no available transgenic zebrafish reporter lines that label the zebrafish excretory urinary tract and urinary bladder, this presented an opportunity to use this line to evaluate the embryological development of the zebrafish urinary tract with respect to morphology.

At 2 weeks and 3 weeks post fertilisation, the GFP expression was localised to the gut, distal pronephros and neutrophils. The distal pronephros/mesonephros, which likely represents the precursor to the urinary bladder, had a tubular appearance. By 4 weeks post fertilisation, the GFP expression was localised to the renal tubules, ducts, and the most distal excretory urinary tract i.e. the urinary bladder. At this stage, the urinary bladder still had a tubular like appearance (Figure 35). By 6 weeks post fertilisation, the urinary bladder became a saccular/expansile structure, and this persisted to adulthood (Figure 36).

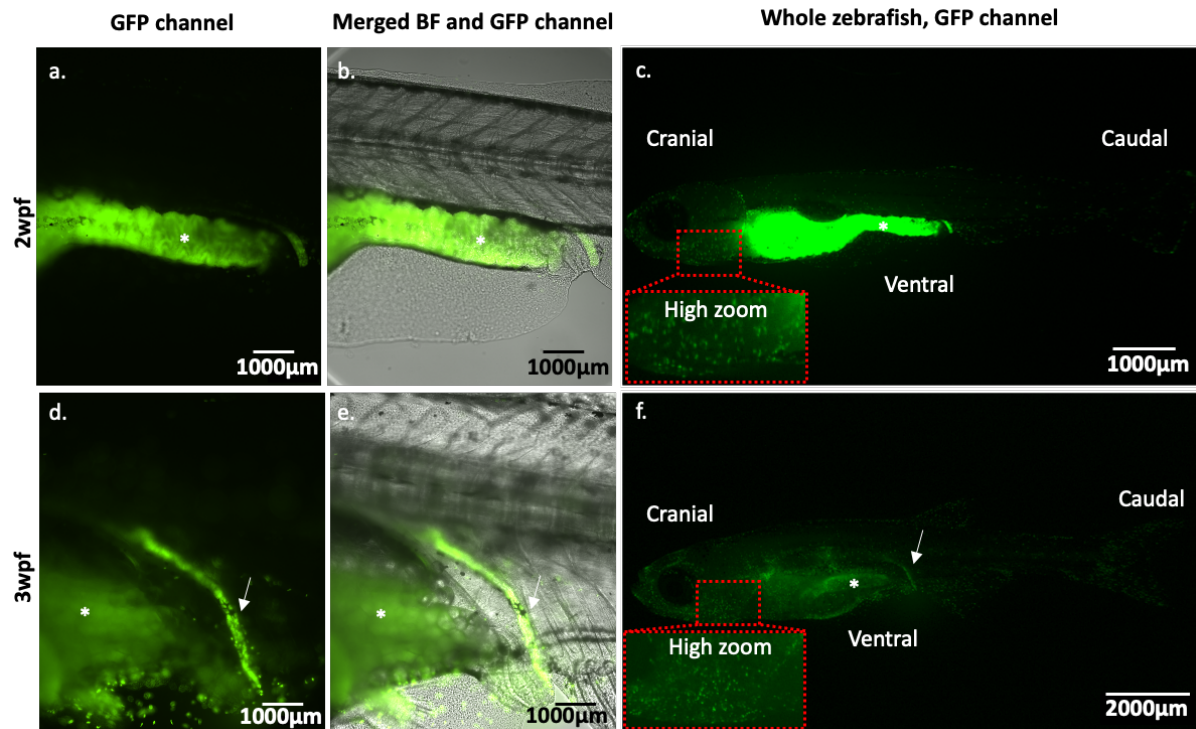


**Figure 35. Analysis of Morphological Development of the Zebrafish Urinary Bladder Using GFP expression in the *TgBac(mpx: GFP) i114* Zebrafish Line Between 2- and 3- Weeks Post Fertilisation.**

(a-c) GFP expression distal urinary tract (White arrow) at 2 weeks post fertilisation (Lateral Orientation). GFP expression in gut (white asterisk) and neutrophils (Red dotted square on zebrafish and red dotted square showed at higher zoom below zebrafish) also shown. (d-f) GFP expression distal urinary tract (White arrow) at 3 weeks post fertilisation (Lateral Orientation). GFP expression in gut (white asterisk) and neutrophils (Red dotted squares on whole zebrafish in (c) and (f)) also shown.

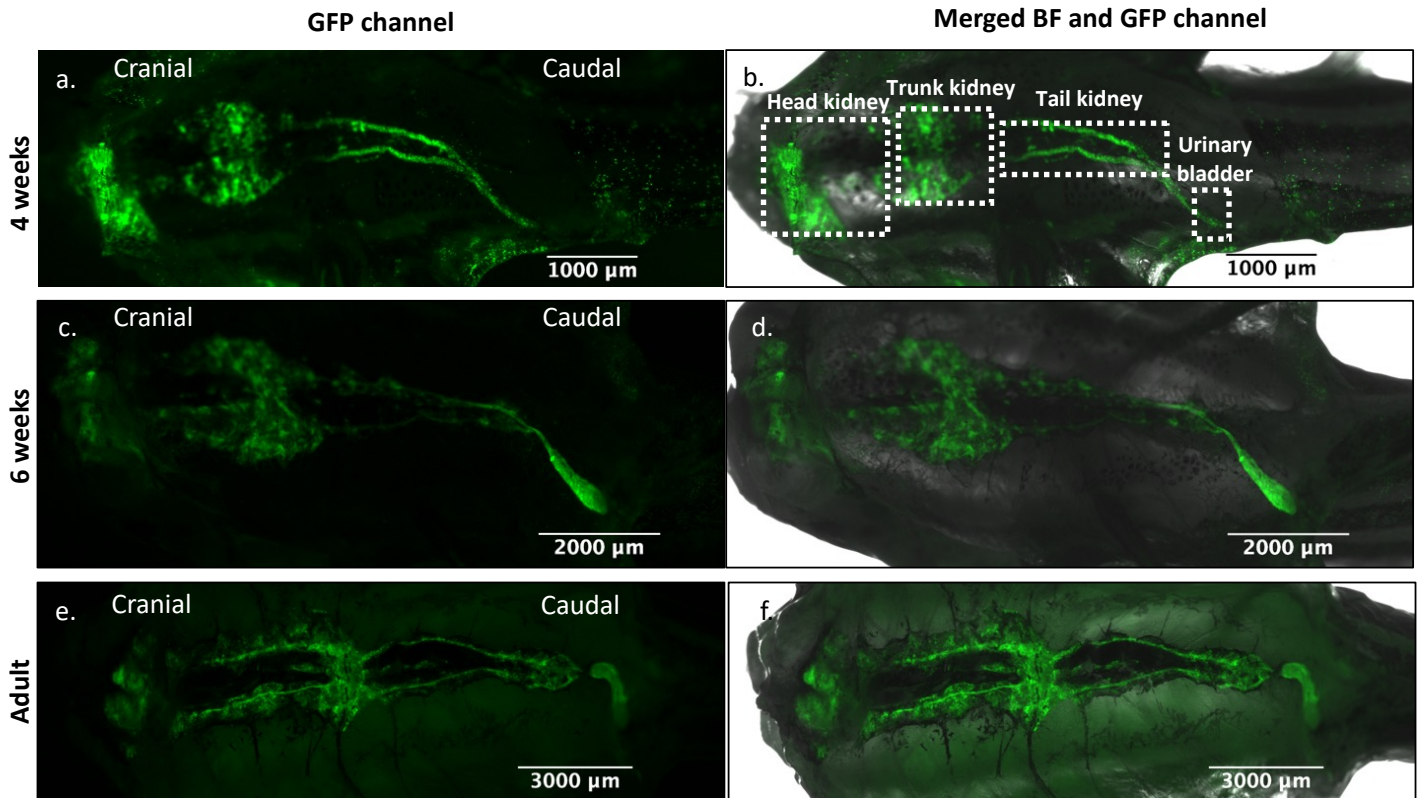


**Figure 36. Analysis of Morphological Development of the Zebrafish Urinary Bladder Using GFP Expression in the *TgBAC(mpx: GFP)i114* Zebrafish Line Between 4-Weeks Post Fertilisation and Adult Stages.**

Ventral abdominal wall incised open, urinary tract exposed (gut, gonads and swim bladder removed) and ventral surface of dorsal abdominal wall imaged. (a-b) 4 weeks old, (c-d) 6 weeks old, (e-f)) Adult ( $\geq 3$  months). Zebrafish urinary bladder develops from a tubular structure at 4 weeks old to a saccular/expansile structure at 6 weeks to adulthood.

#### 4.2.5. Characterisation of Adult Zebrafish Urinary Bladder Morphology Using *TgBAC(mpx:GFP)i114* Line

Having shown for the first time that the *TgBAC(mpx:GFP)i114* zebrafish line, in addition to labelling the neutrophils, also labels the distal urinary tract throughout the lifecycle of the zebrafish, it was possible to characterise, in detail, the morphological structure and anatomical relations of the adult zebrafish urinary bladder (Figure 37). Since the *MPO* gene (Myeloperoxidase, the human orthologue of the promoter used in the zebrafish *TgBAC(mpx:GFP)i114* line) is not known to be expressed in the human urinary bladder (361, 362), this labelling of the urinary bladder in the *TgBAC(mpx:GFP)i114* zebrafish line is likely to be due to position effects. This is a phenomenon whereby upstream or downstream gene promoters or enhancers, both within the BAC and at the genome insertion site of the BAC, can potentially drive reporter gene expression in tissues that are not associated with the zebrafish *mpx* gene promoter.

Two mesonephric ducts (analogous to ureters) run, in parallel, along the dorsal abdominal wall of adult zebrafish with approximately 1000µm in between them. Macroscopically, this region of the dorsal abdominal wall is pigmented which is best visualised in the brightfield channels. The two mesonephric ducts converge at the caudal aspect of the dorsal abdominal wall to a single urinary bladder. The urinary bladder is approximately 2000µm in length and saccular in shape. It tapers inferiorly and caudally to a narrow urethra (Figure 37).

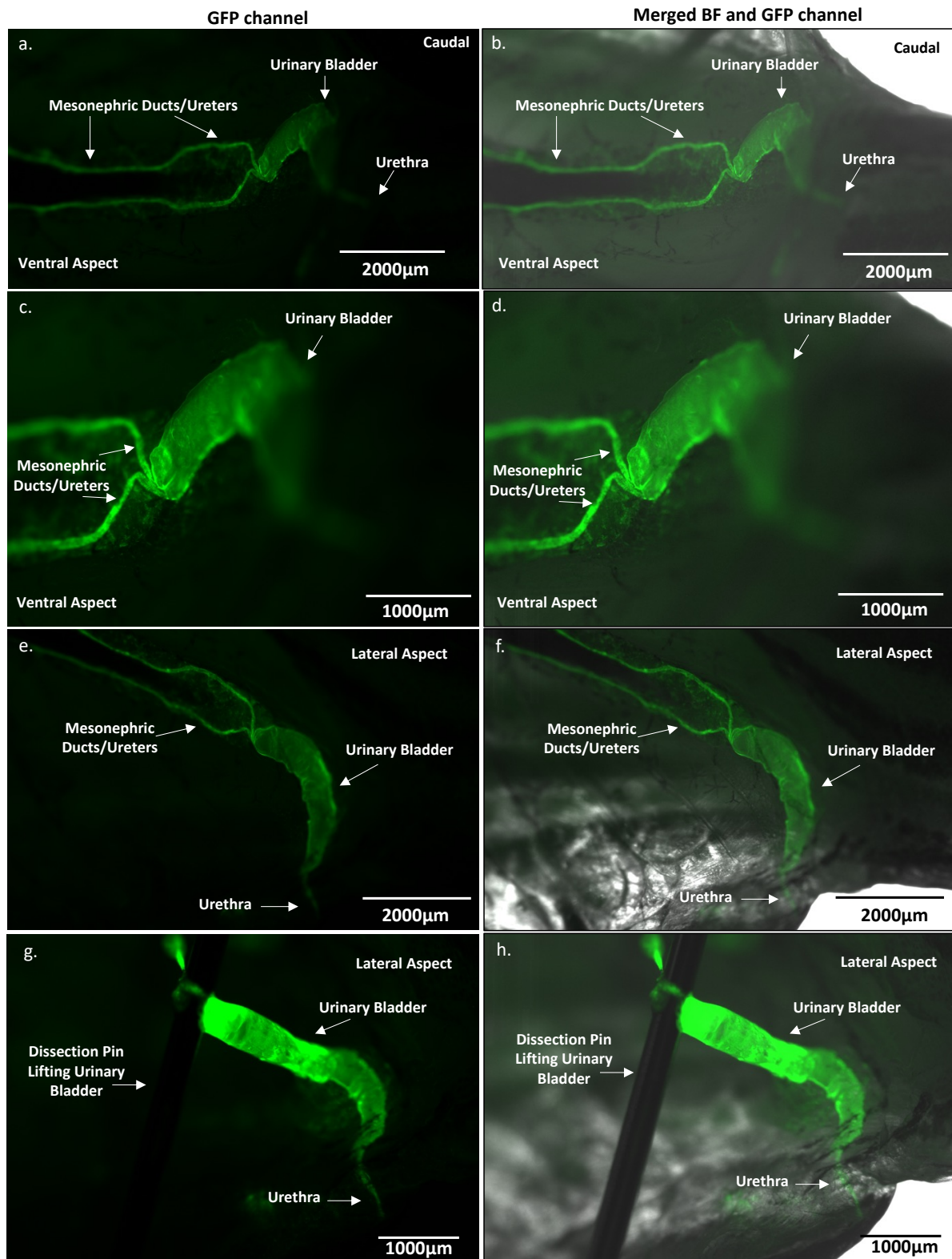


**Figure 37. Analysis of Morphology of Adult Zebrafish Urinary Bladder Using GFP Expression in *TgBAC(mpx:GFP)i114* Zebrafish Line.**

Ventral abdominal wall incised open, urinary tract exposed and left lateral abdominal wall removed. (a-d): Ventral aspect of urinary tract on dorsal abdominal wall imaged. (e-f): Lateral aspect of urinary tract imaged. (g-h). Dissection pin used to lift urinary bladder away from abdominal wall attachments and lateral aspect imaged.

#### **4.2.6. Isolation of Zebrafish Urinary Bladder From Dissected Adult Zebrafish**

During the process of dissecting open zebrafish and exposing the urinary tract, the macroscopic appearances of the zebrafish urinary bladder were investigated. The zebrafish urinary tract tissue in the kidney was traced along the dorsal abdominal wall at the caudal most region of the abdomen to the urinary bladder. The zebrafish urinary bladder is closely adherent to the dorsal abdominal wall with connective tissue and required careful dissection away from this connective tissue. In contrast to the zebrafish kidney which has a pigmented colouration, the zebrafish urinary bladder has a clear to translucent colouration. The zebrafish urinary bladder is approximately 500µm in length.

It was decided to try to attempt to isolate the zebrafish urinary bladder away from the connective tissue along the dorsal abdominal wall. Being able to do this would open the possibility of being able to perform high quality transcriptomic analysis on freshly dissected zebrafish urinary bladders. With careful dissection technique, it was possible to isolate the zebrafish urinary bladder from the surrounding tissue (Figure 38).

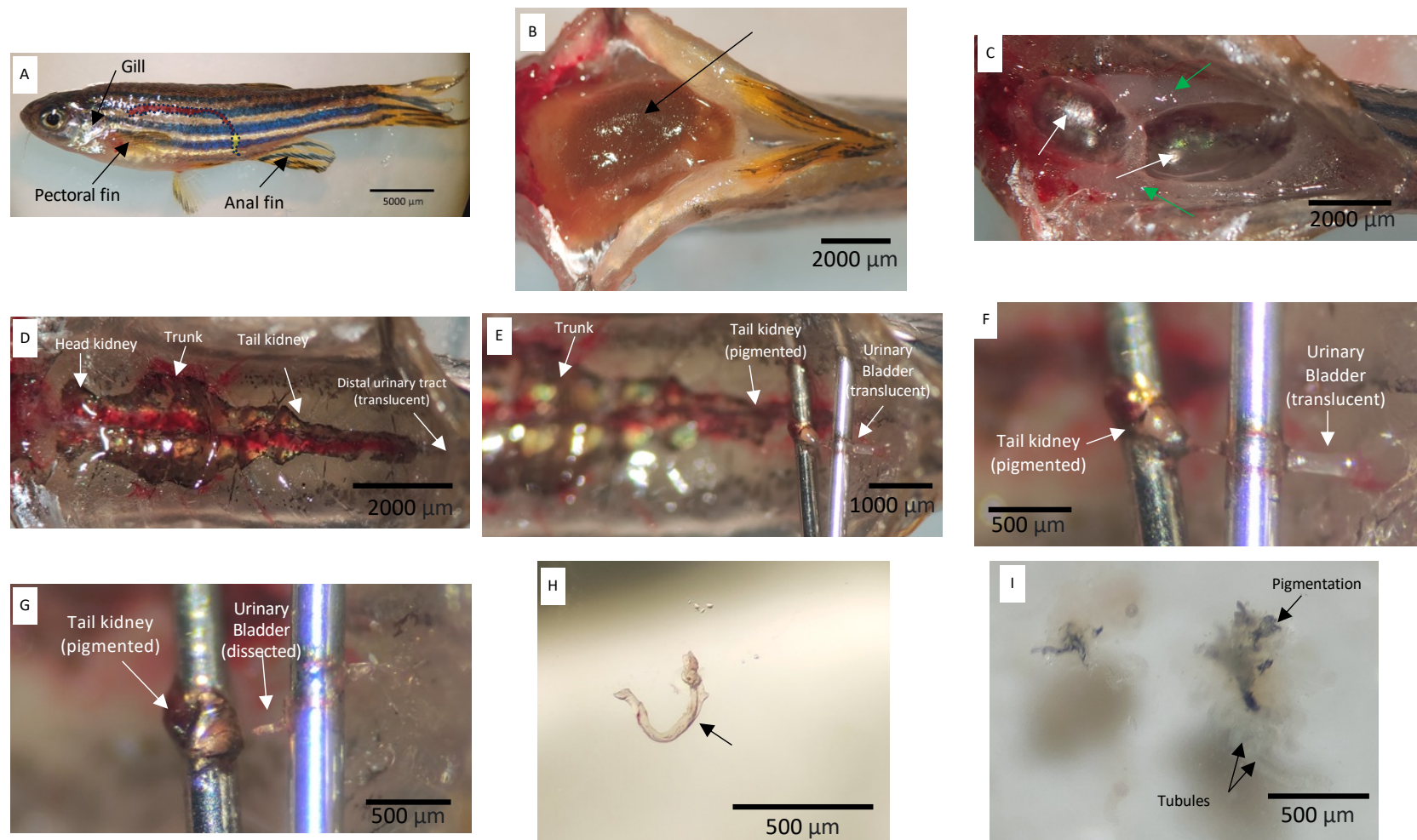


**Figure 38. Dissection of Zebrafish Distal Urinary Tract.**

(a) Overview anatomy of adult zebrafish. Urinary tract outline superimposed: Kidney (red) and Urinary Bladder (yellow). (b) Ventral incision, gut exposed (black arrow). (c) Gut excised, swim bladder (white arrow) and testes (green arrow) exposed. (d) Swim bladder and testes removed, kidney and distal urinary tract exposed. (e) Pin under tail kidney and urinary bladder. (f) Urinary bladder connected distal to the tail kidney. (g) Urinary bladder dissected proximal and distal. (h) Isolated urinary bladder in solution (black arrow). (i) Isolated kidney (obtained from mid-kidney/trunk) in solution. Figure generated with assistance from summer intern student Krithickk Sivakumar.

### 4.3. Discussion

Here we have characterised the distal excretory component of the urinary tract in both larval and adult zebrafish and demonstrated close homology in distal urinary tract anatomy and function between zebrafish and human. We identified expression of *uroplakin 1a*, a characteristic urothelial gene, in the zebrafish embryo pronephros starting at 96 hpf, and characterised key components of the adult zebrafish urinary excretory system (the urinary bladder arising from fusion of the two mesonephric ducts). We demonstrated the zebrafish urinary bladder empties via a distinct urethra, and that in anaesthetised adult zebrafish, urine accumulates in the bladder and is intermittently released.

Using whole mount *in situ* hybridisation, we detected the presence of *uroplakin1a* expression in the zebrafish larval pronephric tubules and ducts at 96 hpf and 120 hpf. This is supported by the results of a previous study demonstrating expression of another uroplakin protein, Upk3l, at the apical surface of the pronephric tubules and ducts (42). Morpholinos against *upk3l* led to embryos with reduced pronephric function believed to be due to defects in epithelial polarity and morphogenesis. The zebrafish pronephric epithelium and the human urothelium both play roles in urine excretion function and are in direct contact with urine. Our findings are suggestive of structural homology between these two structures. Uroplakins are transmembrane proteins that form an asymmetric unit membrane (AUM) on the apical surface of the superficial layer of human urothelium (352). Multiple functions have been reported for uroplakins. Mouse knockout studies suggest that they play a role in apical membrane permeability barrier function of urothelium (354, 355). Abnormal uroplakins have also been linked to urinary tract malformations such as hydronephrosis and vesicoureteric reflux in mouse knockout and human genetic studies (363, 364).

We demonstrated that zebrafish possess two mesonephric ducts arising from the kidneys and uniting into a urinary bladder. The zebrafish mesonephric ducts and urinary bladder are lined by an epithelium expressing proteins characteristic of human urothelium (suggesting structural similarity and evolutionary conservation). These are important findings as

previously there have been conflicting reports regarding the presence of a urinary bladder in zebrafish (25, 26, 358). The presence of mesonephric ducts and a urinary bladder have been described in other teleost species (28, 365). We did note two differences between the zebrafish and human urothelium. Firstly, the zebrafish urinary bladder epithelium is one to two cell layers thick, in comparison to the multi-layered human urothelium. Secondly, human urothelium is composed of superficial ('umbrella'), intermediate, and basal cell layers, which are characterised by differential protein expression (352). The zebrafish urinary bladder epithelium expressed proteins characteristic of both superficial (Uroplakins) and basal (Cytokeratin 5 and Cd44) layers. This may reflect biological adaptation to differences in urinary composition, anatomical simplicity or that proteins characteristic of luminal and basal layers are different in zebrafish and humans.

This study also showed structural similarity in the lower urinary tracts distal to the urinary bladder in zebrafish and humans. We demonstrated that the zebrafish urinary bladder leads to a urethra and urethral orifice that is separate from the hindgut and surrounded by a deeper connective tissue layer rich in collagen. These structures have not previously been described in zebrafish. Furthermore, we demonstrated sex differences in urethral anatomy in zebrafish by demonstrating that the male zebrafish ejaculatory duct joins the urethra (similar to humans) whereas the female oviduct is a separate structure to the urethra throughout its course.

We identified for the first time that the *Tg(mpx: GFP)i114* zebrafish line, which labels neutrophils, also labels the zebrafish urinary tract (and gut) from around 2 weeks post fertilisation to adulthood. This is the only transgenic reporter line to date, known to be expressed specifically in the urinary bladder. It was deemed extremely unlikely that the reporter gene expression pattern in the urinary tract represents neutrophilic infiltration because this would be expected to be a scattered pattern of single neutrophils rather than expression that clearly delineated the zebrafish mesonephric ducts and urinary bladder. The reporter gene expression is likely to be within the urinary tract and gut epithelia rather than other cell layers such as the muscle because expression in the muscle layers underlying the epithelia would be expected to be seen elsewhere in the zebrafish. It is not entirely clear what is driving the reporter gene expression in the excretory urinary tract. The expression

pattern seen in the urinary tract and gut epithelia may be due to regulatory elements from nearby promoters or enhancers (within the BAC) driving the GFP expression. An *in-silico* search of an online human protein expression atlas (The human protein atlas) revealed myeloperoxidase (MPO, the human protein that is analogous to zebrafish *mpx*) to be expressed predominantly in bone marrow and lymphoid tissues (361, 362) and therefore it is unlikely that the GFP expression in the urinary tract is being driven by the zebrafish *mpx* gene regulatory elements. Further work is required to confirm this. Overall, our finding is important as it can be used to study zebrafish urinary bladder structure and function. It is possible that in the future the GFP expression in the zebrafish urinary bladder epithelium could be utilised to isolate specifically the zebrafish urinary bladder epithelial cells using flow cytometry to study gene expression patterns in these cells.

We characterised the change in excretory urinary tract morphology over time using the *Tg(mpx: GFP)*j114** zebrafish line. We showed the distal zebrafish urinary tract changes from a tubular structure (from 2-4 weeks post fertilisation) to a saccular expansile structure from 6 weeks onwards to adulthood. A collaborator (Dr Duncan Morhardt) demonstrated, using a technique of injection of a fluorescent dye into the systemic circulation of adult zebrafish, that intermittent micturition takes place with corresponding expansion and contraction of the urinary bladder (data not shown in thesis) (366). My finding of the development of a saccular/expansile like morphology from around 6 weeks of age suggests that intermittent micturition may start to take place at around that time as it is unlikely that intermittent micturition can take place in a tubular like urinary bladder. Further work is needed to establish when the full urinary bladder function starts in zebrafish.

#### **4.4. Conclusion**

The adult zebrafish distal urinary excretory system shares several features with its human counterpart. The zebrafish system has two mesonephric ducts leading to a urinary bladder lined by a uroplakin expressing urothelium. The urinary bladder, in turn, leads to a urethra and urethral orifice. These findings present an opportunity to model human lower urinary tract diseases in zebrafish.

## Chapter 5. Developing a Transgenic Model of Urinary Tract Cancer in Zebrafish Utilising An Enhancer Trap Line

### 5.1. Introduction

Urinary tract cancers are a significant global health problem (56, 57, 367). Urinary tract cancers include cancers of the kidneys, ureters, bladder and urethra. The most common urinary tract cancer is urothelial cancer which can occur throughout the urinary tract. Urothelial cancers arise from the urothelial cells lining the renal pelvis, ureters, urinary bladder and urethra (367). The most common cancer arising the kidneys is renal cell carcinoma which arises from the renal tubules (57).

Large genomic sequencing efforts have led to significant insights into the molecular events associated with these cancers (118, 368). The cancer genome atlas has identified many mutated and upregulated genes associated with urinary tract cancers. However, these insights would benefit from validation in a high-volume *in vivo* model to determine the driver genetic alterations and the passenger genetic alterations.

The zebrafish model has led to significant insights in other cancers such as melanoma (369) and sarcoma (370). We have previously demonstrated that zebrafish have a urinary tract which shares close homology with the human system. The zebrafish kidney converges into two mesonephric ducts that unite into a single urinary bladder lined by epithelial cells that express uroplakin proteins. Whilst models of zebrafish melanoma and sarcoma exist, a transgenic zebrafish model of urinary tract cancer had not previously been developed.

## 5.2. Aims and Objectives

The aims and objectives of this chapter are as follows:

The overarching aim of this chapter was to develop a novel transgenic model of zebrafish urinary tract cancer. I planned to achieve this aim through the following objectives:

1. To identify a transgenic zebrafish line with tissue specific expression in the urinary tract that could be used to direct expression of genes of interest.
2. To characterise reporter gene expression pattern of transgenic zebrafish urinary tract reporter line during the embryonic, larval, juvenile stages and adult stages.
3. To develop a system whereby genomic alterations associated with human urinary bladder cancer can be expressed and visualised in the zebrafish urinary tract *in vivo*.
4. To raise transgenic zebrafish with human bladder cancer associated genomic alterations in the zebrafish urinary tract and monitor for the development of macroscopic abnormalities.
5. To histologically analyse abnormalities arising from expression of human bladder cancer associated genomic alterations in the zebrafish urinary tract.

## 5.3. Results

### 5.3.1. Identification and Characterisation of Transgenic Et(*gSAIzGFFD*)875b; Tg(*UAS: GFP*) Zebrafish Line

During a lab visit to the Kawakami laboratory (National Institute of Genetics, Japan), a shelf screen of enhancer lines was performed to identify a transgenic zebrafish line with tissue specific expression in the urinary tract. The Kawakami lab have a database of transgenic zebrafish lines with reporter gene expression in a large number of different zebrafish tissues (215). These zebrafish lines were generated by the Kawakami lab using tol2 transposon technology (371) and gene and enhancer trap techniques (372). Gene trapping or enhancer trapping is a technique where a plasmid construct containing transcriptional activator (e.g. Gal4 or GFF; capable of driving reporter gene expression) or containing a

reporter gene (e.g. GFP) is expressed, through one cell stage microinjection, under the control of promoters or enhancers near the insertion point of the plasmid construct (372).

The enhancer trap screen I performed involved fluorescent microscopy imaging of five of these transgenic zebrafish lines during the embryonic and larval developmental stages:

- *Et(hspGGFF)20A; Tg(UAS: GFP)*
- *Et(gSAIzGFFM)1659A; Tg(UAS: GFP)*
- *Et(gSAIzGFFM)619A; Tg(UAS: GFP)*
- *Et(gSAIzGFFD)2262A; Tg(UAS: GFP)*
- *Et(gSAIzGFFD)875b; Tg(UAS: GFP)*

These lines were selected based on a search of the enhancer trap database for lines which had been observed, at the Kawakami lab, to have reporter gene expression in the pronephros. These lines all utilised the Gal4/UAS system (373, 374) i.e. these enhancer trap lines were all generated using plasmids containing the GFF transgene, which is a form of transcriptional activator Gal4, and all had a second transgene (*UAS: GFP*) in their genome. The presence of both of these transgenes enables the transcriptional activator Gal4 (or in this case a modified version of Gal4 called Gal4-VP16 which is also known as GFF), which is expressed under the control of nearby enhancers or promoters, to drive expression of the upstream activating sequence (UAS) and any genes placed downstream of the upstream activating sequence to enable visualisation of the spatial expression pattern of nearby enhancers or promoters in these lines (372).

Of all of the screened transgenic enhancer trap lines, The *Et(gSAIzGFFD)875b; Tg(UAS: GFP)* zebrafish line was determined to have the strongest and most specific expression in the zebrafish urinary tract. This line was transferred to the Bateson centre (MTA K2018-137), University of Sheffield for further characterisation. Data obtained from the Kawakami lab showed the genomic integration site of the p-gSAIzGFFD enhancer trap construct in the *Et(gSAIzGFFD)875b* line to be Chromosome 3: 3,525,857-3,625,856). One of the genes in this region includes: *gucy2c* which encodes the Guanylate Cyclase 2c protein, an enzyme found in the intestinal epithelium (375). This provides an estimation of potential gene

enhancers driving the spatial expression pattern in this transgenic line. However, this is only a rough estimation as the true enhancers or promoters could be further away.

As the overarching aim was to develop a novel transgenic zebrafish model of urinary tract through expression of genes that are associated with human bladder cancer in the zebrafish urinary tract, it was important to understand when the reporter gene expression in the *Et(gSAIzGFFD875b:UAS GFP)* enhancer trap line started and how the expression changes over time.

To determine when the GFP expression in the pronephros starts in the *Et(gSAIzGFFD)875b; Tg(UAS: GFP)* zebrafish line, a fluorescence microscopy time lapse was performed. Embryos were collected from an Incross of *Et(gSAIzGFFD)875b; Tg(UAS: GFP)* parents. Prior to the commencement of imaging at approximately 21.5 hours post fertilisation, embryos were dechorionated, anaesthetised using tricaine MS222, immobilised in low melting point agarose containing tricaine MS222 and drawn up into capillaries for imaging on a Lightsheet microscope (Zeiss).

Analysis of the timelapse fluorescence microscopy imaging revealed the GFP expression to start in the distal pronephros at 23 hours post fertilisation. By 24 hpf, there was an increase in GFP positive cells in the distal pronephros. These GFP positive cells fused with the cloaca by 28 hours post fertilisation (Figure 39).

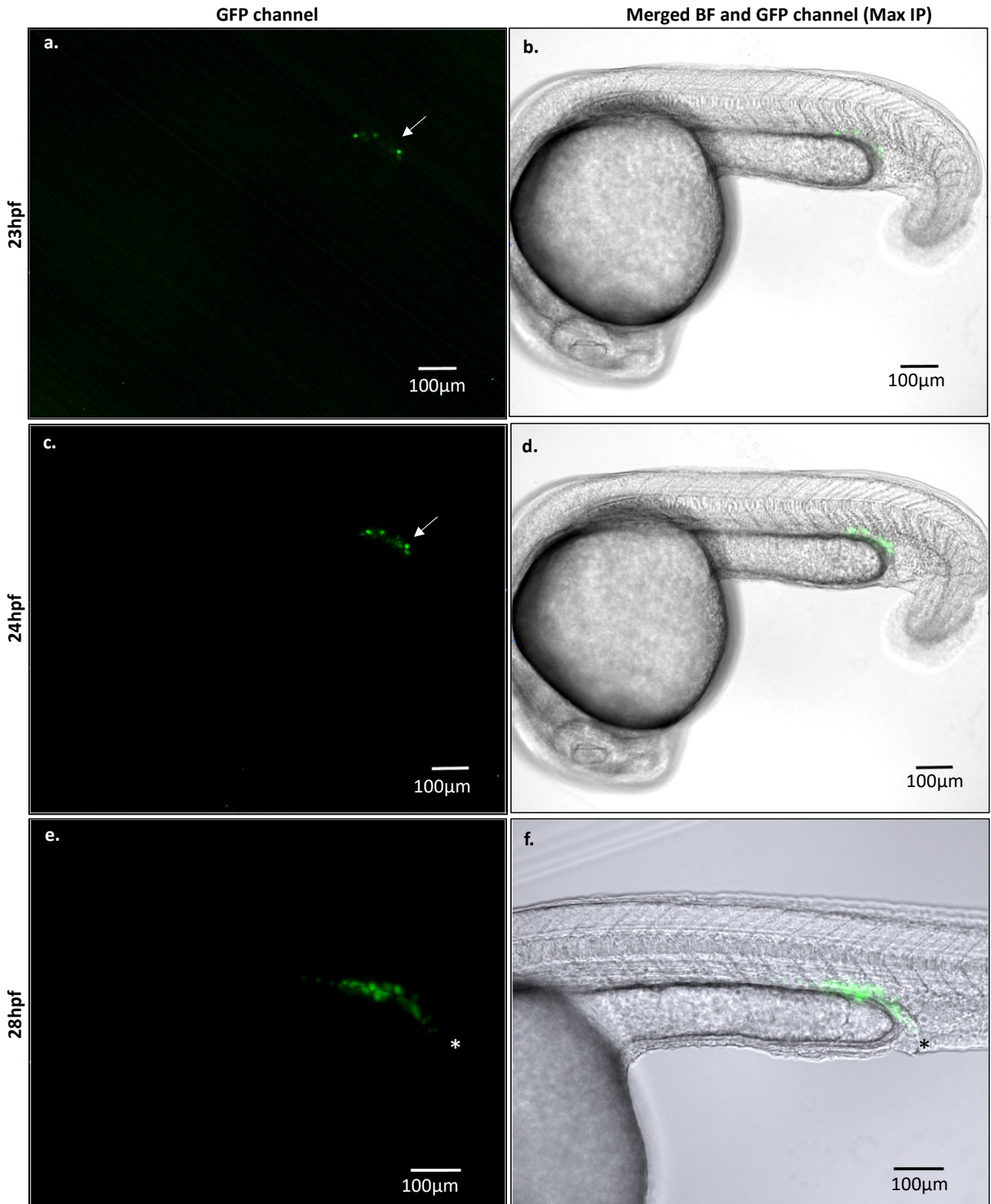


**Figure 39. Early GFP Expression in the Zebrafish Pronephros of the *Et(gSAIzGFFD)875b*; *Tg(UAS:GFP)* Enhancer Trap Zebrafish Line.**

(a-b) at 23 hpf, (c-d) at 24 hpf and (e-f) at 28 hpf. First GFP positive cells to appear at 23 hpf and 24 hpf (White arrows). Fusion of zebrafish pronephros with cloaca is evident at 28 hpf (Asterix).

Fluorescent microscopy images taken using Zeiss Lightsheet Microscope.

Further characterisation was performed at 2-, 3- and 4-days post fertilisation using standard fluorescence microscopy. At days 2 and 3pf, the GFP expression was localised throughout the proximal and middle segments of the pronephros. At 4 days post fertilisation the GFP expression was visualised in the proximal, middle and part of the distal pronephros segments as well as the gut (Figure 40).

Further fluorescence microscopy was performed on older *Et(gSAIzGFFD)875B; Tg(UAS:GFP)* zebrafish larvae at 2 weeks and 3 weeks post fertilisation. These timepoints were selected because mesonephrogenesis occurs at around 10 days post fertilisation. GFP expression was visualised in the proximal, middle and distal urinary tract segments as well as the gut at 2 weeks. At 3 weeks, the GFP expression was localised to the proximal and middle urinary tract segments and the gut but not the distal urinary tract (Figure 41).

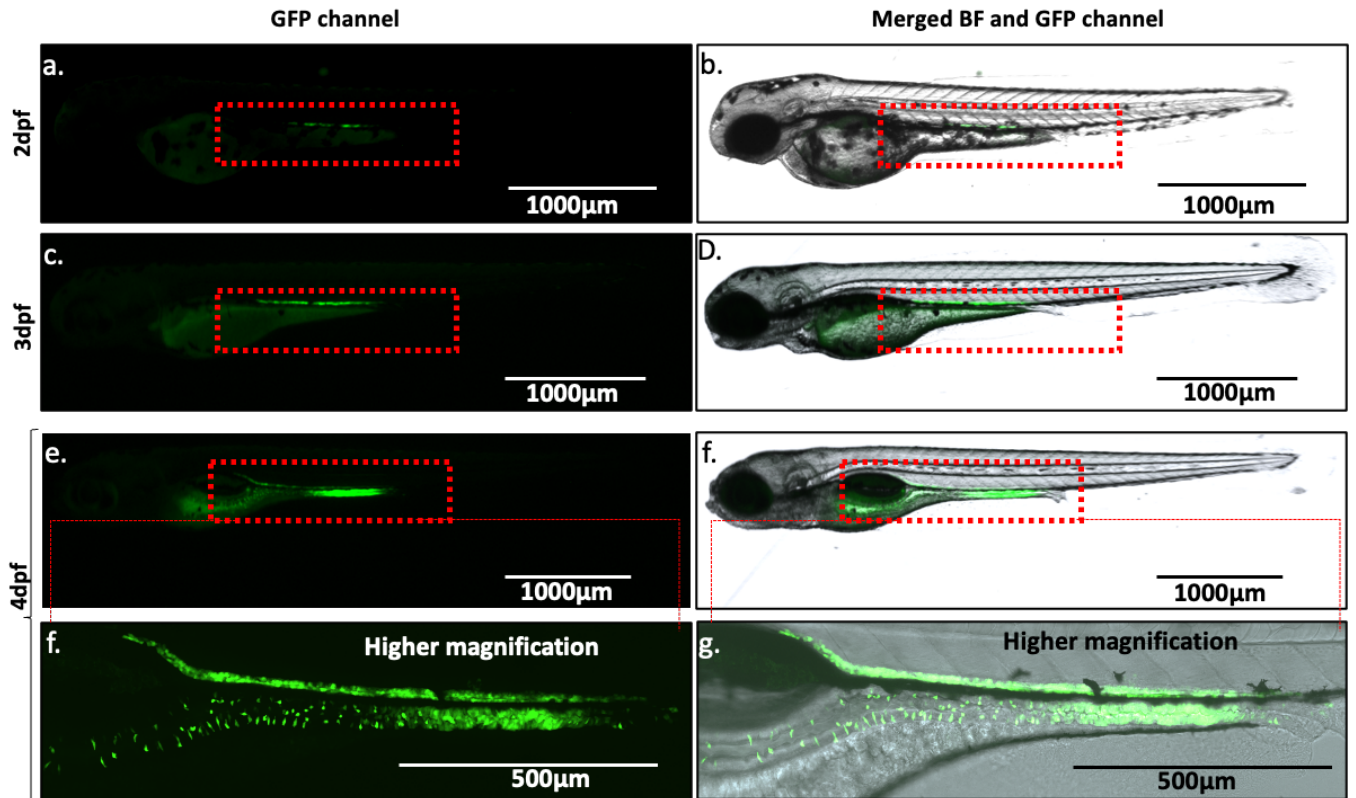


**Figure 40. GFP Expression in Zebrafish *Et(gSAIzGFFD)875b; Tg(UAS:GFP)* Line Between 2- and 4 Days Post Fertilisation.**

(a-b) 2dpf, (c-d) 3dpf, (e-g) 4dpf. Fluorescent microscopy images taken using Leica M205 FA Fluorescent Stereomicroscope (a-f) and Nikon W1 Spinning Disc Fluorescent Microscope (f-g).

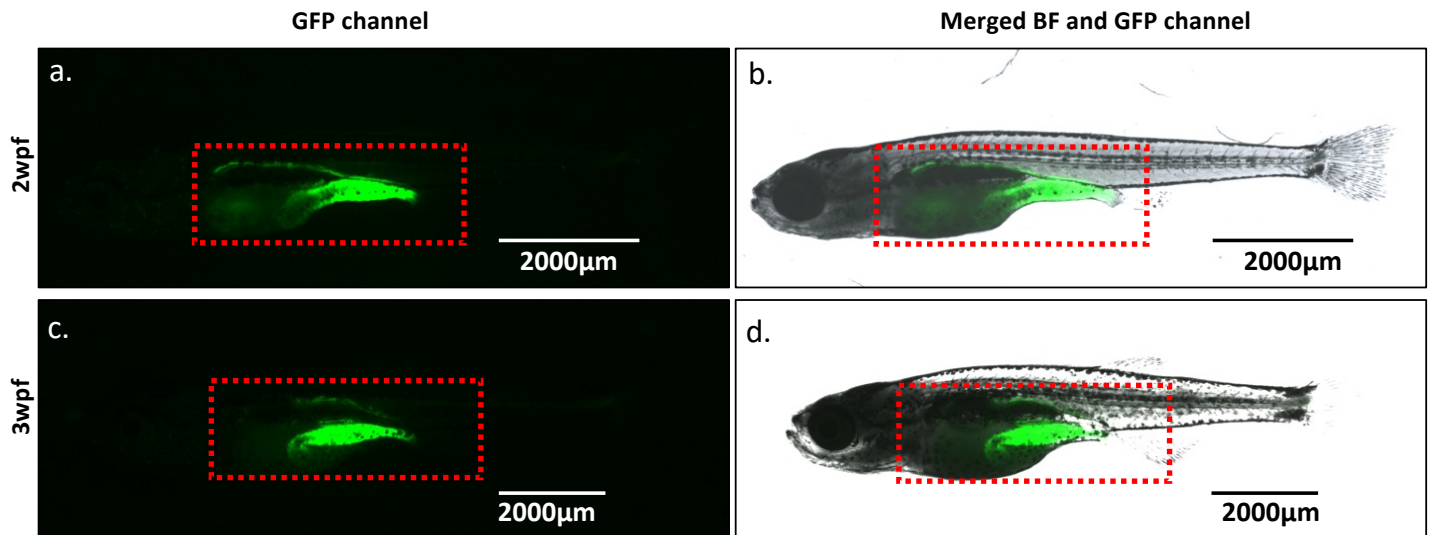


**Figure 41. GFP Expression in Zebrafish *Et(gSAIzGFFD)875b; Tg(UAS:GFP)* Line Between 2- and 3 Weeks Post Fertilisation.**

(a-b) 2wpf, (c-d) 3wpf. GFP expression is seen in pronephros/mesonephros and gut (Red dotted rectangle) at 2 and 3 weeks wpf (during mesonephrogenesis). Fluorescent microscopy images taken using Leica M205 FA Fluorescent Stereomicroscope.

After 3 weeks post fertilisation, the zebrafish tissues became denser, and it was increasingly difficult to visualise the GFP expression pattern in the urinary tract. It was therefore necessary to dissect open (following schedule 1 cull)  $\geq 4$ -week-old *Et(gSAIzGFFD)875B; Tg(UAS:GFP)* zebrafish to visualise GFP expression in the urinary tract.

Dissection involved incising the ventral abdominal wall and removing the gut, swim bladder and gonads to expose the urinary tract along the dorsal abdominal wall. This was immediately followed by fluorescence microscopy at 4 weeks, 6 weeks and 2 years to determine the GFP expression pattern in the juvenile and adult urinary tract.

This imaging demonstrated GFP expression to be localised to the kidney tubules and mesonephric ducts/ureters during the juvenile stages of zebrafish development (4 weeks [Figure 42] and 6 weeks [Figure 43]). There was no GFP expression seen in the most distal aspects of the urinary tract which is where the urinary bladder would be expected to be located.

Based on the lifecycle of zebrafish, whereby the adult stage is reached at 3 months and the laboratory lifespan continues to a maximum of 30 to 36 months, it was decided that it was highly likely that reporter gene expression in zebrafish between 3 months to 36 months would be very similar. The reporter gene expression in the *Et(gSAIzGFFD)875B; Tg(UAS:GFP)* zebrafish line was evaluated at 2 years due to the available adult zebrafish stocks at the time that this work was carried out. There was no GFP expression seen in the adult zebrafish urinary tract at 2 years old (Images not shown).

A summary of the spatial reporter gene expression in the *Et(gSAIzGFFD)875B; Tg(UAS:GFP)* zebrafish line is shown in Table 9.

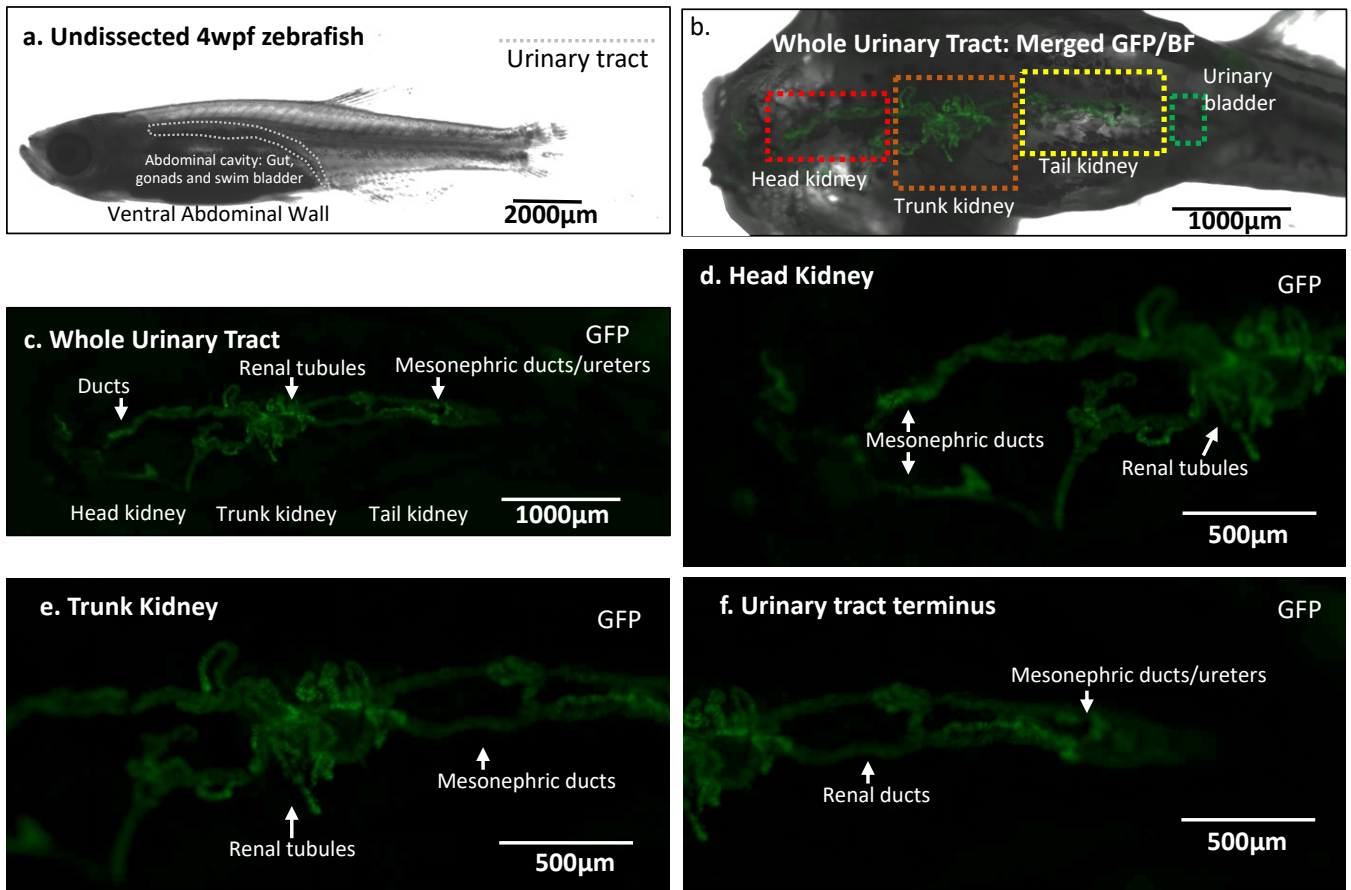


**Figure 42. GFP Expression in Urinary Tract of Dissected Zebrafish *Et(gSAIzGFFD)875b; Tg(UAS:GFP)* Line At 4 Weeks Post Fertilisation.**

Zebrafish dissected open (Ventral abdominal wall incised and gut, gonads and swim bladder removed from abdominal cavity exposing urinary tract) at 4 weeks post fertilisation. Ventral surface imaged. (a) Undissected 4wpf zebrafish brightfield image for reference. (b-c) Whole zebrafish urinary tract, (d) Head kidney, (e) Trunk kidney, (f) Urinary tract terminus. GFP expression is seen in head kidney, body of kidney and tail kidney. GFP localizes to the kidney tubules, major ducts and ureters. Fluorescent microscopy images taken using Leica M205 FA Fluorescent Stereomicroscope.

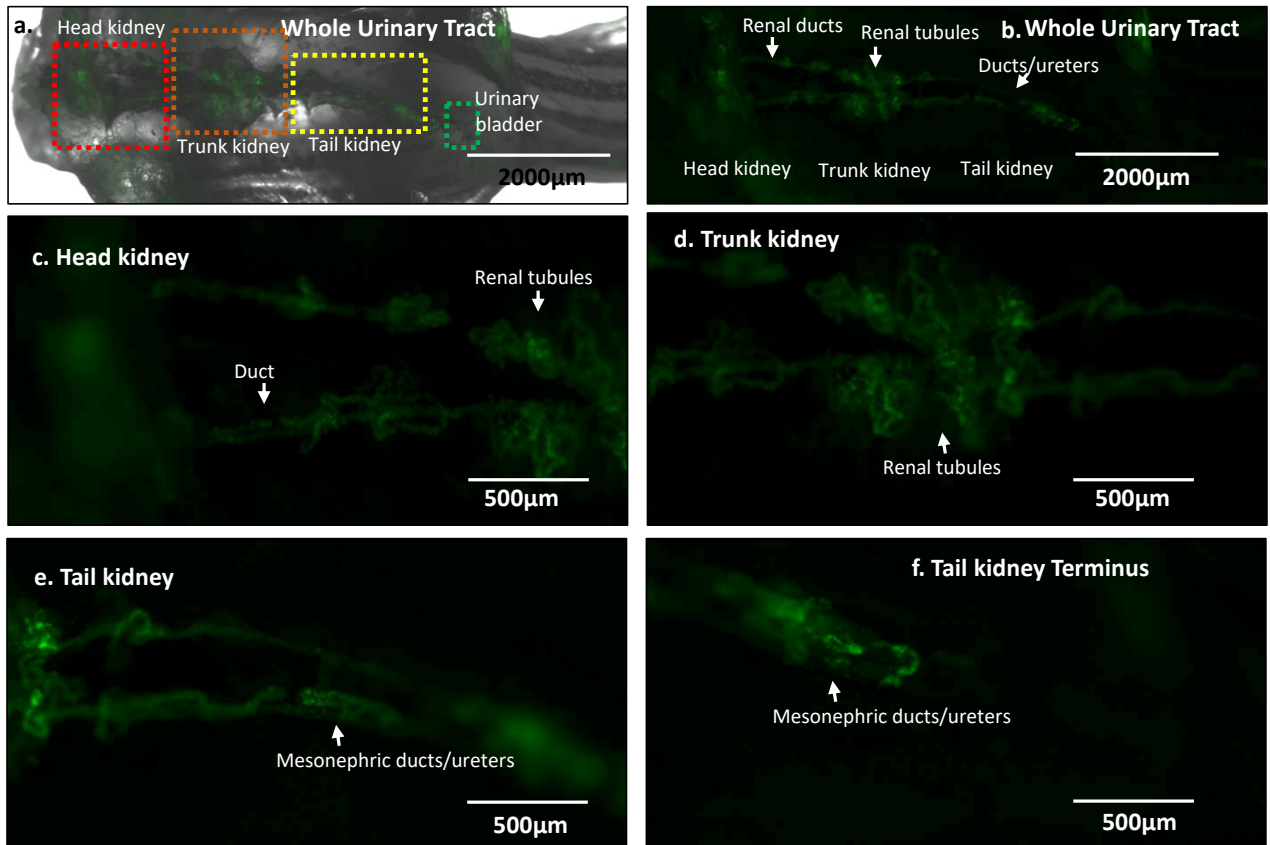


**Figure 43. GFP Expression in Urinary Tract of Dissected Zebrafish *Et(gSAIzGFFD)875b; Tg(UAS:GFP)* Line At 6 Weeks Post Fertilisation.**

Zebrafish Dissected open (Ventral abdominal wall incised and gut, gonads and swim bladder removed exposing urinary tract] at 6 weeks post fertilisation.) (a-b) Whole zebrafish urinary tract, (c) Head kidney, (d) Trunk kidney, (e) Tail kidney, (f) Tail kidney terminus. GFP expression is seen in head kidney, body of kidney and tail kidney. Fluorescent microscopy images taken using Leica M205 FA Fluorescent Stereomicroscope.

<b>Time point</b>	<b>Spatial Fluorescent Reporter Gene Expression Pattern</b>
23 hours pf	Distal pronephros
24 hours pf	Distal pronephros
28 hours pf	Distal pronephros (Fuses with the cloaca)
2 days pf	Middle and distal pronephros
3 days pf	Middle and distal pronephros
4 days pf	Proximal, middle, and distal pronephros. Bowel.
5 days pf	Proximal, middle, and distal pronephros. Bowel.
2 weeks pf	Proximal, middle, and distal mesonephros. Bowel.
3 weeks pf	Proximal and middle mesonephros. Bowel.
4 weeks pf	Head, trunk and tail kidney (tubules and ducts). No expression visualised in urinary bladder.
6 weeks pf	Head, trunk and tail kidney (tubules and ducts). No expression visualised in urinary bladder.
2 years pf	No expression visualised in urinary tract.

**Table 9. Spatial Reporter Gene Expression Pattern in *Et(gSAIzGFFD)875b; Tg(UAS: GFP)* Zebrafish Line.**

Bowel expression was not assessed from 4 weeks post fertilisation onwards as zebrafish reporter gene expression was assessed by dissection and removal of organs overlying urinary tract. Note that mesonephrogenesis occurs at around 10-14 days old, so zebrafish pronephros becomes mesonephros by 2 weeks old(23).

### **5.3.2. Stable *GFP-HRAS\_G12V* Expression in the Zebrafish Urinary Tract**

The *HRAS* gene (belongs to RAS family of GTPases which activates the RAS-RAF-MEK-ERK pathway) has been reported to be commonly mutated in bladder cancer(120, 376). The G12V mutation (Glycine amino acid substituted to valine at amino acid 12) results in

constitutive activation of the RAS signalling pathway. Zebrafish embryos from *Tg(UAS: GFP - HRAS\_G12V)* and *Tg(UAS: GFP-CAAX)* lines were obtained from Dr Yi Feng (University of Edinburgh) and raised to adulthood. The plasmids used to generate them had a GFP heart marker (*clmc: GFP*) within the cassette and therefore the resulting zebrafish had GFP positive hearts. The *Tg(UAS: GFP-CAAX)* zebrafish line possesses the *GFP-CAAX* sequence (encodes GFP with a specific amino acid sequence at the C terminus directing GFP to the cell membrane) downstream of the upstream activating sequence (UAS) and therefore acts as a control for any experiments utilising the *Tg(UAS GFP HRAS\_G12V)* zebrafish line. The *HRAS\_G12V* oncogene has been previously demonstrated to function in zebrafish and drive cancers in other zebrafish tissues (370).

To express *HRAS\_G12V* in the zebrafish urinary tract, adult *Tg(UAS: GFP-HRAS\_G12V)* and *Tg(UAS: GFP-CAAX)* zebrafish were outcrossed to adult *Et(gSAIzGFFD)875b* zebrafish. Embryos were screened for GFP fluorescence in the heart and pronephros and fluorescence microscopy was performed on the GFP positive zebrafish embryos generated from this outcross *Et(gSAIzGFFD)875b; Tg(UAS: GFP-HRAS\_G12V)* to determine if this system could result in visual evidence of GFP-HRAS\_G12V expression in the zebrafish pronephros. This imaging revealed GFP expression (and therefore downstream HRAS\_G12V expression) in the pronephros and gut, but the expression was weak and appeared mosaic (Figure 44). A possible explanation for this weak expression is transcriptional silencing (or reduced expression) of the *UAS: GFP-HRAS\_G12V* component which has been reported to occur with the use of the Gal4/UAS system (377). There are a number of possible explanations for transcriptional silencing that occurs with Gal4/UAS system. Repetitive DNA sequences, present in upstream activating sequences (UAS), can trigger transcriptional silencing. This phenomenon has also been attributed to DNA methylation. Repetitive UAS sequences are CpG-rich structures which are considered prone to methylation (377).

This stable genetics technique of expressing genomic alterations in the zebrafish urinary tract was not pursued further as it was deemed unlikely that the weak GFP expression seen in *Et(gSAIzGFFD)875b; Tg(UAS: GFP-HRAS\_G12V)* larvae would be capable of driving *HRAS\_G12V* expression that would be sufficient for a cancer model.

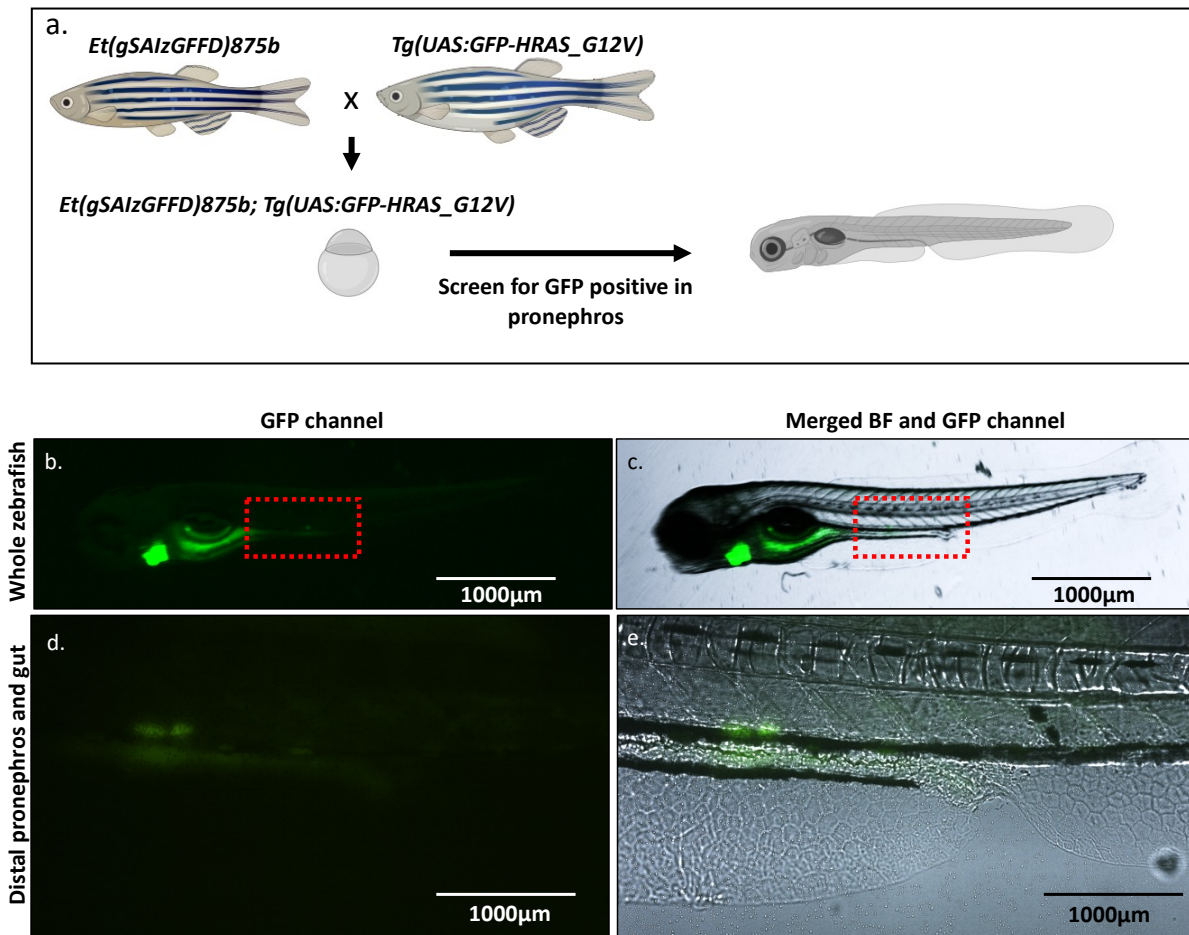


**Figure 44. Attempt at Generating Stable Transgenic Zebrafish *Et(gSAIzGFFD)875b; Tg(UAS:GFP-HRAS\_G12V)* Line for Use in a Urinary Tract Cancer Model.**

(a) Schematic of stable zebrafish transgenic cross. (b-e) Weak GFP expression in pronephros and gut of stable *Et(gSAIzGFFD)875b; Tg(UAS:GFP-HRAS\_G12V)*. Fluorescent microscopy images taken using Leica M205 FA Fluorescent Stereomicroscope (B-C) and Nikon Eclipse TE2000-U (d-e).

### 5.3.3. Mosaic *GFP HRAS\_G12V* Expression in the Zebrafish Urinary Tract

Following the weak *GFP HRAS\_G12V* expression that was visualised in the stable *Et(gSAIzGFFD875b: UAS GFP HRAS\_G12V)* larvae, it was next decided to try to express *GFP HRAS* in the zebrafish pronephros utilising a transient approach in the F0 generation using one cell stage microinjection of plasmids. This technique involves the random incorporation of the p(UAS GFP HRAS\_G12V) construct into the genome of one cell stage *Et(gSAIzGFFD875b)* zebrafish embryos using tol2 transgenesis. The transgenesis process results in incorporation of the plasmid DNA in a proportion of the subsequently dividing cells, but not all of them. This technique was felt to be less likely to be affected by UAS gene silencing. Furthermore, this technique more closely recapitulates the human adult cancer process which arises from genomic alterations in somatic cells.

I performed one cell stage microinjection of *Et(gSAIzGFFD)875b* zebrafish embryos with pDestTol2CG2-UAS: GFP-HRAS\_G12V) and pDestTol2CG2-UAS: GFP-CAAX) plasmids along with tol2 transposase mRNA (encodes the transposase enzyme). This technique relies on tol2 mediated transgenesis whereby the tol2 mRNA is translated into the transposase enzyme, which in turn, mediates the transposition of the plasmid sequences into the genome of the injected zebrafish embryos. Several plasmid concentrations were used until an optimum concentration was identified whereby mosaic transgene expression was seen in the pronephros and minimal embryonic death (due to high plasmid concentrations). Plasmid dilutions used during the optimization process were: 50ng/ul, 25ng/ul, 15ng/ul and in injection volumes used during the optimization process were 1nl and 0.5nl. The plasmid dilution that yielded the strongest expression pattern with the least deformities or death was 15ng/ul with an injection volume of 0.5nl. Injected embryos were screened for GFP expression in the zebrafish pronephros at days 2-4 post fertilisation and imaged using a spinning disc fluorescent microscope. This revealed strong mosaic GFP expression in the pronephros of zebrafish larvae (Figure 45). The GFP expression was localised to the cell membranes as expected. GFP expression was also seen in the gut as expected based on the expression pattern of *Et(gSAIzGFFD)875b; Tg(UAS: GFP)* larvae previously performed.

Based on the results of this experiment, it was decided to use this technique for a zebrafish urinary tract cancer model.

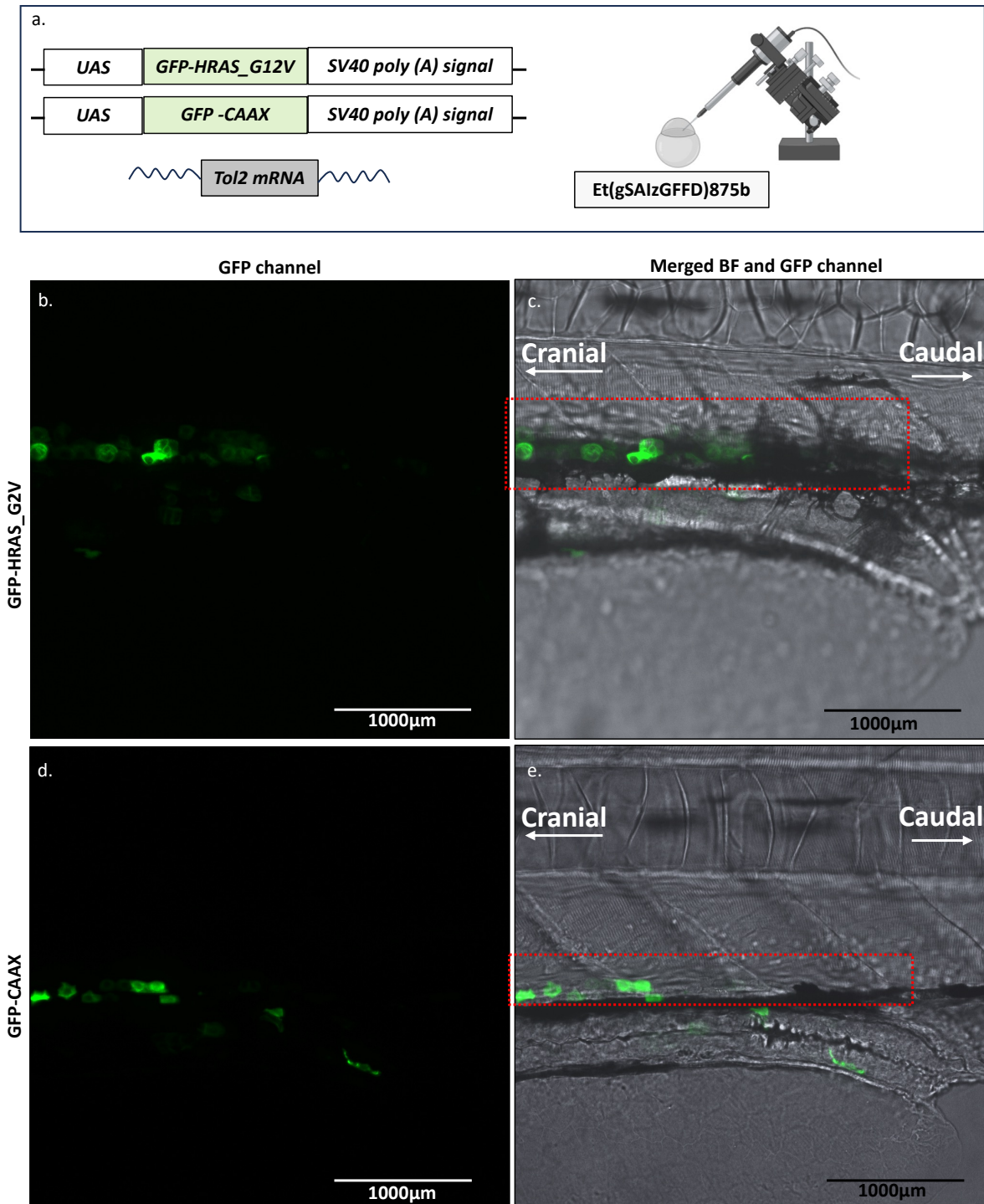


**Figure 45. Mosaic *GFP-HRAS\_G12V* Expression in Zebrafish Distal Pronephros at 4 Days Post Fertilisation.**

(a) Schematic of one-cell stage microinjection procedure of plasmids containing *GFP-HRAS-G12V* and *GFP-CAAX* coding sequences in *Et(gSAIzGFFD)875b* enhancer trap zebrafish line. (b-c) Transient mosaic GFP expression in pronephros of 4dpf *Et(gSAIzGFFD)875b; Tg(UAS:GFP-HRAS\_G12V)* zebrafish demonstrated with fluorescent microscopy. (d-e) Transient mosaic GFP expression in pronephros of 4dpf *Et(gSAIzGFFD)875b; Tg(UAS:GFP-CAAX)* zebrafish demonstrated with fluorescent microscopy. Mosaic membranous expression of *GFP-CAAX* and *GFP-HRAS\_G12V* is seen in pronephros (red dotted rectangle). Fluorescent microscopy images above taken using Perkin Elmer Spinning Disc Fluorescent Microscope at x20 objective.

#### 5.3.4. 5-Ethynyl-2-deoxyuridine Proliferation Assay

Following optimization of the one cell stage pDestTol2CG2-UAS: GFP-HRAS\_G12V and pDestTol2CG2-UAS:GFP-CAAX) plasmids in Et(*gsAlzGFFD*)875b zebrafish and successful visualisation of transgenic expression, I wanted to see if I could use an assay to measure proliferation activity in the zebrafish larval pronephros. There were two reasons for doing this. Firstly, the urothelium in humans has one of the lowest proliferation rates of all human tissues and so I wanted to see if this was also the case in the zebrafish pronephros. Secondly, as proliferation is one of the hallmarks of cancer, a proliferation assay would determine if *GFP HRAS\_G12V* expression in the pronephros is driving proliferation, as an early precursor to cancer. 5-Ethynyl-2-deoxyuridine (EdU) is a nucleoside analogue of thymidine that incorporates into DNA during DNA synthesis and measures cells in the S phase synthesis of the cell cycle i.e. proliferating cells(378). The specific assay I used utilises click chemistry and relies on covalently coupling an azide with an alkyne.

I optimised the assay by generating transgenic F0 Et(*gsAlzGFFD*)875b; *Tg(UAS: GFP-CAAX)* zebrafish with mosaic GFP expression in the pronephros. These were generated using one cell stage microinjection of pDestTol2CG2-UAS:GFP-CAAX into Et(*gsAlzGFFD*)875b zebrafish. I then performed yolk injection of EdU at 3dpf and incubated the EdU for 20 hours prior to co-immunostaining with a GFP antibody. The zebrafish were imaged in a lateral orientation (A field that included the cloaca on the right side of the image and the mid-section of gut/pronephros on the left side of the image). The image channels used with GFP (to image the GFP-CAAX in the Et(*gsAlzGFFD*)875b; *Tg(UAS:GFP-CAAX)* zebrafish line and far red (to image the EdU positive cells).

In the zebrafish where the assay appeared to be successful, it was not possible to reproducibly quantify the proportion of GFP positive pronephros cells that were also positive for EdU (Figure 46) for several reasons. Firstly, it was not possible to reproducibly differentiate between individual GFP stained cells likely due to a combination of the quality of the imaging and degradation of the sample during the protocol. There were areas of the pronephros where it was possible to count and differentiate between individual GFP positive cells and then count individual GFP positive and far-red positive cells, but this was

not a technique that was deemed to be reproducible across all the successfully stained zebrafish. Subjectively, it did appear that the gut was significantly more proliferatively active than the pronephros. Furthermore, the pronephros did not appear to be a proliferatively active tissue at all. However, it was decided not to use this assay to compare proliferation activity between GFP-HRAS\_G12V and GFP-CAAX expression in the zebrafish pronephros.

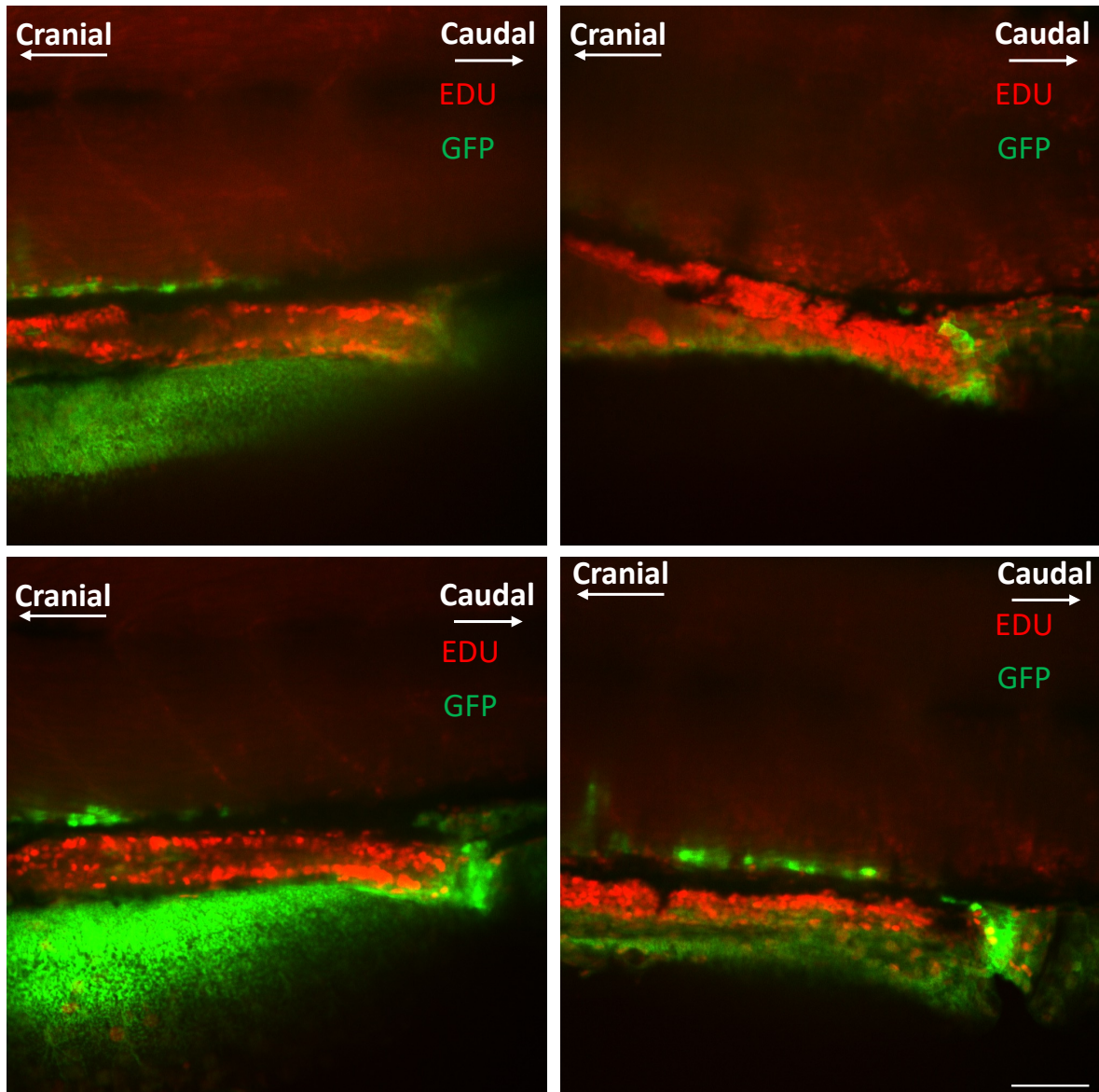


**Figure 46. Optimisation of EdU Proliferation Assay to Visualize Proliferation in Zebrafish Pronephros Using Fluorescence Microscopy.**

Assay performed in *Et(gSAIzGFFD)875b; Tg(UAS:GFP-CAAX)* zebrafish. Transgenic zebrafish larvae had mosaic GFP-CAAX expression in pronephros. Fluorescent microscopy performed using Perkin Elmer Spinning Disc at x20 objective. 4x separate 5-micron z slices are shown. Scale bar 50um.

### 5.3.5. Design and Implementation of Zebrafish Urinary Tract Cancer Model

Following optimisation of the one cell stage microinjection of the pDestTol2CG2-UAS: *GFP\_HRAS\_G12V* and pDestTol2CG2-UAS:*GFP-CAAX* plasmids, an experimental pipeline was designed to induce urinary bladder cancer. It was decided to utilise, in addition to the *HRAS\_G12V* oncogene in zebrafish, the *tp53 zdf1* mutation. This is a global mutation that was generated using N-ethyl-N-nitrosourea (ENU) mutagenesis and results in substitution of Methionine (M) with Lysine (K) at the 214<sup>th</sup> amino acid which is located within the DNA binding domain of the Tp53 protein. This mutation affects the region of the protein that is responsible for DNA binding to TP53 specific consensus sequences (194). The mutation is therefore a loss of function mutation i.e. loss of the ability to induce cell cycle arrest and apoptosis in response to DNA damage.

TP53 protein is 393 amino acids in length and DNA binding domain mutations (between amino acid 102 to 292(379)) in the *TP53* gene are common in human bladder cancer(380, 381). Ideally, the zebrafish *tp53* mutation would be tissue specific to the urinary tract but it was felt that this would complicate the genetics of the experiment and so the global *tp53* mutation that had previously been reported to function was used.

Through zebrafish crosses and genotyping for *GFF* transgene and *tp53 zdf1* mutation, the following zebrafish lines were generated.

1. *Et(gSAIzGFFD)875b*
2. *tp53<sup>zdf1/zdf1</sup>; Et(gSAIzGFFD)875b*

The *tp53<sup>zdf1/zdf1</sup>* homozygous mutation was selected for use in this model over a heterozygous mutation to maximize the probability of cancer formation as a heterozygous *tp53<sup>zdf1/zdf1</sup>* mutation would leave a functioning copy of the zebrafish *tp53* gene.

I performed microinjection of two plasmids (pDestTol2CG2-UAS:*GFP-HRAS\_G12V*] and pDestTol2CG2-UAS: *GFP-CAAX*]) at the one cell stage into *Et(gSAIzGFFD)875b* zebrafish both

with and without the homozygous *tp53 zdf1* mutation background (*tp53<sup>zdf1/zdf1</sup>*) thus giving rise to 4 experimental groups:

1. *tp53<sup>+/+</sup>*, *Et(gSAIzGFFD)875b*; *Tg(UAS: GFP-CAAX)*
2. *tp53<sup>+/+</sup>*, *Et(gSAIzGFFD)875b*; *Tg(UAS: GFP-HRAS\_G12V)*
3. *tp53<sup>zdf1/zdf1</sup>*, *Et(gSAIzGFFD)875b*; *Tg(UAS: GFP-CAAX)*
4. *tp53<sup>zdf1/zdf1</sup>*, *Et(gSAIzGFFD)875b*; *Tg(UAS: GFP-HRAS\_G12V)*

The offspring were screened for the presence of GFP expression in the distal pronephros between days 2-5 post fertilisation and those with good expression were selected to be raised to adulthood and monitored for the development of tumours (Figure 47).

Power calculations were performed based on estimates of tumour development from previous zebrafish models of other cancers and of mouse models of urinary bladder cancer.

As this experiment had not previously been performed on zebrafish, data from mouse experiments were used for estimates. I estimated distal urinary tract/urinary bladder cancer in the following groups:

1. *tp53<sup>+/+</sup>*, *Et(gSAIzGFFD)875b*; *Tg(UAS: GFP-CAAX)*: 0% distal urinary tract/urinary bladder cancers.
2. *tp53<sup>+/+</sup>*, *Et(gSAIzGFFD)875b*; *Tg(UAS: GFP-HRAS\_G12V)*: 20% distal urinary tract/urinary bladder cancers.
3. *tp53<sup>zdf1/zdf1</sup>*, *Et(gSAIzGFFD)875b*; *Tg(UAS: GFP-CAAX)*: 30% distal urinary tract/urinary bladder hyperplasia.
4. *tp53<sup>zdf1/zdf1</sup>*, *Et(gSAIzGFFD)875b*; *Tg(UAS: GFP-HRAS\_G12V)*: 30% distal urinary tract/urinary bladder cancers.

The power calculations provided a guide for how many zebrafish needed to be raised in each group and were based on 80% power, p value of 0.05 I estimated I needed the following numbers of zebrafish:

1. *tp53*<sup>+/+</sup>, Et(*gSAIzGFFD*)875*b*; Tg(*UAS: GFP-CAAX*): 31 zebrafish
2. *tp53*<sup>+/+</sup>, Et(*gSAIzGFFD*)875*b*; Tg(*UAS: GFP-HRAS\_G12V*): 31 zebrafish
3. *tp53*<sup>*zdf1/zdf1*</sup>, Et(*gSAIzGFFD*)875*b*; Tg(*UAS: GFP-CAAX*): 18 zebrafish
4. *tp53*<sup>*zdf1/zdf1*</sup>, Et(*gSAIzGFFD*)875*b*; Tg(*UAS: GFP-HRAS\_G12V*): 18 zebrafish

I added 30% extra zebrafish to each group to account for potential sickness or death due to non-malignancy related causes. I also added 20 extra zebrafish to each group to enable a preliminary histological analysis if no tumours developed at 3 months. This brought to the final numbers to:

1. *tp53*<sup>+/+</sup>, Et(*gSAIzGFFD*)875*b*; Tg(*UAS: GFP-CAAX*): 60 zebrafish
2. *tp53*<sup>+/+</sup>, Et(*gSAIzGFFD*)875*b*; Tg(*UAS: GFP-HRAS\_G12V*): 60 zebrafish
3. *tp53*<sup>*zdf1/zdf1*</sup>, Et(*gSAIzGFFD*)875*b*; Tg(*UAS: GFP-CAAX*): 43 zebrafish
4. *tp53*<sup>*zdf1/zdf1*</sup>, Et(*gSAIzGFFD*)875*b*; Tg(*UAS: GFP-HRAS\_G12V*): 43 zebrafish

The final endpoint was selected at 3 months due to the reporter gene expression pattern of the Et(*gSAIzGFFD*)875*b*; Tg(*UAS: GFP*) zebrafish line. Based on the dissection/fluorescent microscopy experiments on the Et(*gSAIzGFFD*)875*b*; Tg(*UAS: GFP*) zebrafish line, there was no significant reporter gene expression at the adult stage. It was therefore deduced that oncogene expression would similarly cease to be expressed during the adult stage and so it was determined unlikely that tumours would form past 3 months.

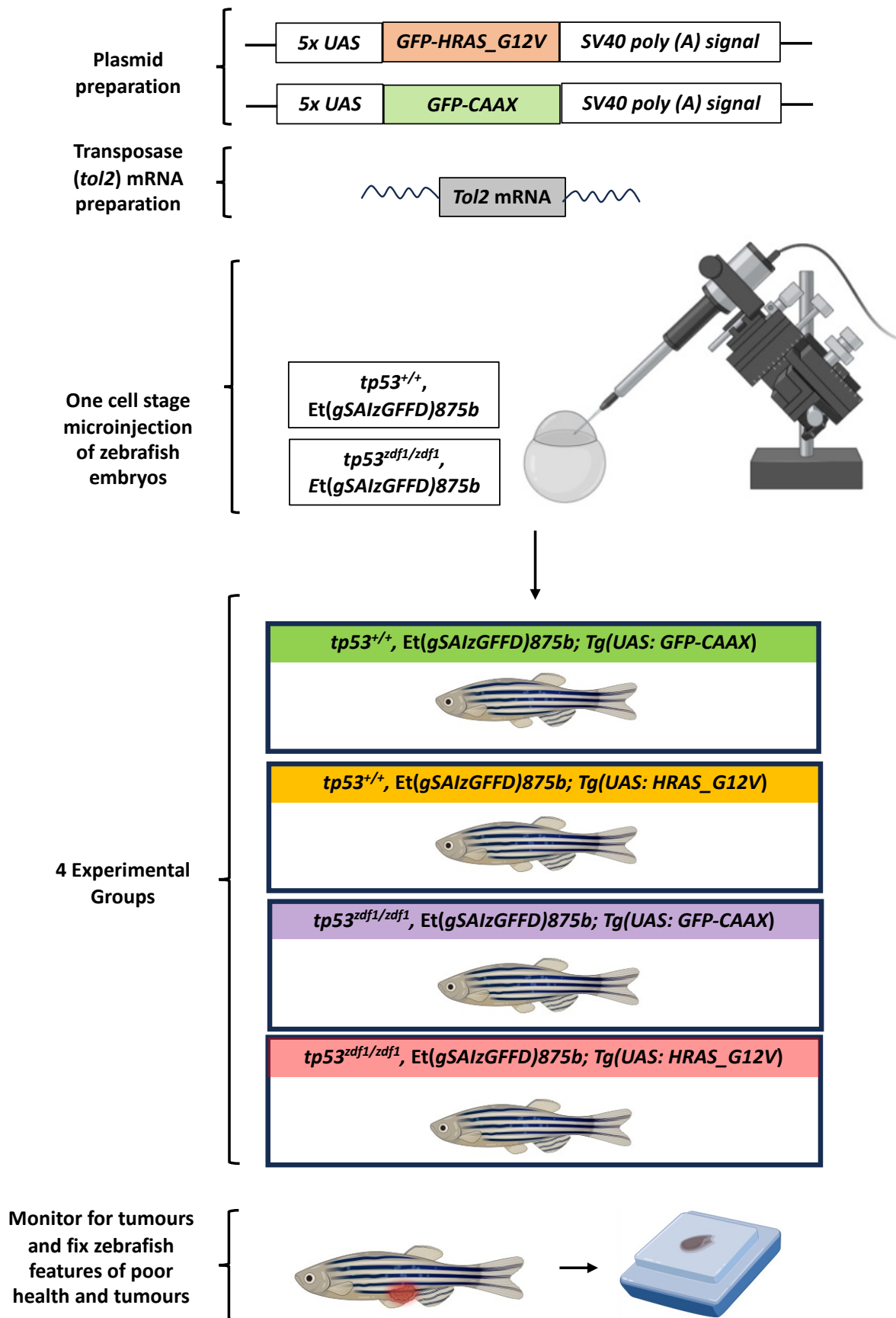


Figure 47. Schematic of the Zebrafish Urinary Tract Cancer Model Pipeline.

### 5.3.6. Abdominal Tumour development in Urinary Tract Cancer Model

The experimental zebrafish were monitored closely for any abnormalities including swimming difficulties, macroscopic lesions, and emaciation. 2-weeks post fertilisation was selected as the time point to start quantifying the onset of tumour development as this was when the zebrafish reached a size where it became more feasible to assess for the presence of a phenotype. This meant that the total number of zebrafish at 2-weeks post fertilisation would be the denominator in any calculations to determine the proportion of zebrafish that developed tumours in the experiment. Two weeks is also the start of mesonephrogenesis in the zebrafish and so is the transition from the temporary embryonic and larval urinary tract to the permanent adult urinary tract.

Between 2 weeks and 3 months of age, the following numbers of zebrafish developed macroscopic abdominal tumours (Figure 48)

- 7.1% (3/42) of the *tp53*<sup>+/+</sup>, *Et(gSAIzGFFD)875b; Tg(UAS: GFP-HRAS\_G12V)* group
- 14.6% (6/41) of the *tp53*<sup>zdf1/zdf1</sup>, *Et(gSAIzGFFD)875b; Tg(UAS: GFP-HRAS\_G12V)* group

There was no significant difference when comparing the proportion of macroscopic abdominal tumours between the 2 groups above ( $p=0.31$ , Fishers exact test).

There were no macroscopic abdominal tumours visualised in the other two groups. One tumour in each group was imaged using fluorescence microscopy to determine if the lesions expressed GFP as this indicates that HRAS\_G12V is likely to also be expressed in the tumour as the GFP transgene is fused to HRAS\_G12V. GFP was expressed in both tumours (Figure 48) suggesting these are related to the HRAS\_G12V overexpression.

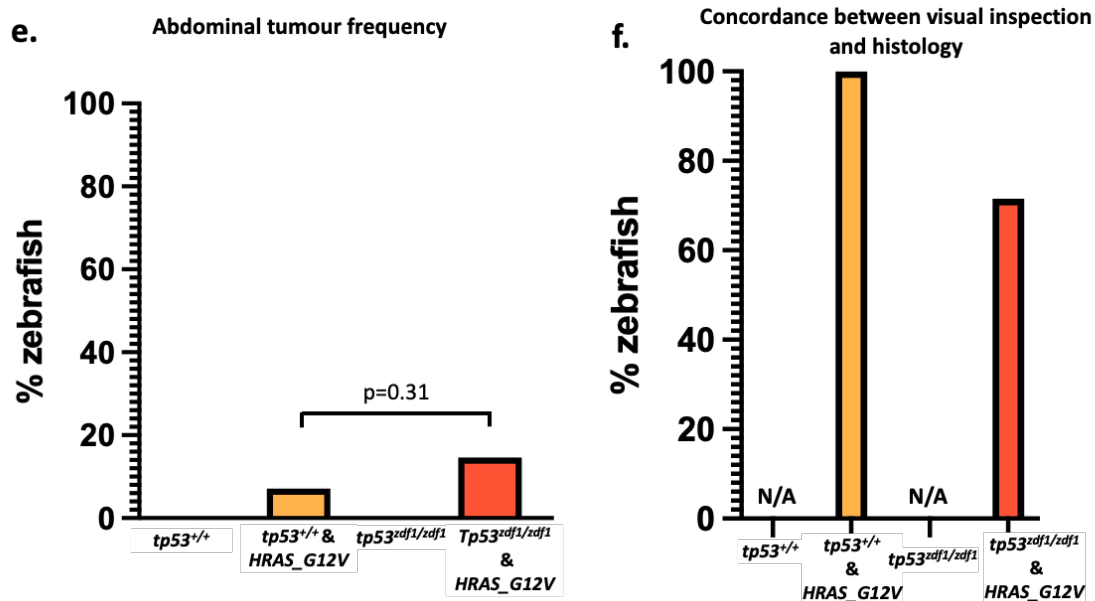
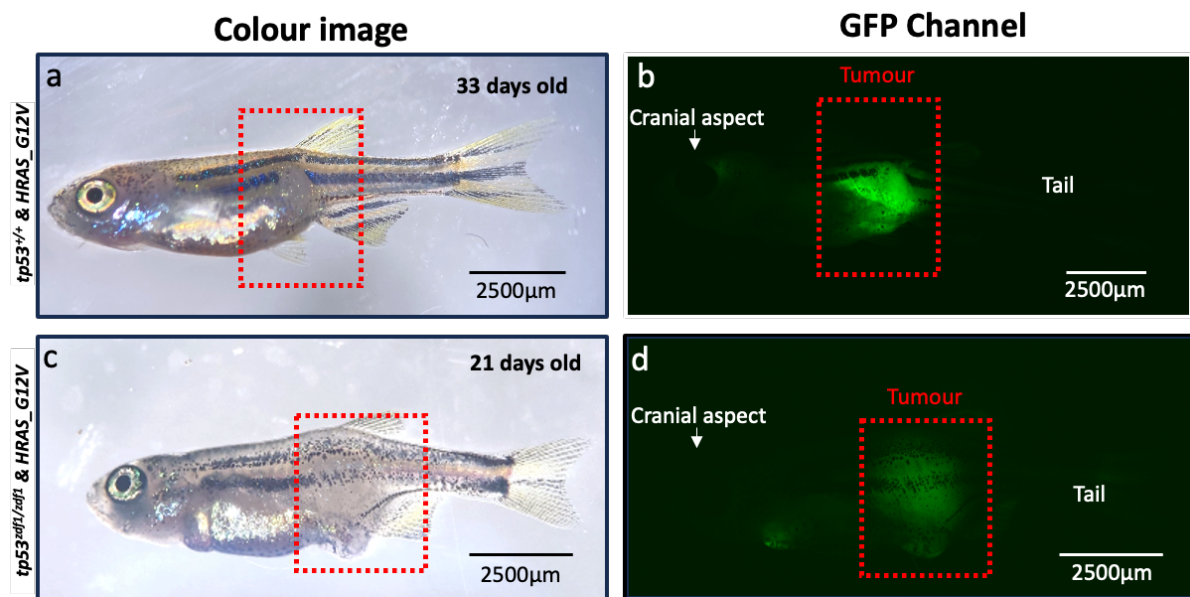


**Figure 48. Zebrafish Tumours Generated in Urinary Tract Cancer Model.**

(a-d) Representative images (Colour and GFP channel fluorescent microscopy images) of zebrafish that developed macroscopic tumours between 2 weeks and 3 months in *tp53*<sup>+/+</sup>, *Et(gSAIzGFFD)875b*; *Tg(UAS: GFP-HRAS\_G12V)* (a,b) and *tp53*<sup>zdf1/zdf1</sup>; *Et(gSAIzGFFD)875b*; *Tg(UAS: GFP-HRAS\_G12V)* (c,d). (e) Proportion of zebrafish developing histologically confirmed macroscopic tumours between 2 weeks and 3 months (n=3/42 zebrafish for *tp53*<sup>+/+</sup>, *Et(gSAIzGFFD)875b*; *Tg(UAS: GFP-HRAS\_G12V)* and n=6/41 for *tp53*<sup>zdf1/zdf1</sup>; *Et(gSAIzGFFD)875b*; *Tg(UAS: GFP-HRAS\_G12V)*). (f) Proportion of zebrafish with visual abdominal tumours based on visual inspection that were confirmed to have cancer histologically (n=3/3 for *tp53*<sup>+/+</sup>, *Et(gSAIzGFFD)875b*; *Tg(UAS: GFP-HRAS\_G12V)* and n=5/7 for *tp53*<sup>zdf1/zdf1</sup>; *Et(gSAIzGFFD)875b*; *Tg(UAS: GFP-HRAS\_G12V)*).

### 5.3.7. Non-Abdominal Tumour Development in Urinary Tract Cancer Model

In addition to abdominal tumour development in the experimental zebrafish, non-abdominal macroscopic tumours were also noted during the experiment in the head and skin (Figure 49). One of these tumours (skin lesion with melanoma like appearance) was evaluated using fluorescence microscopy in the tumour and this showed positive GFP fluorescence strongly suggestive of *HRAS\_G12V* expression in the tumour.

In total, 7.3% of the *tp53<sup>zdf1/zdf1</sup>*, *Et(gSAIzGFFD)875b*; *Tg(UAS: GFP-HRAS\_G12V)* group showed evidence of non-abdominal tumours. There were no non-abdominal tumours visualised in the other groups.

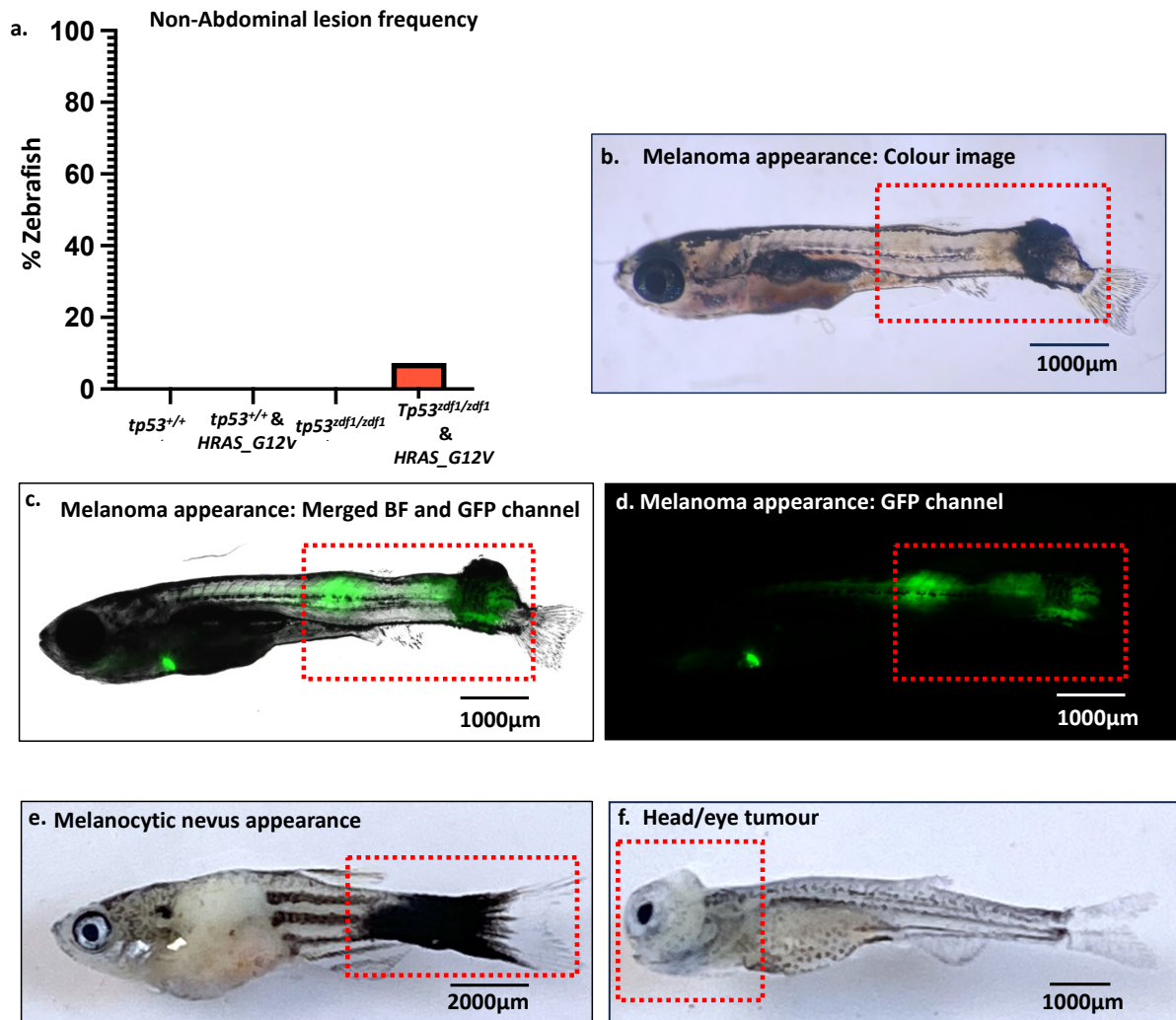


**Figure 49. Non-Abdominal Tumours in the Zebrafish Urinary Tract Cancer Model.**

(a) In total 3/41 (7.3%) zebrafish showed evidence of non-abdominal tumours (visually), all in the *tp53*<sup>zdf1/zdf1</sup>, *Et(gSAIzGFFD)875b*; *Tg(UAS: GFP-HRAS\_G12V)* group. (b-d) 15-day old zebrafish showed evidence of a melanoma like lesion on the tail. (e) 27-day old zebrafish with melanocytic nevus like lesion on tail (In addition to abdominal tumour). (f) 20-day old zebrafish with head/eye tumour.

### **5.3.8. Histological Characteristics of H&E-Stained Tumours in the Urinary Tract Cancer Model**

Zebrafish that developed macroscopic tumours were culled and fixed using an overdose of tricaine anaesthesia followed by immersion in 4% paraformaldehyde and the whole zebrafish were processed histologically (embedded in paraffin wax, sectioned and stained for haematoxylin and eosin (H&E) to evaluate the histological characteristics of the tumours.

Abdominal tumours were stratified based on their location within the abdominal cavity: proximal vs distal abdominal tumours. Based on the histological appearances and anatomical location, it was felt that proximal abdominal tumours were likely to be arising from the proximal urinary tract i.e. kidney tubules and upper urinary tract urothelium. Distal abdominal tumours were likely to be arising from the distal urinary tract i.e. urinary bladder and its early precursor, the distal pronephric duct and distal mesonephric duct. However, it was recognised that further characterisation was needed to determine the exact tissue of origin.

In total, there were 4 individual zebrafish that developed tumour masses that appeared to be arising in the distal abdominal cavity (Figure 50). One of these tumours had an epithelioid appearance and three out of the four tumours had a spindle like morphology.

In total, 5 zebrafish developed tumours masses that appeared to be arising in the proximal abdominal cavity tract (Figures 51-52). These tumour masses all had a spindle-like morphology.

These tumour masses all demonstrated features of cancer i.e. invasion into the surrounding tissues, nuclear pleomorphism and prominent mitoses (Figure 53). These tumours occurred in both the tp53 mutant & HRAS\_G12V and tp53 wild type & HRAS\_G12V groups.

By 3 months, all remaining zebrafish that hadn't developed any macroscopic abnormalities were culled. A sample of these zebrafish were histologically analysed using H&E staining. The regions evaluated included the abdominal cavity, the head kidney, the trunk kidney, the

tail kidney and the urinary bladder. There was no evidence of cancer seen in the regions analyzed (Figure 54) suggesting that if tumours develop in zebrafish in this model, they are likely to manifest macroscopically.

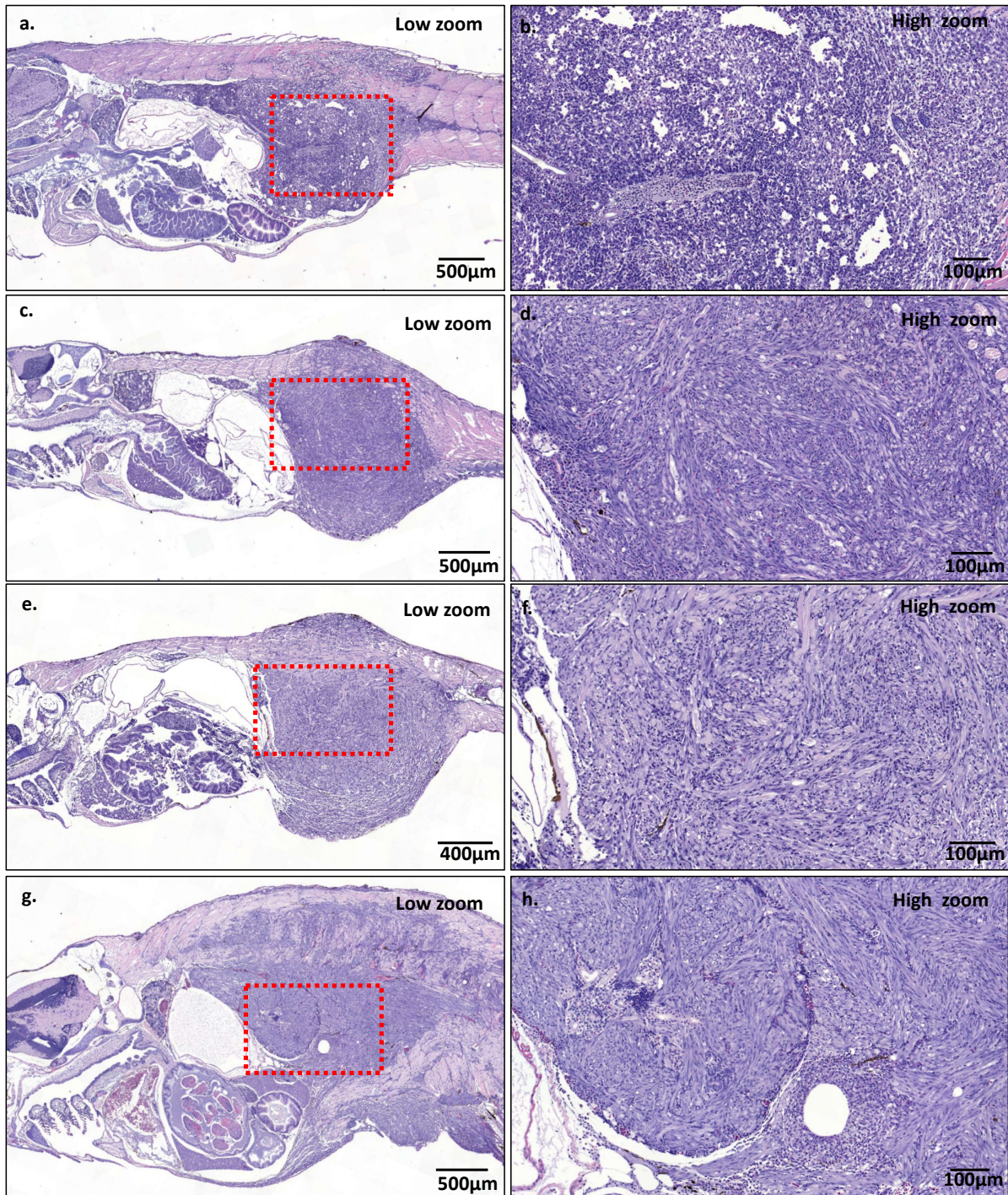


**Figure 50. Histological Characteristics of Zebrafish Distal Abdominal/Pelvic Cancers in Urinary Tract Cancer Model.**

H&E-stained sections from transgenic zebrafish that developed cancers between 2 weeks and 3 months. All cancers developed in in *tp53* wild type & HRAS\_G12V and *tp53* mutant & HRAS\_G12V groups. Each row represents separate zebrafish. (a-b) *tp53* wild type & HRAS\_G12V zebrafish, (c-h) *tp53* mutant & HRAS\_G12V zebrafish. All histology images taken on 3DHISTECH panoramic slide scanner (x20 objective and varying digital zoom).

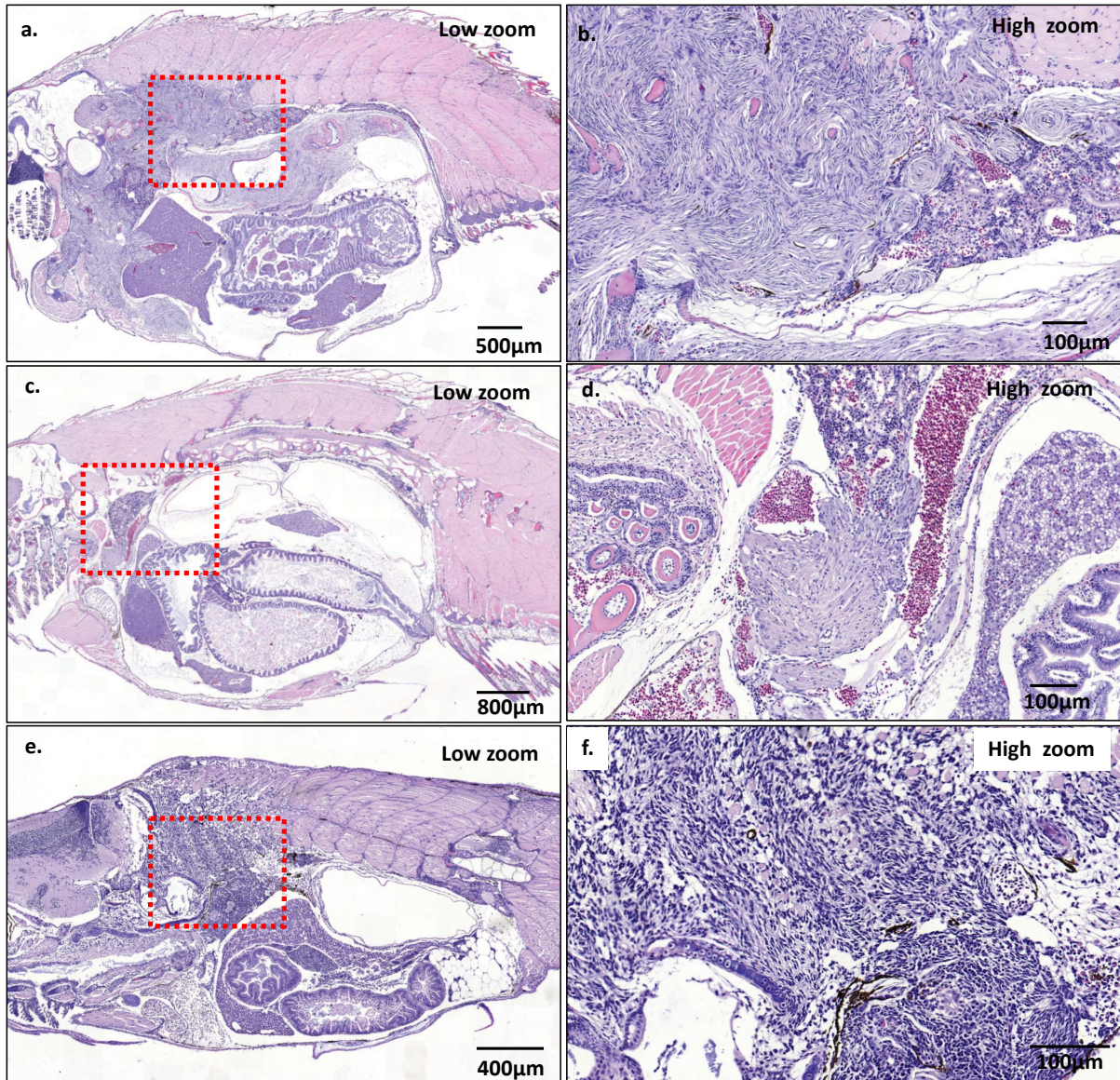


**Figure 51. Histological Characteristics of Zebrafish Proximal Abdominal Cancers in Urinary Tract Cancer Model.**

H&E-stained sections from transgenic zebrafish that developed cancers between 2 weeks and 3 months. All cancers developed in *tp53* wild type & HRAS\_G12V and *tp53* mutant & HRAS\_G12V groups. Each row represents separate zebrafish. (a-d) *tp53* wild type & HRAS\_G12V zebrafish. (e-f) *tp53* mutant & HRAS\_G12V zebrafish. All histology images taken on 3DHISTECH panoramic slide scanner (x20 objective and varying digital zoom).

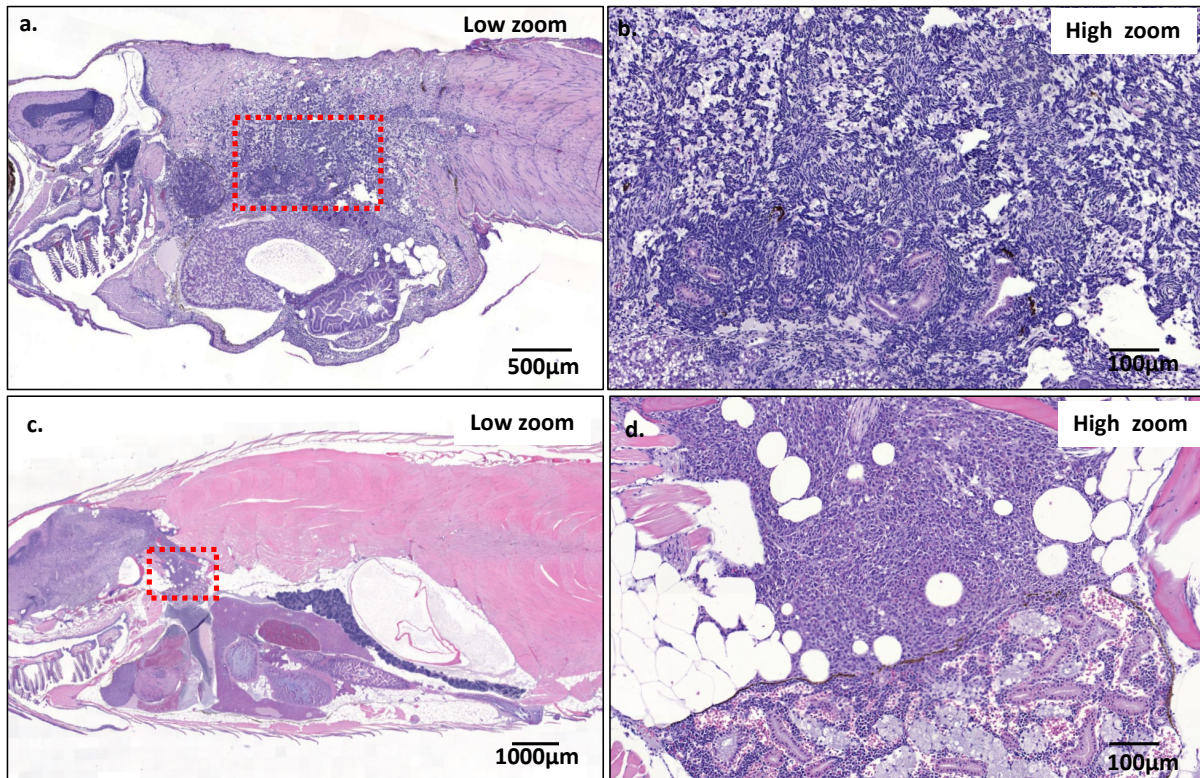


**Figure 52. Histological Characteristics of Zebrafish Proximal Abdominal Cancers in Urinary Tract Cancer Model.**

H&E-stained sections from transgenic zebrafish that developed cancers between 2 weeks and 3 months. All cancers developed in *tp53* wild type & HRAS\_G12V and *tp53* mutant & HRAS\_G12V groups. Each row represents separate zebrafish. (a-b) and (c-d) are both *tp53* mutation & HRAS\_G12V zebrafish. All histology images taken on 3DHISTECH panoramic slide scanner (x20 objective and varying digital zoom).

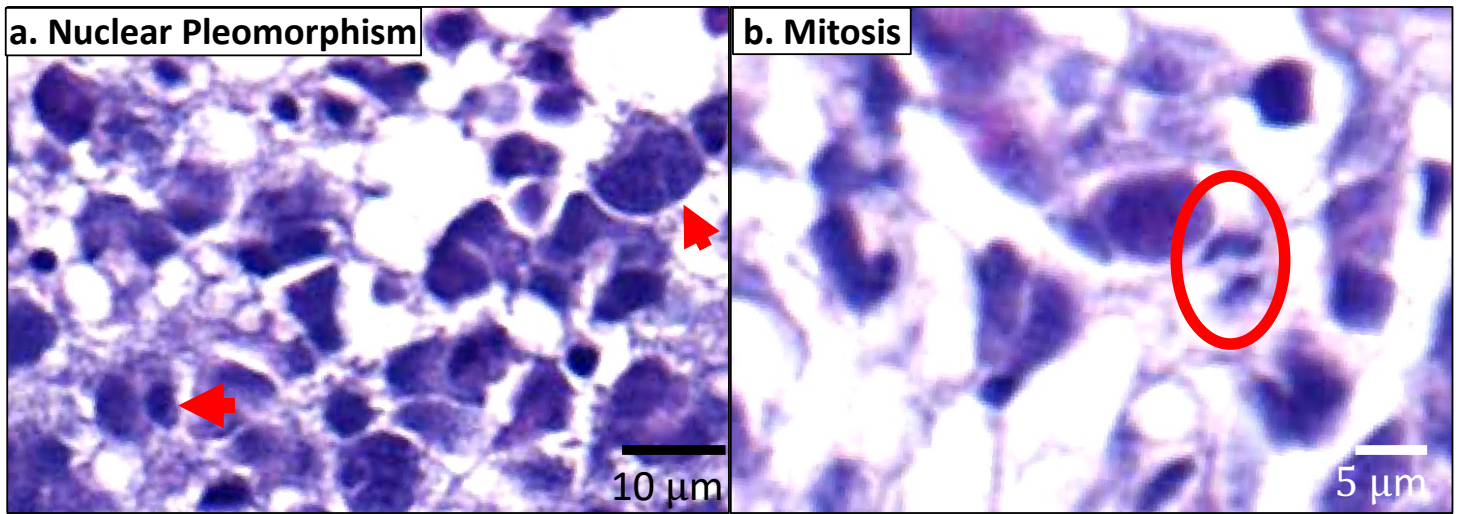


**Figure 53. Histological Features of Cancer in Urinary Tract Cancer Model: Nuclear Pleomorphism and Prominent Mitosis.**

High zoom image of representative example of zebrafish cancer shown in Figure 44 a-b. All histology images taken on 3DHISTECH panoramic slide scanner (x20 objective and varying digital zoom).

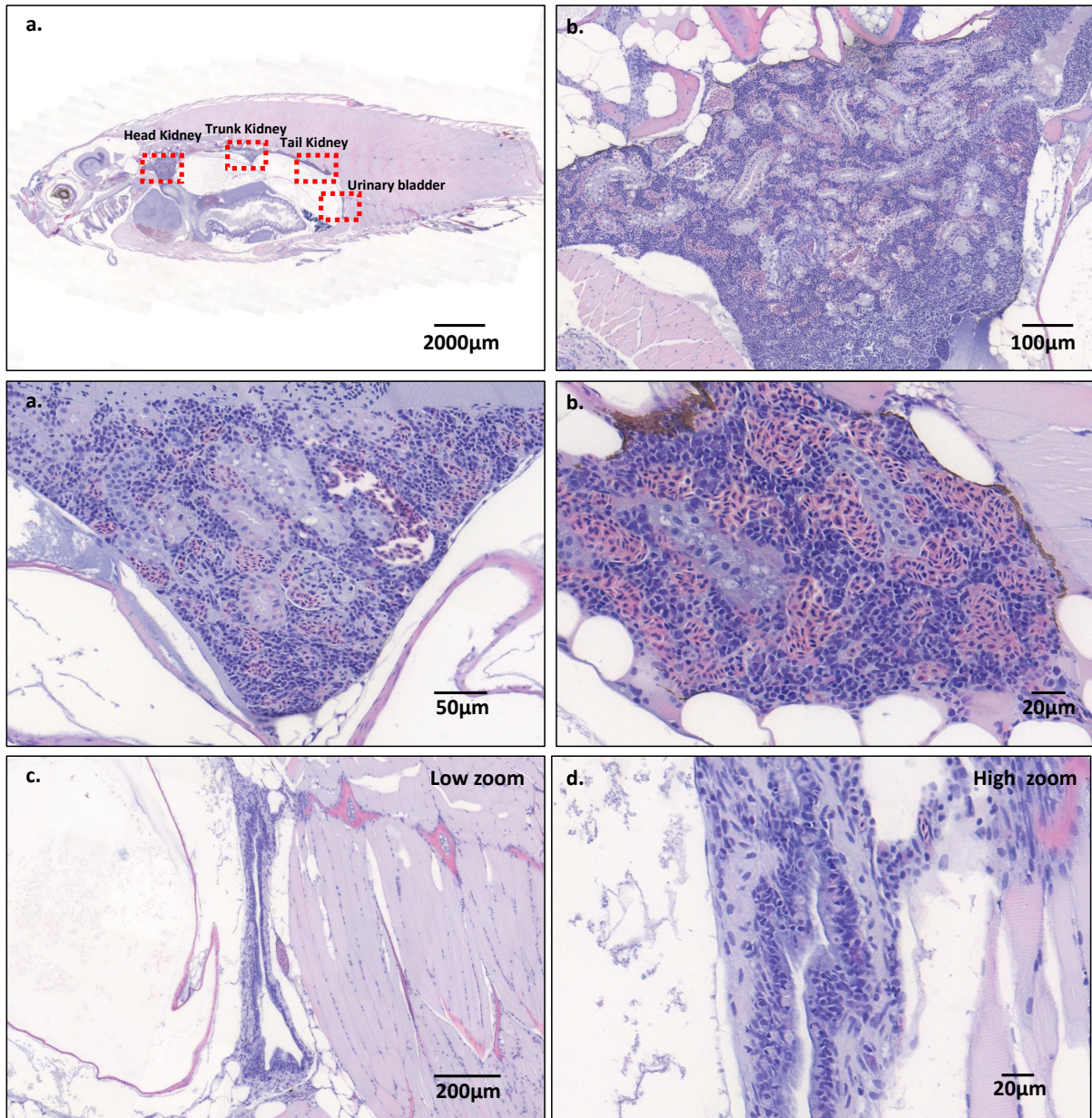


**Figure 54. No Evidence of Macroscopic Tumours in *tp53* Mutant & *HRAS\_G12V* and *tp53* Wild Type & *HRAS\_G12V* Endpoint 3-Month-Old Zebrafish.**

Images shown of representative tissue section from *tp53* mutant & *HRAS\_G12V*. Areas evaluated on tissue sections. (a) Whole zebrafish urinary tract. (b) Head kidney. (c) Trunk Kidney. (d) Tail kidney. (e) Urinary bladder at low zoom and (f) urinary bladder at high zoom. All histology images taken on 3DHISTECH panoramic slide scanner (x20 objective and varying digital zoom).

### **5.3.9. Immunohistochemical Characterisation of Zebrafish Tumours Generated During Urinary Tract Cancer Model**

#### **5.3.9.1. AE1/AE3 Epithelial Marker**

Although H&E staining provided important insights into the morphological characteristics of the tumour cells as well as the anatomical location of the tumours, it was determined that a more in-depth characterisation of the nature of the zebrafish tumours would need immunohistochemistry. Although oncogene expression was driven in the epithelial cells of the urinary tract of the zebrafish, most of the tumours appeared to have a spindle cell appearance which is not characteristic of epithelial tumours. However, it is well established that cancers that are significantly undifferentiated can take on alternative morphological appearances, including spindle cell morphology.

First and foremost, it was necessary to determine if these tumours were epithelial in origin. In clinical practice, a commonly used marker to determine if tumours of unknown primary are epithelial in origin is AE1/AE3 (382). AE1/AE3 are broadly reactive and recognise cytokeratins in epithelial tissues.

Due to the absence of commercially available AE1/AE3 zebrafish antibodies, a mouse recombinant monoclonal AE1/AE3 antibody (Ab961) with reported reactivity (by the manufacturer) in zebrafish was selected. Prior to staining the zebrafish tumours with the AE1/AE3 antibody, optimisation was performed on human and zebrafish epithelial tissues using different concentrations until successful staining was demonstrated. As expected, positive staining (cytoplasmic and membranous staining) was seen in the urothelium of the human bladder, the epithelial lining of the zebrafish urinary bladder and the zebrafish gut epithelium. No primary antibody negative controls all demonstrated an absence of positive staining (Figure 55).

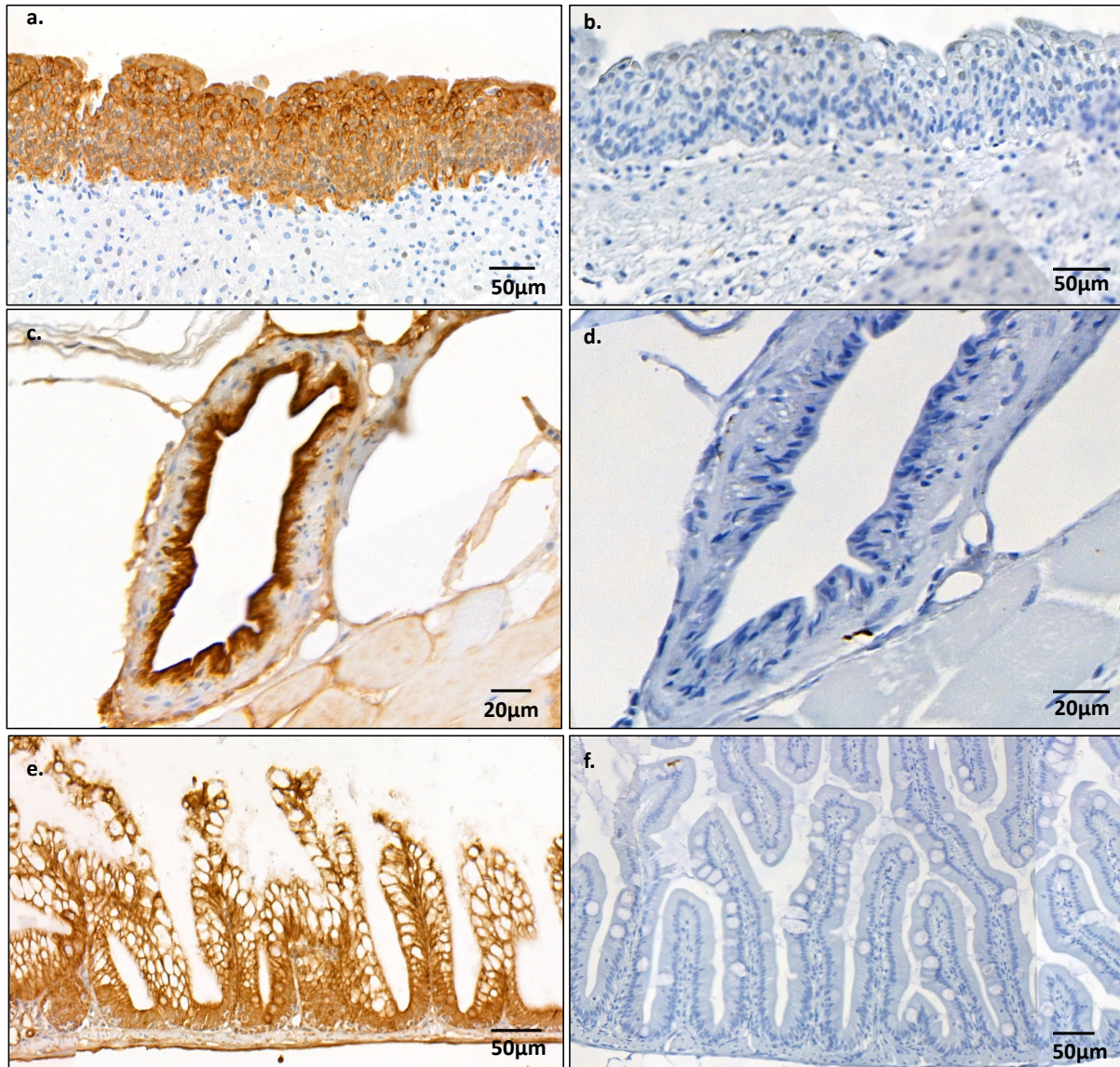


**Figure 55. Immunohistochemistry Validation of AE1/AE3 (Pan-Cytokeratin) Antibody in Zebrafish Epithelia.**

(a) AE1/AE3 staining in human bladder urothelium, (b) no primary antibody control in human bladder urothelium, (c) AE1/AE3 staining in zebrafish urinary bladder epithelium, (d) no primary antibody control in zebrafish urinary bladder epithelium, (e) AE1/AE3 staining in zebrafish gut epithelium, (f) no primary antibody control in zebrafish gut epithelium. All histology images taken on 3DHISTECH panoramic slide scanner (x20 objective and varying digital zoom). Performed with assistance from Jenny Down, histology technician, University of Sheffield.

Following successful optimisation of the AE1/AE3 antibody on normal zebrafish tissues, immunohistochemical staining of the zebrafish tumours was performed to determine if they were epithelial in origin.

Three out of the four zebrafish lower abdominal tumours that were generated demonstrated cytoplasmic and membranous staining for the AE1/AE3 antibody (Figure 56). The AE1/AE3 positive tumours (Figure 56c-h) all had a spindle cell like morphology on H&E staining. This suggests that these AE1/AE3 positive tumours are epithelial in origin tumours that are significantly undifferentiated. The only zebrafish lower abdominal tumour that didn't stain positive for AE1/AE3 (Figure 56a-b) had an epithelioid morphology on H&E staining.

In the five tumours that appeared to be originating in the upper abdominal cavity, two out of the five demonstrated cytoplasmic and membranous staining for the AE1/AE3 antibody (Figures 57-58). The AE1/AE3 positive tumours (Figure 57c-d and Figure 58a-b) also had spindle cell like morphology suggesting they were also significantly undifferentiated epithelial-in-origin tumours.

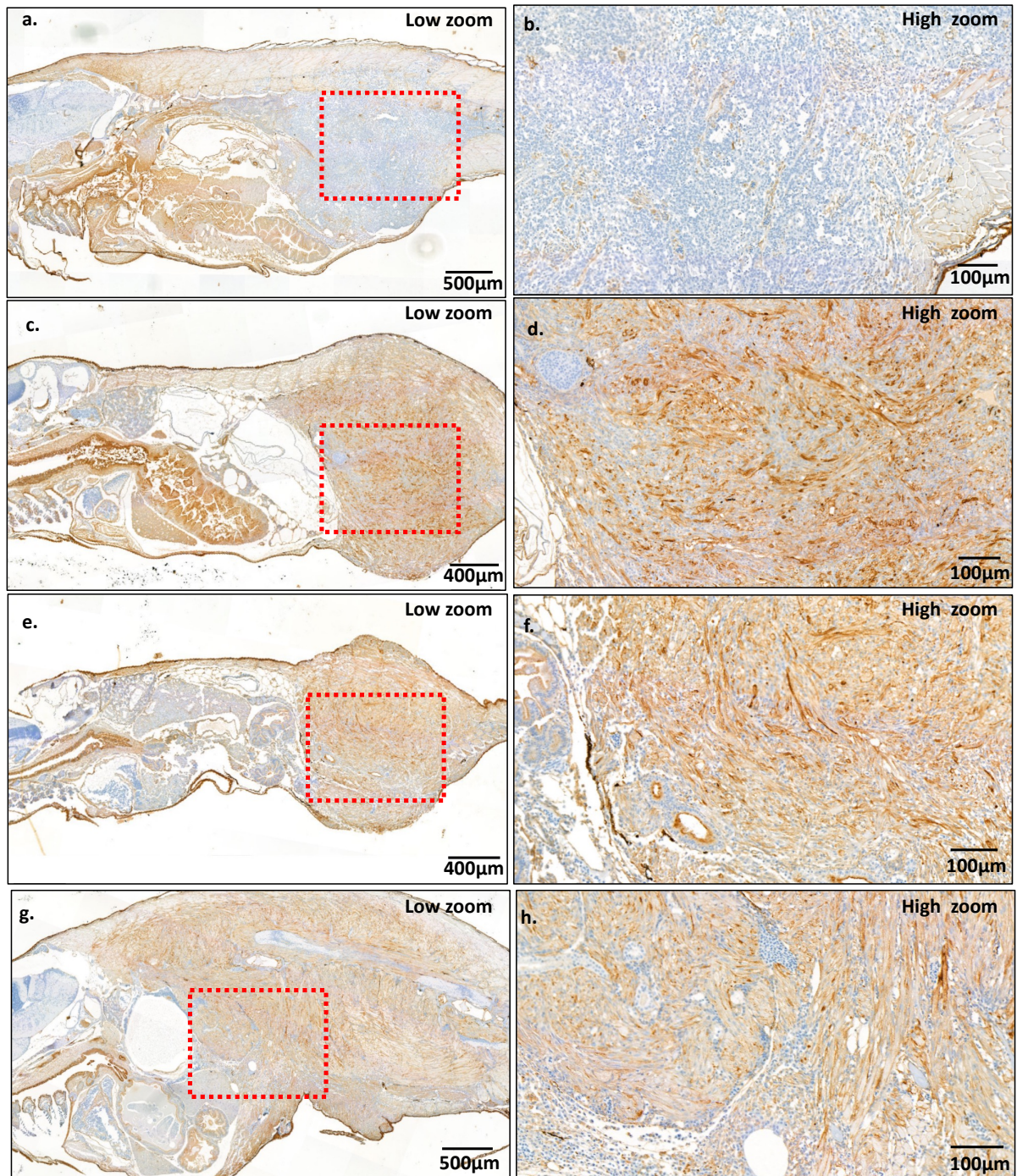


**Figure 56. Immunohistochemistry Using AE1/AE3 (Pan-Cytokeratin) Antibody in Distal Abdominal/Pelvic Tumours in Zebrafish Urinary Tract Cancer Model.**

Each row represents separate zebrafish. (a-b) *tp53* wild type & HRAS\_G12V zebrafish, (c-h) *tp53* mutant & HRAS\_G12V zebrafish. All histology images taken on 3DHISTECH panoramic slide scanner (x20 objective and varying digital zoom). Performed with assistance from Jenny Down, histology technician, University of Sheffield.

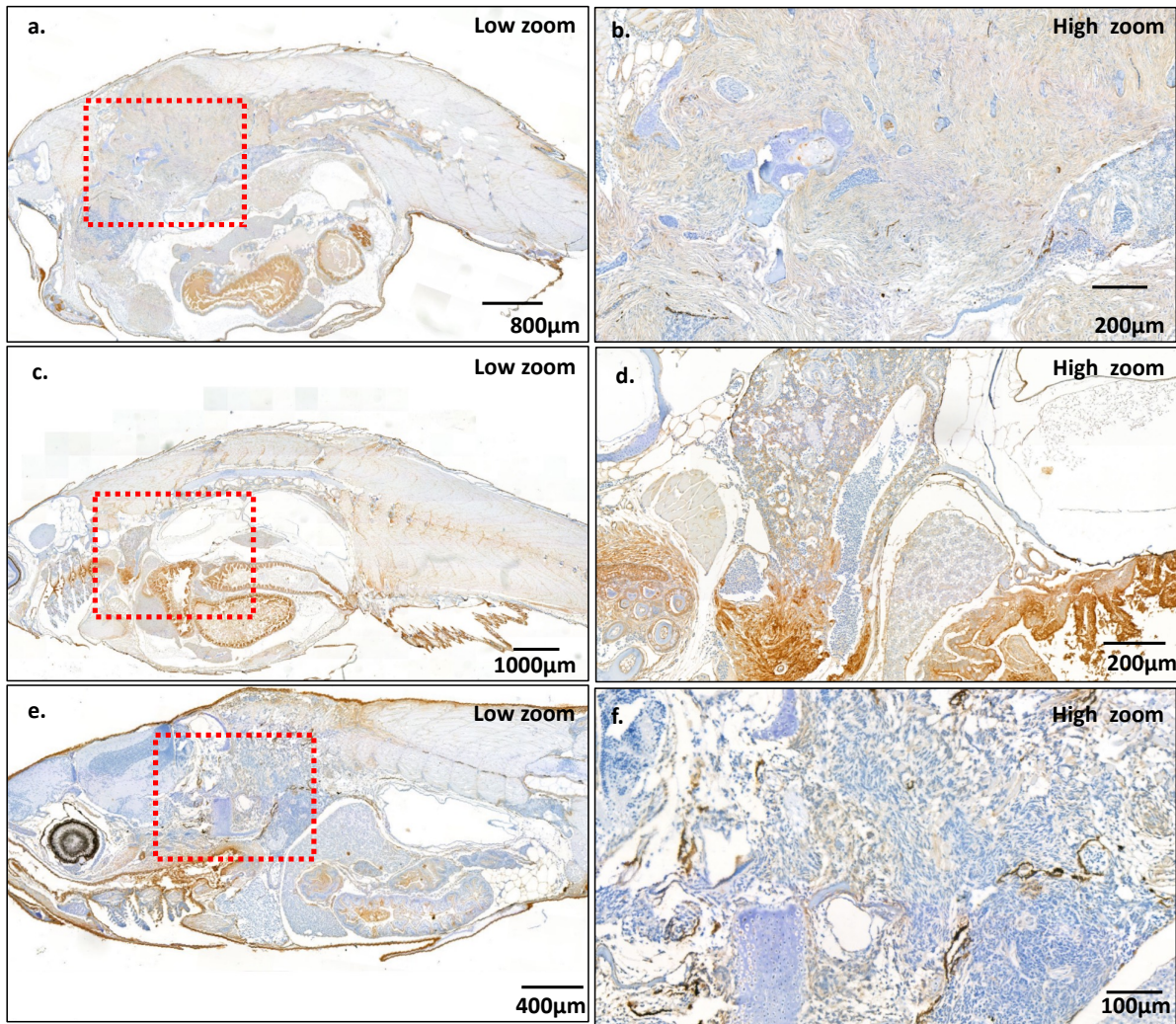


**Figure 57. Immunohistochemistry using AE1/AE3 (Pan-Cytokeratin) Antibody in Proximal Abdominal Tumours in Zebrafish Urinary Tract Cancer Model.**

Each row represents separate zebrafish. (a-d) *tp53* wild type & HRAS\_G12V zebrafish. (e-f) *tp53* mutant & HRAS\_G12V zebrafish. All histology images taken on 3DHISTECH panoramic slide scanner (x20 objective and varying digital zoom). Performed with assistance from Jenny Down, histology technician, University of Sheffield.

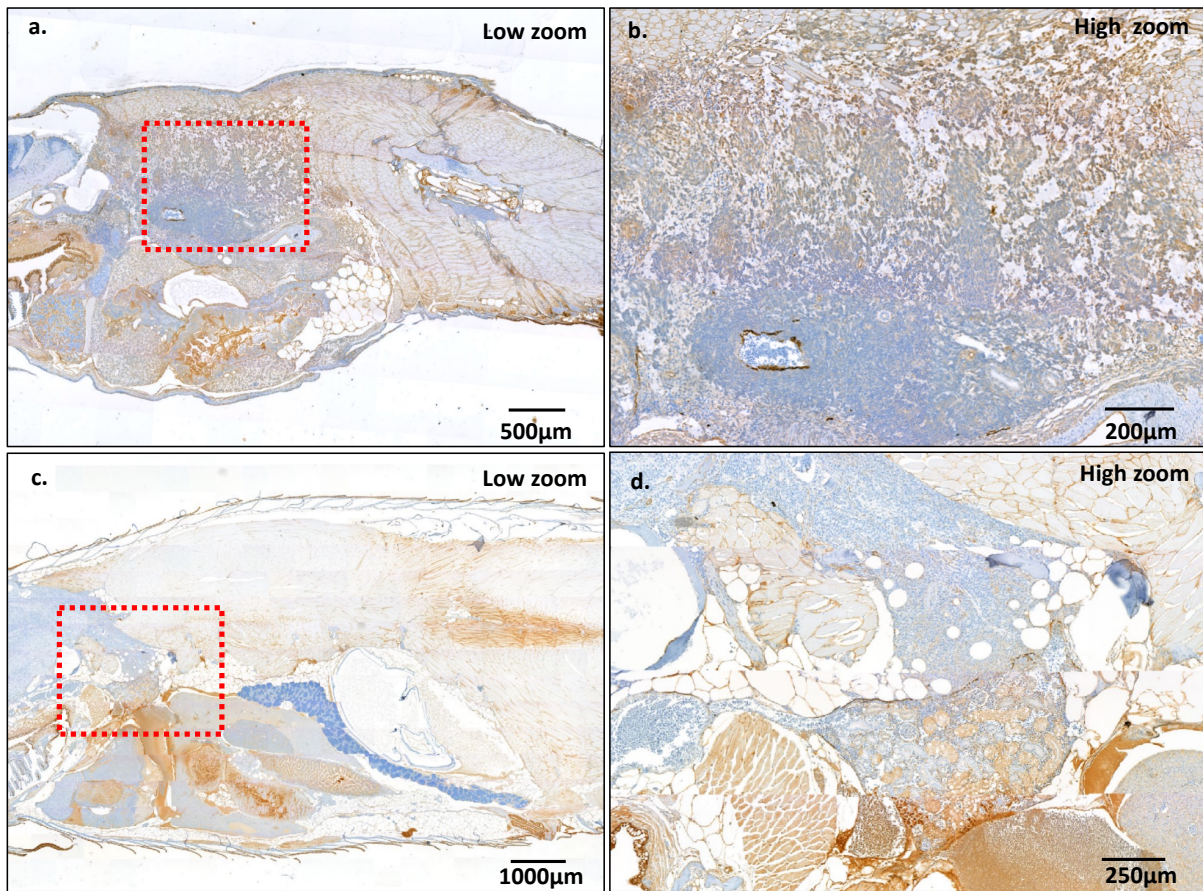


**Figure 58. Immunohistochemistry Using AE1/AE3 (Pan-Cytokeratin) Antibody in Proximal Abdominal Tumours in Zebrafish Urinary Tract Cancer Model.**

Each row represents separate zebrafish. (a-d) *tp53* mutant & *HRAS\_G12V* zebrafish. All histology images taken on 3DHISTECH panoramic slide scanner (x20 objective and varying digital zoom). Performed with assistance from Jenny Down, histology technician, University of Sheffield.

### 5.3.9.2. Urothelial Immunohistochemistry Markers

Three out of the five AE1/AE3 positive zebrafish tumours were selected for further immunohistochemical characterisation with urothelial markers. This selection was based on tumours that had a distal or middle abdominal anatomical location as it was hypothesised these would be most likely to be urothelial cancers. The markers that were selected to be used were GATA3 and Uroplakin 1a (UPK1A). UPK1a was selected over UPK2 due to closer homology between zebrafish and humans. These markers had already been optimised on zebrafish earlier in this project (see Chapter 4. GATA3 is from the GATA family of transcription factors and is expressed in a number of epithelial cancers including urothelial cancer. It is often used in clinical practice to differentiate metastatic urothelial or breast carcinoma from other metastatic carcinomas (90, 359).

In the GATA3 immunohistochemistry staining experiment, of the three zebrafish tumours evaluated (Figure 59), one of the zebrafish tumours demonstrated positive nuclear staining for GATA3 (Figure 59c-d).

However, in the UPK1A immunohistochemical staining, none of the zebrafish tumours demonstrated the cytoplasmic and membranous staining that would be expected in positive uroplakin 1a staining (Figure 60).

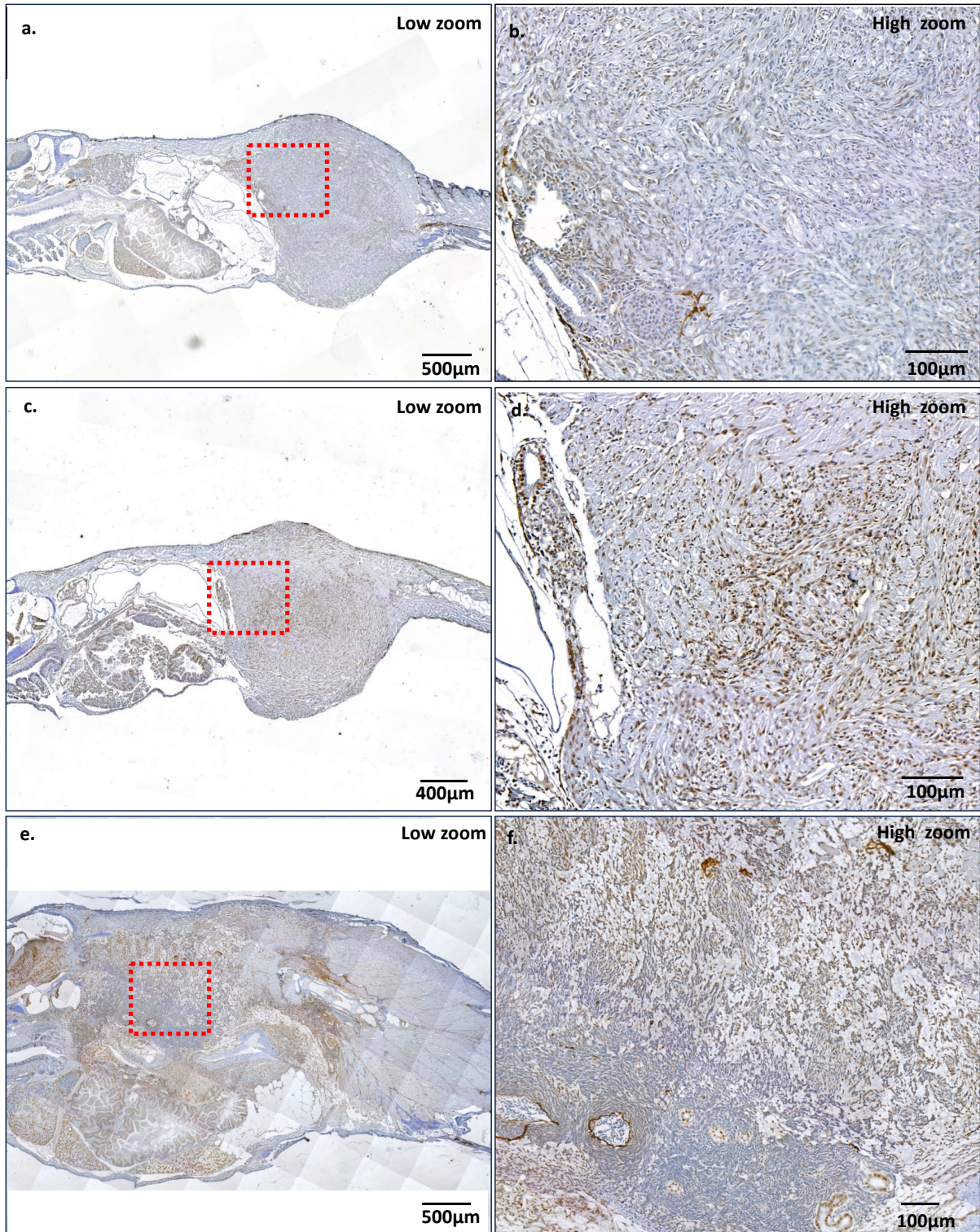


**Figure 59. Immunohistochemistry Using GATA 3 Antibody in IHC Determined Epithelial Tumours Generated in Zebrafish Urinary Tract Cancer Model.**

Each row represents a separate zebrafish. All zebrafish tumours shown from *tp53* mutant & HRAS\_G12V zebrafish. There is tiling artefact evident in image (e). All histology images taken on 3DHISTECH panoramic slide scanner (x20 objective and varying digital zoom). Performed with assistance from Jenny Down, histology technician, University of Sheffield.

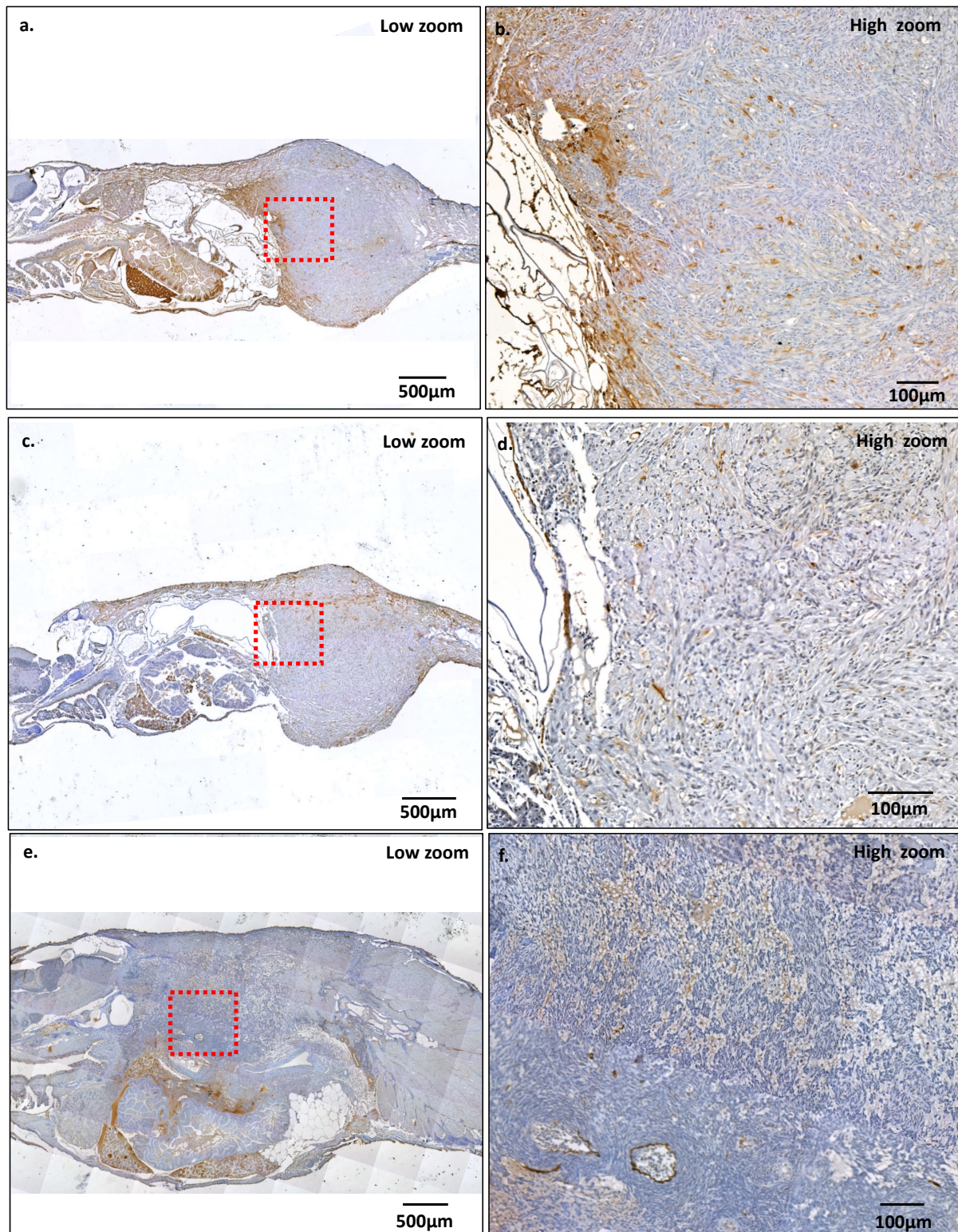


**Figure 60. Immunohistochemistry Using Uroplakin-1a Antibody in IHC Determined Epithelial Tumours Generated in Zebrafish Urinary Tract Tumours in Urinary Tract Cancer Model.** Each row represents a separate zebrafish. All zebrafish tumours shown from *tp53* mutant & *HRAS\_G12V* zebrafish. There is tiling artefact evident in image (e). All histology images taken on 3DHISTECH panoramic slide scanner (x20 objective and varying digital zoom). Performed with assistance from Jenny Down, histology technician, University of Sheffield.

### 5.3.9.3. Renal Immunohistochemistry Markers

As the spatial expression pattern of the zebrafish *Et(gSAIzGFFD)875b; Tg(UAS:GFP)* line was throughout the zebrafish pronephros and mesonephros, it was hypothesised that these zebrafish tumours may be renal in origin. In clinical practice, a commonly used renal immunohistochemical marker used in the diagnosis of renal cell carcinoma is transcription factor PAX8 (383).

As there were no commercially available zebrafish Pax8 antibodies, a mammalian antibody targeting the human PAX8 protein would have to be used. The human and zebrafish Pax8 amino acid sequences were aligned, and it was determined that there was significant homology in the N terminus. A rabbit monoclonal PAX8 antibody targeting the N terminus of the human PAX8 sequence was selected.

This antibody was first optimised on mouse kidney tissue to validate the protocol. This successfully demonstrated nuclear staining of the renal tubular epithelial cells (Figure 61). However, no staining was demonstrated in normal zebrafish kidney tissue suggesting either an absence of PAX8 in the zebrafish kidney or insufficient homology between the amino acid sequences to facilitate binding of the antibody to the protein.

a.

Zebrafish	3	NSTGRGHGGLNQLGGMFVNGRPLPEVIRQRIVDMAHQGVPCDISRQLRVSHGCVSKILG	62
Human	4	NS GHGGLNQLGG FVNGRPLPEV+RQRIVD+AHQGVPCDISRQLRVSHGCVSKILG	63
Zebrafish	63	RYETGSIKPGVIGGSKPKVATPKVVEKIAEYKRNPTMFAWEIRDRLAEGVCDGDTVP	122
Human	64	RYETGSI+PGVIGGSKPKVATPKVVEKI +YKRNPTMFAWEIRDRLAEGVCD DTVP	123
Zebrafish	123	SVSSINRIIRTQVQPFNLPD----TKGLSPGHTLIPSSAVTPPESQSDSLGSTYSIN	178
Human	124	SVSSINRIIRTQVQPFNLP+D TK LSPGHTLIPSSAVTPPESQSDSLGSTYSIN	183
Zebrafish	179	GLLGITQTTADGKRGHDDSDQESCRHSVDSQSGGGARKQLRTEHFPS---AALDCGFER	235
Human	184	GLLGI Q +D KR DSDQ+SCR S+DSQ S G RK LRT+ F L+C FER	242
Zebrafish	236	HYSSDSF---SQSKAEQQLYLALMNPGLDEGKGA-----SSISRNLAAHQYAVVTEAL	287
Human	243	+ +++ S +K EQ LYPL L+N LD+GK + + RNL+ HQ Y VV +	302
Zebrafish	288	QPLPLCLKQEVSPVNSLSPSPHIIISGSAFLDLSAIISSPSSAPVASSCGSAHLSHGFFSF	347
Human	303	P +KQE +PEV+S S +P +S SAFLDL + S F++F	345
Zebrafish	348	SHHAPVHGQFSSPSLMAGREVAASSMLPGYPPHIPTAQTG-FSSSTIAGMVSAPYETGQSY	406
Human	346	H A V+GQF+ +L++GRE+ LPGYPPHIPT+ G ++SS IAGMV+ EY+G +Y	405
Zebrafish	407	SHPAYSSYSEAWRFNSSLILGSPYYYSSATR---PPPPAAAYDHL	448
Human	406	H YSSYSEAWRF NSS+L SPYYYSS +R PP A A+DHL	450

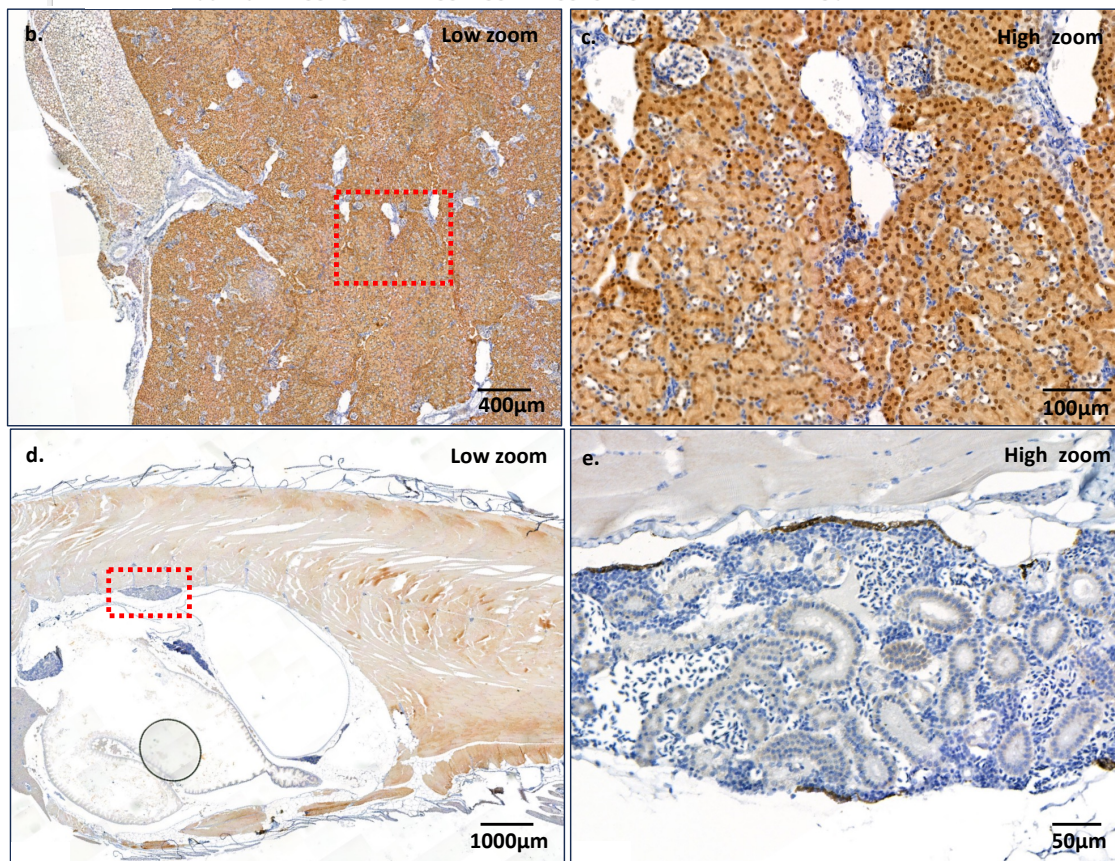


**Figure 61. Optimization of Pax8 Immunohistochemistry in Zebrafish Kidney.**

(a) Zebrafish and human PAX8 sequences aligned using the online National Center for Biotechnology Information (NCBI) BLAST tool (233). Significant homology between sequences identified at N terminus. (b-c) PAX8 immunohistochemistry staining in normal mouse kidney (positive control). (d-e) No Pax8 staining is seen in normal zebrafish kidney. All histology images taken on 3DHISTECH panoramic slide scanner (x20 objective and varying digital zoom). Performed with assistance from Jenny Down, histology technician, University of Sheffield.

## 5.4. Discussion

This is the first known study to drive urinary cancer associated genomic alterations HRAS\_G12V and *tp53* DNA binding domain mutation in the zebrafish urinary tract. There were a number of important findings. Firstly, a new enhancer trap transgenic zebrafish line was identified with reporter gene expression in the pronephros and mesonephros during the larval and juvenile stages. Secondly, this study demonstrated that it is possible to use this enhancer trap transgenic zebrafish line to direct (and visualise) the expression of HRAS\_G12V in the zebrafish urinary tract. Thirdly, abdominal cancers resulted from overexpression HRAS\_G12V and a combination of HRAS\_G12V overexpression and *tp53* mutation. Fourthly, many of these cancers were determined to be epithelial in origin but unlikely to be urothelial in origin based on immunohistochemistry i.e. positive for AE1/AE3 (epithelial marker) but negative for GATA3 and UPK1A (urothelial markers).

This study identified and characterised the *Et(gSAIzGFFD)875b; Tg(UAS: GFP)* zebrafish line. This is an enhancer trap line that expresses GFP under the control of enhancers in the vicinity of the genomic insertion of the GFF transgene. The GFP expression pattern evolved over time. At 2- and 3-days post fertilisation, the GFP expression was restricted to the pronephros and from 4 days post fertilisation onwards, the expression was also in the gut. From 3-weeks post fertilisation onwards, the GFP expression was restricted to just proximal and middle segments of the mesonephros but not the distal mesonephros or urinary bladder region. No GFP expression was seen in the adult *Et(gSAIzGFFD)875b; Tg(UAS: GFP)* zebrafish urinary tract. The identification of this line is an important finding because it can be used as a resource in the study of urinary tract diseases as well as bowel diseases. It is important to note that this reporter line, whilst labelling the whole urinary tract in larvae, does not label the urinary bladder in juvenile and adult zebrafish.

There is no previous literature on the embryology of the zebrafish mesonephric ducts and urinary bladder. Previous work on segmentation patterns of the pronephros reported that the most distal portion likely represents the excretory system or collecting system of the zebrafish larval urinary tract based on expression of mammalian nephric duct markers *ret1*, *gata3*, and *emx1* (32). In mammals, the urinary bladder develops from the anterior

urogenital sinus which develops from partitioning of the cloaca. The mesonephric duct fuses to the anterior urogenital sinus and the ureteric bud develops as an outgrowth from the mesonephric duct and grows upwards to fuse to the metanephric kidney (6). The embryological processes of the zebrafish urinary tract are likely to be different to the mammalian system because the final zebrafish kidney is the mesonephric kidney and they do not develop a metanephric kidney (31). In the *Et(gSAIzGFFD)875b; Tg(UAS: GFP)* zebrafish line, combination of GFP expression in the distal pronephros prior to day 5pf but absence of GFP expression in the urinary bladder region 3 weeks post fertilisation onwards suggests that there may be an embryological change to the structure of the urinary tract at this stage that involves the urinary bladder. Although it is logical the zebrafish distal pronephros is the precursor to the adult urinary bladder, our findings suggest that this may not be the case. It is possible that the zebrafish urinary bladder doesn't exist prior to around 3-weeks post fertilisation at which point it may start to develop. Potential tissues it could arise from are the cloacal tissue or from the mesonephric ducts. Further work is needed to determine the embryology of the zebrafish distal urinary tract.

*In vivo* expression of *GFP-HRAS\_G12V* in the zebrafish pronephros was demonstrated. Two different approaches to express *GFP-HRAS\_G12V* in the zebrafish pronephros are demonstrated: stable expression and mosaic expression. The stable approach utilised stable zebrafish line crosses with a *Tg(UAS: GFP-HRAS\_G12V)* zebrafish line crossed with the *Et(gSAIzGFFD)875b* zebrafish line. In contrast, the mosaic approach utilised one cell stage microinjection of *p-UAS: GFP-HRAS\_G12V* plasmid with *tol2 transposase* mRNA. It was decided not to use the stable approach for the cancer model because the transgene expression was too low. A possible explanation for the poor transgene expression with the stable approach is UAS gene silencing (377). This is an issue associated with using the Gal4/UAS system whereby the UAS sequences become methylated over subsequent generations leading to silencing of expression of downstream genes and diminished expression over time (377). In contrast, the mosaic approach resulted in good expression. Furthermore, the mosaic expression of oncogene approach more closely recapitulates most adult human urinary tract cancers that arise due to somatic genomic alterations.

We demonstrated, utilising the Gal4/UAS system, that driving HRAS\_G12V in combination with a global *tp53* homozygous mutation (M214K) under the control of an enhancer that drives expression in the pronephros and mesonephros can drive cancers in the abdominal cavity. We demonstrated that the combination of *tp53* homozygous M214K mutation and HRAS\_G12V expression in the urinary tract leads to more tumours (14.6% vs 7.14%) than HRAS\_G12V expression alone, though the difference was not statistically significant. In other zebrafish models of cancer, a combination of *tp53* mutation with *RAS* overexpression leads to more carcinogenesis compared to *HRAS* overexpression alone (384). An important advantage of this model is the speed of onset of cancers and the majority of cancers in this model developed prior to 6 weeks post fertilisation. This rapid onset of cancer development is important because mechanistic data on the initiation and progression of cancer can potentially be generated in a short amount of time.

These cancers can have a range of gross morphological appearances and can take on both epithelioid and spindle cell like appearances histologically. Immunohistochemistry for a pan cytokeratin (AE1/AE3) demonstrated that several of these cancers are likely to be epithelial in origin including cancers that appeared morphologically epithelioid on H&E staining. It is possible that in zebrafish cancers with spindle-cell like appearances on H&E sections but positive AE1/AE3 immunohistochemical profiles, there was significant undifferentiation and epithelial to mesenchymal transition as this is a known phenomenon that can occur with aggressive subtypes of carcinomas (385). The Gal4/UAS system, which was utilised to drive *HRAS\_G12V* overexpression, is reported to result in significant overexpression of transgenes placed downstream of the upstream activating sequence (386). This is a possible explanation of the potential undifferentiated tumours.

None of the cancers that were positive for AE1/AE3 staining stained positive for both urothelial panel markers (GATA3 and UPK1A). However, it may be the case that these tumours are significantly undifferentiated and no longer express markers that human urothelial cancers would be expected to express. It is recognised that human urothelial carcinomas can stain negative for uroplakins, particularly invasive and metastatic urothelial carcinomas (387, 388). Furthermore, it is possible that zebrafish urothelial cancers don't

express these markers. Further work is needed to characterise the transcriptomic profile of the tumours to determine which human cancer subtype they are most likely to resemble.

A particularly interesting finding is the wide range of different morphological appearances of the zebrafish cancers. The zebrafish cancers were in both proximal and distal abdominal locations, had both epithelioid and spindle cell like appearances on H&E staining, and were in both abdominal and non-abdominal regions. There are likely to be several reasons for this. Firstly, the enhancer trap *Et(gSAizGFFD)875b; Tg(UAS:GFP)* zebrafish line is expressed throughout the zebrafish pronephros and mesonephros and the gut. Therefore, mosaic expression of *HRAS\_G12V* in these tissues is likely to lead to differing levels of expression in different regions of the pronephros and mesonephros. It is important to note that the pronephros and mesonephros epithelial layer is not one homogenous structure but has different regions that are likely to have different functions and different gene expression patterns. Previous studies have established different gene expression levels in different regions of the pronephros. Further work is needed to identify zebrafish gene promoter sequences that drive reporter gene expression in more specific areas of the zebrafish urinary tract as this may enable more homogenous cancers to develop.

The non-abdominal cancers that were observed in this cancer model in the skin and the head region are likely to be secondary to small amounts of previously unidentified expression *Et(gSAizGFFD)875b; Tg(UAS:GFP)* in these regions. Another explanation is *tol2* mediated migration of the p-gSAizGFFD enhancer trap cassette within the zebrafish genome. As the enhancer trap *Et(gSAizGFFD)875b* zebrafish line was made using *tol2* transgenesis, the p-gSAizGFFD enhancer trap cassette has *tol2* sequences that can theoretically be driven by *tol2* transposase enzyme to migrate to other parts of the zebrafish genome. If this happens, then the GFF transcriptional activator could be driven by different regulatory elements leading to different tissue specific expression patterns. However, it is important to note that this is a theoretical risk and has not been seen previously (389). To try to reduce this potential risk, it was also attempted during this project to inject the plasmid into one cell stage embryos without *tol2 transposase* mRNA. In the absence of *tol2 transposase* mRNA, the transgenesis efficiency is significantly reduced (389). However, the potential risk of *tol2* transposase mediated movement of the p-

gSAIzGFFD enhancer trap cassette would be diminished. Our findings were, in the absence of *tol2 mRNA*, that the mosaic expression of the transgenes in injected plasmids was either very weak or absent in the F0 generation. Therefore, it was determined that the *tol2* transgenesis system was essential for mosaic expression of transgenes of interest in the F0 generation.

## **5.5. Conclusion**

Driving urinary tract cancer associated genomic alterations HRAS\_G12V and tp53 mutation under the control of the enhancer trap Et(gSAIzGFFD)875b leads to abdominal cancers which are predominantly epithelial in origin. Further work is needed in characterising the nature of these tumours and their homology to human cancers to determine the feasibility of this model for studying urinary tract cancers.

## Chapter 6. Developing A Transgenic Zebrafish Model of Urinary Tract Cancer Utilising the Zebrafish *cdh17* Gene Promoter

### 6.1. Introduction

In Chapter 5. , I developed a zebrafish model where expression of HRAS\_G12V in combination with a *tp53* mutation in the zebrafish pronephros and mesonephros (and gut) drives cancer. However, it was determined that this model required optimisation for a number of reasons:

Firstly, the reporter gene in the *Et(gSAIzGFFD)875b; Tg(UAS:GFP)* zebrafish line was expressed in both the zebrafish urinary tract (pronephros/mesonephros) and gut. This lack of specificity means that in some zebrafish, genes of interest under the control of the UAS (e.g. oncogenes) were also expressed in the gut as well as the urinary tract.

Secondly, the driver for the model was an enhancer trap and so the promoter or enhancer driving expression of the oncogene is unknown. Whilst neighbouring promoters/enhancers can be mapped and identified, these are not always responsible for expression, and so this limits replication of our model and biological insights. Reproduction would always require offspring from our *Et(gSAIzGFFD)875b* enhancer trap zebrafish line.

Thirdly, our zebrafish *Et(gSAIzGFFD)875b* enhancer trap line that was originally used was made using *tol2* transgenesis. Therefore, injection of *tol2* transposase mRNA into *Et(gSAIzGFFD)875b* larvae could, in theory, result in transposition of the GFF cassette to other sites within the genome. This is less of a problem for cassettes containing simple promoter/reporter constructs, but the enhancer trap is designed to catch nearby genes and drive expression in diverse tissues, meaning that it is possible for the tissue in which the oncogenes are expressed could vary from fish to fish, leading to problems with specificity and reproducibility.

In this chapter I describe my work to derive a more specific transgenic zebrafish line that overcomes these limitations.

## 6.2. Aims and Objectives

This chapter had the following aims and objectives:

### Aim

Develop a new zebrafish cancer model expressing urothelial bladder cancer-associated oncogenes (*HRAS\_G12V*, *erbb2\_A301F* and *pik3ca\_E545K*) under the control of a promoter with more specificity for the zebrafish urinary tract.

### Objectives

I will address this aim through the following objectives:

1. Evaluate, in detail, the expression patterns of different gene promoter-reporter gene constructs with previously reported expression in the zebrafish urinary tract
2. Select a gene promoter with good expression in the zebrafish urinary tract and establish a stable reporter line for this promoter.
3. Characterise the expression of this new transgenic zebrafish line in larvae and adults to determine the feasibility of utilising this promoter for a cancer model.
4. Generate new plasmids to express bladder cancer associated oncogenes (*HRAS\_G12V*, *erbb2\_A301F* and *pik3ca\_E545K*) fused to GFP under the control of this new gene promoter.
5. Inject newly generated plasmids into one cell stage offspring embryos from an incross of *tp53<sup>zdf1/zdf1</sup>* zebrafish and raise the zebrafish to adulthood, monitoring for the development of any abnormalities and histologically characterise any abnormalities that arise.

## 6.3. Results

### 6.3.1. Identification of a New Urinary Tract Specific Promoter

I searched for gene promoters that had previously been used to drive reporter gene expression in the zebrafish urinary tract. In the literature, there were 2 zebrafish gene promoters; *Enpep* (390) and *cdh17* (391), reported to drive gene expression in the zebrafish pronephros/mesonephros.

Three expression vectors were acquired from other research groups:

- An expression vector was acquired from Dr Lowe, University Manchester, UK which contained approximately 2kb of the zebrafish *enpep* promoter sequence upstream of the GFP coding sequence (pT2KXIGdeltaIN- *enpep*: GFP).
- An expression vector was acquired from Dr Freek Van Eeden, University of Sheffield, UK (Made by Dr Aylin Metzner) which contained approximately 2kb of the zebrafish *enpep* promoter sequence upstream of the *Gal4* coding sequence (pDestTol2CG2- *enpep*: *Gal4*).
- An expression vector was acquired from Dr Iain Drummond, Mount Desert Island Biological Laboratory, USA which contained approximately 4kb of the zebrafish *cdh17* promoter driving the *Gal4* coding sequence (pDestTol2CG2-*cdh17*: *Gal4*)

These plasmids were injected into one cell stage zebrafish embryos with tol2 transposase mRNA (into wild type zebrafish embryos for pT2KXIGdeltaIN-*enpep*: GFP and *Tg(UAS: Kaede)s1999t* zebrafish embryos for pDestTol2CG2-*enpep*: *Gal4* and pDestTol2CG2-*cdh17*: *Gal4* plasmids). The F0 offspring were evaluated with fluorescent microscopy for fluorescent protein expression to determine the spatial expression pattern associated with the promoters.

Pre- day 5 post fertilisation, the *Tg(enpep:Gal4); Tg(UAS: Kaede)s1999t* zebrafish had expression throughout the pronephros but with significant off target expression in the muscle. There was also yolk fluorescence (Figure 62a). Pre- day 5 post fertilisation, the

*Tg(enpep: GFP)* zebrafish had expression throughout the pronephros but without the significant off target expression in the muscle. There was also yolk fluorescence (Figure 62b).

Pre- day 5 post fertilisation, the *Tg(cdh17:Gal4); Tg(UAS: Kaede)s1999t* offspring had expression throughout the pronephros but without the muscle expression. There was also yolk fluorescence (Figure 63). When comparing the pronephros expression pattern between the *Tg(enpep:GFP)* and the *Tg(cdh17:Gal4); Tg(UAS: Kaede)s1999t* zebrafish larvae, the expression in the *Tg(cdh17:Gal4); Tg(UAS: Kaede)s1999t* zebrafish larvae pronephros was more distal than the expression in *Tg(enpep: GFP) larvae*.

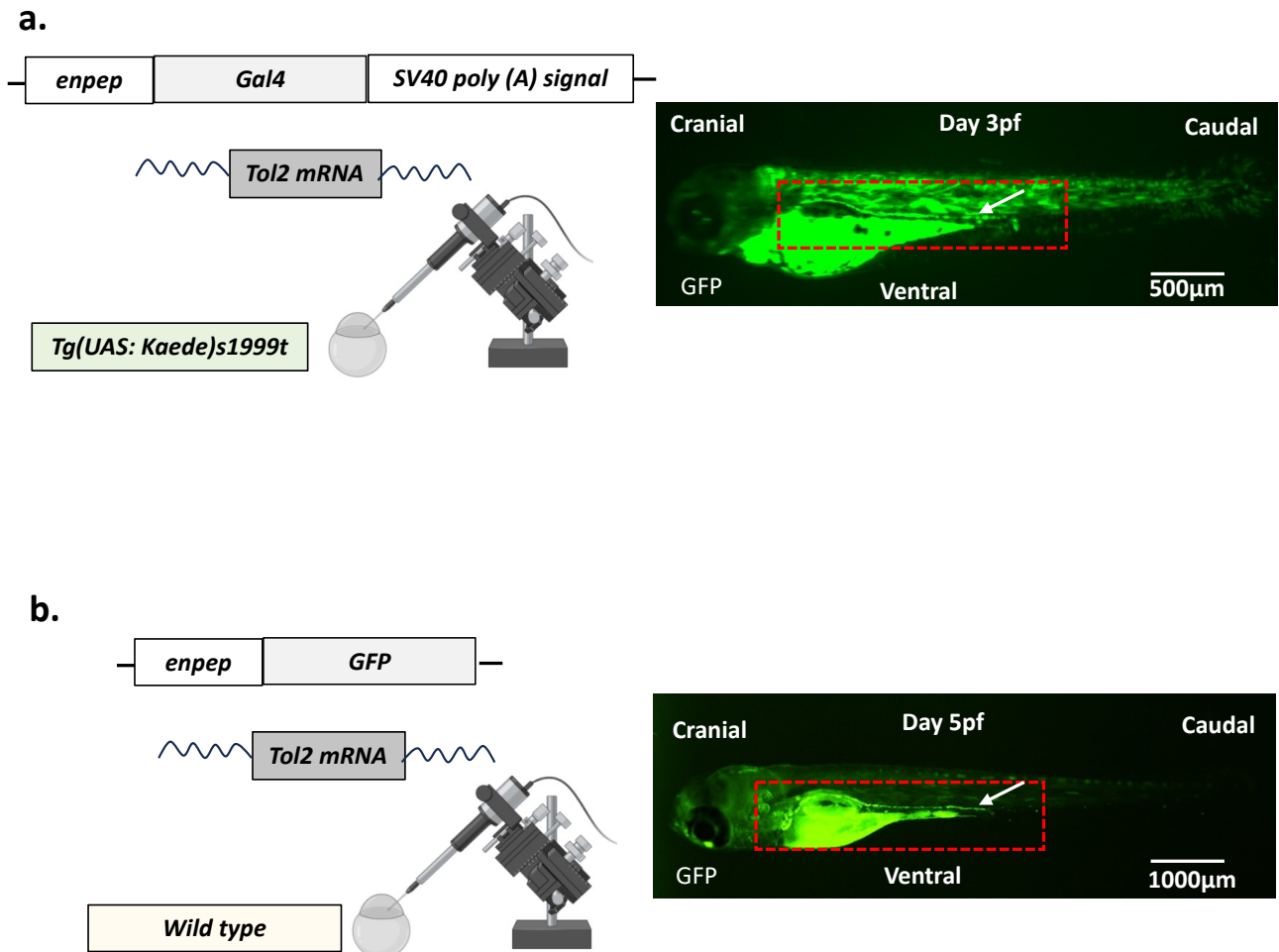


**Figure 62. Zebrafish *In Vivo* Mosaic Expression Patterns of Zebrafish *enpep* Promoter**  
 Expression of fluorescent proteins (Kaede and GFP) under the control of zebrafish 2kb *enpep* promoter at (a) day 3 and (b) day 5 post fertilisation. (a) Utilisation of Gal4/UAS system by injecting pDestTol2CG2-*enpep*: *Gal4* plasmid into one cell stage *Tg(UAS: Kaede)* zebrafish. (b) Zebrafish *enpep* promoter directly driving GFP expression by injecting pT2KXIGdeltaIN-*enpep*: *GFP* plasmid into one cell stage wild type zebrafish. Fluorescent microscopy images above performed in GFP channel using Leica M205 FA fluorescent stereomicroscope (a) and Nikon Eclipse TE2000-U fluorescent microscope (b).

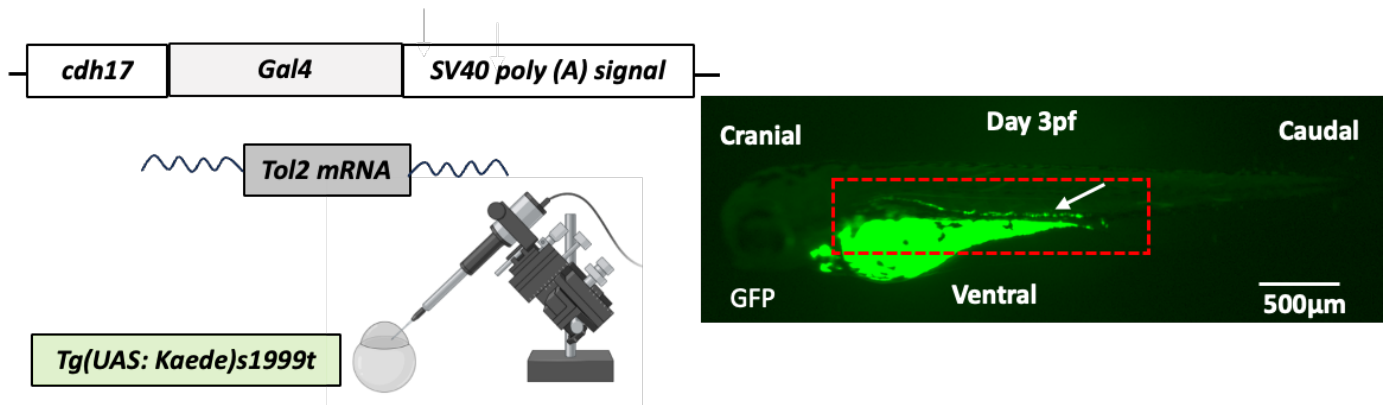


**Figure 63. Zebrafish *In Vivo* Mosaic Expression Pattern of Zebrafish *cdh17* Promoter**

Expression of fluorescent protein (Kaede) under the control of zebrafish 4kb *cdh17* promoter at day 3 post fertilisation. The Gal4/UAS system was utilised by injecting the pDestTol2CG2-*cdh17: Gal4* plasmid into one cell stage *Tg(UAS: Kaede)* zebrafish. Fluorescent microscopy images above performed in GFP channel using Leica M205 FA fluorescent stereomicroscope.

The *cdh17* promoter was therefore selected to make a stable zebrafish reporter line and for further fluorescent microscopy characterisation. Published expression patterns existed for a previous zebrafish *cdh17* reporter line utilising a 2kb promoter fragment (391). However, this was before our report of the zebrafish urinary bladder and ureters and so I wanted to determine *cdh17* was expressed in the zebrafish urinary bladder and ureters. In addition, no in-depth reports of expression patterns from the 4kb promoter fragment plasmid that was acquired for this experiment.

Before making a zebrafish *cdh17* reporter line, the zebrafish Cdh17 amino acid sequence was inputted into the online National Center for Biotechnology Information (NCBI) BLAST tool(233) to determine what the zebrafish Cdh17 protein sequence corresponds to in humans. It was found to be most similar to human CDH17. There were similarities between the two sequences except for a region near the N-terminus of the protein with extra amino acids in zebrafish that weren't present in humans (Figure 64).

Zebrafish	6	LLHLTLLVSIGHGIDLEDK-KGPLIDTVLDVPEATVPVYAFFKFTSAVEDVSSYRVSGET	64
		L L L ++ G+G E K GPL + E F+F + V+ + ++GET	
Human	10	LCLLMLYLATGYG--QEGKFSGPKPMTFSIYEGQEPSQIIFQFKANPPAVT-FELTGET	66
Zebrafish	65	EDKIRISSDGWLYLEQPLEWSPEKKHLLIEALSEDGKTLDGPAQVVLQVIDVNNPPVF	124
		++ I +G LY + L+ H+L + AL +G ++GP + ++V D+N+N P F	
Human	67	DNIFVIEREGLLYYNRALDRETRSTHNLQVAALDANGIIVEGVPVITIEVKDINDNRPTF	126
Zebrafish	125	SESQYSGSIREHSPAGVPFVQVFASDADDPNTENTQLRFSIVNQIPIVGQTFFFGINPNN	184
		+S+Y GS+R++S G PF+ V A+D DDP T N QL + IV Q+P++ +F IN	
Human	127	LQSKYEGSVRQNSRPGKPFVYNATDLDDPATPNGQLYYQIVIQLPMINNVMYFQINNKT	186
Zebrafish	185	GQIFTTEEGAEFLKARPSVTYSRGEVRGSPDVLKKKFEDYCIPKNNIALENNPFYKCV	244
		G I T R	
Human	187	GAISLT-----R	193
Zebrafish	245	AERRTVNVLQDPDYALIVRAEDLGGNAVNSLSSTTRVNIAILQNLWVSPGPITIRENTDE	304
		+ +N ++P Y L++ +D+GG + NS S TT V+I + +N+W +P P+ + EN+ +	
Human	194	EGSQELNPAKNPSYNLVISVKDMGGQSENSFSDTTSVDIIVTENIWKAPKPVEMVENSTD	253
Zebrafish	305	EYPMYLATMRANPTALYRLEQKEIL-SFPFTINQDGDYVVTGPLDREEKEMYILVIAE	363
		+P+ + +R N+P A Y L KE L FPF+I+Q+GDYVVT PLDREEK+ Y+ +A+	
Human	254	PHPIKITQVRWNDPGAQYSLVDKEKLPFRPFSDIQEGDIYVVTQPLDREEKDAYVFYAVAK	313
Zebrafish	364	DEQGVLELEKPMIIPVLVQDENDNPPMCDE--ALFEVQEKEPVGNSIGHLPAHDNDKEGTL	421
		DE G L P+EI V V+D NDNPP C +FEVQE E +GNSIG L AHD D+E T	
Human	314	DEYGKPLSYPLEIHVKVKDINDNPPTCPSPVTVFEVQENERLGNISIGTLTAHDRDEENTA	373
Zebrafish	422	SSALTYTLRSQTPTKPSDKMFSIDPNTGEIKVANQNFQRKQVPQYELTFEVDQVFFTKC	481
		+S L Y + QTP P D +F I G +++A Q+ +++ PQY LT EV+D+ F T C	
Human	374	NSFLNYRIVEQTPKLPMDGLFLIQTAYAGMLQLAKQSLKKQDTPQYNLTIEVSDKDFKTL	433
Zebrafish	482	KAIKVIDINDEIPIFEKNDYGTYSVPELAEVGTLLNIKATDADDTGTGSSRVEYHITA	541
		I VIDIND+IPIFEK+DYG ++ E +G+T+L I+ATDAD+ TGSS++ YHI	
Human	434	FVQINVIDINDQIPIFEKSDYGNLTLAEDTNIGSTILTIQATDADEPFTGSSKILYHIK	493
Zebrafish	542	GDPQNLFAIEVDEETGEGRVYIAQPLDYELQSVYNLKIDARNPEPLIAGVEYNDSSSTTSV	601
		GD + ++ D T G V I +PLD+E +V N+ A NPEPL+ GV+YN SS	
Human	494	GDSEGR LGVDTDPHTNTGYVVIKKPLDFETA AVSNIVFKAENPEPLVFGVKYNASSFAKF	553
Zebrafish	602	VIELVDVDEPPKFEVEGLNVNVPENITVGTLKMAEAKDPEGKTIKFKMEGDEHKWLELN	661
		+ + DV+E P+F V E++ +GT + AKDPEG I + + GD WL+++	
Human	554	TLIVTDVNEAPQFSQHVFAQKVSQVDAIGTKVGNVTAKDPEGLDISYSLRGDTRGWLKID	613
Zebrafish	662	VDTGELKTKAALDRETVDHFTLTITAYETEGSKMEAEMKVDIHLQDVNDNYPKLQK--TQ	719
		TGE+ + A LDRE + + + A E GS + + + + L DVNDN P+L K T	
Human	614	HVTGEIFSVAPLDREAGSPYRVQVATEVGGSSLSSVSEFHLILMDVNDNPPRLAKDYTG	673
Zebrafish	720	GFICLQDMTP--LTLTAMDKDADPYGEP-FTFAISRKS--QNFEIKPVDGTSAKLILK	774
		F C P L A D D + P FTF++ S ++E+ ++GT A+L +	
Human	674	LFFCHPLSAPGSLIFEATDDDQHLFRGPHFTFSLGSGSLQNDWEVSKINGTHARLSTRHT	733
Zebrafish	775	PSSEQNVTVPINVLNAG--LGITQKFDVTRICNCTKLGICYIEPASHSWKL-SMGSTIGI	831
		E+ V I + D L V C+C + G C+ PA H + ++G +GI	
Human	734	DFEEREYVVLIRINDGGRPPLEGIVSLPVTFCSCVE-GSCF-RPAGHQTGIPTVGMVGI	791
Zebrafish	832	LAGVFGVIGLFLGICLYQIKK---KDKQRATAEGETKAM 867	
		L VIG+ L + +IKK KD + E K +	
Human	792	LLTLLVIGIILAVVFIRIKKDKGKDNVESQAQASEVKPL 830	

**Figure 64. Alignment of Zebrafish and Human CDH17 Amino Acid Sequences.**

Amino acid alignment performed using online National Center for Biotechnology Information (NCBI) BLAST tool (233).

### 6.3.2. Generation of Tg(*cdh17 Gal4*); Tg(UAS: Kaede) Stable Line

Due to the tissue specific expression in the *Tg(cdh17 Gal4); Tg(UAS: Kaede)s1999t* mosaic zebrafish larvae generated from single cell injection of plasmid, it was decided to set up a stable *Tg(cdh17 Gal4); Tg(UAS: Kaede)s1999t* zebrafish line for two reasons: Firstly, a stable line would enable an accurate determination of the expression pattern of the *cdh17* promoter at different ages. Secondly, a stable *Tg(cdh17: Gal4)* zebrafish line could be used for a future cancer model utilising the Gal4/UAS system (if the cancer model without the Gal4/UAS system does not result in sufficient expression for tumourigenesis).

Following one cell stage microinjection of the pDestTol2CG2-*cdh17: Gal4* plasmid into transgenic zebrafish line *Tg(UAS: Kaede)s1999t*, offspring were screened between days 3-5pf for the presence of Kaede expression in the pronephros as well as the GFP expression in the heart to confirm successful integration of the plasmid resulting in good expression (Figure 65). The zebrafish with good expression were raised to adulthood and outcrossed to nacre wild type zebrafish. The next generation (F1 generation) were screened for GFP expression in the pronephros to confirm successful transmission of the *cdh17:Gal4* transgene sequence to the germline (Figure 65). This F1 generation was raised to adulthood and outcrossed again. The offspring were screened for GFP expression in the pronephros and in the heart to identify a founder with a single transgene insertion based on a Mendelian inheritance pattern (Figure 66).

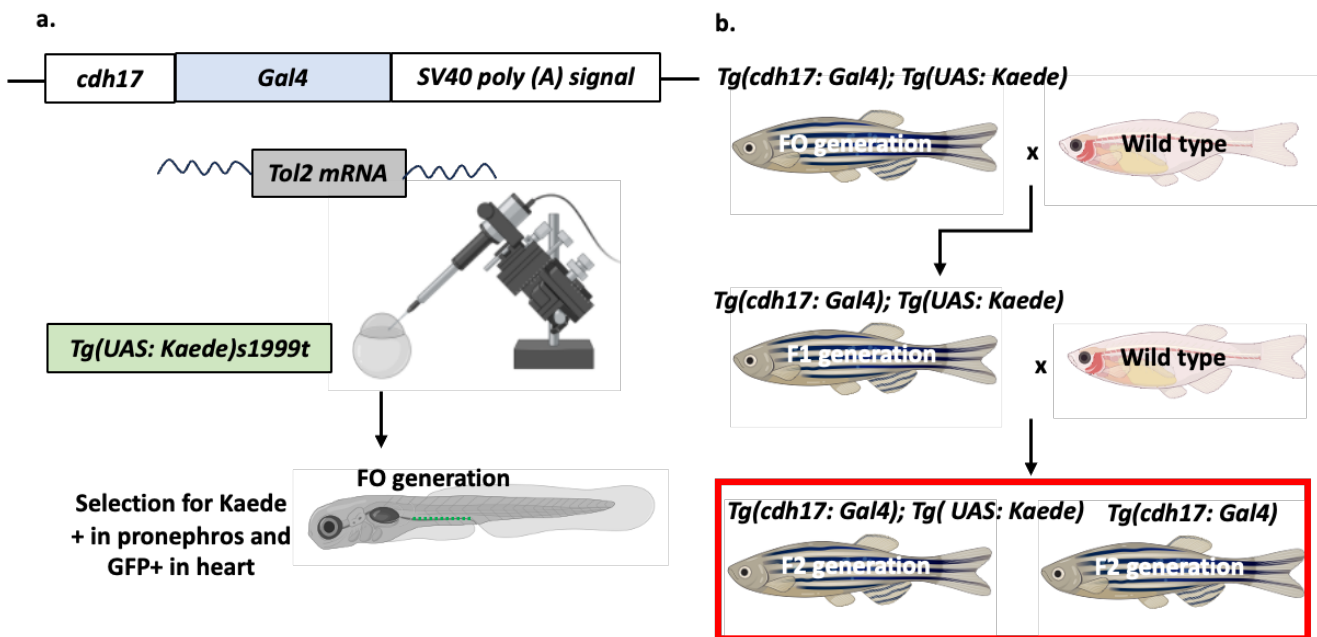


**Figure 65. Generation of *Tg(cdh17: Gal4)sh681; Tg(UAS: Kaede)s1999t* and *Tg(cdh17: Gal4)shs681* Stable Transgenic Zebrafish Lines.**

(a) Schematic demonstrating creation of the F0 generation: Single cell injection of pDestTol2CG2-*cdh17: Gal4* plasmid with *tol2* transposase mRNA into *Tg(UAS: Kaede)s1999t* zebrafish and screening for Kaede expression in pronephros and GFP expression in heart. (b) Subsequent outcrosses of F0 generation to wild type zebrafish to generate stable F1 generation and outcross of stable F1 generation to wild type to generate stable F2 generation for *Tg(cdh17: Gal4)sh681;Tg(UAS: Kaede)s1999t* and *Tg(cdh17:Gal4) sh681* zebrafish lines.

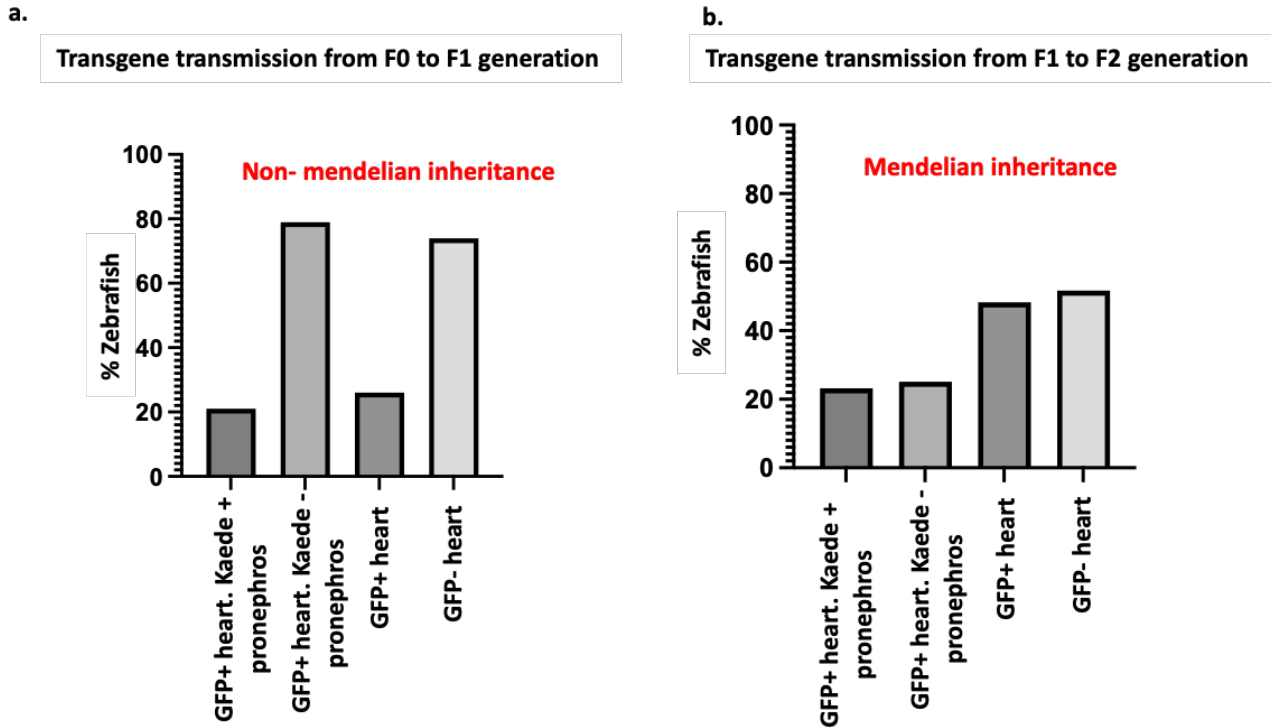


**Figure 66. Identification of Founder with Single Transgene Insertion in Newly Generated *Tg(cdh17: Gal4)sh681*; *Tg(UAS: Kaede)s1999t* and *Tg(cdh17: Gal4)shs681* Stable Transgenic Zebrafish Lines.**

(a) Transmission of *cdh17: Gal4* and *UAS: Kaede* transgenes from F0 to F1 generation. (b) Transmission of *cdh17: Gal4* and *UAS: Kaede* transgenes from F1 to F2 generation.

### **6.3.3. Characterisation of Kaede Expression Pattern in *Tg(cdh17: Gal4)sh681; Tg(UAS: Kaede)s1999t* From Larval To Adult Stages**

During the larval stages (4 days post fertilisation) of this zebrafish line, Kaede was expressed throughout the zebrafish pronephros (Tubules and ducts). There was no expression elsewhere visualised. At high magnification, the lumen of the pronephric duct was visualised and the cellular expression pattern was nuclear and membranous as expected. There was also a small amount of expression visualised in the gut. At 2 weeks, the expression pattern was similar (Figure 67).

By 3 weeks, mesonephrogenesis had started and the expression was seen throughout the mesonephros down to the urethra. However, the expression was significantly weaker in the most distal urinary tract (Figure 67).

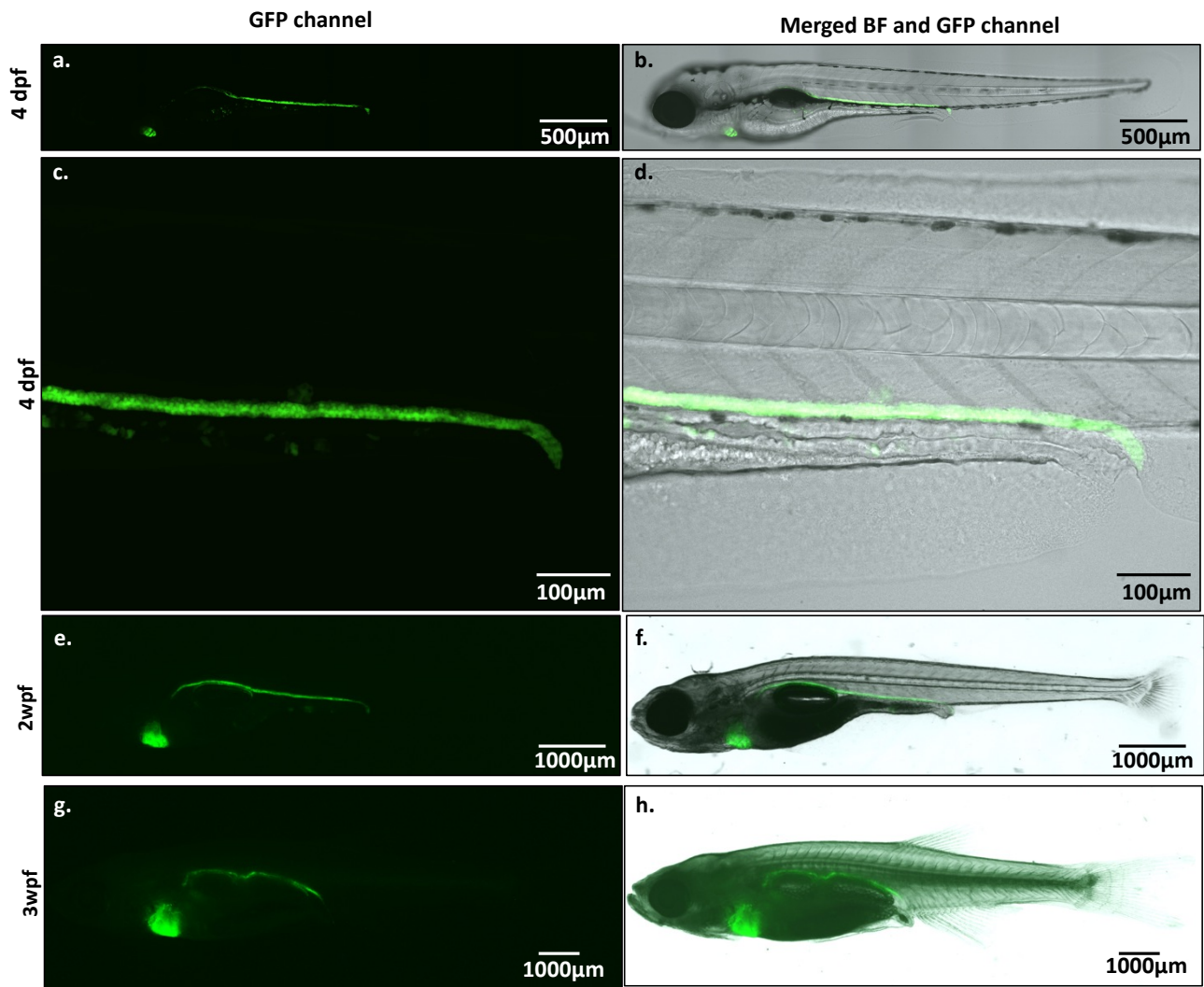


**Figure 67. Fluorescence Microscopy of Stable *Tg(cdh17: Gal4)sh681; UAS: Kaede)s1999t* Transgenic Zebrafish Larvae at 4 days, 2 Weeks and 3 Weeks Post Fertilisation.**

(a-d) 4dpf, (e-f) 2 wpf and (g-h) 3wpf. Kaede expression is seen in the pronephros and subsequently the mesonephros. GFP expression also seen in the heart (*cm1c*:GFP sequence in pDestTol2CG2-*cdh17:Gal4* construct). Fluorescent microscopy images above performed in GFP channel using Leica M205 FA fluorescent stereomicroscope.

By 6 weeks, in dissected zebrafish, Kaede expression was evident throughout the kidney, in the mesonephric tubules, ducts and ureters along the dorsal abdominal wall of the zebrafish. However, expression was not seen in the urinary bladder (Figure 68). At 3 months, no significant expression was seen in the urinary tract (data not shown).

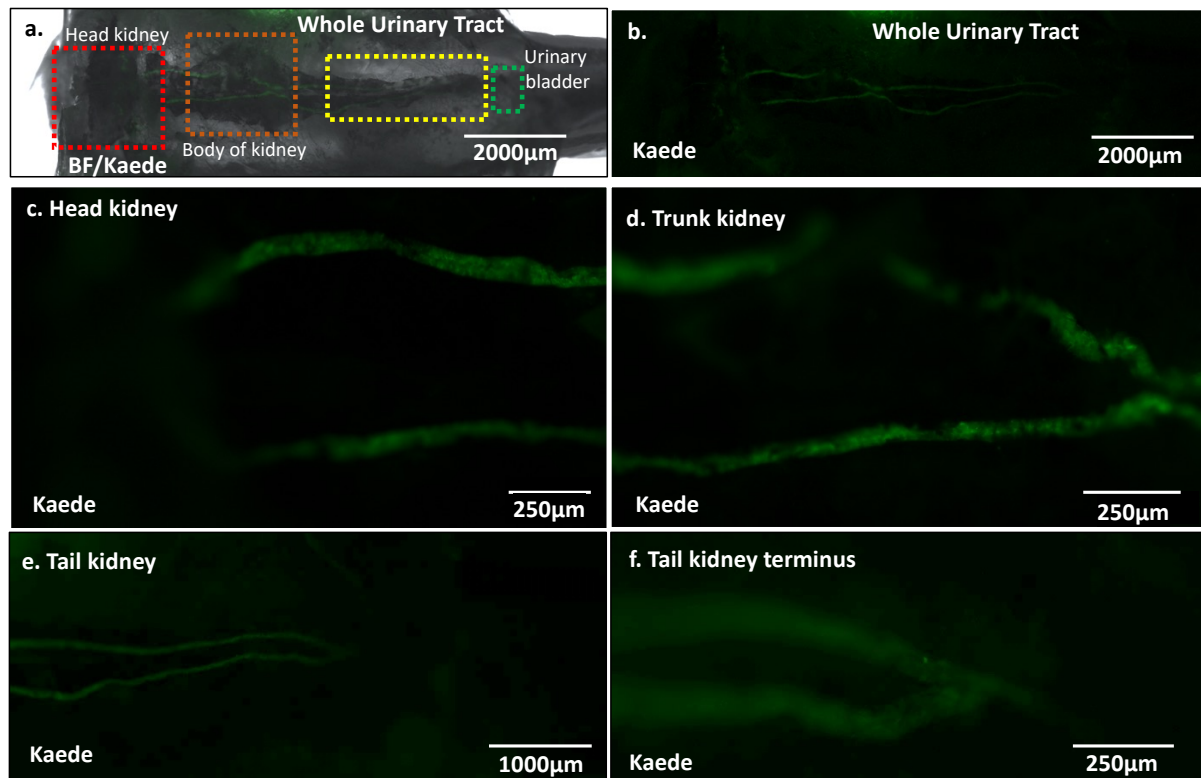


**Figure 68. Fluorescence Microscopy of Stable *Tg(cdh17: Gal4)sh681; UAS: Kaede)s1999t* Transgenic Zebrafish Line at 6-Weeks Post Fertilisation.**

Imaged zebrafish have been dissected open (Ventral abdominal wall incised and gut, gonads and swim bladder removed exposing urinary tract). Ventral abdominal wall facing up. Imaging shows urinary tract on the inside of the dorsal abdominal wall. (a-b) GFP expression is seen in throughout urinary tract, (c) in head kidney, (d) in trunk kidney, (e) in tail kidney and (f) in tail kidney terminus/ureters. Fluorescent microscopy images above performed in GFP channel using Leica M205 FA fluorescent stereomicroscope.

#### 6.3.4. Generation of Plasmids to Drive GFP-HRAS-G12V Expression Under Control of the *cdh17* promoter.

Having characterised the spatial reporter gene expression in the *Tg(cdh17: Gal4)sh681; UAS: Kaede)s1999t* zebrafish line, it was decided to generate plasmids to express oncogenes under the control of the *cdh17* promoter. Although *cdh17* expression was not present in juvenile urinary bladder region, it was expressed in the most distal urinary tract of larvae which is the site of the precursor to the urinary bladder. Furthermore, *cdh17* expression was present in the mesonephric ducts which are structurally homologous to ureters. Therefore, it was determined that this promoter would still be suitable for a urothelial cancer model.

Having previously shown (in Chapter 5. ) that the *HRAS\_G12V* transgene can successfully generate tumours in the zebrafish, it was decided to make the following plasmids (compatible with tol2 mediated transgenesis) using previously described gateway cloning LR recombination reactions:

- pDestTol2CG2-*cdh17*: GFP-HRAS\_G12V
- pDestTol2CG2-*cdh17*:GFP-CAAX).

Briefly, this is a technique whereby three component plasmids are brought together in a recombination reaction with LR clonase II plus enzyme to produce expression vectors: a p5E plasmid, a pME plasmid and a p3E plasmid. The component plasmids I used were as follows:

1. p5E-*cdh17* promoter
2. pME-GFP-HRAS\_G12V or pME-GFP-CAAX
3. p3E-polyadenylation tail

The final plasmid maps were electronically constructed using SnapGene® software (from Dotmatics available at [snapgene.com](http://snapgene.com)). Diagnostic digests were used to confirm correct recombination of the plasmids purified from the colonies picked (Figure 69). The final plasmid sequences were subsequently confirmed using whole plasmid sequencing (Plasmidsaurus, Oregon USA).

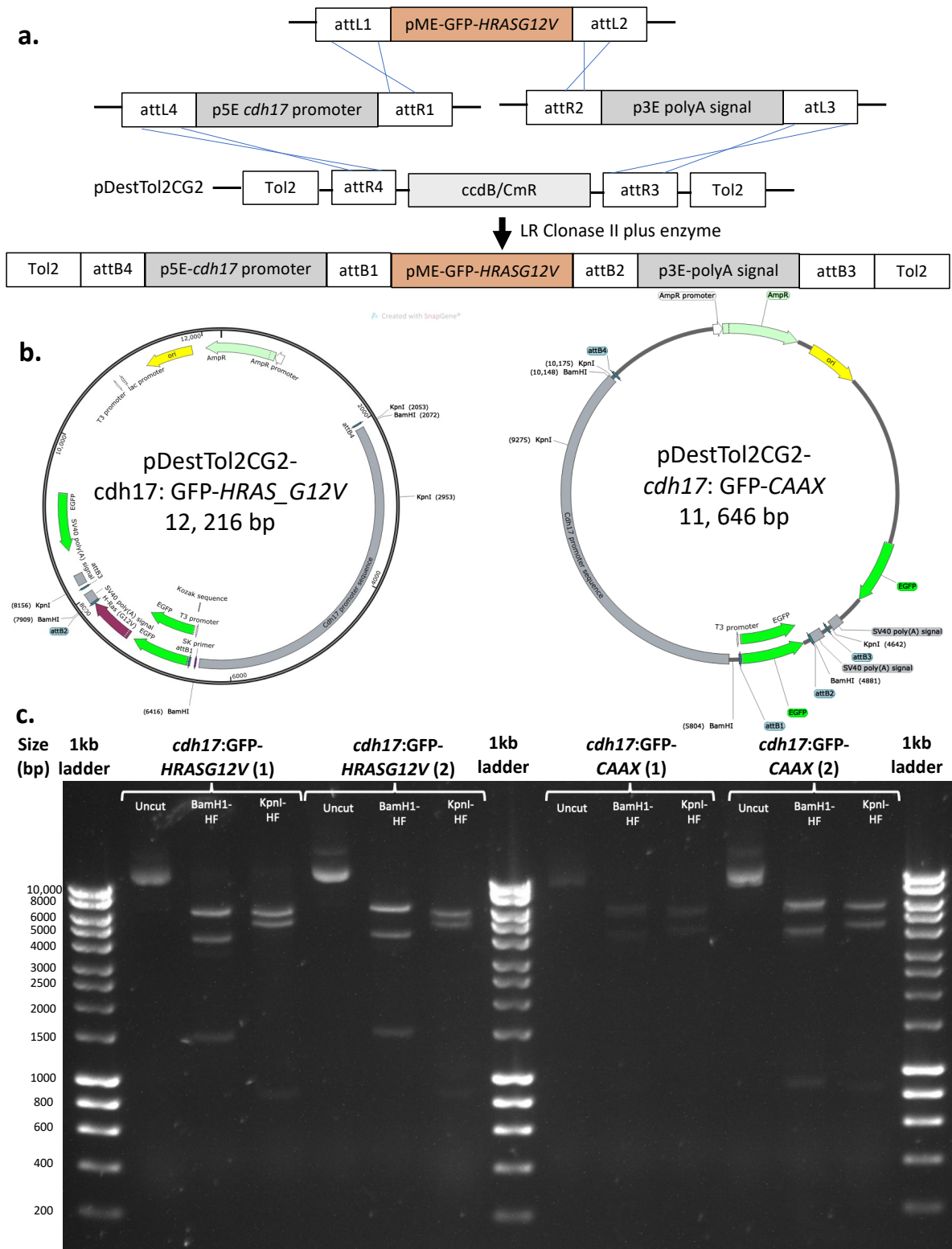


**Figure 69. Generating pDestTol2CG2-*cdh17*: GFP-HRAS\_G12V and pDestTol2CG2-*cdh17*: GFP-CAAX expression vectors.**

(a) Schematic of Gateway LR reaction used to generate final expression vectors. (b) Plasmid maps for final expression vectors. (c) Diagnostic digest and gel electrophoresis to confirm correct recombination for expression vectors generated using LR reactions. Results shown for plasmids purified from 2 separate colonies grown on LB agar plates for each plasmid: (1) and (2).

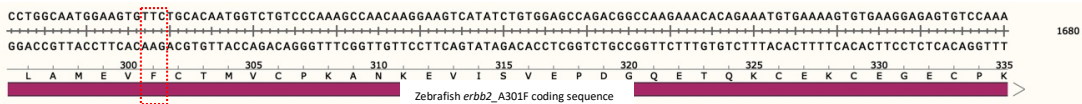
### 6.3.5. Generation of plasmids to drive oncogenic *erb2* and *pik3ca* expression under control of the zebrafish *cdh17* promoter.

Following an *in silico* search of the COSMIC catalogue(380) and TCGA bladder cancer mutation data(118), two other genes were selected as oncogenes to drive carcinogenesis in the urinary tract: *erb2* and *pik3ca*. For these, the most common mutations in human urothelial BC were identified from the COSMIC catalogue as: ERBB2 S310F and PIK3CA E545K. These are missense substitutions causing constitutive activation in humans.

Zebrafish and human amino acid sequences were aligned for ERBB2 and PIK3CA proteins and there was significant homology for both. This also enabled the identification of the corresponding amino acid to be mutated in the zebrafish protein based on the amino acid alignments. Amino acid number 310 (Serine) in the human ERBB2 protein corresponded to amino acid 301 (Alanine) in zebrafish. Amino acid 545 (Glutamic acid) in the human PIK3CA protein also corresponded to amino acid 545 (Glutamic acid) in the zebrafish PIK3CA protein. The substitutions were performed in the sequences in SnapGene software® (from Dotmatics; available at [snapgene.com](http://snapgene.com)) (A->F for ERBB2 and E->K for PIK3CA). The stop codon was subsequently removed, a Kozak sequence(392) was added in front of the start of the ATG open reading frame and the GFP sequence to create a C-terminal fusion (Figure 70). The sequence was then synthesised within a pDonor 221 plasmid to create a middle entry construct compatible with gateway cloning technology (Thermofisher GeneArt™). This plasmid was transformed, grown in LB broth and purified. LR reactions were subsequently performed using the pDestTol2CG2 backbone to create the following plasmids: pDestTol2CG2-*cdh17: erb2\_A301F*-GFP and pDestTol2CG2-*cdh17: pik3ca\_E545K*-GFP (Figure 71).

A

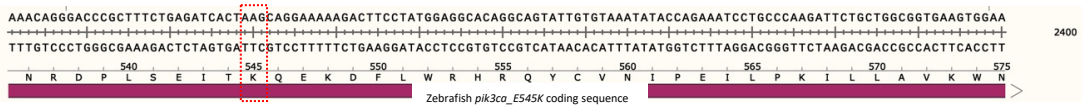
Zebrafish	196	CWGEKQDQCQLTSVNCSSGCSRCKGPKPSDCCHVQCAAGCTGPKDSDCLACRHFNDSGT	255
Human	204	CWGE +DCQ+LT C+ GC+RCKGP P+DCCH QCAAGCTGPK SDCLAC HFN SG	263
Zebrafish	256	CKDSCPPPTIYDPITFQSKPNKDKKFSFGATCVKQCPHNYLAMEV- <b>ACTM</b> VCPKANKEVI	314
Human	264	CELHCPALVTYNTDTTFESMPNPEGRYTFGASCVTACPYNYLSTDV <b>GSCT</b> LVCPLHNQEV	323
Zebrafish	315	SVEPDGQETQKCEKCEGECPKVCYGLGMGNLQGVSVVNSTNIGMFTGCEKIYGLAFLSD	374
Human	324	+ DG TQ+CEKC C +VCYGLGM +L+ V V S NI F GC+KI+GSLAFL +	379
		A--EDG--TQRCEKCSKPCARVCYGLGMEHLREVRVTSANIQEFAGCKKIFGSLAFLPE	



Site of new zebrafish *erb2\_A301F* mutation (homologous to human *ERBB2\_S310F* mutation)

B.

Zebrafish	481	SSPVKFPDMATIEDHANWIIISREMGYNYCQSGQSSRVARDHAMTEADIEQLRQLGNRDPL	540
Human	481	SSVKFPDM+ IE+HANW +SRE G++Y +G S+R+ARD+ + E D EQL+ + RDPL	540
Zebrafish	541	SEITE <b>DEKDFL</b> WRHROYCVNIPEILPKILLAVKWNRSRDEVAQMYCLLDWPAIKPEQAME	600
Human	541	SEITEDEKDFL+ HR YCV IPEILPK+LL+VKWNSRDEVAQMYCL+KDWP IKPEQAME	600
Zebrafish	601	LLDCNYPDPMIRDFAVRCLEKYLTDKLSQYLIQLVQVLKYEQYLDNPLVRFLLKKALTN	660
Human	601	LLDCNYPDPM+R FAVRCLEKYLTDKLSQYLIQLVQVLKYEQYLDN LVRFLKKALTN	660



Site of new zebrafish *pik3ca\_E545K* mutation (homologous to human *PIK3CA\_E545K* mutation)

C. Designing middle entry gateway cloning plasmid for C-terminal fusion protein with GFP in zebrafish

L1 att site	Extra 2 bases to keep in frame	Kozak sequence (GCCGCC)	CDS of oncogene (ATG.....)	Remove stop codon	Extra base to keep in frame	L2 att site
-------------	--------------------------------	-------------------------	----------------------------	-------------------	-----------------------------	-------------

**Figure 70. Designing Zebrafish Middle Entry Plasmids Containing *erb2* and *pik3ca* Coding Sequences With Mutations Associated With Urothelial Bladder Cancer.**

Common mutations associated with human bladder cancer include: *PIK3CA\_E545K* and *ERBB2\_S310F*. Firstly, coding nucleotide sequences were retrieved from Ensembl and input into SnapGene® software (from Dotmatics; available at [snappgene.com](http://snappgene.com)). Amino acid alignments of human and zebrafish proteins were generated using the online National Center for Biotechnology Information (NCBI) BLAST tool(233) and amino acid substitutions were performed in correctly aligned positions. (a) Human *ERBB2* amino acid 310 (Ser or S) corresponds to zebrafish *Erb2* amino acid 301 (Ala or A) (Red dotted square). (b) Human *PIK3CA* amino acid 545 (Glu or E) corresponds to zebrafish *Pik3ca* amino acid 545 (Glu or E) (Red dotted square). (c) DNA components required to make middle entry gateway cloning plasmid compatible with C-terminal fusion to GFP in zebrafish.



### **6.3.6. Testing Newly Generated Plasmids Designed to Drive Oncogenic *HRAS*, *erbb2* and *pik3ca* Under the Control of the Zebrafish *cdh17* Promoter**

All plasmids were injected into one cell stage wild type zebrafish embryos and the offspring evaluated for GFP expression in the pronephros (to confirm plasmids integration into the genome and that the plasmids express GFP). Fluorescence microscopy was performed on day 3 post-fertilisation. Of these plasmids, pDestTol2CG2-*cdh17*: GFP-*HRAS\_G12V* and pDestTol2CG2-*cdh17*: GFP-*CAAX* resulted in GFP positive heart marker expression and pronephros expression (Figure 72). The GFP expression for pDestTol2CG2-*cdh17*: GFP-*HRAS\_G12V* was considerably weaker than pDestTol2CG2-*cdh17*: GFP-*CAAX* but it was present (Figure 72).

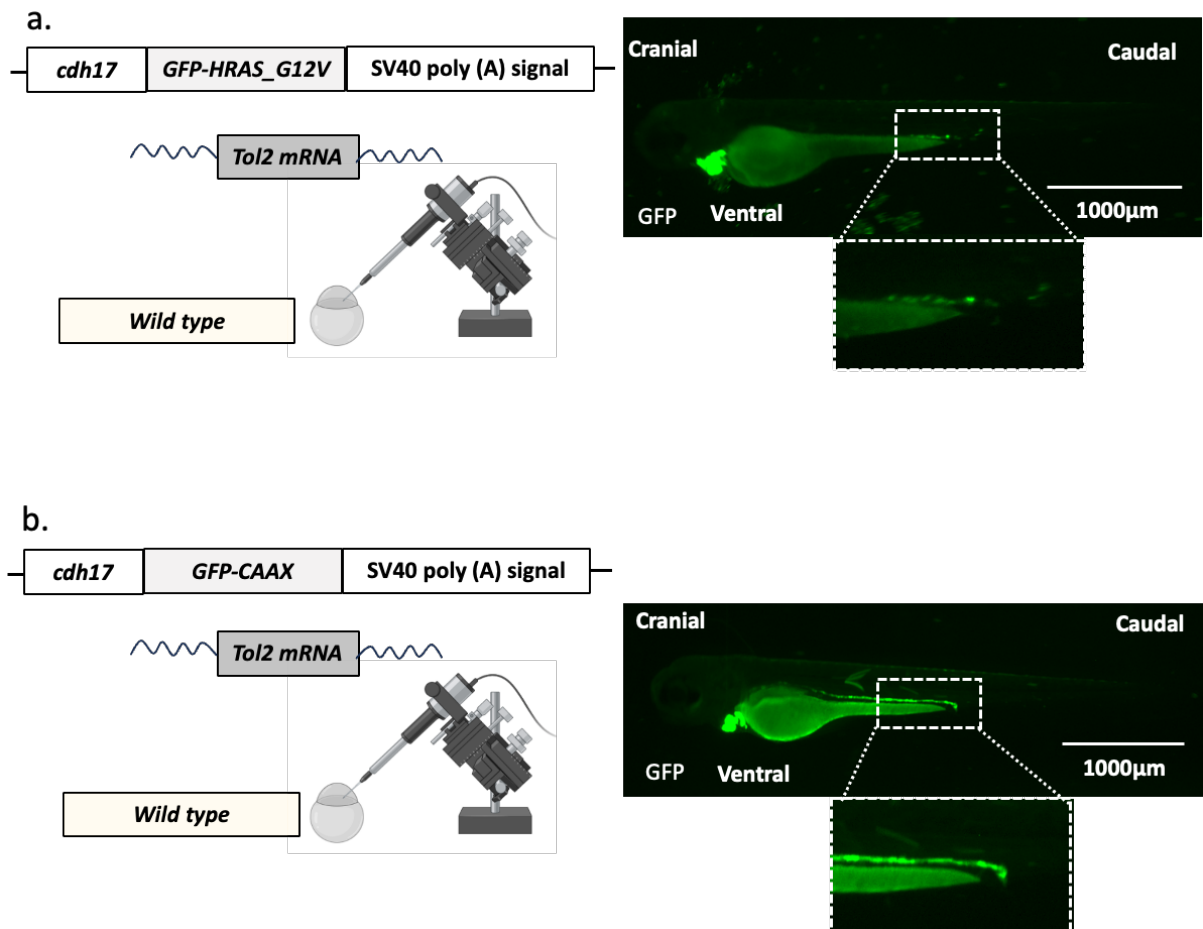


**Figure 72. One Cell Stage Zebrafish Microinjection of Newly Constructed *cdh17: GFP-HRAS\_G12V* and *cdh17: GFP-CAAX* Expression Vectors and Subsequent Fluorescence Microscopy.**

Schematic of technique (left column) and fluorescent microscopy (GFP channel, right column) shown for (a) pDestTol2CG2-*cdh17: GFP-HRAS\_G12V* and (b) pDestTol2CG2-*cdh17: GFP-CAAX*. GFP positive heart (*cm1c: GFP* marker in pDestTol2CG2 backbone) seen in both transgenic lines. GFP expression in pronephros for *cdh17: GFP-HRAS\_G12V* and *cdh17: GFP-CAAX* expression vectors. Fluorescent microscopy images on the right side of figure performed using Leica M205 FA fluorescent stereomicroscope.

However, although pDestTol2CG2-*cdh17: erbb2\_A301F-GFP* and pDestTol2CG2-*cdh17: pik3ca\_E545K-GFP* resulted in good GFP heart marker expression, there was no GFP expression in the pronephros (Figure 73).

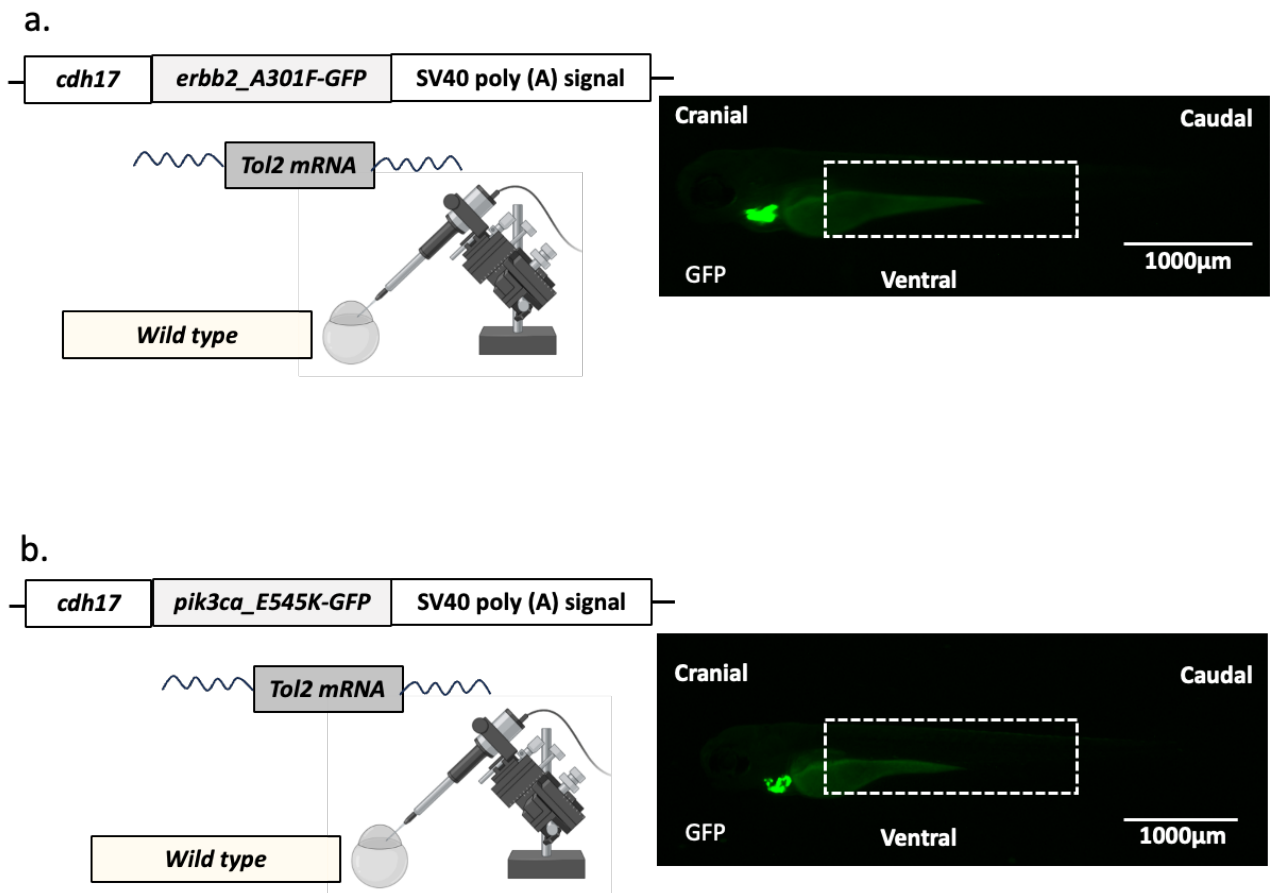


**Figure 73. One Cell Stage Zebrafish Microinjection of Newly Constructed *cdh17: erbb2\_A301F-GFP* and *cdh17: pik3ca\_E545K-GFP* Expression Vectors and Subsequent Fluorescence Microscopy**

Schematic of technique (left column) and fluorescent microscopy (GFP channel, right column) shown for (a) pDestTol2CG2-*cdh17: erbb2\_A301F-GFP* and (b) pDestTol2CG2-*cdh17: pik3ca\_E545K-GFP*. GFP positive heart (*cm1c: GFP* marker in pDestTol2CG2 backbone) seen in both transgenic lines. No GFP expression seen in pronephros for *cdh17: erbb2\_A301F-GFP* and *cdh17: pik3ca\_E545K-GFP* expression vectors. Fluorescent microscopy images on the right side of figure performed using Leica M205 FA fluorescent stereomicroscope.

### 6.3.7. Design of urinary tract cancer model utilising *cdh17* promoter/driver

The two newly generated plasmids that I had demonstrated to be functioning (pDestTol2CG2-*cdh17*: GFP-*HRAS\_G12V* and pDestTol2CG2-*cdh17*: GFP-*CAAX*) were injected at the one cell stage into an in-cross of *tp53<sup>zdf1/zdf1</sup>*, *Et(gSAIzGFFD)875b* zebrafish. The reason for using zebrafish homozygous for the *zdf1 tp53* mutation that also had the *Et(gSAIzGFFD)875b* enhancer trap transgene in its genetic background was that this line was maintained from the zebrafish urinary tract cancer model from Chapter 5. of this thesis. I determined that the '*Et(gSAIzGFFD)875b*' transgene in the background would be unlikely to have any unwanted effects on this experiment and the background would be present both in test and control groups. Furthermore, the *GFF* transgene would not affect the expression of the *HRAS\_G12V* because I was not using plasmids with a UAS sequence.

The F0 generation were screened at days 3-5pf for mosaic expression in the pronephros. The mosaic expression was throughout the pronephros. F0 generation zebrafish with the strongest expression patterns were raised (Figure 74).

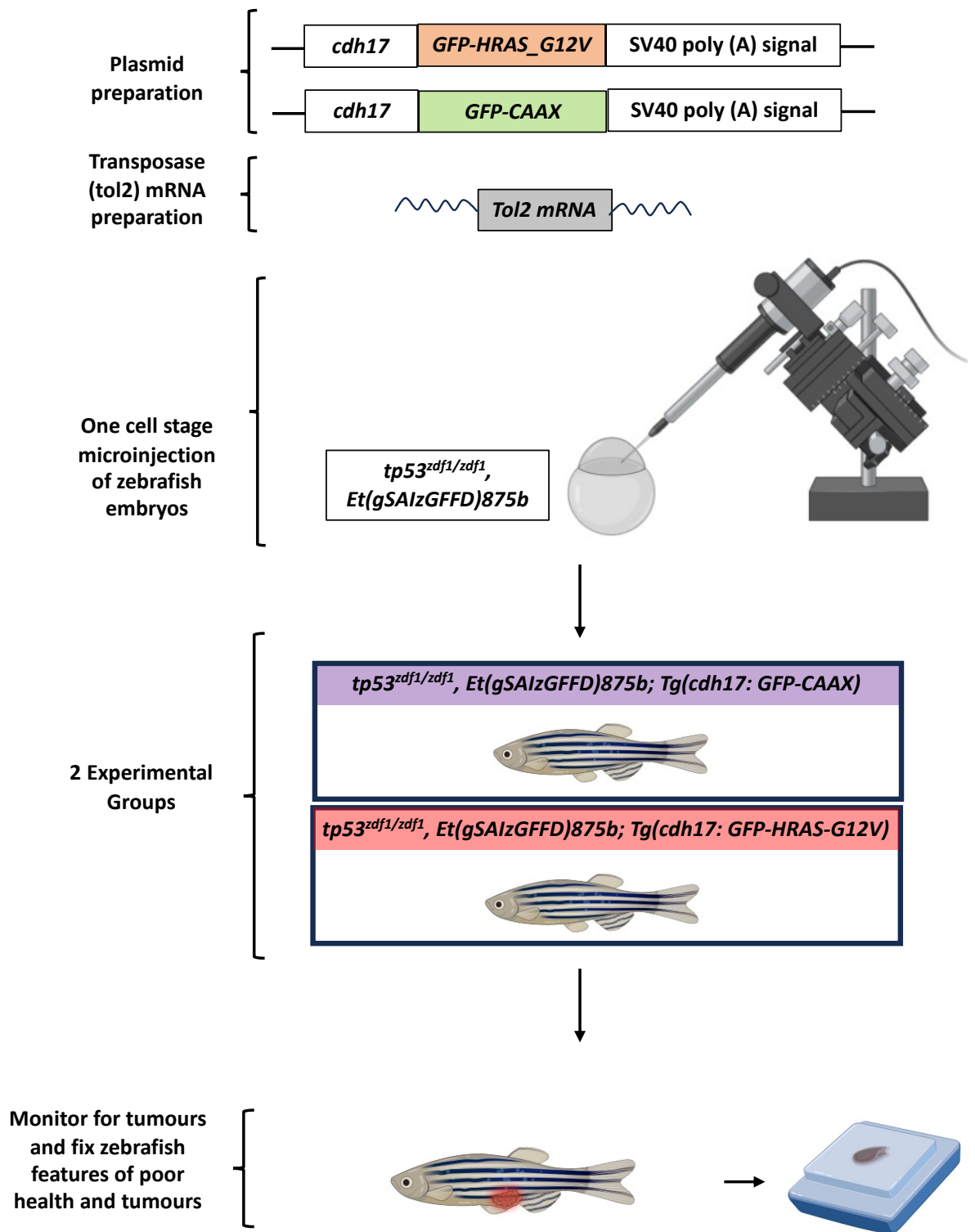
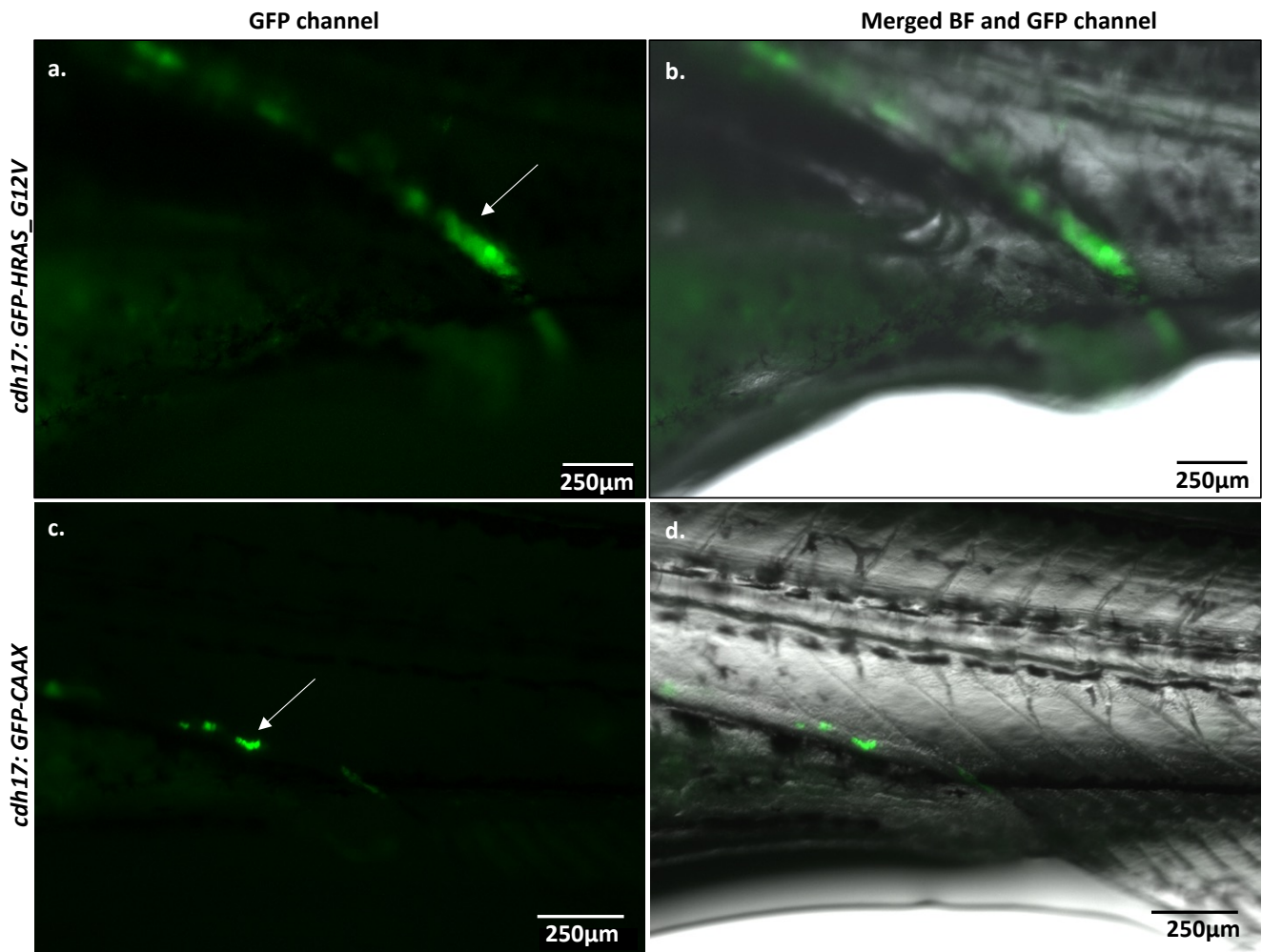


Figure 74. Schematic of New Zebrafish Urinary Tract Cancer Model Utilising Zebrafish *cdh17* Gene Promoter.

### 6.3.8. Mosaic expression of GFP-HRAS\_G12V and GFP-CAAX in the Distal Mesonephros Under the Control of the Zebrafish *cdh17* Promoter at 3 Weeks Post Fertilisation

To confirm ongoing mosaic expression during the juvenile stages, F0 zebrafish at 3 weeks old were imaged under anaesthetic (and subsequently culled) and reporter gene expression was evidence throughout the mesonephros (Figure 75).



**Figure 75. Mosaic Expression of GFP-HRAS\_G12V and GFP-CAAX in Distal Mesonephros Under the Control of the *cdh17* Gene Promoter.**

All zebrafish are homozygous for *tp53<sup>zdf1/zdf1</sup>* mutation. Zebrafish shown are 3 weeks post-fertilisation. GFP expression seen in distal mesonephros (White arrow). Fluorescent microscopy above performed using Leica M205 FA fluorescent stereomicroscope.

### 6.3.9. Identification of Zebrafish Abnormalities in New Urinary Tract Cancer Model

Zebrafish were monitored daily for the development of macroscopic tumours or any abnormal phenotype or signs of distress. Abnormal phenotypes that were identified included: abdominal swelling, cardiac oedema, swimming difficulties, general poor condition (Figure 76).

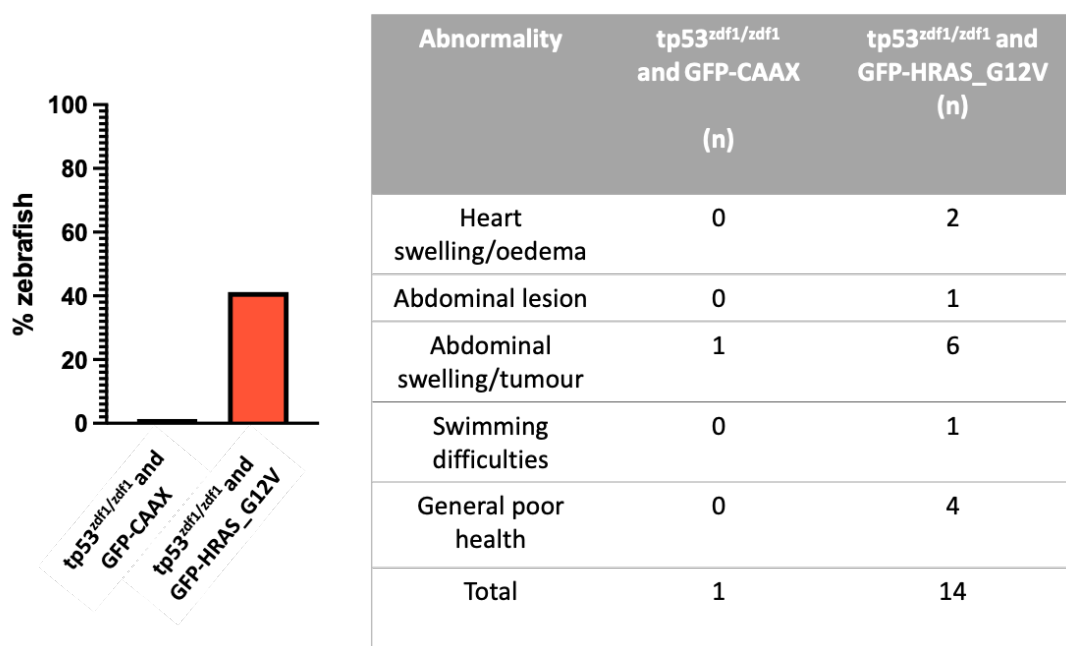


**Figure 76. Macroscopic Phenotypes in *tp53<sup>zdf1/zdf1</sup>*, *Tg(cdh17: GFP-HRAS\_G12V)* and *tp53<sup>zdf1/zdf1</sup>*, *Tg(cdh17: GFP-CAAX)* Zebrafish Between 2 Weeks and 3 Months.**

15 zebrafish in total were culled due to abnormalities. 42.4% (14/33) *tp53<sup>zdf1/zdf1</sup>* and GFP-*HRAS\_G12V* zebrafish and 1.5% (1/68) *tp53<sup>zdf1/zdf1</sup>* and GFP-CAAX zebrafish were culled due to abnormalities between 2 weeks and 3 months.

### 6.3.10. Histological Analysis of Zebrafish With Macroscopic Abnormalities in Cancer Model Utilising *cdh17* Promoter

All zebrafish with macroscopic abnormalities were processed histologically. Wax embedded specimens were sectioned so that the urinary tract was visible. These sections were stained for H&E and were analysed with a histopathologist to look for the presence of any cancers. Areas of the zebrafish that were analysed included the components of the zebrafish kidney (head kidney, trunk, tail and urinary bladder [if present in the section]) and gastrointestinal tract. No cancers were visualised in any of the 15 zebrafish that were culled due to visual abnormalities. Representative H&E stained histological slides are shown below of *tp53<sup>zdf1/zdf1</sup>, Tg(cdh17: GFP- HRAS\_G12V)* zebrafish that were culled due to heart swelling at 4 weeks old (Figure 77), heart swelling at 6 weeks old (Figure 78), abdominal swelling at 6 weeks old (Figure 79) and abdominal swelling at 2 months old (Figure 80).

In zebrafish that were culled due to heart swelling there were no overt histological abnormalities in the abdominal organs analysed (Figures 77 and 78). In zebrafish that were culled due to abdominal swelling, histological analysis either revealed distended bowels (Figures 79 and 80) or a large number of eggs (Figure 80), but no evidence of cancers.

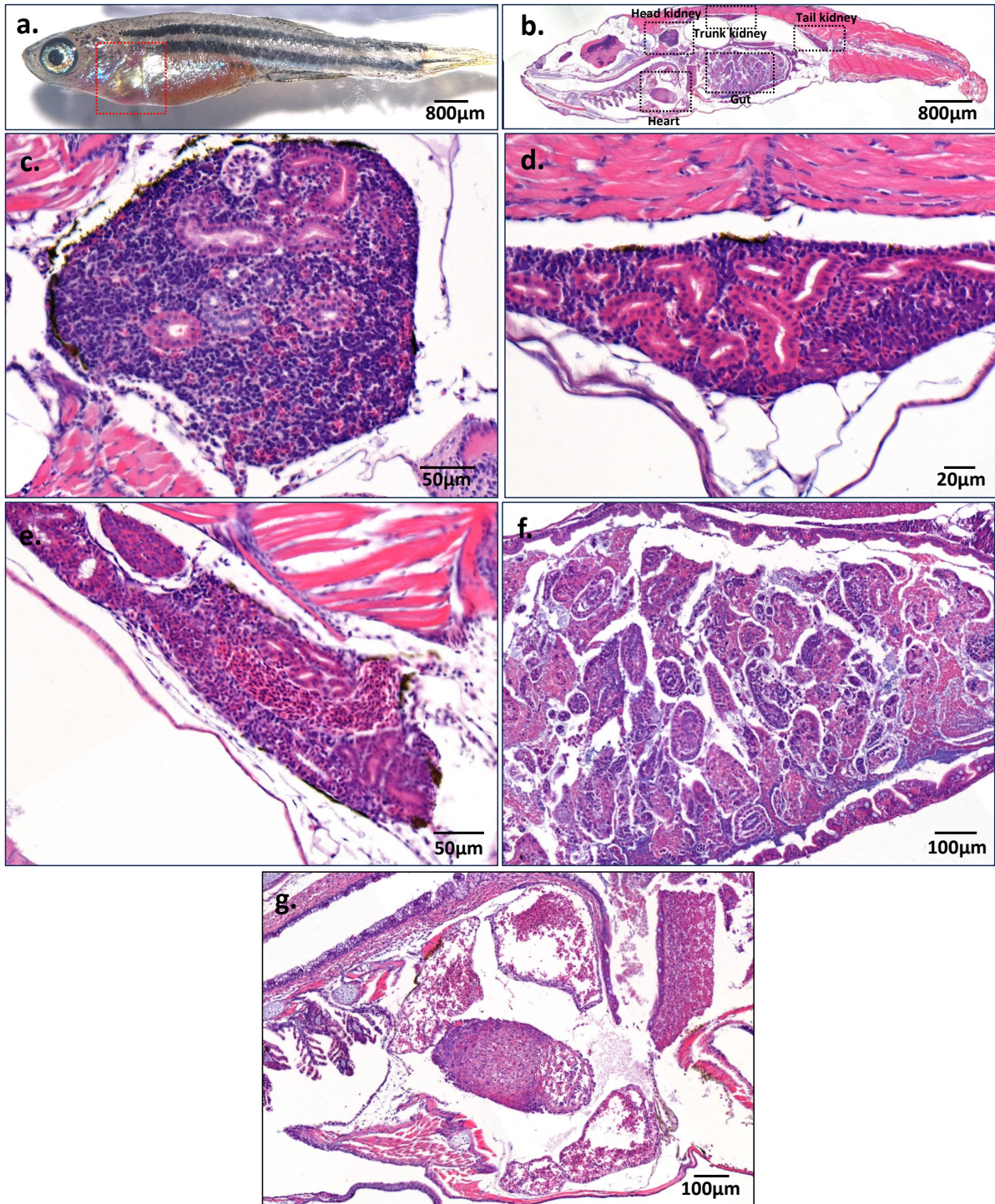


**Figure 77. H&E-Stained Sections of Approximately 4-Week Post Fertilisation  $tp53^{zdf1/zdf1}$ ,  $Tg(cdh17: GFP- HRAS\_G12V)$  Zebrafish Culled Due To Heart Swelling.**

(a) Whole zebrafish photograph shown for comparison (heart swelling in red dotted square). No evidence of cancer seen in (b) whole zebrafish, (c) Head kidney, (d) trunk kidney, (e) tail kidney and distal urinary tract or (f) gut. (g) Section of swollen heart shown.

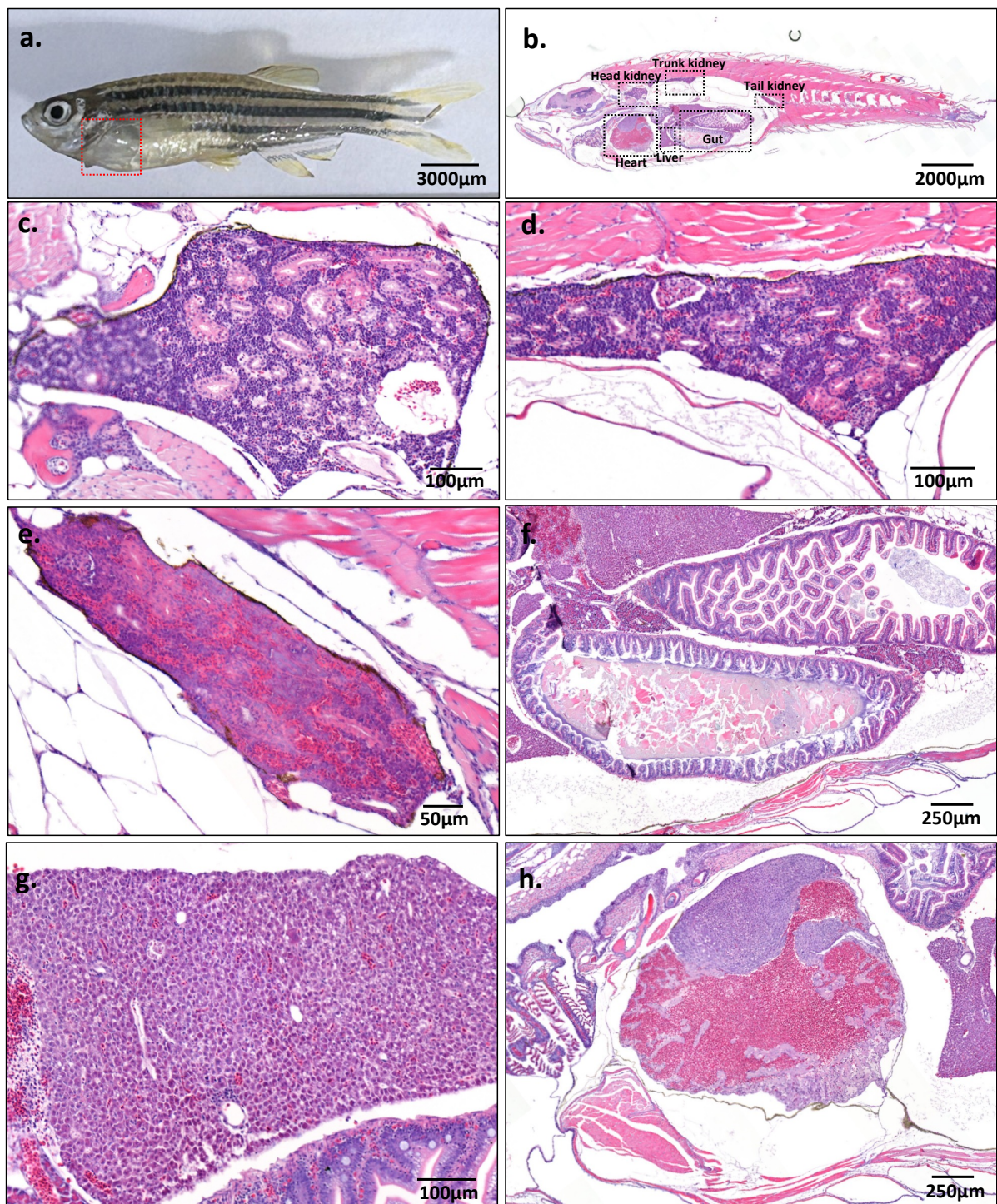


**Figure 78. H&E-Stained Sections of Approximately 6-Week Post Fertilisation *tp53<sup>zdf1/zdf1</sup>*, *Tg(cdh17: GFP- HRAS\_G12V)* Zebrafish Culled Due To Heart Swelling.**

(a) Whole zebrafish photograph shown for comparison (heart swelling in red dotted square). No evidence of cancer seen in (b) whole zebrafish, (c) Head kidney, (d) trunk kidney, (e) tail kidney and distal urinary tract, (f) gut or (g) liver. (h) Section of swollen heart shown.

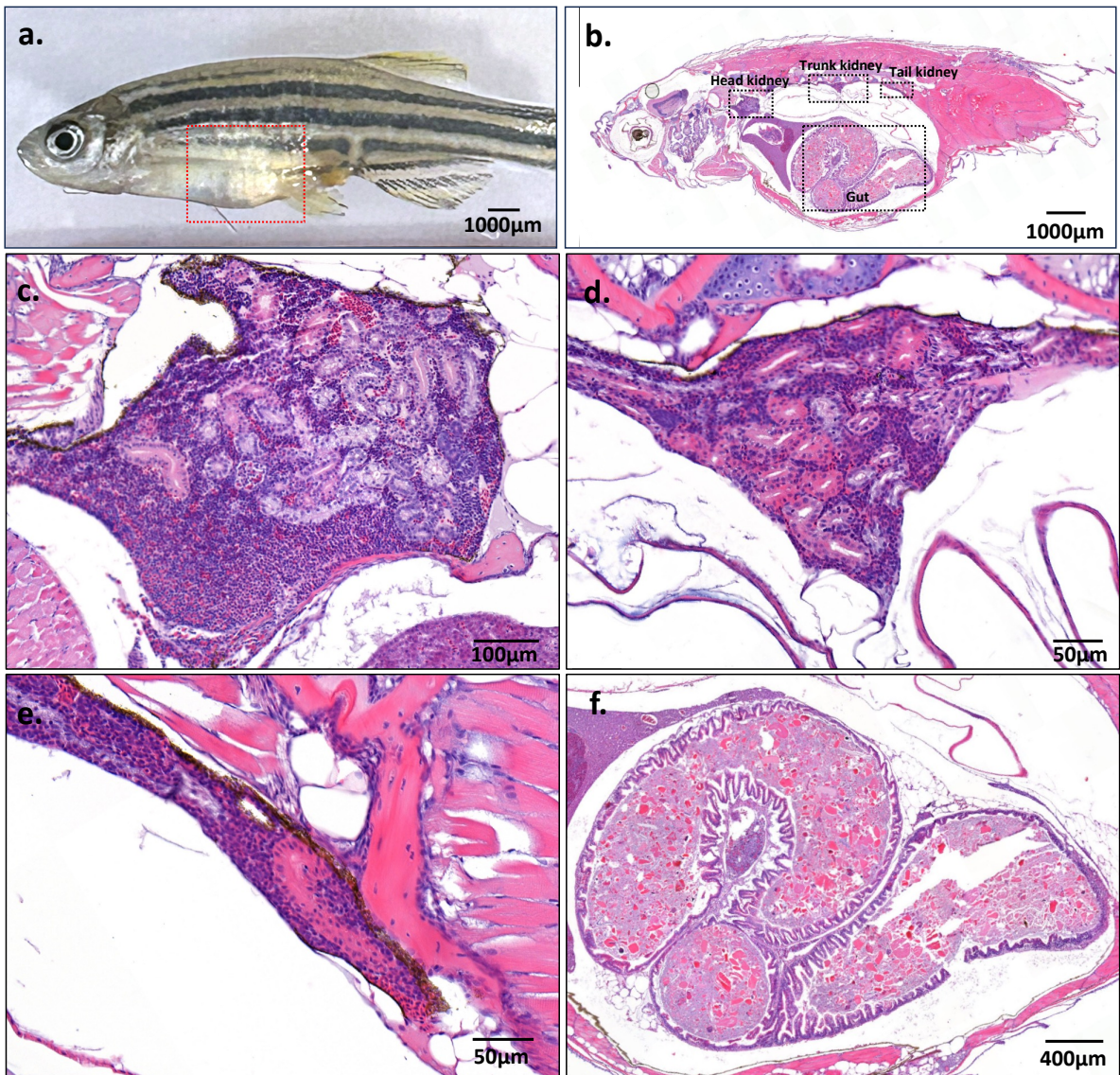


**Figure 79. H&E-Stained Sections of Approximately 6-Week Post Fertilisation  $tp53^{zdf1/zdf1}$ ,  $Tg(cdh17: GFP- HRAS\_G12V)$  Zebrafish Culled Due To Abdominal Swelling.**

(a) Whole zebrafish photograph shown for comparison (abdominal swelling in red dotted square). No evidence of cancer seen in (b) whole zebrafish, (c) Head kidney, (d) trunk kidney, (e) tail kidney or (f) Gut.

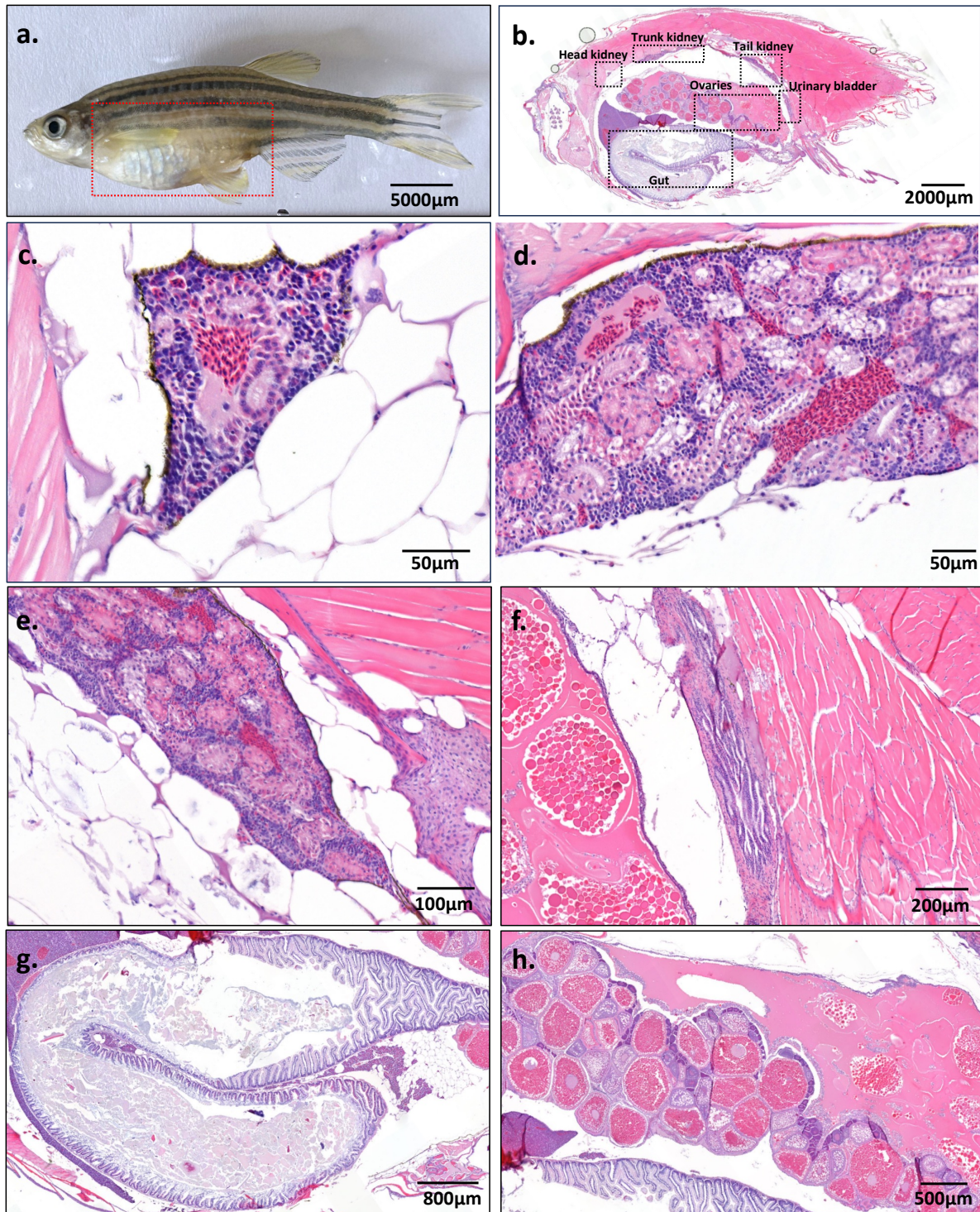


**Figure 80. H&E-Stained Sections of Approximately 2-month-old *tp53<sup>zdf1/zdf1</sup>*, *Tg(cdh17: GFP-HRAS\_G12V)* Zebrafish Culled Due To Abdominal Swelling.**

(a) Whole zebrafish photograph shown for comparison (abdominal swelling in red dotted square). No evidence of cancer seen in (b) whole zebrafish, (c) Head kidney, (d) trunk kidney, (e) tail kidney, (f) urinary bladder, (g) gut or (h) ovaries.

## 6.4. Discussion

This chapter has provided some important findings. Firstly, it provides an up-to-date characterisation of the zebrafish *cdh17* promoter expression pattern throughout the life course of the zebrafish. Secondly, this study has shown that driving *HRAS\_G12V* under the control of the zebrafish *cdh17* promoter, both with and without global *tp53* mutation does not lead to cancer up to 3 months of age in these zebrafish.

The *cdh17* promoter in our study drove reporter gene expression throughout the zebrafish pronephros during the larval stages. At 3-weeks post fertilisation, the reporter expression was throughout the urinary tract. An important finding is that between 3 weeks post fertilisation and 6 weeks post fertilisation, the reporter gene expression diminished in the most distal parts of the urinary tract. By 6 weeks post fertilisation, the reporter expression was visible in both mesonephric ducts, but not distal to the fusion of the mesonephric ducts where the urinary bladder would be located. This is the first time this has been described in the literature. A previous study using a 2.3kb *cdh17* promoter fragment previously reported gene expression throughout the urinary tract at 1 month and 6 months old i.e. down to the cloaca (391). However, this was not our experience. It is important to note that due to our previous identification and characterisation of the zebrafish urinary bladder, I was specifically interested in expression in this structure and focussed specifically on this. It is likely that previous groups didn't focus specifically on expression in the urinary bladder and so this region may have been overlooked. A similar expression pattern was seen with the *Et(gSAIzGFFD)875b; Tg(UAS: GFP)* enhancer trap zebrafish line. However, the *Tg(mpx:GFP)i114* zebrafish line demonstrated reporter gene expression in the distal pronephros/mesonephros at 3 weeks post fertilisation and this reporter gene expression persisted in the mesonephric ducts and the urinary bladder to adulthood. Further work is needed to characterise the embryology of the zebrafish distal urinary tract to determine the origin of the zebrafish mesonephric ducts and urinary bladder.

One of the potential reasons for the lack of cancers in these zebrafish by 3 months is that the method used the *cdh17* promoter without utilising the Gal4/UAS amplification system. The Gal4/UAS system has previously been reported to potentiate and amplify transgene

expression (393). It may be the case that to drive cancers in the pronephros/mesonephros, the GAL4/UAS system is required to increase the expression of oncogenes beyond the levels of an endogenous gene promoter. The cancer experiment was halted at 3 months as this study sought to determine if this zebrafish model could serve as a useful high-throughput cancer model with a fast turnaround time. It is possible that cancers could have developed after 3 months, although we saw no Kaede urinary tract expression after 3 months in the stable *Tg(cdh17: Gal4) sh681; Tg(UAS: Kaede) s1999t* transgenic line.

Whilst it was planned to evaluate the phenotype with oncogenic *erbb2* and *pik3ca* expression in the zebrafish pronephros/mesonephros, the plasmids containing C-terminal fusions between the oncogene and GFP did not result in any reporter gene expression in the pronephros. This is most likely related to the linker sequence used. The C-terminal fusion that was created between *erbb2* and *pik3ca* coding sequences and GFP was the att site which was 24 bp long which would result in a protein with 8 amino acids (Asp, Pro, Ala, Phe, Leu, Tyr, Lys, Val). It is possible that this linker sequence was not long enough and therefore the 3D tertiary structure of the Erbb2-GFP and Pik3ca-GFP fusion proteins that were translated did not fold properly. Use of *in-silico* proteomic tools that analyse the 3D tertiary protein structure based on an inputted amino acid sequence may help to predict the likelihood that the final fusion protein will fold properly. Furthermore, changing the linker sequence to a longer flexible linker or to a self-cleaving peptide such as T2A may resolve this issue in the future.

## 6.5. Conclusions

The zebrafish *cdh17* promoter can drive expression of transgenes in the pronephros and mesonephros throughout the larval and juvenile stages but not the adult urinary bladder from 6 weeks post fertilisation. Expression of *HRAS\_G12V* under the control of the zebrafish *cdh17* promoter on a background of a *tp53* DNA binding domain mutation does not lead to cancer in the examined window. In future, increased expression of *HRAS\_G12V* using, for example, the Gal4/UAS system, may drive cancer formation.

## Chapter 7. Overall Discussion and Future Work

### 7.1. Overall Discussion

Urinary tract cancers are a significant global health problem (56, 57, 367). Urothelial cancers and renal cell carcinoma are the commonest urinary tract cancers (excluding prostate cancer) and are a source of significant morbidity and mortality.

Our systematic review of BC provides a contemporary update of the epidemiology, incidence, prevalence and mortality of bladder cancer. One of the most striking findings from this systematic review is that global age standardised rates for BC incidence have not changed significantly from 1990 to 2019, but there has been a significant shift in incidence and mortality in specific world regions. For example, there have been significant increased incidences noted in East Asia, North Africa, Middle East and Central Europe. Furthermore, the greatest percentage increases in BC incidence over the next 20 years is predicted to be in Africa, Latin America, Caribbean, Asia and Oceania. This is likely to be related, in part, to the rapid industrialisation taking place in these areas. In addition to the well-established risk factors of smoking and occupational exposures, the review highlighted the evidence for opium consumption and firefighting. Furthermore, the systematic review reported new correlative evidence for specific dietary factors, gene-external risk factor interactions, pelvic radiotherapy, and diesel exhaust emission exposure. These findings are important because they can potentially inform prevention strategies to reduce cancer incidence in the future. Identification of groups at high risk of getting bladder cancer can also potentially help with targeted screening. There is ongoing work in the literature to determine the efficacy of screening high risk populations for bladder cancer (394).

Animal models are an important resource for deepening understanding of the mechanistic pathways involved in cancer initiation and progression. High-throughput *in-vivo* transgenic models for urinary tract cancers are lacking. Zebrafish models have been an attractive model for cancer due to their advantages with regards to the potential for high throughput experimental methods, ease of genetic manipulation and high-quality *in vivo* imaging at younger ages (209). Our work on the characterisation of the zebrafish urinary tract

represents the first in-depth characterisation of the excretory urinary tract in zebrafish. We demonstrated the anatomy of the zebrafish urinary collecting system including the mesonephric ducts (homologous to ureters), urinary bladder and urethra both histologically level and using fluorescent microscopy. We demonstrate the anatomy of the zebrafish kidneys along the dorsal abdominal wall with two major mesonephric ducts running either side of the midline. The two mesonephric ducts merge caudally into a single saccular shape urinary bladder which leads to the urethra situated posterior to the gut. The zebrafish urinary collecting system expresses several proteins that are also expressed in the human urinary collecting system suggesting homology. The zebrafish urinary bladder has a collagen rich lamina propria-like structure underlying the epithelium and also has a thin muscle layer mirroring the human urinary bladder wall structure. The zebrafish pelvic floor also shares similarities with its human counterpart. Following the zebrafish urinary bladder inferiorly leads to a distinct urethra that is separate from the rectum but receives drainage from the testis via an epididymis-like structure.

However, there are differences between the zebrafish and human excretory urinary tracts. In contrast to human ureters, zebrafish mesonephric ducts don't have an underlying muscle layer. Furthermore, the zebrafish urinary bladder epithelium has only one to two cell layers which is different to the multicellular urothelium. A urinary bladder has been described in other teleost fish species and has been described as a thin-walled organ (395) which matches our findings. These differences in structure between zebrafish and human are likely to be related to differing physiological demands and differing environments.

The purpose of the zebrafish urinary bladder is unclear. In humans, the human urinary bladder is a compliant waterproof reservoir that stores urine at low pressures until it is socially convenient to pass urine (5). Work from a collaborator (Dr Duncan Morhardt (366)) demonstrated intermittent filling and emptying of the zebrafish urinary bladder. It has been postulated in other fish species that intermittent micturition may confer a survival advantage in an environment where olfactory signals are important (395). However, this theory suggests an element of voluntary control over micturition. As zebrafish do not have a cerebral cortex structure, their intermittent voiding may be reflex in nature and not subject to voluntary control. Further work is needed to establish this mechanism. Another potential

function of the zebrafish urinary bladder is osmoregulation. Previous work in other freshwater teleost species (freshwater rainbow trout) has reported sodium and chloride reabsorption take place in the urinary bladder (28, 396).

Our work on developing a zebrafish model of urinary tract cancer utilised several elements: the *Et(gSAIzGFFD)875b* enhancer trap line, zebrafish *tp53* mutation, *HRASG12V* overexpression in the tissues that the GFF transgene are expressed (which include the urinary tract) in and use of the Gal4/UAS system. We demonstrated invasive cancers in the abdominal cavity. These cancers are likely to predominantly arise from the epithelial cells in the urinary tract based on the anatomical location and immunohistochemistry for AE1/AE3. However, it has proven difficult in this project to determine the specific epithelial tissues that they arise from with histological morphology analysis and immunohistochemistry alone. The enhancer trap line that was used is expressed throughout the pronephros, mesonephros and gut and zebrafish in the experiment were raised on the basis of mosaic expression in the distal pronephros as a minimum but they often had expression more proximally and in the gut. Furthermore, the reporter gene expression in the zebrafish *Et(gSAIzGFFD)875b* enhancer trap line did not continue to the adult stage nor was the reporter gene expression present in the adult saccular and expansile urinary bladder. Although it is logical that the most distal aspects of the pronephros give rise to the mesonephric ducts (homologous to ureters) and urinary bladder, and the more proximal aspects of the pronephros and mesonephros give rise to the renal tubules and ducts, this not known for sure. Despite this, this study demonstrated as a proof of principle that it is possible to induce cancers in the F0 generation through mosaic expression of *HRASG12V* under the control of an enhancer trap zebrafish line with expression in the urinary tract. Whilst various other groups have used a stable line approach to generating cancers in other models, the mosaic F0 generation model more closely recapitulates the cancer process in adults which often results from mutations in somatic cells.

The attempt at optimisation of the cancer model shown in Chapter 6. led to a number of important insights. Firstly, it involved a direct comparison of the in-vivo expression of two different zebrafish promoter fragments and a further characterisation of a 4kb *cdh17* promoter fragment during the larval, juvenile and adult stages. Whilst there is a published

characterisation of the expression pattern of a 2.3kb *cdh17* promoter during the larval and juvenile stages (391), I decided that further characterisation was required for this 4kb *cdh17* promoter fragment with an emphasis on characterising the expression pattern in the excretory elements such as the urinary bladder and urethra. This is because these structures were likely to have been previously overlooked as they were not known about. We show that driving *HRASG12V* in the distal urinary tract under the control of the *cdh17* promoter with a global *tp53* mutation in the background leads to macroscopic phenotypes including cardiac swelling and abdominal swelling due to bowel distension, but no cancers in the abdominal cavity. This suggests that there may be a physiological effect of the *HRAS\_G12V* expression in the urinary tract (combined with *tp53* DNA binding domain mutation) causing possible oedema/congestive cardiac failure/reduced gut transit. This possibility would require further experimental testing to confirm a link between the genomic alterations and the non-malignant observations. The Gal4/UAS system is likely to be important for cancer generation in these tissues in the zebrafish, as the same genomic alterations driven in similar tissues resulted in cancers when the Gal4/UAS system was used in Chapter 5.

## 7.2. Future Work

Having an in depth understanding of the embryology of the zebrafish excretory urinary tract is key for any future cancer model. One of the difficulties with a zebrafish urinary tract cancer model is expressing genes in the zebrafish larval pronephros and using their expression in the larval pronephros as a basis for where these genes will be expressed in the adults. An early assumption made in this project was that if genes are expressed in the distal pronephros early on then they will be expressed in the mesonephric ducts and urinary bladder as adults i.e. the distal pronephros is a precursor to the mesonephric ducts and adult urinary bladder. However, whilst this is true for the *TgBAC(mpx: GFP) i114* zebrafish line, this is not true for the *cdh17* reporter line or the *Et(gSAIzGFFD)875b* enhancer trap line. This could either be because when the urinary bladder becomes more expansile and saccular in nature, it stops expressing *cdh17* or the enhancer trap regulatory genes. Or it could be because the urinary bladder actually doesn't exist pre-3 weeks old and the urinary bladder develops after 3 weeks post fertilisation, either from the mesonephric duct or from the cloaca as occurs in humans. If this was the case, then the most distal segments of

zebrafish the urinary tract before 3 weeks post fertilisation would be mesonephric ducts. The urinary bladder in other teleost fish species has been described as a morphological extension of the kidney originating from the mesonephric duct and has been used as a model of renal tubular function in other fish species (29). However, there is no evidence in the literature to support this mesonephric duct origin urinary bladder in teleost fish.

It is known that in humans the urinary bladder predominantly arises from the anterior urogenital sinus (endodermal in origin) and the ureters arise from the ureteric bud that comes from the mesonephric duct (mesodermal in origin) and ascends up to fuse to the metanephric kidney (6). A key difference between the zebrafish urinary tract embryology and human counterpart is that the zebrafish have been reported not to develop a metanephros (23). Therefore, the epithelial-to-mesenchymal interactions and embryological processes that occur in the human urinary tract (the ureteric bud arises from the mesonephric duct and ascends and fuses to the metanephric tissue as well as the distal ureter and mesonephric migrating to form bladder trigone (6)) are likely to be different in zebrafish.

Potential ways in which the zebrafish distal urinary tract embryology can be explored is using a spatial transcriptomics. This could help to characterise the gene expression patterns in specific regions of the larval urinary tract in order to determine the larval urinary tract structures that give rise to the urinary bladder, mesonephric ducts and kidney. Another method to further characterise the embryological processes occurring in the zebrafish urinary tract is using fluorescent microscopy of a zebrafish reporter line that labels the zebrafish urinary bladder specifically. The *Tg(mpx: GFP) i114* urinary tract morphology experiments in this thesis provided important insights into the morphological development of the excretory urinary tract structures and supported a zebrafish urinary bladder structure that embryological arose from the distal pronephros. However, this study didn't explain whether the zebrafish urinary bladder arose and grew from the distal pronephros or if the distal pronephros is a precursor to the mesonephric ducts and urinary bladder. Having a stronger grasp of these embryological processes in the zebrafish urinary tract will be key to the optimisation of any transgenic zebrafish urinary tract cancer model to ensure that any

oncogenes of interest being expressed in zebrafish larval tissues are in fact being expressed in the desired specific adult tissues.

The experiments in this thesis to characterise the larval, juvenile and adult reporter expression patterns in the *cdh17* promoter reporter line and the *Et(gSAIzGFFD)875b* reporter line both demonstrated a similar pattern of urinary tract expression. They both demonstrated expression in the most distal most pronephros segments but then during the juvenile stages, the expression diminished in the most distal segments. Therefore, a model of adult bladder cancer will need to use a promoter or enhancer with transgene expression in the larval pronephros but continues to express specifically in the adult urinary bladder. Apart from the *Tg(mpx:GFP) i114* zebrafish line which we found to have reporter gene expression in the zebrafish urinary bladder in addition to neutrophils, there are no known reporter lines for the zebrafish urinary bladder. Transgenic mouse models of bladder cancer have previously used the mouse *uroplakin-2* gene promoter which is highly specific for the urinary bladder. The Immunohistochemistry experiments in Chapter 4. demonstrate *uroplakin-1a* and *2*- expression in the zebrafish ureters and urinary bladder suggesting this may be an effective regulatory element to use to drive genes of interest in the zebrafish adult urinary bladder. Utilising these regulatory elements from the zebrafish *uroplakin 1-a* or *uroplakin-2* genes will involve cloning up to 10kb of the nucleotide sequence upstream of the ATG translation start site into a plasmid and placing, downstream of this, the nucleotide sequence for transcriptional activator *Gal4* or *GFP* to see if a stable line can be established. A new method that is reported to bypass some of the difficulties associated with estimating the regulatory elements of a gene is CRISPR/Cas 9 mediated 'knock in' whereby a reporter or transcriptional activator sequence can be 'knocked in' just upstream of the ATG translation start site using CRISPR/Cas9 technology (397). This means that one is not constrained by the maximum nucleotide sequence size possible to place into a plasmid or inherent issues of transgenesis efficiency with BAC transgenesis.

If a *uroplakin-1a* or *uroplakin-2* reporter line does not result in expression in in the adult urinary bladder, then further work is required to identify other genes that are expressed in the zebrafish urinary bladder and ureters and to identify regulatory sequences from these. It is important that the gene chosen is as specific to the urothelium as possible for a urothelial

cancer model. One potential issue with developing a tissue specific reporter line for the zebrafish urinary epithelium to label the ureters and the urinary bladder is the *uropalakin* genes may not actually be tissue specific for the urinary epithelium in zebrafish. If this is shown to be the case, then a full transcriptomic profile of the zebrafish urinary bladder and mesonephric ducts/ureters will be needed to identify potential candidate genes that are expressed in the zebrafish urinary bladder. With this data, one can then develop reporter lines for these candidate genes and identify candidates with the best tissue specificity. I have optimised a technique (data not shown in thesis) to extract good quality RNA from 3-4 pooled freshly dissected zebrafish urinary bladders and so this technique can be used to generate RNA sequencing data for the zebrafish urinary bladder.

With regards to the cancers that I generated in Chapter 5. of this thesis, a future experiment that would help to characterise the nature of these cancers and provide definitive evidence that they were 'urothelial' in origin or 'mesonephric duct/ureter' in origin or 'renal tubule' in origin would involve evaluation of the gene expression patterns within the tumours. There are several methods to potentially extract RNA from these zebrafish tumours and perform transcriptomic profiling. Methods that can be used to perform transcriptomic profiling of the tumours include a) laser capture microdissection from FFPE tissue sections or b) laser capture microdissection of snap frozen cryosections with subsequent microarray or RNA sequencing analysis (398). An alternative approach is c) spatial transcriptomic analysis using snap-frozen and cryo-sectioned tissue (399). There are pros and cons to these methods. RNA extracted from FFPE tissue is often fragmented but it is generally good enough for microarray but not RNA sequencing. RNA extracted from snap frozen tissue is less degraded than RNA from FFPE tissue and so RNA sequencing is an option, but this method requires more skills with respect to snap freezing and cryosectioning. Spatial transcriptomic methods are excellent for performing in depth analysis of gene expression profiles in different regions of the tumour, but the use of this technology is hindered by its significant cost.

A marker of poor prognosis in bladder cancer in clinical practice is Ki-67 immunohistochemistry staining. Ki-67 is a nuclear protein expressed in the G1, S, G2 and M phases of the cell cycle but not detectable in the G0 or early G1 phase. It is thus a marker of cell proliferation (400). Zebrafish do not possess the Ki-67 protein. However, zebrafish do

possess proliferating circulating nuclear antigen (PCNA) which is another protein which can be used as a marker of proliferation. PCNA is a nuclear protein which plays a role in DNA synthesis and repair. This marker has been used successfully in zebrafish previously (401). Future work could use PCNA on the zebrafish cancers to determine their aggressiveness.

The logical next step in the optimisation of the *cdh17* cancer model is to attempt the cancer model utilising the Gal4/UAS system. The Gal4/UAS system is reported to increase transgene expression beyond the expression that can occur under the control of a native promoter (393). As *cdh17* is not expressed in the adult urinary bladder this may be a larval model of urinary bladder cancer at around 3 weeks post fertilisation or an adult model of upper tract urothelial cancer or an adult model of renal cell carcinoma. This experiment would require crossing the *tp53 zdf1* mutation into our newly generated zebrafish *Tg(cdh17: Gal4) sh681* line to generate a *tp53<sup>zdf1/zdf1</sup>, Tg(cdh17: Gal4) sh681* zebrafish line and then injecting pDestTol2CG2- *UAS:GFP-HRAS\_G12V* and pDestTol2CG2- *UAS:GFP-CAAX* plasmids into embryos from an Incross of this line. Immunohistochemistry and transcriptomic profiling will then be required to determine the specific cancer subtype that has been generated.

The cancer models in this thesis utilised two genomic alterations: the *HRAS\_G12V* transgene and *tp53* M214K mutation. One of the commonest genomic alterations in human bladder cancer is mutation in the receptor tyrosine kinase FGFR3 leading to constitutive activation (118, 120). Overexpression of zebrafish *fgfr3* in the zebrafish pronephros was attempted in the zebrafish in this project by injecting a previously published plasmid (pCM326[pDestTol2CG2,*crya*:Venus]-UAS: *fgfr3*-2AEGFP) (229) into one cell stage Et(gSAIzGFFD)875b zebrafish embryos. Although, there was evidence of the Venus fluorescent protein expression in the eye (demonstrating integration and functioning of *crya*: Venus component of the plasmid), there was no evidence of GFP expression in the pronephros (Data not shown). It was therefore determined, due to the absence of GFP expression in the pronephros, that use of this plasmid would not be suitable for use in a cancer model. One possible explanation for the absence of GFP expression in the pronephros could be related to issues related to the use of the 2A self-cleaving peptide such as incomplete cleavage (402). However, it is important that future zebrafish urinary tract

cancer models attempt to overexpress mutant *fgfr3* to recapitulate common forms of human bladder cancer. A method that could be tried in the future is to assemble a plasmid containing a mutant *fgfr3* DNA sequence fused to a reporter gene sequence with different linker sequences in between.

### **7.3. Conclusions**

Urinary tract cancers are common and are associated with significant morbidity and mortality. Large scale sequencing data sets are revealing new genomic alterations associated with these cancers. High throughput transgenic animal models of urinary tract cancers are needed to mechanistically test the roles and functions of these genomic alterations. The zebrafish excretory urinary tract shares several similarities with its human counterpart supporting its use as a model of urinary tract diseases. A transgenic zebrafish model of urinary tract cancer whereby an oncogene associated with human bladder cancer, *HRAS\_G12V*, is overexpressed in the zebrafish urinary tract both with and without a zebrafish global *tp53* DNA binding domain mutation, can lead to invasive abdominal cancers in up to 6 weeks. However, this model requires further validation. Further work is needed to characterise the zebrafish cancers generated from this model and determine their homology to human urinary tract cancers. Furthermore, further work is needed in the future to further understand the functional segmentation pattern and embryological origin of the zebrafish excretory urinary tract in order to improve expression of genes of interest to specific regions of the adult zebrafish urinary tract.

## References

1. Mullins M. Genetic methods: conventions for naming zebrafish genes In: Westerfield M, editor. *The Zebrafish Book A Guide for the Laboratory Use of Zebrafish* 3rd ed. Eugene, OR: University of Oregon Press; 1995.
2. Wood R. *Trends in Genetics: Genetic Nomenclature Guide with Information on Websites*. Cambridge, UK: Elsevier Trends Journals; 1998.
3. The Zebrafish Information Network (ZFIN). ZFIN Zebrafish Nomenclature Conventions: The Zebrafish Information Network (ZFIN); 2022 [Available from: <https://zfin.atlassian.net/wiki/spaces/prot/pages/356155900/Conventions+For+Naming+Zebrafish+Genes>].
4. Elkoushy M, Andonian S. Surgical, Radiologic, and Endoscopic Anatomy of the Kidney and Ureter. In: AW. P, editor. *Campbell-Walsh-Wein Urology*. 2. 12th ed. Philadelphia, PA, USA: Elsevier; 2021.
5. Timbrook Brown E, Wein A, Dmochowski R. Pathophysiology and Classification of Lower Urinary Tract Dysfunction. In: Partin A, Dmochowski R, Kavoussi L, Peters C, editors. *Campbell-Walsh-Wein Urology*. 3. 12th ed. Philadelphia, PA, USA: Elsevier; 2021.
6. Baskin L, Cunha G. Embryology of the Genitourinary Tract. In: Partin A, Peters C, Kavoussi L, Dmochowski R, Wein A, editors. *Campbell Walsh Wein Urology*. 1. 12th Edition ed: Elsevier Health Sciences; 2020.
7. Velagapudi C, Nilsson RP, Lee MJ, Burns HS, Ricono JM, Arar M, et al. Reciprocal induction of simple organogenesis by mouse kidney progenitor cells in three-dimensional co-culture. *The American journal of pathology*. 2012;180(2).
8. O'Rahilly R MF. *Human embryology and teratology*. 2nd ed. New York: Wiley-Liss.; 1996 1996.
9. Moore KL, Persaud TVN, Torchia MG. *The Developing Human: Clinically Oriented Embryology*. 11th ed: Elsevier Health Sciences; 2019.
10. Weiss JP. Embryogenesis of ureteral anomalies: a unifying theory. *The Australian and New Zealand journal of surgery*. 1988;58(8).
11. Batourina E, Tsai S, Lambert S, Sprenkle P, Viana R, Dutta S, et al. Apoptosis induced by vitamin A signaling is crucial for connecting the ureters to the bladder. *Nat Genet*. 2005;37(10).
12. Tanaka ST, Ishii K, Demarco RT, Pope Jc, Brock JW, 3rd, Hayward SW. Endodermal origin of bladder trigone inferred from mesenchymal-epithelial interaction. *J Urol*. 2010;183(1):386-91.
13. Moore K, Persaud T, Torchia M. *The Developing Human: Clinically Oriented Embryology*. 9th ed. Philadelphia, PA, USA: Elsevier; 2013.
14. Birder LA, de Groat WC. Mechanisms of disease: involvement of the urothelium in bladder dysfunction. *Nature clinical practice Urology*. 2007;4(1):46-54.
15. Jost SP. Cell cycle of normal bladder urothelium in developing and adult mice. *Virchows Archiv B, Cell pathology including molecular pathology*. 1989;57(1).
16. Romih R, Koprivec D, Martincic DS, Jezernik K. Restoration of the rat urothelium after cyclophosphamide treatment. *Cell biology international*. 2001;25(6).
17. Shin K, Lee J, Guo N, Kim J, Lim A, Qu L, et al. Hedgehog/Wnt feedback supports regenerative proliferation of epithelial stem cells in bladder. *Nature*. 2011;472(7341).
18. Amin M, Grignon D, Srigley J, Eble J. *Urological Pathology*. Philadelphia, PA, USA.: Wolters Kluwer; 2013.
19. *The Histology of Human Urinary Bladder: The Human Protein Atlas*; [Available from: <https://www.proteinatlas.org/learn/dictionary/normal/urinary+bladder>].

20. Volff JN. Genome evolution and biodiversity in teleost fish. *Heredity* (Edinb). 2005;94(3):280-94.
21. Kimmel CB, Ballard WW, Kimmel SR, Ullmann B, Schilling TF. Stages of embryonic development of the zebrafish. *Dev Dyn*. 1995;203(3):253-310.
22. The Zebrafish Information Network (ZFIN). Zebrafish Developmental Staging Series [cited 2024 14th June]. Available from: [https://zfin.org/zf\\_info/zfbook/stages/](https://zfin.org/zf_info/zfbook/stages/).
23. Diep CQ, Peng Z, Ukah TK, Kelly PM, Daigle RV, Davidson AJ. Development of the zebrafish mesonephros. *Genesis* 2015;53(3-4):257-69.
24. Menke AL, Spitsbergen JM, Wolterbeek AP, Woutersen RA. Normal anatomy and histology of the adult zebrafish. *Toxicol Pathol*. 2011;39(5):759-75.
25. Baranowska Körberg I, Hofmeister W, Markljung E, Cao J, Nilsson D, Ludwig M, et al. WNT3 involvement in human bladder exstrophy and cloaca development in zebrafish. *Hum Mol Genet*. 2015;24(18):5069-78.
26. Holden JA, Layfield LL, Matthews JL. Kidney The Zebrafish Atlas of Macroscopic and Microscopic Anatomy. 1 ed. USA: Cambridge University Press; 2013. p. 98-100.
27. Chen T, Song G, Yang H, Mao L, Cui Z, Huang K. Development of the Swimbladder Surfactant System and Biogenesis of Lysosome-Related Organelles Is Regulated by BLOS1 in Zebrafish. *Genetics*. 2018;208(3):1131-46.
28. Curtis J, Wood C. The Function of the Urinary Bladder In Vivo in the Freshwater Rainbow Trout. *Journal of Experimental Biology*. 1991;155(1):567-83.
29. McDonald MD, Walsh PJ, Wood CM. Transport physiology of the urinary bladder in teleosts: a suitable model for renal urea handling? *The Journal of experimental zoology*. 2002;292(7):604-17.
30. Gerlach GF, Schrader LN, Wingert RA. Dissection of the adult zebrafish kidney. *J Vis Exp*. 2011(54).
31. Drummond IA. Kidney development and disease in the zebrafish. *Journal of the American Society of Nephrology : JASN*. 2005;16(2).
32. Naylor RW, Davidson AJ. Pronephric tubule formation in zebrafish: morphogenesis and migration. *Pediatric nephrology (Berlin, Germany)*. 2017;32(2):211-6.
33. Drummond IA, Majumdar A, Hentschel H, Elger M, Solnica-Krezel L, Schier AF, et al. Early development of the zebrafish pronephros and analysis of mutations affecting pronephric function. *Development (Cambridge, England)*. 1998;125(23).
34. Pyati UJ, Cooper MS, Davidson AJ, Nechiporuk A, Kimelman D. Sustained Bmp signaling is essential for cloaca development in zebrafish. *Development (Cambridge, England)*. 2006;133(11).
35. Slanchev K, Pütz M, Schmitt A, Kramer-Zucker A, Walz G. Nephrocystin-4 is required for pronephric duct-dependent cloaca formation in zebrafish. *Hum Mol Genet*. 2011;20(16).
36. Wingert RA, Selleck R, Yu J, Song HD, Chen Z, Song A, et al. The cdx genes and retinoic acid control the positioning and segmentation of the zebrafish pronephros. *PLoS Genet*. 2007;3(10):1922-38.
37. Naylor RW, Przepiorski A, Ren Q, Yu J, Davidson AJ. HNF1 $\beta$  is essential for nephron segmentation during nephrogenesis. *Journal of the American Society of Nephrology : JASN*. 2013;24(1).
38. Wingert RA, Davidson AJ. Zebrafish nephrogenesis involves dynamic spatiotemporal expression changes in renal progenitors and essential signals from retinoic acid and irx3b. *Developmental dynamics : an official publication of the American Association of Anatomists*. 2011;240(8).

39. Diep CQ, Ma D, Deo RC, Holm TM, Naylor RW, Arora N, et al. Identification of adult nephron progenitors capable of kidney regeneration in zebrafish. *Nature*. 2011;470(7332).
40. Curtin E, Hickey G, Kamel G, Davidson AJ, Liao EC. Zebrafish *wnt9a* is expressed in pharyngeal ectoderm and is required for palate and lower jaw development. *Mechanisms of development*. 2011;128(1-2).
41. Carroll TJ, Park JS, Hayashi S, Majumdar A, McMahon AP. Wnt9b plays a central role in the regulation of mesenchymal to epithelial transitions underlying organogenesis of the mammalian urogenital system. *Developmental cell*. 2005;9(2).
42. Mitra S, Lukianov S, Ruiz WG, Cianciolo Cosentino C, Sanker S, Traub LM, et al. Requirement for a uroplakin 3a-like protein in the development of zebrafish pronephric tubule epithelial cell function, morphogenesis, and polarity. *PLoS one*. 2012;7(7):e41816.
43. Garcia-España A, Chung PJ, Zhao X, Lee A, Pellicer A, Yu J, et al. Origin of the tetraspanin uroplakins and their co-evolution with associated proteins: implications for uroplakin structure and function. *Molecular phylogenetics and evolution*. 2006;41(2).
44. Kolvenbach CM, Dworschak GC, Frese S, Japp AS, Schuster P, Wenzlitschke N, et al. Rare Variants in BNC2 Are Implicated in Autosomal-Dominant Congenital Lower Urinary-Tract Obstruction. *American journal of human genetics*. 2019;104(5).
45. Brown JS, Amend SR, Austin RH, Gatenby RA, Hammarlund EU, Pienta KJ. Updating the Definition of Cancer. *Mol Cancer Res*. 2023;21(11):1142-7.
46. Sung H, Ferlay J, Siegel RL, Laversanne M, Soerjomataram I, Jemal A, et al. Global Cancer Statistics 2020: GLOBOCAN Estimates of Incidence and Mortality Worldwide for 36 Cancers in 185 Countries. *CA Cancer J Clin*. 2021;71(3):209-49.
47. Riva L, Pandiri AR, Li YR, Droop A, Hewinson J, Quail MA, et al. The mutational signature profile of known and suspected human carcinogens in mice. *Nat Genet*. 2020;52(11):1189-97.
48. Fowler JC, Jones PH. Somatic Mutation: What Shapes the Mutational Landscape of Normal Epithelia? *Cancer Discov*. 2022;12(7):1642-55.
49. Hill W, Lim EL, Weeden CE, Lee C, Augustine M, Chen K, et al. Lung adenocarcinoma promotion by air pollutants. *Nature*. 2023;616(7955):159-67.
50. Hanahan D, Weinberg RA. The hallmarks of cancer. *Cell*. 2000;100(1).
51. Hanahan D, Weinberg RA. Hallmarks of cancer: the next generation. *Cell*. 2011;144(5).
52. Hanahan D. Hallmarks of Cancer: New Dimensions. *Cancer Discov*. 2022;12(1):31-46.
53. Wu S, Zhu W, Thompson P, Hannun YA. Evaluating intrinsic and non-intrinsic cancer risk factors. *Nat Commun*. 2018;9(1):3490.
54. Lichtenstein P, Holm NV, Verkasalo PK, Iliadou A, Kaprio J, Koskenvuo M, et al. Environmental and heritable factors in the causation of cancer--analyses of cohorts of twins from Sweden, Denmark, and Finland. *N Engl J Med*. 2000;343(2):78-85.
55. Mucci LA, Hjelmborg JB, Harris JR, Czene K, Havelick DJ, Scheike T, et al. Familial Risk and Heritability of Cancer Among Twins in Nordic Countries. *JAMA*. 2016;315(1):68-76.
56. Cumberbatch MGK, Jubber I, Black PC, Esperto F, Figueroa JD, Kamat AM, et al. Epidemiology of Bladder Cancer: A Systematic Review and Contemporary Update of Risk Factors in 2018. *Eur Urol*. 2018;74(6):784-95.
57. Bukavina L, Bensalah K, Bray F, Carlo M, Challacombe B, Karam JA, et al. Epidemiology of Renal Cell Carcinoma: 2022 Update. *Eur Urol*. 2022;82(5):529-42.

58. Soualhi A, Rammant E, George G, Russell B, Enting D, Nair R, et al. The incidence and prevalence of upper tract urothelial carcinoma: a systematic review. *BMC Urol.* 2021;21(1):110.
59. Roupert M, Babjuk M, Burger M, Capoun O, Cohen D, Comperat EM, et al. European Association of Urology Guidelines on Upper Urinary Tract Urothelial Carcinoma: 2020 Update. *Eur Urol.* 2021;79(1):62-79.
60. Hsieh JJ, Purdue MP, Signoretti S, Swanton C, Albiges L, Schmidinger M, et al. Renal cell carcinoma. *Nat Rev Dis Primers.* 2017;3:17009.
61. Mungan NA, Aben KK, Schoenberg MP, Visser O, Coebergh JW, Witjes JA, et al. Gender differences in stage-adjusted bladder cancer survival. *Urology.* 2000;55(6):876-80.
62. Greiman AK, Rosoff JS, Prasad SM. Association of Human Development Index with global bladder, kidney, prostate and testis cancer incidence and mortality. *BJU international.* 2017;120(6):799-807.
63. Cumberbatch MG, Rota M, Catto JW, La Vecchia C. The Role of Tobacco Smoke in Bladder and Kidney Carcinogenesis: A Comparison of Exposures and Meta-analysis of Incidence and Mortality Risks. *Eur Urol.* 2016;70(3):458-66.
64. Hoffmann D, Hoffmann I, El-Bayoumy K. The less harmful cigarette: a controversial issue. a tribute to Ernst L. Wynder. *Chem Res Toxicol.* 2001;14(7):767-90.
65. Barnes JL, Zubair M, John K, Poirier MC, Martin FL. Carcinogens and DNA damage. *Biochem Soc Trans.* 2018;46(5):1213-24.
66. Momas I, Daures JP, Festy B, Bontoux J, Gremy F. Bladder cancer and black tobacco cigarette smoking. Some results from a French case-control study. *Eur J Epidemiol.* 1994;10(5):599-604.
67. Burch JD, Rohan TE, Howe GR, Risch HA, Hill GB, Steele R, et al. Risk of bladder cancer by source and type of tobacco exposure: a case-control study. *Int J Cancer.* 1989;44(4):622-8.
68. Reed O, Jubber I, Griffin J, Noon AP, Goodwin L, Hussain S, et al. Occupational bladder cancer: A cross section survey of previous employments, tasks and exposures matched to cancer phenotypes. *PloS one.* 2020;15(10).
69. Hadkhale K, Martinsen JI, Weiderpass E, Kjaerheim K, Sparen P, Tryggvadottir L, et al. Occupational exposure to solvents and bladder cancer: A population-based case control study in Nordic countries. *International Journal of Cancer.* 2017;140(8):1736-46.
70. García-Closas M, Malats N, Silverman D, Dosemeci M, Kogevinas M, Hein DW, et al. NAT2 slow acetylation, GSTM1 null genotype, and risk of bladder cancer: results from the Spanish Bladder Cancer Study and meta-analyses. *Lancet (London, England).* 2005;366(9486).
71. Figueroa JD, Middlebrooks CD, Banday AR, Ye Y, Garcia-Closas M, Chatterjee N, et al. Identification of a novel susceptibility locus at 13q34 and refinement of the 20p12.2 region as a multi-signal locus associated with bladder cancer risk in individuals of European ancestry. *Hum Mol Genet.* 2016;25(6):1203-14.
72. Pils D, Bachmayr-Heyda A, Auer K, Svoboda M, Auner V, Hager G, et al. Cyclin E1 (CCNE1) as independent positive prognostic factor in advanced stage serous ovarian cancer patients - a study of the OVCAD consortium. *Eur J Cancer.* 2014;50(1):99-110.
73. Roberts SA, Lawrence MS, Klimczak LJ, Grimm SA, Fargo D, Stojanov P, et al. An APOBEC cytidine deaminase mutagenesis pattern is widespread in human cancers. *Nat Genet.* 2013;45(9).

74. Stewart G. The emerging physiological roles of the SLC14A family of urea transporters. *Br J Pharmacol.* 2011;164(7):1780-92.
75. Strassburg CP, Kalthoff S, Ehmer U. Variability and function of family 1 uridine-5'-diphosphate glucuronosyltransferases (UGT1A). *Crit Rev Clin Lab Sci.* 2008;45(6):485-530.
76. Zhou SF, Wang B, Yang LP, Liu JP. Structure, function, regulation and polymorphism and the clinical significance of human cytochrome P450 1A2. *Drug Metab Rev.* 2010;42(2):268-354.
77. Morrissette JD, Colliton RP, Spinner NB. Defective intracellular transport and processing of JAG1 missense mutations in Alagille syndrome. *Hum Mol Genet.* 2001;10(4):405-13.
78. Chen Z, Guo Y, Zhao D, Zou Q, Yu F, Zhang L, et al. Comprehensive Analysis Revealed that CDKN2A is a Biomarker for Immune Infiltrates in Multiple Cancers. *Front Cell Dev Biol.* 2021;9:808208.
79. Marjon K, Cameron MJ, Quang P, Clasquin MF, Mandley E, Kunii K, et al. MTAP Deletions in Cancer Create Vulnerability to Targeting of the MAT2A/PRMT5/RIOK1 Axis. *Cell Rep.* 2016;15(3):574-87.
80. Bartel CA, Parameswaran N, Cipriano R, Jackson MW. FAM83 proteins: Fostering new interactions to drive oncogenic signaling and therapeutic resistance. *Oncotarget.* 2016;7(32):52597-612.
81. Sui X, Lei L, Chen L, Xie T, Li X. Inflammatory microenvironment in the initiation and progression of bladder cancer. *Oncotarget.* 2017;8(54).
82. Hanada T, Nakagawa M, Emoto A, Nomura T, Nasu N, Nomura Y. Prognostic value of tumor-associated macrophage count in human bladder cancer. *International journal of urology : official journal of the Japanese Urological Association.* 2000;7(7).
83. Lima L, Oliveira D, Tavares A, Amaro T, Cruz R, Oliveira MJ, et al. The predominance of M2-polarized macrophages in the stroma of low-hypoxic bladder tumors is associated with BCG immunotherapy failure. *Urologic Oncology.* 2014;32(4):449-57.
84. Martin JW, Jefferson FA, Huang M, Sung JM, Chang J, Piranviseh K, et al. A California Cancer Registry Analysis of Urothelial and Non-urothelial Bladder Cancer Subtypes: Epidemiology, Treatment, and Survival. *Clin Genitourin Cancer.* 2020;18(3):e330-e6.
85. Comperat EM, Burger M, Gontero P, Mostafid AH, Palou J, Roupert M, et al. Grading of Urothelial Carcinoma and The New "World Health Organisation Classification of Tumours of the Urinary System and Male Genital Organs 2016". *Eur Urol Focus.* 2019;5(3):457-66.
86. Amin MB. Histological variants of urothelial carcinoma: diagnostic, therapeutic and prognostic implications. *Mod Pathol.* 2009;22 Suppl 2:S96-S118.
87. Mundy AR, Fitzpatrick J, Neal DE, George NJR. Transitional Cell Carcinoma of the Bladder. *The Scientific Basis of Urology.* Third ed: CRC Press; 2010. p. 374-85.
88. Babjuk M, Burger M, Capoun O, Cohen D, Compérat EM, Dominguez Escrig JL, et al. European Association of Urology Guidelines on Non-muscle-invasive Bladder Cancer (Ta, T1, and Carcinoma in Situ). *European urology.* 2022;81(1).
89. Leivo MZ, Elson PJ, Tacha DE, Delahunt B, Hansel DE. A combination of p40, GATA-3 and uroplakin II shows utility in the diagnosis and prognosis of muscle-invasive urothelial carcinoma. *Pathology.* 2016;48(6):543-9.
90. Qiang Z, Jubber I, Lloyd K, Cumberbatch M, Griffin J. Gene of the month: GATA3. *J Clin Pathol.* 2023;76(12):793-7.

91. Cumberbatch MGK, Foerster B, Catto JWF, Kamat AM, Kassouf W, Jubber I, et al. Repeat Transurethral Resection in Non-muscle-invasive Bladder Cancer: A Systematic Review. *Eur Urol.* 2018;73(6):925-33.
92. Sylvester RJ, van der Meijden AP, Oosterlinck W, Witjes JA, Bouffouix C, Denis L, et al. Predicting recurrence and progression in individual patients with stage Ta T1 bladder cancer using EORTC risk tables: a combined analysis of 2596 patients from seven EORTC trials. *Eur Urol.* 2006;49(3):466-77.
93. Schrier BP, Hollander MP, van Rhijn BW, Kiemeny LA, Witjes JA. Prognosis of muscle-invasive bladder cancer: difference between primary and progressive tumours and implications for therapy. *Eur Urol.* 2004;45(3):292-6.
94. von der Maase H, Sengelov L, Roberts JT, Ricci S, Dogliotti L, Oliver T, et al. Long-term survival results of a randomized trial comparing gemcitabine plus cisplatin, with methotrexate, vinblastine, doxorubicin, plus cisplatin in patients with bladder cancer. *Journal of clinical oncology : official journal of the American Society of Clinical Oncology.* 2005;23(21).
95. Spruck CH, Ohneseit PF, Gonzalez-Zulueta M, Esrig D, Miyao N, Tsai YC, et al. Two molecular pathways to transitional cell carcinoma of the bladder. *Cancer research.* 1994;54(3).
96. Rosin MP, Cairns P, Epstein JI, Schoenberg MP, Sidransky D. Partial allelotype of carcinoma in situ of the human bladder. *Cancer research.* 1995;55(22).
97. Chatterjee SJ, Datar R, Youssefzadeh D, George B, Goebell PJ, Stein JP, et al. Combined effects of p53, p21, and pRb expression in the progression of bladder transitional cell carcinoma. *Journal of clinical oncology : official journal of the American Society of Clinical Oncology.* 2004;22(6).
98. Billerey C, Chopin D, Aubriot-Lorton MH, Ricol D, Gil Diez de Medina S, Van Rhijn B, et al. Frequent FGFR3 mutations in papillary non-invasive bladder (pTa) tumors. *The American journal of pathology.* 2001;158(6).
99. Cappellen D, De Oliveira C, Ricol D, de Medina S, Bourdin J, Sastre-Garau X, et al. Frequent activating mutations of FGFR3 in human bladder and cervix carcinomas. *Nat Genet.* 1999;23(1).
100. López-Knowles E, Hernández S, Malats N, Kogevinas M, Lloreta J, Carrato A, et al. PIK3CA mutations are an early genetic alteration associated with FGFR3 mutations in superficial papillary bladder tumors. *Cancer research.* 2006;66(15).
101. Platt FM, Hurst CD, Taylor CF, Gregory WM, Harnden P, Knowles MA. Spectrum of phosphatidylinositol 3-kinase pathway gene alterations in bladder cancer. *Clinical cancer research : an official journal of the American Association for Cancer Research.* 2009;15(19).
102. Visvanathan KV, Pockock RD, Summerhayes IC. Preferential and novel activation of H-ras in human bladder carcinomas. *Oncogene research.* 1988;3(1).
103. Kompier LC, Lurkin I, van der Aa MN, van Rhijn BW, van der Kwast TH, Zwarthoff EC. FGFR3, HRAS, KRAS, NRAS and PIK3CA mutations in bladder cancer and their potential as biomarkers for surveillance and therapy. *PloS one.* 2010;5(11).
104. Bakkar AA, Wallerand H, Radvanyi F, Lahaye JB, Pissard S, Lecerf L, et al. FGFR3 and TP53 gene mutations define two distinct pathways in urothelial cell carcinoma of the bladder. *Cancer research.* 2003;63(23).
105. van Rhijn BW, van der Kwast TH, Vis AN, Kirkels WJ, Boevé ER, Jöbsis AC, et al. FGFR3 and P53 characterize alternative genetic pathways in the pathogenesis of urothelial cell carcinoma. *Cancer research.* 2004;64(6).

106. Jebar AH, Hurst CD, Tomlinson DC, Johnston C, Taylor CF, Knowles MA. FGFR3 and Ras gene mutations are mutually exclusive genetic events in urothelial cell carcinoma. *Oncogene*. 2005;24(33).
107. Pathology Outlines. Bladder & urothelial tract 2024 [Available from: <https://www.pathologyoutlines.com/bladder.html>].
108. Ornitz DM, Itoh N. The Fibroblast Growth Factor signaling pathway. Wiley interdisciplinary reviews Developmental biology. 2015;4(3).
109. di Martino E, L'Hôte CG, Kennedy W, Tomlinson DC, Knowles MA. Mutant fibroblast growth factor receptor 3 induces intracellular signaling and cellular transformation in a cell type- and mutation-specific manner. *Oncogene*. 2009;28(48).
110. Foth M, Ismail NFB, Kung JSC, Tomlinson D, Knowles MA, Eriksson P, et al. FGFR3 mutation increases bladder tumourigenesis by suppressing acute inflammation. *J Pathol*. 2462018. p. 331-43.
111. Knowles M. FGFR3 – a Central Player in Bladder Cancer Pathogenesis? *Bladder Cancer*. 2020;6(4):403-23.
112. Ross RL, Askham JM, Knowles MA. PIK3CA mutation spectrum in urothelial carcinoma reflects cell context-dependent signaling and phenotypic outputs. *Oncogene*. 2013;32(6).
113. Rodriguez-Viciano P, Warne PH, Dhand R, Vanhaesebroeck B, Gout I, Fry MJ, et al. Phosphatidylinositol-3-OH kinase as a direct target of Ras. *Nature*. 1994;370(6490).
114. Macaluso M, Russo G, Cinti C, Bazan V, Gebbia N, Russo A. Ras family genes: an interesting link between cell cycle and cancer. *Journal of cellular physiology*. 2002;192(2).
115. Ascione CM, Napolitano F, Esposito D, Servetto A, Belli S, Santaniello A, et al. Role of FGFR3 in bladder cancer: Treatment landscape and future challenges. *Cancer Treat Rev*. 2023;115:102530.
116. Pineda S, Milne RL, Calle ML, Rothman N, López de Maturana E, Herranz J, et al. Genetic variation in the TP53 pathway and bladder cancer risk. a comprehensive analysis. *PLoS One*. 2014;9(5):e89952.
117. Knowles MA, Hurst CD. Molecular biology of bladder cancer: new insights into pathogenesis and clinical diversity. *Nature reviews Cancer*. 2015;15(1).
118. Robertson AG, Kim J, Al-Ahmadie H, Bellmunt J, Guo G, Cherniack AD, et al. Comprehensive Molecular Characterization of Muscle-Invasive Bladder Cancer. *Cell*. 2017;171(3):540-56.e25.
119. Comprehensive molecular characterization of urothelial bladder carcinoma. *Nature*. 2014;507(7492).
120. Hurst CD, Alder O, Platt FM, Droop A, Stead LF, Burns JE, et al. Genomic Subtypes of Non-invasive Bladder Cancer with Distinct Metabolic Profile and Female Gender Bias in KDM6A Mutation Frequency. *Cancer Cell*. 2017;32(5).
121. Glaser AP, Fantini D, Wang Y, Yu Y, Rimar KJ, Podojil JR, et al. APOBEC-mediated mutagenesis in urothelial carcinoma is associated with improved survival, mutations in DNA damage response genes, and immune response. *Oncotarget*. 2017;9(4).
122. Liu W, Newhall KP, Khani F, Barlow L, Nguyen D, Gu L, et al. The Cytidine Deaminase APOBEC3G Contributes to Cancer Mutagenesis and Clonal Evolution in Bladder Cancer. *Cancer Res*. 2023;83(4):506-20.
123. Alexandrov LB, Kim J, Haradhvala NJ, Huang MN, Tian Ng AW, Wu Y, et al. The repertoire of mutational signatures in human cancer. *Nature*. 2020;578(7793):94-101.

124. Perou CM, Sørli T, Eisen MB, van de Rijn M, Jeffrey SS, Rees CA, et al. Molecular portraits of human breast tumours. *Nature*. 2000;406(6797).
125. Seiler R, Ashab HAD, Erho N, van Rhijn BWG, Winters B, Douglas J, et al. Impact of Molecular Subtypes in Muscle-invasive Bladder Cancer on Predicting Response and Survival after Neoadjuvant Chemotherapy. *Eur Urol*. 2017;72(4):544-54.
126. Rosenberg JE, Hoffman-Censits J, Powles T, van der Heijden MS, Balar AV, Necchi A, et al. Atezolizumab in patients with locally advanced and metastatic urothelial carcinoma who have progressed following treatment with platinum-based chemotherapy: a single-arm, multicentre, phase 2 trial. *Lancet (London, England)*. 2016;387(10031).
127. Sylvester RJ, Oosterlinck W, van der Meijden AP. A single immediate postoperative instillation of chemotherapy decreases the risk of recurrence in patients with stage Ta T1 bladder cancer: a meta-analysis of published results of randomized clinical trials. *J Urol*. 2004;171(6 Pt 1):2186-90, quiz 435.
128. Tolley DA, Parmar MK, Grigor KM, Lallemand G, Benyon LL, Fellows J, et al. The effect of intravesical mitomycin C on recurrence of newly diagnosed superficial bladder cancer: a further report with 7 years of follow up. *J Urol*. 1996;155(4):1233-8.
129. Gandhi NM, Morales A, Lamm DL. Bacillus Calmette-Guerin immunotherapy for genitourinary cancer. *BJU Int*. 2013;112(3):288-97.
130. Boorjian SA, Alemozaffar M, Konety BR, Shore ND, Gomella LG, Kamat AM, et al. Intravesical nadofaragene firadenovec gene therapy for BCG-unresponsive non-muscle-invasive bladder cancer: a single-arm, open-label, repeat-dose clinical trial. *Lancet Oncol*. 2021;22(1):107-17.
131. Inman BA, Hahn NM, Stratton K, Kopp R, Sankin A, Skinner E, et al. A Phase 1b/2 Study of Atezolizumab with or Without Bacille Calmette-Guerin in Patients with High-risk Non-muscle-invasive Bladder Cancer. *Eur Urol Oncol*. 2023;6(3):313-20.
132. Grossman HB, Natale RB, Tangen CM, Speights VO, Vogelzang NJ, Trump DL, et al. Neoadjuvant chemotherapy plus cystectomy compared with cystectomy alone for locally advanced bladder cancer. *N Engl J Med*. 2003;349(9):859-66.
133. Tunio MA, Hashmi A, Qayyum A, Mohsin R, Zaeem A. Whole-pelvis or bladder-only chemoradiation for lymph node-negative invasive bladder cancer: single-institution experience. *Int J Radiat Oncol Biol Phys*. 2012;82(3):e457-62.
134. Stein JP, Lieskovsky G, Cote R, Groshen S, Feng AC, Boyd S, et al. Radical cystectomy in the treatment of invasive bladder cancer: long-term results in 1,054 patients. *J Clin Oncol*. 2001;19(3):666-75.
135. Kotwal S, Choudhury A, Johnston C, Paul AB, Whelan P, Kiltie AE. Similar treatment outcomes for radical cystectomy and radical radiotherapy in invasive bladder cancer treated at a United Kingdom specialist treatment center. *Int J Radiat Oncol Biol Phys*. 2008;70(2):456-63.
136. Rosario DJ, Catto JW, Cutinha PE, Anderson JB, Ferguson C, Kirkbride P, et al. Similar treatment outcomes for radical cystectomy and radical radiotherapy in invasive bladder cancer treated at a United Kingdom specialist treatment center: in regard to Kotwal et al. (*Int J Radiat Oncol Biol Phys* 2008;70:456-463). *Int J Radiat Oncol Biol Phys*. 2008;71(5):1601-2; author reply 2.
137. Advanced Bladder Cancer Meta-analysis C. Neoadjuvant chemotherapy in invasive bladder cancer: update of a systematic review and meta-analysis of individual patient data advanced bladder cancer (ABC) meta-analysis collaboration. *Eur Urol*. 2005;48(2):202-5; discussion 5-6.

138. Witjes JA, Bruins HM, Carrion A, Cathomas R, Comperat EM, Efstathiou JA, et al. EAU Guidelines on Muscle-invasive and Metastatic Bladder Cancer. <http://uroweb.org/guidelines/compilations-of-all-guidelines/>: EAU Guidelines Office, Arnhem, The Netherlands.; 2022.
139. Advanced Bladder Cancer Meta-analysis Collaborators G. Adjuvant Chemotherapy for Muscle-invasive Bladder Cancer: A Systematic Review and Meta-analysis of Individual Participant Data from Randomised Controlled Trials. *Eur Urol.* 2022;81(1):50-61.
140. Bajorin DF, Witjes JA, Gschwend JE, Schenker M, Valderrama BP, Tomita Y, et al. Adjuvant Nivolumab versus Placebo in Muscle-Invasive Urothelial Carcinoma. *N Engl J Med.* 2021;384(22):2102-14.
141. Balar AV, Castellano D, O'Donnell PH, Grivas P, Vuky J, Powles T, et al. First-line pembrolizumab in cisplatin-ineligible patients with locally advanced and unresectable or metastatic urothelial cancer (KEYNOTE-052): a multicentre, single-arm, phase 2 study. *Lancet Oncol.* 2017;18(11):1483-92.
142. Balar AV, Galsky MD, Rosenberg JE, Powles T, Petrylak DP, Bellmunt J, et al. Atezolizumab as first-line treatment in cisplatin-ineligible patients with locally advanced and metastatic urothelial carcinoma: a single-arm, multicentre, phase 2 trial. *Lancet.* 2017;389(10064):67-76.
143. Powles T, O'Donnell PH, Massard C, Arkenau HT, Friedlander TW, Hoimes CJ, et al. Efficacy and Safety of Durvalumab in Locally Advanced or Metastatic Urothelial Carcinoma: Updated Results From a Phase 1/2 Open-label Study. *JAMA oncology.* 2017;3(9):e172411.
144. Sharma P, Retz M, Siefker-Radtke A, Baron A, Necchi A, Bedke J, et al. Nivolumab in metastatic urothelial carcinoma after platinum therapy (CheckMate 275): a multicentre, single-arm, phase 2 trial. *Lancet Oncol.* 2017;18(3):312-22.
145. Powles T, Park SH, Voog E, Caserta C, Valderrama BP, Gurney H, et al. Avelumab Maintenance Therapy for Advanced or Metastatic Urothelial Carcinoma. *N Engl J Med.* 2020;383(13):1218-30.
146. Powles T, Rosenberg JE, Sonpavde GP, Loriot Y, Duran I, Lee JL, et al. Enfortumab Vedotin in Previously Treated Advanced Urothelial Carcinoma. *N Engl J Med.* 2021;384(12):1125-35.
147. Loriot Y, Necchi A, Park SH, Garcia-Donas J, Huddart R, Burgess E, et al. Erdafitinib in Locally Advanced or Metastatic Urothelial Carcinoma. *N Engl J Med.* 2019;381(4):338-48.
148. Tagawa ST, Balar AV, Petrylak DP, Kalebasty AR, Loriot Y, Flechon A, et al. TROPHY-U-01: A Phase II Open-Label Study of Sacituzumab Govitecan in Patients With Metastatic Urothelial Carcinoma Progressing After Platinum-Based Chemotherapy and Checkpoint Inhibitors. *J Clin Oncol.* 2021;39(22):2474-85.
149. Alfred Witjes J, Max Bruins H, Carrion A, Cathomas R, Comperat E, Efstathiou JA, et al. European Association of Urology Guidelines on Muscle-invasive and Metastatic Bladder Cancer: Summary of the 2023 Guidelines. *Eur Urol.* 2024;85(1):17-31.
150. Almas B, Halvorsen OJ, Johannesen TB, Beisland C. Higher than expected and significantly increasing incidence of upper tract urothelial carcinoma. A population based study. *World J Urol.* 2021;39(9):3385-91.
151. Hassler MR, Bray F, Catto JWF, Grollman AP, Hartmann A, Margulis V, et al. Molecular Characterization of Upper Tract Urothelial Carcinoma in the Era of Next-generation Sequencing: A Systematic Review of the Current Literature. *Eur Urol.* 2020;78(2):209-20.

152. Cosentino M, Palou J, Gaya JM, Breda A, Rodriguez-Faba O, Villavicencio-Mavrich H. Upper urinary tract urothelial cell carcinoma: location as a predictive factor for concomitant bladder carcinoma. *World Journal of Urology*. 2013;31(1):141-5.
153. Singla N, Fang D, Su X, Bao Z, Cao Z, Jafri SM, et al. A Multi-Institutional Comparison of Clinicopathological Characteristics and Oncologic Outcomes of Upper Tract Urothelial Carcinoma in China and the United States. *J Urol*. 2017;197(5):1208-13.
154. Xylinas E, Rink M, Margulis V, Karakiewicz P, Novara G, Shariat SF, et al. Multifocal carcinoma in situ of the upper tract is associated with high risk of bladder cancer recurrence. *Eur Urol*. 2012;61(5):1069-70.
155. Li WM, Shen JT, Li CC, Ke HL, Wei YC, Wu WJ, et al. Oncologic outcomes following three different approaches to the distal ureter and bladder cuff in nephroureterectomy for primary upper urinary tract urothelial carcinoma. *Eur Urol*. 2010;57(6):963-9.
156. van Doeveren T, van de Werken HJG, van Riet J, Aben KKH, van Leeuwen PJ, Zwarthoff EC, et al. Synchronous and metachronous urothelial carcinoma of the upper urinary tract and the bladder: Are they clonally related? A systematic review. *Urol Oncol*. 2020;38(6):590-8.
157. Margulis V, Shariat SF, Matin SF, Kamat AM, Zigeuner R, Kikuchi E, et al. Outcomes of radical nephroureterectomy: a series from the Upper Tract Urothelial Carcinoma Collaboration. *Cancer*. 2009;115(6):1224-33.
158. Catto JW, Yates DR, Rehman I, Azzouzi AR, Patterson J, Sibony M, et al. Behavior of urothelial carcinoma with respect to anatomical location. *J Urol*. 2007;177(5):1715-20.
159. Colin P, Koenig P, Ouzzane A, Berthon N, Villers A, Biserte J, et al. Environmental factors involved in carcinogenesis of urothelial cell carcinomas of the upper urinary tract. *BJU Int*. 2009;104(10):1436-40.
160. Yates DR, Catto JW. Distinct patterns and behaviour of urothelial carcinoma with respect to anatomical location: how molecular biomarkers can augment clinicopathological predictors in upper urinary tract tumours. *World J Urol*. 2013;31(1):21-9.
161. Moss TJ, Qi Y, Xi L, Peng B, Kim TB, Ezzedine NE, et al. Comprehensive Genomic Characterization of Upper Tract Urothelial Carcinoma. *Eur Urol*. 2017;72(4):641-9.
162. Schneider B, Glass A, Jagdmann S, Huhns M, Claus J, Zettl H, et al. Loss of Mismatch-repair Protein Expression and Microsatellite Instability in Upper Tract Urothelial Carcinoma and Clinicopathologic Implications. *Clin Genitourin Cancer*. 2020;18(5):e563-e72.
163. O'Brien T, Ray E, Singh R, Coker B, Beard R, British Association of Urological Surgeons Section of O. Prevention of bladder tumours after nephroureterectomy for primary upper urinary tract urothelial carcinoma: a prospective, multicentre, randomised clinical trial of a single postoperative intravesical dose of mitomycin C (the ODMIT-C Trial). *Eur Urol*. 2011;60(4):703-10.
164. Birtle A, Johnson M, Chester J, Jones R, Dolling D, Bryan RT, et al. Adjuvant chemotherapy in upper tract urothelial carcinoma (the POUT trial): a phase 3, open-label, randomised controlled trial. *Lancet*. 2020;395(10232):1268-77.
165. Seisen T, Peyronnet B, Dominguez-Escrig JL, Bruins HM, Yuan CY, Babjuk M, et al. Oncologic Outcomes of Kidney-sparing Surgery Versus Radical Nephroureterectomy for Upper Tract Urothelial Carcinoma: A Systematic Review by

- the EAU Non-muscle Invasive Bladder Cancer Guidelines Panel. *Eur Urol.* 2016;70(6):1052-68.
166. Cutress ML, Stewart GD, Wells-Cole S, Phipps S, Thomas BG, Tolley DA. Long-term endoscopic management of upper tract urothelial carcinoma: 20-year single-centre experience. *BJU Int.* 2012;110(11):1608-17.
167. Moschini M, Shariat SF, Roupret M, De Santis M, Bellmunt J, Sternberg CN, et al. Impact of Primary Tumor Location on Survival from the European Organization for the Research and Treatment of Cancer Advanced Urothelial Cancer Studies. *J Urol.* 2018;199(5):1149-57.
168. Bellmunt J, de Wit R, Vaughn DJ, Fradet Y, Lee JL, Fong L, et al. Pembrolizumab as Second-Line Therapy for Advanced Urothelial Carcinoma. *N Engl J Med.* 2017;376(11):1015-26.
169. Muglia VF, Prando A. Renal cell carcinoma: histological classification and correlation with imaging findings. *Radiol Bras.* 2015;48(3):166-74.
170. Fuhrman SA, Lasky LC, Limas C. Prognostic significance of morphologic parameters in renal cell carcinoma. *Am J Surg Pathol.* 1982;6(7):655-63.
171. Cancer Genome Atlas Research N. Comprehensive molecular characterization of clear cell renal cell carcinoma. *Nature.* 2013;499(7456):43-9.
172. Delahunt B, Eble JN, Samarasinghe H, Thunders M, Yaxley JW, Egevad L. Staging of renal cell carcinoma: current progress and potential advances. *Pathology.* 2021;53(1):120-8.
173. Ljungberg B, Albiges L, Abu-Ghanem Y, Bedke J, Capitanio U, Dabestani S, et al. European Association of Urology Guidelines on Renal Cell Carcinoma: The 2022 Update. *Eur Urol.* 2022;82(4):399-410.
174. Bedke J, Albiges L, Capitanio U, Giles RH, Hora M, Lam TB, et al. The 2021 Updated European Association of Urology Guidelines on Renal Cell Carcinoma: Immune Checkpoint Inhibitor-based Combination Therapies for Treatment-naïve Metastatic Clear-cell Renal Cell Carcinoma Are Standard of Care. *Eur Urol.* 2021;80(4):393-7.
175. Wakefield L, Agarwal S, Tanner K. Preclinical models for drug discovery for metastatic disease. *Cell.* 2023;186(8):1792-813.
176. Kobayashi T, Owczarek TB, McKiernan JM, Abate-Shen C. Modeling bladder cancer in mice: opportunities and challenges. *Nature reviews Cancer.* 2015;15(1):42-54.
177. Zhang ZT, Pak J, Shapiro E, Sun TT, Wu XR. Urothelium-specific expression of an oncogene in transgenic mice induced the formation of carcinoma in situ and invasive transitional cell carcinoma. *Cancer research.* 1999;59(14).
178. Zhang ZT, Pak J, Huang HY, Shapiro E, Sun TT, Pellicer A, et al. Role of Ha-ras activation in superficial papillary pathway of urothelial tumor formation. *Oncogene.* 2001;20(16).
179. Ahmad I, Patel R, Liu Y, Singh LB, Taketo MM, Wu XR, et al. Ras mutation cooperates with  $\beta$ -catenin activation to drive bladder tumorigenesis. *Cell death & disease.* 2011;2(3).
180. He F, Melamed J, Tang MS, Huang C, Wu XR. Oncogenic HRAS Activates Epithelial-to-Mesenchymal Transition and Confers Stemness to p53-Deficient Urothelial Cells to Drive Muscle Invasion of Basal Subtype Carcinomas. *Cancer research.* 2015;75(10).
181. Gao J, Huang HY, Pak J, Cheng J, Zhang ZT, Shapiro E, et al. p53 deficiency provokes urothelial proliferation and synergizes with activated Ha-ras in promoting urothelial tumorigenesis. *Oncogene.* 2004;23(3).

182. He F, Mo L, Zheng XY, Hu C, Lepor H, Lee EY, et al. Deficiency of pRb family proteins and p53 in invasive urothelial tumorigenesis. *Cancer research*. 2009;69(24).
183. Puzio-Kuter AM, Castillo-Martin M, Kinkade CW, Wang X, Shen TH, Matos T, et al. Inactivation of p53 and Pten promotes invasive bladder cancer. *Genes & development*. 2009;23(6).
184. Ahmad I, Singh LB, Foth M, Morris CA, Taketo MM, Wu XR, et al. K-Ras and  $\beta$ -catenin mutations cooperate with Fgfr3 mutations in mice to promote tumorigenesis in the skin and lung, but not in the bladder. *Disease models & mechanisms*. 2011;4(4).
185. Shi MJ, Fontugne J, Moreno-Vega A, Meng XY, Groeneveld C, Dufour F, et al. FGFR3 Mutational Activation Can Induce Luminal-like Papillary Bladder Tumor Formation and Favors a Male Sex Bias. *Eur Urol*. 2023;83(1):70-81.
186. Ahmad I, Morton JP, Singh LB, Radulescu SM, Ridgway RA, Patel S, et al.  $\beta$ -Catenin activation synergizes with PTEN loss to cause bladder cancer formation. *Oncogene*. 2011;30(2).
187. Lieschke GJ, Currie PD. Animal models of human disease: zebrafish swim into view. *Nature reviews Genetics*. 2007;8(5):353-67.
188. Langenau DM, Traver D, Ferrando AA, Kutok JL, Aster JC, Kanki JP, et al. Myc-induced T cell leukemia in transgenic zebrafish. *Science (New York, NY)*. 2003;299(5608).
189. Elliot A, Myllymäki H, Feng Y. Inflammatory Responses during Tumour Initiation: From Zebrafish Transgenic Models of Cancer to Evidence from Mouse and Man. *Cells*. 2020;9(4):1018.
190. Howe K, Clark MD, Torroja CF, Torrance J, Berthelot C, Muffato M, et al. The zebrafish reference genome sequence and its relationship to the human genome. *Nature*. 2013;496(7446):498-503.
191. Kawakami K. Transgenesis and gene trap methods in zebrafish by using the Tol2 transposable element. *Methods in cell biology*. 2004;77.
192. White RM, Sessa A, Burke C, Bowman T, LeBlanc J, Ceol C, et al. Transparent adult zebrafish as a tool for in vivo transplantation analysis. *Cell Stem Cell*. 2008;2(2):183-9.
193. Ignatius MS, Hayes MN, Moore FE, Tang Q, Garcia SP, Blackburn PR, et al. tp53 deficiency causes a wide tumor spectrum and increases embryonal rhabdomyosarcoma metastasis in zebrafish. *eLife*. 2018;7.
194. Berghmans S, Murphey RD, Wienholds E, Neuberg D, Kutok JL, Fletcher CD, et al. tp53 mutant zebrafish develop malignant peripheral nerve sheath tumors. *Proc Natl Acad Sci U S A*. 2005;102(2):407-12.
195. Shive HR, West RR, Embree LJ, Azuma M, Sood R, Liu P, et al. brca2 in zebrafish ovarian development, spermatogenesis, and tumorigenesis. *Proceedings of the National Academy of Sciences of the United States of America*. 2010;107(45).
196. Solin SL, Shive HR, Woolard KD, Essner JJ, McGrail M. Rapid tumor induction in zebrafish by TALEN-mediated somatic inactivation of the retinoblastoma1 tumor suppressor rb1. *Sci Rep*. 2015;5.
197. Noonan HR, Metelo AM, Kamei CN, Peterson RT, Drummond IA, Iliopoulos O. Loss of vhl in the zebrafish pronephros recapitulates early stages of human clear cell renal cell carcinoma. *Disease models & mechanisms*. 2016;9(8).
198. Rankin EB, Tomaszewski JE, Haase VH. Renal cyst development in mice with conditional inactivation of the von Hippel-Lindau tumor suppressor. *Cancer Res*. 2006;66(5):2576-83.

199. Santoriello C, Deflorian G, Pezzimenti F, Kawakami K, Lanfrancone L, d'Adda di Fagagna F, et al. Expression of H-RASV12 in a zebrafish model of Costello syndrome causes cellular senescence in adult proliferating cells. *Disease models & mechanisms*. 2009;2(1-2).
200. Patton EE, Widlund HR, Kutok JL, Kopani KR, Amatruda JF, Murphey RD, et al. BRAF mutations are sufficient to promote nevi formation and cooperate with p53 in the genesis of melanoma. *Current biology : CB*. 2005;15(3).
201. Anelli V, Villefranc JA, Chhangawala S, Martinez-McFaline R, Riva E, Nguyen A, et al. Oncogenic BRAF disrupts thyroid morphogenesis and function via twist expression. *eLife*. 2017;6.
202. Park SW, Davison JM, Rhee J, Hruban RH, Maitra A, Leach SD. Oncogenic KRAS induces progenitor cell expansion and malignant transformation in zebrafish exocrine pancreas. *Gastroenterology*. 2008;134(7).
203. Yang Q, Yan C, Wang X, Gong Z. Leptin induces muscle wasting in a zebrafish kras-driven hepatocellular carcinoma (HCC) model. *Disease models & mechanisms*. 2019;12(2).
204. Enya S, Kawakami K, Suzuki Y, Kawaoka S. A novel zebrafish intestinal tumor model reveals a role for cyp7a1-dependent tumor-liver crosstalk in causing adverse effects on the host. *Disease models & mechanisms*. 2018;11(8).
205. Ju B, Chen W, Orr BA, Spitsbergen JM, Jia S, Eden CJ, et al. Oncogenic KRAS promotes malignant brain tumors in zebrafish. *Molecular cancer*. 2015;14(1).
206. Langenau DM, Keefe MD, Storer NY, Guyon JR, Kutok JL, Le X, et al. Effects of RAS on the genesis of embryonal rhabdomyosarcoma. *Genes & development*. 2007;21(11).
207. Liu S, Leach SD. Screening pancreatic oncogenes in zebrafish using the Gal4/UAS system. *Methods in cell biology*. 2011;105:367-81.
208. Ung CY, Guo F, Zhang X, Zhu Z, Zhu S. Mosaic zebrafish transgenesis for functional genomic analysis of candidate cooperative genes in tumor pathogenesis. *Journal of visualized experiments : JoVE*. 2015(97).
209. White R, Rose K, Zon L. Zebrafish cancer: the state of the art and the path forward. *Nature reviews Cancer*. 2013;13(9):624-36.
210. Ignatius MS, Chen E, Elpek NM, Fuller AZ, Tenente IM, Clagg R, et al. In vivo imaging of tumor-propagating cells, regional tumor heterogeneity, and dynamic cell movements in embryonal rhabdomyosarcoma. *Cancer Cell*. 2012;21(5):680-93.
211. Marques IJ, Weiss FU, Vlecken DH, Nitsche C, Bakkers J, Lagendijk AK, et al. Metastatic behaviour of primary human tumours in a zebrafish xenotransplantation model. *BMC Cancer*. 2009;9:128.
212. Lombardini ED, Hard GC, Harshbarger JC. Neoplasms of the urinary tract in fish. *Veterinary pathology*. 2014;51(5).
213. Bugman AM, Langer PT, Hadzima E, Rivas AE, Mitchell MA. Evaluation of the anesthetic efficacy of alfaxalone in oscar fish (*Astronotus ocellatus*). *Am J Vet Res*. 2016;77(3):239-44.
214. Westerfield M. *The Zebrafish Book: A Guide for the Laboratory Use of Zebrafish (Danio Rerio)*: University of Oregon Press; 2000.
215. Kawakami K, Abe G, Asada T, Asakawa K, Fukuda R, Ito A, et al. zTrap: zebrafish gene trap and enhancer trap database. *BMC developmental biology*. 2010;10:105.
216. Isles HM, Loynes CA, Alasmari S, Kon FC, Henry KM, Kadochnikova A, et al. Pioneer neutrophils release chromatin within in vivo swarms. *eLife*. 2021;10:e68755.

217. Renshaw SA, Loynes CA, Trushell DM, Elworthy S, Ingham PW, Whyte MK. A transgenic zebrafish model of neutrophilic inflammation. *Blood*. 2006;108(13):3976-8.
218. Ramezani T, Laux DW, Bravo IR, Tada M, Feng Y. Live imaging of innate immune and preneoplastic cell interactions using an inducible Gal4/UAS expression system in larval zebrafish skin. *J Vis Exp*. 2015(96).
219. Santoriello C, Gennaro E, Anelli V, Distel M, Kelly A, Koster RW, et al. Kita driven expression of oncogenic HRAS leads to early onset and highly penetrant melanoma in zebrafish. *PLoS One*. 2010;5(12):e15170.
220. Myllymaki H, Astorga Johansson J, Grados Porro E, Elliot A, Moses T, Feng Y. Metabolic Alterations in Preneoplastic Development Revealed by Untargeted Metabolomic Analysis. *Front Cell Dev Biol*. 2021;9:684036.
221. Lister JA, Robertson CP, Lepage T, Johnson SL, Raible DW. nacre encodes a zebrafish microphthalmia-related protein that regulates neural-crest-derived pigment cell fate. *Development*. 1999;126(17):3757-67.
222. Rosen JN, Sweeney MF, Mably JD. Microinjection of zebrafish embryos to analyze gene function. *Journal of visualized experiments : JoVE*. 2009(25).
223. Westerfield M. Whole-Mount In Situ Hybridization. *The zebrafish book A guide for the laboratory use of zebrafish (Danio rerio)*. 4th ed. Eugene, Oregon: Univ. of Oregon Press; 2000.
224. Stefansson IM, Salvesen HB, Akslen LA. Loss of p63 and cytokeratin 5/6 expression is associated with more aggressive tumors in endometrial carcinoma patients. *Int J Cancer*. 2006;118(5):1227-33.
225. Walusimbi SS, Pate JL. Luteal cells from functional and regressing bovine corpora lutea differentially alter the function of gamma delta T cells. *Biol Reprod*. 2014;90(6):140.
226. Guan GF, Zhang DJ, Zheng Y, Wen LJ, Yu DJ, Lu YQ, et al. Significance of ATP-binding cassette transporter proteins in multidrug resistance of head and neck squamous cell carcinoma. *Oncol Lett*. 2015;10(2):631-6.
227. Jung IH, Jung DE, Park YN, Song SY, Park SW. Aberrant Hedgehog ligands induce progressive pancreatic fibrosis by paracrine activation of myofibroblasts and ductular cells in transgenic zebrafish. *PLoS One*. 2011;6(12):e27941.
228. Qiu P, Jie Y, Ma C, Chen H, Qin Y, Tu K, et al. Paired box 8 facilitates the c-MYC related cell cycle progress in TP53-mutation uterine corpus endometrial carcinoma through interaction with DDX5. *Cell Death Discov*. 2022;8(1):276.
229. D'Agati G, Cabello EM, Frontzek K, Rushing EJ, Klemm R, Robinson MD, et al. Active receptor tyrosine kinases, but not Brachyury, are sufficient to trigger chordoma in zebrafish. *Disease models & mechanisms*. 2019;12(7).
230. Kwan KM, Fujimoto E, Grabher C, Mangum BD, Hardy ME, Campbell DS, et al. The Tol2kit: a multisite gateway-based construction kit for Tol2 transposon transgenesis constructs. *Dev Dyn*. 2007;236(11):3088-99.
231. Martin FJ, Amode MR, Aneja A, Austine-Orimoloye O, Azov AG, Barnes I, et al. Ensembl 2023. *Nucleic Acids Res*. 2023;51(D1):D933-D41.
232. UniProt C. UniProt: the Universal Protein Knowledgebase in 2023. *Nucleic Acids Res*. 2023;51(D1):D523-D31.
233. Johnson M, Zaretskaya I, Raytselis Y, Merezuk Y, McGinnis S, Madden TL. NCBI BLAST: a better web interface. *Nucleic Acids Res*. 2008;36(Web Server issue):W5-9.

234. Page MJ, McKenzie JE, Bossuyt PM, Boutron I, Hoffmann TC, Mulrow CD, et al. The PRISMA 2020 statement: an updated guideline for reporting systematic reviews. *Rev Esp Cardiol (Engl Ed)*. 2021;74(9):790-9.
235. Bray F, Ferlay J, Soerjomataram I, Siegel RL, Torre LA, Jemal A. Global cancer statistics 2018: GLOBOCAN estimates of incidence and mortality worldwide for 36 cancers in 185 countries. *CA Cancer J Clin*. 2018;68(6):394-424.
236. Catto JWF, Gordon K, Collinson M, Poad H, Twiddy M, Johnson M, et al. Radical Cystectomy Against Intravesical BCG for High-Risk High-Grade Nonmuscle Invasive Bladder Cancer: Results From the Randomized Controlled BRAVO-Feasibility Study. *J Clin Oncol*. 2021;39(3):202-14.
237. Witjes JA, Bruins HM, Cathomas R, Comperat EM, Cowan NC, Gakis G, et al. European Association of Urology Guidelines on Muscle-invasive and Metastatic Bladder Cancer: Summary of the 2020 Guidelines. *Eur Urol*. 2021;79(1):82-104.
238. Ramirez D, Gupta A, Canter D, Harrow B, Dobbs RW, Kucherov V, et al. Microscopic haematuria at time of diagnosis is associated with lower disease stage in patients with newly diagnosed bladder cancer. *BJU Int*. 2016;117(5):783-6.
239. Comperat E, Amin MB, Cathomas R, Choudhury A, De Santis M, Kamat A, et al. Current best practice for bladder cancer: a narrative review of diagnostics and treatments. *Lancet*. 2022;400(10364):1712-21.
240. Bilano V, Gilmour S, Moffiet T, d'Espaignet ET, Stevens GA, Commar A, et al. Global trends and projections for tobacco use, 1990-2025: an analysis of smoking indicators from the WHO Comprehensive Information Systems for Tobacco Control. *Lancet*. 2015;385(9972):966-76.
241. Islami F, Stoklosa M, Drope J, Jemal A. Global and Regional Patterns of Tobacco Smoking and Tobacco Control Policies. *Eur Urol Focus*. 2015;1(1):3-16.
242. Bao W, Xu G, Lu J, Snetselaar LG, Wallace RB. Changes in Electronic Cigarette Use Among Adults in the United States, 2014-2016. *JAMA*. 2018;319(19):2039-41.
243. Cumberbatch MG, Cox A, Teare D, Catto JW. Contemporary Occupational Carcinogen Exposure and Bladder Cancer: A Systematic Review and Meta-analysis. *JAMA oncology*. 2015;1(9):1282-90.
244. Burger M, Catto JW, Dalbagni G, Grossman HB, Herr H, Karakiewicz P, et al. Epidemiology and risk factors of urothelial bladder cancer. *Eur Urol*. 2013;63(2):234-41.
245. Page MJ, McKenzie JE, Bossuyt PM, Boutron I, Hoffmann TC, Mulrow CD, et al. The PRISMA 2020 statement: an updated guideline for reporting systematic reviews. *BMJ*. 2021;372:n71.
246. Ferlay J, Ervik M, Lam F, Colombet M, Mery L, Piñeros M, et al. Global Cancer Observatory: Cancer Today: Lyon, France: International Agency for Research on Cancer.; [cited 2020 December]. Available from: <https://gco.iarc.fr/today>.
247. Ferlay J, Colombet M, Soerjomataram I, Parkin DM, Pineros M, Znaor A, et al. Cancer statistics for the year 2020: An overview. *Int J Cancer*. 2021;149:778-89.
248. Cancer Research UK. Bladder cancer incidence statistics: Cancer Research UK; 2022 [cited 2024 10th June]. Available from: <https://www.cancerresearchuk.org/health-professional/cancer-statistics/statistics-by-cancer-type/bladder-cancer/incidence#ref-1>.
249. Roser M, Ritchie H. Cancer: Our World in Data; [updated November, 2019; cited 2015 July]. Available from: <https://ourworldindata.org/cancer>.
250. Safiri S, Kolahi AA, Naghavi M, Global Burden of Disease Bladder Cancer C. Global, regional and national burden of bladder cancer and its attributable risk

- factors in 204 countries and territories, 1990-2019: a systematic analysis for the Global Burden of Disease study 2019. *BMJ Glob Health*. 2021;6(11):e004128.
251. Ferlay J, Laversanne M, Ervik M, Lam F, Colombet M, Mery L, et al. *Global Cancer Observatory: Cancer Tomorrow.*: Lyon, France: International Agency for Research on Cancer.; [cited 2020 December]. Available from: <https://gco.iarc.fr/tomorrow>.
252. Mossanen M, Nassar AH, Stokes SM, Martinez-Chanza N, Kumar V, Nuzzo PV, et al. Incidence of Germline Variants in Familial Bladder Cancer and Among Patients With Cancer Predisposition Syndromes. *Clin Genitourin Cancer*. 2022;20(6):568-74.
253. Vosoughi A, Zhang T, Shohdy KS, Vlachostergios PJ, Wilkes DC, Bhinder B, et al. Common germline-somatic variant interactions in advanced urothelial cancer. *Nat Commun*. 2020;11(1):6195.
254. List of classifications by cancer sites with sufficient or limited evidence in humans, IARC Monographs Volumes 1–132: International Agency for Research on Cancer; [cited 2022 July 1st]. Available from: [https://monographs.iarc.who.int/wp-content/uploads/2019/07/Classifications\\_by\\_cancer\\_site.pdf](https://monographs.iarc.who.int/wp-content/uploads/2019/07/Classifications_by_cancer_site.pdf).
255. Freedman ND, Silverman DT, Hollenbeck AR, Schatzkin A, Abnet CC. Association between smoking and risk of bladder cancer among men and women. *JAMA*. 2011;306(7):737-45.
256. Jacob L, Freyn M, Kalder M, Dinas K, Kostev K. Impact of tobacco smoking on the risk of developing 25 different cancers in the UK: a retrospective study of 422,010 patients followed for up to 30 years. *Oncotarget*. 2018;9(25):17420-9.
257. Laaksonen MA, MacInnis RJ, Canfell K, Giles GG, Hull P, Shaw JE, et al. The future burden of kidney and bladder cancers preventable by behavior modification in Australia: A pooled cohort study. *Int J Cancer*. 2020;146(3):874-83.
258. Zhao X, Wang Y, Liang C. Cigarette smoking and risk of bladder cancer: a dose-response meta-analysis. *Int Urol Nephrol*. 2022;54(6):1169-85.
259. Li Y, Tindle HA, Hendryx MS, Xun P, He K, Liang X, et al. Smoking Cessation and the Risk of Bladder Cancer among Postmenopausal Women. *Cancer Prev Res*. 2019;12(5):305-14.
260. Yan H, Ying Y, Xie H, Li J, Wang X, He L, et al. Secondhand smoking increases bladder cancer risk in nonsmoking population: a meta-analysis. *Cancer Manag Res*. 2018;10:3781-91.
261. Fuller TW, Acharya AP, Meyyappan T, Yu M, Bhaskar G, Little SR, et al. Comparison of Bladder Carcinogens in the Urine of E-cigarette Users Versus Non E-cigarette Using Controls. *Sci Rep*. 2018;8(1):507.
262. Bjurlin MA, Matulewicz RS, Roberts TR, Dearing BA, Schatz D, Sherman S, et al. Carcinogen Biomarkers in the Urine of Electronic Cigarette Users and Implications for the Development of Bladder Cancer: A Systematic Review. *Eur Urol Oncol*. 2021;4(5):766-83.
263. Huang J, Huang D, Ruan X, Huang J, Xu D, Heavey S, et al. Association between cannabis use with urological cancers: A population-based cohort study and a mendelian randomization study in the UK biobank. *Cancer Med*. 2023;12(3):3468-76.
264. Sheikh M, Shakeri R, Poustchi H, Pourshams A, Etemadi A, Islami F, et al. Opium use and subsequent incidence of cancer: results from the Golestan Cohort Study. *Lancet Glob Health*. 2020;8(5):e649-e60.
265. Brown KF, Rungay H, Dunlop C, Ryan M, Quartly F, Cox A, et al. The fraction of cancer attributable to modifiable risk factors in England, Wales, Scotland,

- Northern Ireland, and the United Kingdom in 2015. *Br J Cancer*. 2018;118(8):1130-41.
266. Hadkhale K, Martinsen JI, Weiderpass E, Kjaerheim K, Sparen P, Tryggvadottir L, et al. Occupational variation in bladder cancer in Nordic males adjusted with approximated smoking prevalence. *Acta Oncol*. 2019;58(1):29-37.
267. Demers PA, DeMarini DM, Fent KW, Glass DC, Hansen J, Adetona O, et al. Carcinogenicity of occupational exposure as a firefighter. *Lancet Oncol*. 2022;23(8):985-6.
268. Jalilian H, Ziaei M, Weiderpass E, Rueegg CS, Khosravi Y, Kjaerheim K. Cancer incidence and mortality among firefighters. *Int J Cancer*. 2019;145(10):2639-46.
269. Diet, nutrition, physical activity and bladder cancer. Continuous Update Project Expert Report: World Cancer Research Fund/American Institute for Cancer Research; [updated 2018; cited 2015. Available from: <http://dietandcancerreport.org/>.
270. Witlox WJA, van Osch FHM, Brinkman M, Jochems S, Goossens ME, Weiderpass E, et al. An inverse association between the Mediterranean diet and bladder cancer risk: a pooled analysis of 13 cohort studies. *Eur J Nutr*. 2020;59(1):287-96.
271. Dianatinasab M, Wesselius A, Salehi-Abargouei A, Yu EYW, Brinkman M, Fararouei M, et al. Adherence to a Western dietary pattern and risk of bladder cancer: A pooled analysis of 13 cohort studies of the Bladder Cancer Epidemiology and Nutritional Determinants international study. *Int J Cancer*. 2020;147(12):3394-403.
272. Yu EYW, Wesselius A, Mehrkanon S, Brinkman M, van den Brandt P, White E, et al. Grain and dietary fiber intake and bladder cancer risk: a pooled analysis of prospective cohort studies. *Am J Clin Nutr*. 2020;112(5):1252-66.
273. Sarich P, Canfell K, Egger S, Banks E, Joshy G, Grogan P, et al. Alcohol consumption, drinking patterns and cancer incidence in an Australian cohort of 226,162 participants aged 45 years and over. *Br J Cancer*. 2021;124(2):513-23.
274. Vartolomei MD, Iwata T, Roth B, Kimura S, Mathieu R, Ferro M, et al. Impact of alcohol consumption on the risk of developing bladder cancer: a systematic review and meta-analysis. *World J Urol*. 2019;37(11):2313-24.
275. Hong X, Xu Q, Lan K, Huang H, Zhang Y, Chen S, et al. The Effect of Daily Fluid Management and Beverages Consumption on the Risk of Bladder Cancer: A Meta-analysis of Observational Study. *Nutr Cancer*. 2018;70(8):1217-27.
276. Yu EYW, Dai Y, Wesselius A, van Osch F, Brinkman M, van den Brandt P, et al. Coffee consumption and risk of bladder cancer: a pooled analysis of 501,604 participants from 12 cohort studies in the BLadder Cancer Epidemiology and Nutritional Determinants (BLEND) international study. *Eur J Epidemiol*. 2020;35(6):523-35.
277. Al-Zalabani AH, Wesselius A, Yi-Wen Yu E, van den Brandt P, Grant EJ, White E, et al. Tea consumption and risk of bladder cancer in the Bladder Cancer Epidemiology and Nutritional Determinants (BLEND) Study: Pooled analysis of 12 international cohort studies. *Clin Nutr*. 2022;41(5):1122-30.
278. Larsson SC, Andersson SO, Johansson JE, Wolk A. Cultured milk, yogurt, and dairy intake in relation to bladder cancer risk in a prospective study of Swedish women and men. *Am J Clin Nutr*. 2008;88(4):1083-7.

279. Acham M, Wesselius A, van Osch FHM, Yu EY, van den Brandt PA, White E, et al. Intake of milk and other dairy products and the risk of bladder cancer: a pooled analysis of 13 cohort studies. *Eur J Clin Nutr.* 2020;74(1):28-35.
280. Dianatinasab M, Wesselius A, de Loeij T, Salehi-Abargouei A, Yu EYW, Fararouei M, et al. The association between meat and fish consumption and bladder cancer risk: a pooled analysis of 11 cohort studies. *Eur J Epidemiol.* 2021;36(8):781-92.
281. Jochems SHJ, Reulen RC, van Osch FHM, Witlox WJA, Goossens ME, Brinkman M, et al. Fruit consumption and the risk of bladder cancer: A pooled analysis by the Bladder Cancer Epidemiology and Nutritional Determinants Study. *Int J Cancer.* 2020;147(8):2091-100.
282. Yu EY, Wesselius A, Mehrkanoon S, Goossens M, Brinkman M, van den Brandt P, et al. Vegetable intake and the risk of bladder cancer in the BLadder Cancer Epidemiology and Nutritional Determinants (BLEND) international study. *BMC Med.* 2021;19(1):56.
283. Abufaraj M, Tabung FK, Shariat SF, Moschini M, Devore E, Papantoniou K, et al. Association between Inflammatory Potential of Diet and Bladder Cancer Risk: Results of 3 United States Prospective Cohort Studies. *J Urol.* 2019;202(3):484-9.
284. Dunn JA, Jefferson K, MacDonald D, Iqbal G, Bland R. Low serum 25-hydroxyvitamin D is associated with increased bladder cancer risk: A systematic review and evidence of a potential mechanism. *J Steroid Biochem Mol Biol.* 2019;188:134-40.
285. Boot IWA, Wesselius A, Yu EYW, Brinkman M, van den Brandt P, Grant EJ, et al. Dietary B group vitamin intake and the bladder cancer risk: a pooled analysis of prospective cohort studies. *Eur J Nutr.* 2022;61(5):2397-416.
286. IARC Working Group on the Evaluation of Carcinogenic Risks to Humans. Some Drinking-water Disinfectants and Contaminants, including Arsenic. Lyon, France: International Agency for Research on Cancer, International Agency for Research on Cancer; 2004.
287. Boffetta P, Borron C. Low-Level Exposure to Arsenic in Drinking Water and Risk of Lung and Bladder Cancer: A Systematic Review and Dose-Response Meta-Analysis. *Dose Response.* 2019;17(3):1559325819863634.
288. IARC Working Group on the Evaluation of Carcinogenic Risks to Humans. Outdoor Air Pollution. . Lyon, France: International Agency for Research on Cancer, International Agency for Research on Cancer; 2015.
289. Koutros S, Kogevinas M, Friesen MC, Stewart PA, Baris D, Karagas MR, et al. Diesel exhaust and bladder cancer risk by pathologic stage and grade subtypes. *Environ Int.* 2020;135:105346.
290. Chen J, Rodopoulou S, Strak M, de Hoogh K, Taj T, Poulsen AH, et al. Long-term exposure to ambient air pollution and bladder cancer incidence in a pooled European cohort: the ELAPSE project. *Br J Cancer.* 2022;126(10):1499-507.
291. Turner MC, Gracia-Lavedan E, Cirac M, Castano-Vinyals G, Malats N, Tardon A, et al. Ambient air pollution and incident bladder cancer risk: Updated analysis of the Spanish Bladder Cancer Study. *Int J Cancer.* 2019;145(4):894-900.
292. Arafa A, Ewis A, Eshak E. Chronic exposure to nitrate in drinking water and the risk of bladder cancer: a meta-analysis of epidemiological evidence. *Public Health.* 2022;203:123-9.
293. Helte E, Save-Soderbergh M, Ugge H, Fall K, Larsson SC, Akesson A. Chlorination by-products in drinking water and risk of bladder cancer - A population-based cohort study. *Water Res.* 2022;214:118202.

294. Zhang Y, Birmann BM, Han J, Giovannucci EL, Speizer FE, Stampfer MJ, et al. Personal use of permanent hair dyes and cancer risk and mortality in US women: prospective cohort study. *BMJ*. 2020;370:m2942.
295. Delon C, Brown KF, Payne NWS, Kotrotsios Y, Vernon S, Shelton J. Differences in cancer incidence by broad ethnic group in England, 2013-2017. *Br J Cancer*. 2022;126(12):1765-73.
296. Carrot-Zhang J, Chambwe N, Damrauer JS, Knijnenburg TA, Robertson AG, Yau C, et al. Comprehensive Analysis of Genetic Ancestry and Its Molecular Correlates in Cancer. *Cancer Cell*. 2020;37(5):639-54 e6.
297. Teoh JY, Huang J, Ko WY, Lok V, Choi P, Ng CF, et al. Global Trends of Bladder Cancer Incidence and Mortality, and Their Associations with Tobacco Use and Gross Domestic Product Per Capita. *Eur Urol*. 2020;78(6):893-906.
298. Densmore R, Hajizadeh M, Hu M. Trends in socio-economic inequalities in bladder cancer incidence in Canada: 1992-2010. *Can J Public Health*. 2019;110(6):722-31.
299. Li Y, Hendryx MS, Xun P, He K, Shadyab AH, Lane DS, et al. Physical activity and risk of bladder cancer among postmenopausal women. *Int J Cancer*. 2020;147(10):2717-24.
300. Ihira H, Sawada N, Yamaji T, Goto A, Shimazu T, Inoue M, et al. Physical activity and subsequent risk of kidney, bladder and upper urinary tract cancer in the Japanese population: the Japan Public Health Centre-based Prospective Study. *Br J Cancer*. 2019;120(5):571-4.
301. Kim SY, Yoo DM, Min C, Choi HG. Association between Coffee Consumption/Physical Exercise and Gastric, Hepatic, Colon, Breast, Uterine Cervix, Lung, Thyroid, Prostate, and Bladder Cancer. *Nutrients*. 2021;13(11):3927.
302. Song Y, Qi X, Liu X. N-acetyltransferase 2 polymorphism is associated with bladder cancer risk: An updated meta-analysis based on 54 case-control studies. *Gene*. 2020;757:144924.
303. Chen L, Zhernakova DV, Kurilshikov A, Andreu-Sanchez S, Wang D, Augustijn HE, et al. Influence of the microbiome, diet and genetics on inter-individual variation in the human plasma metabolome. *Nat Med*. 2022;28(11):2333-43.
304. Zhou T, Li HY, Xie WJ, Zhong Z, Zhong H, Lin ZJ. Association of Glutathione S-transferase gene polymorphism with bladder Cancer susceptibility. *BMC Cancer*. 2018;18(1):1088.
305. Song Y, Chen J, Liu K, Zhou K, Lu Y, Wang X, et al. Glutathione S-Transferase Pi 1 (GSTP1) Gene 313 A/G (rs1695) polymorphism is associated with the risk of urinary bladder cancer: Evidence from a systematic review and meta-analysis based on 34 case-control studies. *Gene*. 2019;719:144077.
306. Song Y, Jin D, Chen J, Liang W, Liu X. Effects of Arsenic (+3 Oxidation State) Methyltransferase Gene Polymorphisms and Expression on Bladder Cancer: Evidence from a Systematic Review, Meta-analysis and TCGA Dataset. *Toxicol Sci*. 2020;177(1):27-40.
307. Bayne CE, Farah D, Herbst KW, Hsieh MH. Role of urinary tract infection in bladder cancer: a systematic review and meta-analysis. *World J Urol*. 2018;36(8):1181-90.
308. Dorsher PT, McIntosh PM. Neurogenic bladder. *Adv Urol*. 2012;2012:816274.
309. Bothig R, Tiburtius C, Fiebag K, Kowald B, Hirschfeld S, Thietje R, et al. Traumatic spinal cord injury confers bladder cancer risk to patients managed without permanent urinary catheterization: lessons from a comparison of clinical data with the national database. *World J Urol*. 2020;38(11):2827-34.

310. Ismail S, Karsenty G, Chartier-Kastler E, Cussenot O, Comperat E, Roupret M, et al. Prevalence, management, and prognosis of bladder cancer in patients with neurogenic bladder: A systematic review. *Neurourol Urodyn*. 2018;37(4):1386-95.
311. Hird AE, Saskin R, Liu Y, Lee Y, Ajib K, Matta R, et al. Association between chronic bladder catheterisation and bladder cancer incidence and mortality: a population-based retrospective cohort study in Ontario, Canada. *BMJ Open*. 2021;11(9):e050728.
312. Yu Z, Yue W, Jiuzhi L, Youtao J, Guofei Z, Wenbin G. The risk of bladder cancer in patients with urinary calculi: a meta-analysis. *Urolithiasis*. 2018;46(6):573-9.
313. Fang CW, Liao CH, Wu SC, Muo CH. Association of benign prostatic hyperplasia and subsequent risk of bladder cancer: an Asian population cohort study. *World J Urol*. 2018;36(6):931-8.
314. Fang CW, Hsieh VC, Huang SK, Tsai IJ, Muo CH, Wu SC. A population-based cohort study examining the association of documented bladder diverticulum and bladder cancer risk in urology patients. *PLoS One*. 2019;14(10):e0222875.
315. Guo X, Liu M, Hou H, Liu S, Zhang X, Zhang Y, et al. Impact of prostate cancer radiotherapy on the biological behavior and specific mortality of subsequent bladder cancer. *Int J Clin Oncol*. 2019;24(8):957-65.
316. Moschini M, Zaffuto E, Karakiewicz PI, Andrea DD, Foerster B, Abufaraj M, et al. External Beam Radiotherapy Increases the Risk of Bladder Cancer When Compared with Radical Prostatectomy in Patients Affected by Prostate Cancer: A Population-based Analysis. *Eur Urol*. 2019;75(2):319-28.
317. Zhao S, Xie Q, Yang R, Wang J, Zhang C, Luo L, et al. High prevalence of secondary bladder cancer in men on radiotherapy for prostate cancer: evidence from a meta-analysis. *Cancer Manag Res*. 2019;11:587-98.
318. Mazzone E, Mistretta FA, Knipper S, Palumbo C, Tian Z, Pecoraro A, et al. Long-term incidence of secondary bladder and rectal cancer in patients treated with brachytherapy for localized prostate cancer: a large-scale population-based analysis. *BJU Int*. 2019;124(6):1006-13.
319. Mossanen M, Carvalho FLF, Muralidhar V, Preston MA, Reardon B, Conway JR, et al. Genomic Features of Muscle-invasive Bladder Cancer Arising After Prostate Radiotherapy. *Eur Urol*. 2022;81(5):466-73.
320. Wen L, Zhong G, Zhang Y, Zhong M. Risk and prognosis of secondary bladder cancer after post-operative radiotherapy for gynecological cancer. *Bosn J Basic Med Sci*. 2022;22(3):471-80.
321. Choi JB, Kim JH, Hong SH, Han KD, Ha US. Association of body mass index with bladder cancer risk in men depends on abdominal obesity. *World J Urol*. 2019;37(11):2393-400.
322. Teleka S, Haggstrom C, Nagel G, Bjorge T, Manjer J, Ulmer H, et al. Risk of bladder cancer by disease severity in relation to metabolic factors and smoking: A prospective pooled cohort study of 800,000 men and women. *Int J Cancer*. 2018;143(12):3071-82.
323. Ahmadinezhad M, Arshadi M, Hesari E, Sharafoddin M, Azizi H, Khodamoradi F. The relationship between metabolic syndrome and its components with bladder cancer: a systematic review and meta-analysis of cohort studies. *Epidemiol Health*. 2022;44:e2022050.
324. Pan Y, Lee CY, Lee LM, Wen YC, Huang JY, Yang SF, et al. Incidence of Bladder Cancer in Type 2 Diabetes Mellitus Patients: A Population-Based Cohort Study. *Medicina (Kaunas)*. 2020;56(9):441.

325. Li Y, Hendryx MS, Xun P, He K, Shadyab AH, Pan K, et al. The association between type 2 diabetes mellitus and bladder cancer risk among postmenopausal women. *Cancer Causes Control*. 2020;31(5):503-10.
326. Kim SK, Jang JY, Kim DL, Rhyu YA, Lee SE, Ko SH, et al. Site-specific cancer risk in patients with type 2 diabetes: a nationwide population-based cohort study in Korea. *Korean J Intern Med*. 2020;35(3):641-51.
327. Tybjerg AJ, Babore AD, Olsen TS, Andersen KK. Types of occult cancer in stroke and the relation to smoking. *Acta Neurol Scand*. 2020;142(5):486-92.
328. Feng S, Shao Z, Ju L, Zhang Y. Atopy, asthma, and risk of bladder cancer: Systematic review and meta-analysis of cohort studies. *European Journal of Inflammation*. 2021;19.
329. Yeo J, Seo MS, Hwang IC, Shim JY. An Updated Meta-analysis on the Risk of Urologic Cancer in Patients with Systemic Lupus Erythematosus. *Arch Iran Med*. 2020;23(9):614-20.
330. Choi ST, Ahn SV, Lee PH, Moon CM. The cancer risk according to three subtypes of ANCA-associated vasculitis: A propensity score-matched analysis of a nationwide study. *Semin Arthritis Rheum*. 2021;51(4):692-9.
331. Oh YJ, Lee YJ, Lee E, Park B, Kwon JW, Heo J, et al. Cancer risk in Korean patients with gout. *Korean J Intern Med*. 2022;37(2):460-7.
332. Feng D, Yang Y, Wang Z, Wei W, Li L. Inflammatory bowel disease and risk of urinary cancers: a systematic review and pooled analysis of population-based studies. *Transl Androl Urol*. 2021;10(3):1332-41.
333. Zhang C, Liu S, Peng L, Wu J, Zeng X, Lu Y, et al. Does inflammatory bowel disease increase the risk of lower urinary tract tumors: a meta-analysis. *Transl Androl Urol*. 2021;10(1):164-73.
334. Lizakowski S, Kolonko A, Imko-Walczyk B, Komorowska-Jagielska K, Rutkowski B, Wiecek A, et al. Solid Organ Cancer and Melanoma in Kidney Transplant Recipients: TumorTx Base Preliminary Results. *Transplant Proc*. 2018;50(6):1881-8.
335. Altieri M, Seree O, Lobbedez T, Segol P, Abergel A, Blaizot X, et al. Risk factors of de novo malignancies after liver transplantation: a French national study on 11004 adult patients. *Clin Res Hepatol Gastroenterol*. 2021;45(4):1015-14.
336. Li H, Zhu C, Wu J, Ma Y, Jin X, Wei X, et al. Urological second malignant neoplasms in testicular nonseminoma survivors: a population-based analysis. *Int Urol Nephrol*. 2021;53(3):471-7.
337. Tang H, Shi W, Fu S, Wang T, Zhai S, Song Y, et al. Pioglitazone and bladder cancer risk: a systematic review and meta-analysis. *Cancer Med*. 2018;7(4):1070-80.
338. Adil M, Khan RA, Ghosh P, Venkata SK, Kandhare AD, Sharma M. Pioglitazone and risk of bladder cancer in type 2 diabetes mellitus patients: A systematic literature review and meta-analysis of observational studies using real-world data. *Clinical Epidemiology and Global Health*. 2018;6(2):61-8.
339. Cardwell CR, McDowell RD, Hughes CM, Hicks B, Murchie P. Exposure to Ranitidine and Risk of Bladder Cancer: A Nested Case-Control Study. *Am J Gastroenterol*. 2021;116(8):1612-9.
340. Wandell P, Carlsson AC, Li X, Sundquist J, Sundquist K. Levothyroxine treatment is associated with an increased relative risk of overall and organ specific incident cancers - a cohort study of the Swedish population. *Cancer Epidemiol*. 2020;66:101707.

341. Xie Y, Xu P, Wang M, Zheng Y, Tian T, Yang S, et al. Antihypertensive medications are associated with the risk of kidney and bladder cancer: a systematic review and meta-analysis. *Aging (Albany NY)*. 2020;12(2):1545-62.
342. Dicembrini I, Nreu B, Mannucci E, Monami M. Sodium-glucose co-transporter-2 (SGLT-2) inhibitors and cancer: A meta-analysis of randomized controlled trials. *Diabetes Obes Metab*. 2019;21(8):1871-7.
343. Hu J, Chen JB, Cui Y, Zhu YW, Ren WB, Zhou X, et al. Association of metformin intake with bladder cancer risk and oncologic outcomes in type 2 diabetes mellitus patients: A systematic review and meta-analysis. *Medicine (Baltimore)*. 2018;97(30):e11596.
344. Santucci C, Gallus S, Martinetti M, La Vecchia C, Bosetti C. Aspirin and the risk of nondigestive tract cancers: An updated meta-analysis to 2019. *Int J Cancer*. 2021;148(6):1372-82.
345. Tsoi KKF, Ho JMW, Chan FCH, Sung JJY. Long-term use of low-dose aspirin for cancer prevention: A 10-year population cohort study in Hong Kong. *Int J Cancer*. 2019;145(1):267-73.
346. Guercio V, Turati F, Bosetti C, Polesel J, Serraino D, Montella M, et al. Bladder cancer risk in users of selected drugs for cardiovascular disease prevention. *Eur J Cancer Prev*. 2019;28(2):76-80.
347. Santella C, Rouette J, Brundage MD, Filion KB, Azoulay L. Androgen deprivation therapy for prostate cancer and the risk of bladder cancer: A systematic review of observational studies. *Urol Oncol*. 2020;38(11):816-25.
348. Kim A, Kim MS, Ahn JH, Choi WS, Park HK, Kim HG, et al. Clinical significance of 5-alpha reductase inhibitor and androgen deprivation therapy in bladder cancer incidence, recurrence, and survival: a meta-analysis and systemic review. *Aging Male*. 2020;23(5):971-8.
349. Sathianathen NJ, Fan Y, Jarosek SL, Lawrentschuk NL, Konety BR. Finasteride does not prevent bladder cancer: A secondary analysis of the Medical Therapy for Prostatic Symptoms Study. *Urol Oncol*. 2018;36(7):338 e13- e17.
350. Zhu D, Srivastava A, Agalliu I, Fram E, Kovac EZ, Aboumohamed A, et al. Finasteride Use and Risk of Bladder Cancer in a Multiethnic Population. *J Urol*. 2021;206(1):15-21.
351. Liaw A, Cunha GR, Shen J, Cao M, Liu G, Sinclair A, et al. Development of the human bladder and ureterovesical junction. *Differentiation*. 2018;103:66-73.
352. Dalghi MG, Montalbetti N, Carattino MD, Apodaca G. The Urothelium: Life in a Liquid Environment. *Physiological reviews*. 2020;100(4):1621-705.
353. Garcia-Espana A, Chung PJ, Zhao X, Lee A, Pellicer A, Yu J, et al. Origin of the tetraspanin uroplakins and their co-evolution with associated proteins: implications for uroplakin structure and function. *Molecular phylogenetics and evolution*. 2006;41(2):355-67.
354. Hu P, Meyers S, Liang FX, Deng FM, Kachar B, Zeidel ML, et al. Role of membrane proteins in permeability barrier function: uroplakin ablation elevates urothelial permeability. *Am J Physiol Renal Physiol*. 2002;283(6):F1200-7.
355. Hu P, Deng FM, Liang FX, Hu CM, Auerbach AB, Shapiro E, et al. Ablation of uroplakin III gene results in small urothelial plaques, urothelial leakage, and vesicoureteral reflux. *The Journal of cell biology*. 2000;151(5):961-72.
356. Steurer S, Riemann C, Buscheck F, Luebke AM, Kluth M, Hube-Magg C, et al. p63 expression in human tumors and normal tissues: a tissue microarray study on 10,200 tumors. *Biomark Res*. 2021;9(1):7.

357. Volkel C, De Wispelaere N, Weidemann S, Gorbokon N, Lennartz M, Luebke AM, et al. Cytokeratin 5 and cytokeratin 6 expressions are unconnected in normal and cancerous tissues and have separate diagnostic implications. *Virchows Arch*. 2022;480(2):433-47.
358. Outtandy P, Russell C, Kleta R, Bockenbauer. Zebrafish as a model for kidney function and disease. *Pediatric nephrology (Berlin, Germany)*. 2019;34(5):751-62.
359. Miettinen M, McCue PA, Sarlomo-Rikala M, Rys J, Czapiewski P, Wazny K, et al. GATA3: a multispecific but potentially useful marker in surgical pathology: a systematic analysis of 2500 epithelial and nonepithelial tumors. *The American journal of surgical pathology*. 2014;38(1):13-22.
360. McKenney JK, Desai S, Cohen C, Amin MB. Discriminatory immunohistochemical staining of urothelial carcinoma in situ and non-neoplastic urothelium: an analysis of cytokeratin 20, p53, and CD44 antigens. *The American journal of surgical pathology*. 2001;25(8):1074-8.
361. Uhlen M, Fagerberg L, Hallstrom BM, Lindskog C, Oksvold P, Mardinoglu A, et al. Proteomics. Tissue-based map of the human proteome. *Science*. 2015;347(6220):1260419.
362. The Human Protein Atlas. 2024 [Available from: <https://www.proteinatlas.org/>].
363. Jenkins D, Bitner-Glindzicz M, Malcolm S, Hu CC, Allison J, Winyard PJ, et al. De novo Uroplakin IIIa heterozygous mutations cause human renal adysplasia leading to severe kidney failure. *J Am Soc Nephrol*. 2005;16(7):2141-9.
364. Kong XT, Deng FM, Hu P, Liang FX, Zhou G, Auerbach AB, et al. Roles of uroplakins in plaque formation, umbrella cell enlargement, and urinary tract diseases. *J Cell Biol*. 2004;167(6):1195-204.
365. Macri F, Passantino A, Pugliese M, Pietro SD, Zacccone D, Giorgianni P, et al. Retrograde positive contrast urethrocytography of the fish urogenital system. *TheScientificWorldJournal*. 2014;2014:384165.
366. Jubber I, Morhardt DR, Griffin J, Cumberbatch MG, Glover M, Zheng Y, et al. Analysis of the distal urinary tract in larval and adult zebrafish reveals homology to the human system. *Disease models & mechanisms*. 2023;16(7).
367. Yaxley JP. Urinary tract cancers: An overview for general practice. *J Family Med Prim Care*. 2016;5(3):533-8.
368. Ricketts CJ, De Cubas AA, Fan H, Smith CC, Lang M, Reznik E, et al. The Cancer Genome Atlas Comprehensive Molecular Characterization of Renal Cell Carcinoma. *Cell Rep*. 2018;23(12):3698.
369. Kaufman CK, Mosimann C, Fan ZP, Yang S, Thomas AJ, Ablain J, et al. A zebrafish melanoma model reveals emergence of neural crest identity during melanoma initiation. *Science*. 2016;351(6272):aad2197.
370. Shive HR. Zebrafish models for human cancer. *Vet Pathol*. 2013;50(3):468-82.
371. Kawakami K. Tol2: a versatile gene transfer vector in vertebrates. *Genome Biol*. 2007;8 Suppl 1(Suppl 1):S7.
372. Asakawa K, Kawakami K. The Tol2-mediated Gal4-UAS method for gene and enhancer trapping in zebrafish. *Methods (San Diego, Calif)*. 2009;49(3):275-81.
373. Asakawa K, Kawakami K. Targeted gene expression by the Gal4-UAS system in zebrafish. *Development, growth & differentiation*. 2008;50(6):391-9.
374. Kawakami K, Asakawa K, Hibi M, Itoh M, Muto A, Wada H. Gal4 Driver Transgenic Zebrafish: Powerful Tools to Study Developmental Biology, Organogenesis, and Neuroscience. *Adv Genet*. 2016;95:65-87.

375. Entezari AA, Snook AE, Waldman SA. Guanylyl cyclase 2C (GUCY2C) in gastrointestinal cancers: recent innovations and therapeutic potential. *Expert Opin Ther Targets*. 2021;25(5):335-46.
376. Sugita S, Enokida H, Yoshino H, Miyamoto K, Yonemori M, Sakaguchi T, et al. HRAS as a potential therapeutic target of salirasib RAS inhibitor in bladder cancer. *Int J Oncol*. 2018;53(2):725-36.
377. Halpern ME, Rhee J, Goll MG, Akitake CM, Parsons M, Leach SD. Gal4/UAS transgenic tools and their application to zebrafish. *Zebrafish*. 2008;5(2):97-110.
378. Zeng C, Pan F, Jones LA, Lim MM, Griffin EA, Sheline YI, et al. Evaluation of 5-ethynyl-2'-deoxyuridine staining as a sensitive and reliable method for studying cell proliferation in the adult nervous system. *Brain Res*. 2010;1319:21-32.
379. Baugh EH, Ke H, Levine AJ, Bonneau RA, Chan CS. Why are there hotspot mutations in the TP53 gene in human cancers? *Cell Death Differ*. 2018;25(1):154-60.
380. Tate JG, Bamford S, Jubb HC, Sondka Z, Beare DM, Bindal N, et al. COSMIC: the Catalogue Of Somatic Mutations In Cancer. *Nucleic acids research*. 2019;47(D1).
381. Wellcome Sanger Institute. COSMIC – the Catalogue of Somatic Mutations in Cancer: Wellcome Sanger Institute; 2024 [Available from: [cancer.sanger.ac.uk](http://cancer.sanger.ac.uk)].
382. Selves J, Long-Mira E, Mathieu MC, Rochaix P, Ilie M. Immunohistochemistry for Diagnosis of Metastatic Carcinomas of Unknown Primary Site. *Cancers (Basel)*. 2018;10(4).
383. Tong GX, Yu WM, Beaubier NT, Weeden EM, Hamele-Bena D, Mansukhani MM, et al. Expression of PAX8 in normal and neoplastic renal tissues: an immunohistochemical study. *Mod Pathol*. 2009;22(9):1218-27.
384. Dovey M, White RM, Zon LI. Oncogenic NRAS cooperates with p53 loss to generate melanoma in zebrafish. *Zebrafish*. 2009;6(4):397-404.
385. Gu L, Ai Q, Cheng Q, Ma X, Wang B, Huang Q, et al. Sarcomatoid variant urothelial carcinoma of the bladder: a systematic review and meta-analysis of the clinicopathological features and survival outcomes. *Cancer Cell Int*. 2020;20(1):550.
386. Deng H, Kerppola TK. Visualization of the Genomic Loci That Are Bound by Specific Multiprotein Complexes by Bimolecular Fluorescence Complementation Analysis on Drosophila Polytene Chromosomes. *Methods Enzymol*. 2017;589:429-55.
387. Li W, Liang Y, Deavers MT, Kamat AM, Matin SF, Dinney CP, et al. Uroplakin II is a more sensitive immunohistochemical marker than uroplakin III in urothelial carcinoma and its variants. *Am J Clin Pathol*. 2014;142(6):864-71.
388. Moll R, Wu XR, Lin JH, Sun TT. Uroplakins, specific membrane proteins of urothelial umbrella cells, as histological markers of metastatic transitional cell carcinomas. *Am J Pathol*. 1995;147(5):1383-97.
389. Kawakami K. Tol2: a versatile gene transfer vector in vertebrates. *Genome Biol*. 82007. p. S7.
390. Seiler C, Pack M. Transgenic labeling of the zebrafish pronephric duct and tubules using a promoter from the enpep gene. *Gene expression patterns : GEP*. 2011;11(1-2).
391. Zhou W, Boucher RC, Bollig F, Englert C, Hildebrandt F. Characterization of mesonephric development and regeneration using transgenic zebrafish. *American journal of physiology Renal physiology*. 2010;299(5):F1040-7.
392. Kozak M. Compilation and analysis of sequences upstream from the translational start site in eukaryotic mRNAs. *Nucleic Acids Res*. 1984;12(2):857-72.

393. Yamada M, Nagasaki SC, Suzuki Y, Hirano Y, Imayoshi I. Optimization of Light-Inducible Gal4/UAS Gene Expression System in Mammalian Cells. *iScience*. 2020;23(9):101506.
394. Catto JW, North B, Goff M, Carter A, Sleeth M, Mandrik O, et al. Protocol for the YORKSURE prospective multistage study testing the feasibility for early detection of bladder cancer in populations with high disease-specific mortality risk. *BMJ Open*. 2023;13(9):e076612.
395. McCarthy M, McCarthy L. The evolution of the urinary bladder as a storage organ: scent trails and selective pressure of the first land animals in a computational simulation. *SN Applied Sciences*. 2019;1(12):1727.
396. Curtis J, Wood C. Kidney And Urinary Bladder Responses Of Freshwater Rainbow Trout To Isosmotic NaCl And NaHCO<sub>3</sub> Infusion . *J exp Biol*. 1992(173):181-203.
397. Zhang Y, Marshall-Phelps K, de Almeida RG. Fast, precise and cloning-free knock-in of reporter sequences in vivo with high efficiency. *Development*. 2023;150(12).
398. Foley JW, Zhu C, Jolivet P, Zhu SX, Lu P, Meaney MJ, et al. Gene expression profiling of single cells from archival tissue with laser-capture microdissection and Smart-3SEQ. *Genome Res*. 2019;29(11):1816-25.
399. Hunter MV, Moncada R, Weiss JM, Yanai I, White RM. Spatially resolved transcriptomics reveals the architecture of the tumor-microenvironment interface. *Nat Commun*. 2021;12(1):6278.
400. Scholzen T, Gerdes J. The Ki-67 protein: from the known and the unknown. *J Cell Physiol*. 2000;182(3):311-22.
401. Leung AY, Leung JC, Chan LY, Ma ES, Kwan TT, Lai KN, et al. Proliferating cell nuclear antigen (PCNA) as a proliferative marker during embryonic and adult zebrafish hematopoiesis. *Histochem Cell Biol*. 2005;124(2):105-11.
402. Chng J, Wang T, Nian R, Lau A, Hoi KM, Ho SC, et al. Cleavage efficient 2A peptides for high level monoclonal antibody expression in CHO cells. *MAbs*. 2015;7(2):403-12.